NASA CONTRACTOR REPORT

NASA CR-637

NASA CR-637

PROPORTIONAL SOLID PROPELLANT SECONDARY INJECTION THRUST VECTOR CONTROL STUDY

Prepared by
SPERRY RAND CORP.
Troy, Mich.
for Langley Research Center

NATIONAL AERONAUTICS AND SPACE ADMINISTRATION • WASHINGTON, D. C. • NOVEMBER 1966

NASA CR-637

PROPORTIONAL SOLID PROPELLANT SECONDARY INJECTION THRUST VECTOR CONTROL STUDY

Prepared under Contract No. NAS 1-2962 by
SPERRY RAND CORP.
Troy, Mich.

for Langley Research Center

NATIONAL AERONAUTICS AND SPACE ADMINISTRATION

For sale by the Clearinghouse for Federal Scientific and Technical Information
Springfield, Virginia 22151 – Price $3.75

ABSTRACT

The objective of this contract was to investigate the performance characteristics of a proportional hot gas secondary injection thrust vector control system to permit the application of such TVC systems to large solid fuel rockets. This objective was accomplished through a combined analytical and experimental program. The experiments were conducted on a high energy solid propellant rocket motor under sea level conditions.

Thrust vector control by the method of secondary fluid injection has been investigated both analytically and on scale models over the past few years. Although many types of fluid have been considered, the major operational systems presently use liquids as the injectant.

Theory has predicted that the injection of a high temperature gas will greatly improve secondary injection system performance. Specifically, the injection of high temperature gas will result in a larger specific impulse and magnification factor. The results of this program have shown the theory to be correct. Specific impulse levels of 330 seconds and a magnification factor of 2.3 were obtained with a 2000^{o}F gas.

Past secondary injection systems generally have used on-off type controls. The TVC system analyzed and evaluated during this

program was of the proportional type. The degree of thrust vector control applied to the rocket motor can be varied and modulated in proportion to a programmed input signal. The high temperature pneumatic valve used to modulate the secondary injection gas flow in response to the electrical input signals was based on a design developed by Vickers under contract to NASA Marshall Space Flight Center.

FOREWORD

This report describes the results of work accomplished under NASA Contract NAS 1-2962 entitled "Proportional Hot Gas Secondary Injection Program". The contract was performed under the technical cognizance of John Riebe, Chief, Aerospace Controls Section, Applied Physics and Materials Division, Langley Research Center.

In support of this program, the Allegany Ballistics Laboratory, Cumberland, Maryland, furnished the rocket motor and test stand; conducted the test firings in conjunction with Vickers Incorporated; and provided the instrumentation and data acquisition system.

TABLE OF CONTENTS

LIST OF FIGURES

LIST OF TABLES

NOMENCLATURE

Symbol	Definition	Units
A	Orifice area	in^2
A_{j*}	Injection nozzle throat area	in^2
A_j	Injection nozzle exit area	in^2
A_3	Area of Zone 3 = $A_e - 4A_4$	in^2
A_o	Area of motor nozzle in plane of shock apex	in^2
A_4	Area of each Zone 4 $\tilde{=} \frac{1}{2}h^2$	in^2
A_{e1}	Exit area first nozzle	in^2
A_{e2}	Exit area second nozzle	in^2
A_*	Nozzle throat area	in^2
a	Numerator of secondary injection transfer function	$\frac{in^2 rad}{sec}$
b	Corner frequency for secondary injection	rad/sec
C_1	Gas flow coefficient	$\sqrt{^oR}/sec$
C_d	Orifice discharge coefficient	
D	Translational damping term	lbsec/ft
D_o	Diameter of motor nozzle at shock apex	in
D_j	Diameter of motor nozzle in plane of injection	in
D_e	Diameter of motor nozzle in exit plane	in

Symbol	Definition	Units
F_s	Side force from single injection nozzle	lb
F_1	Thrust from first injection nozzle used as vernier rocket	lb
F_2	Thrust from second injection nozzle used as vernier rocket	lb
F_3	Axial thrust contribution of primary stream	lb
F_4	Total axial thrust contribution of secondary streams	lb
F_j	Measured side force	lb
F_{app}	Force applied to system by secondary injection	lb
F_{meas}	Sum of load cell readings = $F_{34} + F_{56}$	lb
F_{56}	Force on aft load cell = kx_{56}	lb
F	Axial thrust of system	lb
F_{34}	Force on forward load cell = kx_{34}	lb
F_{th}	Theoretical side force	lb
g	Gravitational constant	ft/sec^2
h	Accommodation height	in
I	Primary gas specific impulse	secs
I_j	Injectant gas specific impulse	secs
J	System moment of inertia about c.g.	$slug\ ft^2$
K	Defined by equation 4.4	lbm/sec

Symbol	Definition	Units
k	Spring constant of load cells	lb/ft
L_s	Distance between shock apex to exit plane parallel to nozzle axis	in
L_j	Distance from injection plane to nozzle exit plane parallel to nozzle axis	in
ℓ_1	Distance between forward load cell and test stand c.g	ft
ℓ_2	Distance between aft load cell and test stand c.g	ft
ℓ_3	Distance between aft load cell and injection plane	ft
M_o	Free stream Mach No.	
M_j	Injection nozzle Mach No.	
M_3	Primary stream Mach No. at exit plane	
M_4	Secondary stream Mach No. at exit plane	
$\dot{m}_1$	Mass flow first nozzle	lbm/sec
$\dot{m}_2$	Mass flow second nozzle	lbm/sec
m	System mass	slugs
P	Gas total pressure	psia
P_4	Secondary stream pressure at exit plane	psia
P_o	Primary stream pressure at shock apex	psia
P_2	Pressure along shock	psia
$\bar{P}_2$	Average pressure, shock region	psia

Symbol	Definition	Units
P_s	Boundary layer separation pressure	psia
$\bar{P}_s$	Average pressure in separated region	psia
P_j	Injection nozzle exit pressure	psia
P_{jc}	Injection nozzle chamber pressure	psia
P_3	Primary stream pressure at exit plane	psia
P_c	Rocket engine chamber pressure	psia
P_{e1}	Exit pressure first nozzle	psia
P_{a1}	Ambient pressure at first nozzle	psia
P_{e2}	Exit pressure - second nozzle	psia
P_{a2}	Ambient pressure at second nozzle	psia
P_{c1}	Chamber pressure first nozzle	psia
P_{c2}	Chamber pressure second nozzle	psia
ΔP_{jc}	Difference in injector chamber pressures	psi
Q	Volumetric flow	in^3/sec
R	Gas constant	$ft/^oR$
R_j	Gas constant injected gas	$ft/^oR$
S	Laplace transform	1/sec
T	Gas total temperature	^oR
T_c	Primary gas total temperature	^oR
T_j	Injectant total temperature	^oR
v_j	Injection nozzle exit velocity	ft/sec

Symbol	Definition	Units
v_1	Exit velocity first nozzle	ft/sec
v_2	Exit velocity second nozzle	ft/sec
$\dot{w}$	Primary gas weight flow	lb/sec
$\dot{w}_j$	Injection nozzle weight flow	lb/sec
$\Delta\dot{w}_j$	Differential injection nozzle flow	lb/sec
X	Distance along nozzle wall from shock apex to injection point	in
x_{34}	Deflection of forward load cell	ft
x_{56}	Deflection of aft load cell	ft
X/L	Length of throat to injection plane divided by throat to exit plane	
Y	Chord in plane of injection between injected point to actual shock azimuth	in
Z	Lateral translation of system c.g	ft
α	Primary nozzle half-angle	degrees
γ	Specific heat ratio primary gas	
γ_j	Specific heat ratio injection gas	
Γ	$\gamma\left(\frac{2}{\gamma+1}\right)^{\frac{\gamma+1}{2(\gamma-1)}}$ for $\gamma = 1.3$ $\Gamma = 0.761$	

Symbol	Definition	Units
δ	Boundary layer separation angle	degrees
ε	Angle between injection nozzle center-line and a line perpendicular to the motor nozzle axis	degrees
θ_1	System rotation about c.g	degrees
θ_{exp}	Experimental shock angle - defined by equation 9.3	degrees
Φ_e	Azimuth of shock on nozzle wall at exit plane	degrees
Φ_j	Azimuth of shock on nozzle wall in injection plane	degrees
ζ_d	Nozzle discharge correction factor	
ζ_v	Nozzle velocity correction factor	
μ	Rotational damping term	ft lb sec
ω	System driving frequency	rads/sec
ψ	Effective shock angle along nozzle wall	degrees

SECTION 1

INTRODUCTION

1.1 Program Objectives

The overall purpose of this program was to investigate the performance characteristics of a proportional hot gas secondary injection thrust vector control system. This was accomplished through a combined analytical and experimental program. The specific objectives were:

1. To establish an analytical model to predict the secondary injection phenomena.
2. To conduct an experimental program on a high energy solid propellant rocket motor.
3. To establish the correlation between the analytical model and the experimental data.
4. To determine the effect of secondary injection nozzle configuration and injection angle on system performance.
5. To evaluate the effect of a continuously flowing secondary injection system on the performance of the rocket engine.
6. To establish the dynamics of the proportional secondary injection thrust vector control system.

The results of this program can be directly applied to the design of a high temperature proportional secondary injection thrust vector control system for use on future solid fuel rockets. The high specific impulse levels achieved will allow a significant weight reduction when compared to liquid injection systems and potentially increased reliability because of the use of fewer components.

1.2 System Description

A schematic of the secondary injection system for one axis TVC is shown in Figure 1.1. For the last test in the series in which control was applied in two mutually perpendicular planes two independent systems as shown in Figure 1.1 were installed on the rocket motor.

Gas at 2000°F at a nominal pressure of 2700 psi and mass flow of .61 lb/sec is produced in the gas generator by burning OMAX 453D solid propellant

The load orifice in the generator outlet provides a constant output impedance for the gas generator.

The control valve metering area is sized to produce a system pressure of 1000 psi at the valve inlet.

With the control valve in the null position the gas flow is ported equally to each secondary injection nozzle.

An electrical input signal to the valve results in a proportional displacement of the valve spool which simultaneously increases the flow of gas to one nozzle and decreases the flow to the second nozzle. The maximum signal level one side of the valve is completely closed, and the total gas flow from the generator is ported through one nozzle. The injection nozzle throat area is designed to provide a chamber pressure in the injection nozzle of 600 psia under full flow conditions. The pressure at the nozzle exit, for supersonic injection, is matched to the pressures in the rocket motor nozzle by the configuration of the injection nozzle extension cone.

Since the valve operates in the "choked" region the differential mass flow from the valve is directly proportional to the input signal magnitude. Since the injection nozzle pressure is effectively linear with mass flow, then the differential injection pressure between the two nozzles is also proportional to the input signal magnitude.

This type of gaseous secondary injection system is described as "continuously flowing" since the total gas flow is always injected into the rocket motor nozzle.

Figure 1.2 shows schematically the valve in the null and two extreme positions, with the resulting thrust vector control.

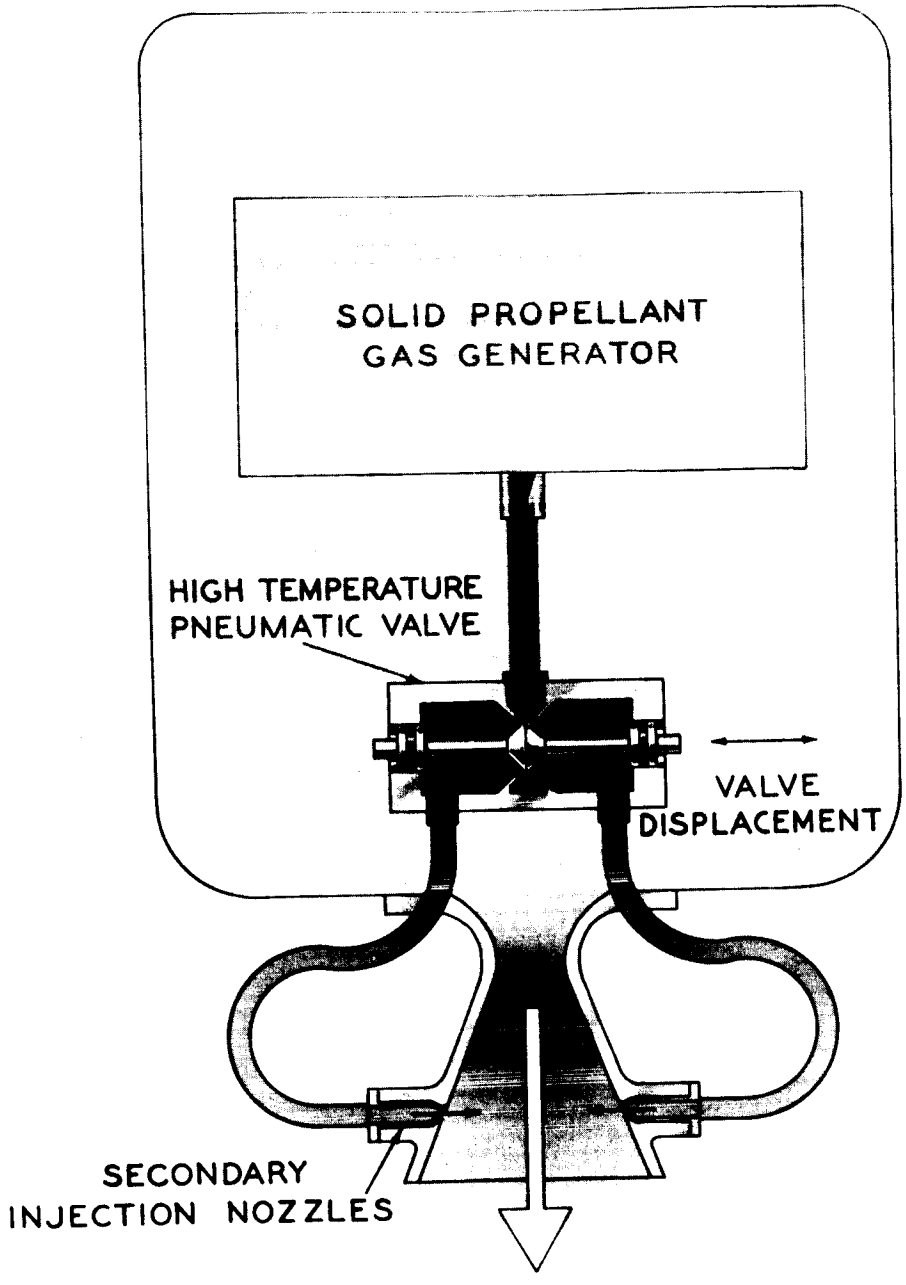

CONTINUOUS FLOWING, PROPORTIONAL, SOLID PROPELLANT SECONDARY INJECTION TVC SYSTEM

FIGURE - 1.1

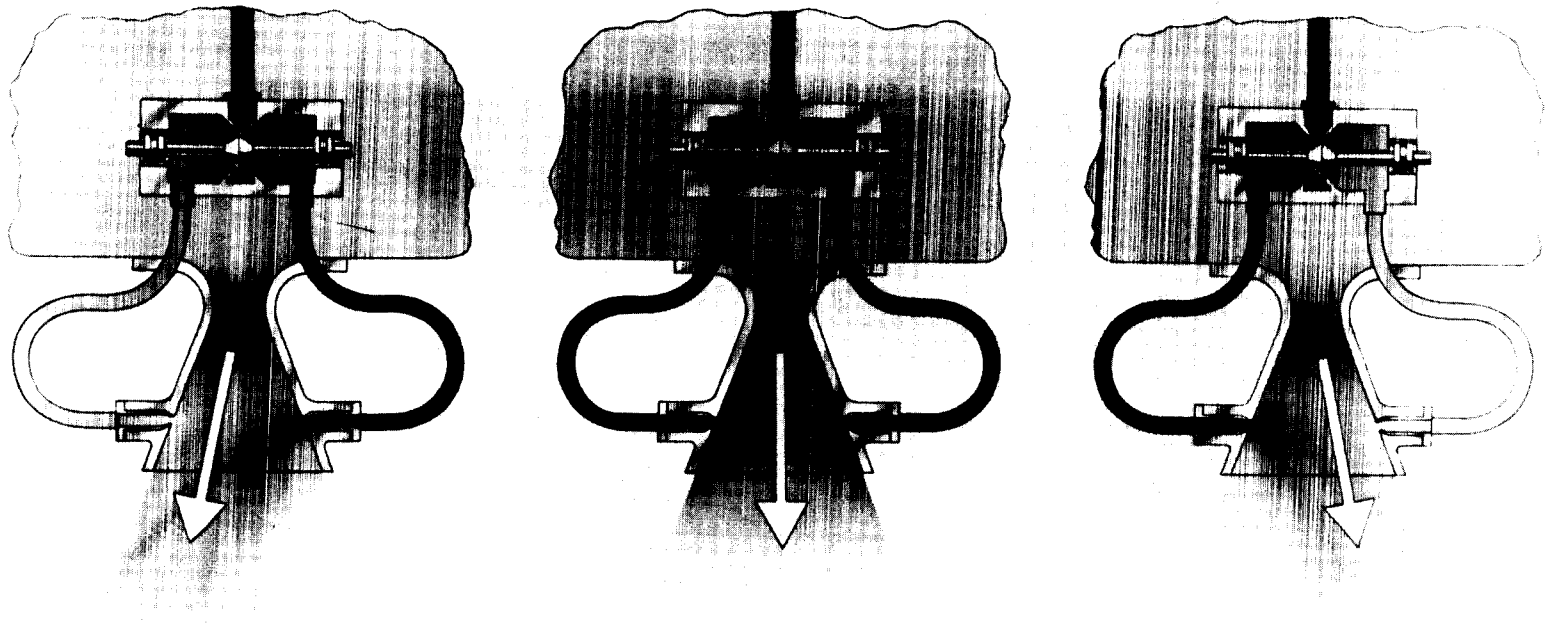

YAW LEFT STRAIGHTAWAY YAW RIGHT

FIGURE - 1.2

FUNCTIONAL DIAGRAM OF TVC SYSTEM

SECTION 2

SECONDARY INJECTION SYSTEM DESIGN AND DEVELOPMENT

The secondary injection system used for this contract consists of the following components:

1. Gas generator assembly consisting of the heavyweight gas generator, solid propellant grain and igniter system.
2. Proportional, open center, high temperature pneumatic control vlave.
3. Secondary injection nozzles.
4. Gas manifolding between the gas generator, valve, and injection nozzles.
5. Mounting frame and brackets as required to install the system on the rocket motor.

The system is shown in Figure 2.1 installed on the EM72 motor.

The installation of two systems on the motor is shown in Figure 2.2; in this case the motor and thrust stand are mounted for a vertical firing.

2.1 Gas Generator Assembly

The gas generator provides the source of hot gas to power the secondary injection system.

The heavyweight gas generator is made of 4140 steel with the end caps threaded onto the cylinder, and sealed by Viton A "O" rings. An asbestos reinforced phenolic liner is inserted into the cylinder to insulate it from the solid propellant gas.

The solid propellant is installed as two half grains and burns on two faces to provide the required mass flow of gas.

Each inhibited half grain is 5.56 inches long, 8.35 inches O.D. and weighs 15.9 lbs. The propellant formulation is OMAX 453D prepared by the Olin Corporation.

A load orifice is installed in the gas generator outlet flange to maintain a constant back pressure to the propellant. Figure 2.3 shows the variation of gas flow from the generator versus the pressure in the generator.

2.2 Proportional Control Valve

2.2.1 Valve Operating

A cut-away view of the high temperature solid propellant gas open center control valve is shown in Figure 2.4.

The flow of gas into the valve is modulated by the spool poppet to the two outlet ports. With the poppet in the null position the flo

is divided equally to both outlets; as the spool is moved from the null position the flow of gas to one outlet is proportionally increased and simultaneously the flow to the other outlet is decreased. With the spool in its extreme position the total flow into the valve is ported from one outlet, the other being completely shut off. The valve and injection nozzle areas are sized so that the flow across the valve metering area is chocked (i.e. at sonic velocity) so that the flow modulation is proportional to valve area and hence to valve stroke.

The valve is operated by a small hydraulic actuator in a closed loop system. The feedback transducer which senses the position of the pneumatic valve poppet is mounted on top of the valve; it is necessary to pick off this position over the center of the valve to minimize the null shift as the valve heats up. A photograph of the valve and actuator assembly is shown in Figure 2.5. The block diagram of the valve and actuator combination is given in Figure 2.6.

2.2.2 Valve Setup

Before each hot test the valve stroke is adjusted and valve flow checked using high pressure room temperature gaseous nitrogen (N_2).

The flow of N_2 into the valve is measured using a standard turbine flowmeter. This volumetric flow is converted into weight flow by the gas equation

$$PQ = \dot{w}RT$$

where P = upstream pressure psia

Q = volumetric flow in^3/sec

$\dot{w}$ = weight flow lb/sec

R = gas constant lb in/lb M ^oR

T = gas total temperature ^oR

Due to the different thermodynamic constants and gas temperature between the OMAX 453D propellant gas and the N_2, the weight flow of the gas through the valve at a given valve inlet pressure will be greater with N_2 than with propellant gas. For choked conditions the weight flow is determined by

$$\dot{w} = C_1 C_d \frac{AT}{\sqrt{T}} \text{ lb/sec}$$

where $C_1 = \sqrt{\dfrac{gk}{R\left(\frac{k+1}{2}\right)^{\frac{k+1}{k-1}}}}$ $\sqrt{^oR}/sec$

C_d = valve discharge coefficient

A = valve metering area, in^2

P = valve inlet pressure, psia

T = gas total temperature, ^oR

R = gas constant, lb in/lb M ^oR

k = ratio of specific heats

For constant values of C_d, A and P then the ratio of gas flow is given by

$$\frac{\dot{w}_c}{\dot{w}_h} = \frac{(C_1)_c}{(C_1)_h} \sqrt{\frac{T_h}{T_c}}$$

Where subscripts c and h refer to cold and hot conditions respectively.

For OMAX 453D gas at 2000^oF and N_2 at 60^oF

$$\frac{\dot{w}_c}{\dot{w}_h} = \frac{.522}{.413} \sqrt{\frac{2460}{520}} = 2.76$$

2.2.3 Valve Development

The basic design of the high temperature pneumatic valve as conceived at the start of the contract has been proved successful over

a series of 14 hot firings on the valve conducted at Vickers and at ABL during TVC test firings.

The only area requiring some modification was the method of valve actuation.

Initially the valve was actuated directly by an electrical torque motor. Because of the stroke limitations imposed by the torque motor it was necessary to use a valve inlet pressure of 2000 psi to pass the required mass flow through the valve.

The flow forces acting on the valve poppet are a function of mass flow and velocity distribution over the poppet face, and these factors are not the same for cold test as they are for hot firing conditions.

To reduce the development required in this area it was decided to modify the valve actuating mechanism to produce a higher driving force with a longer valve stroke capability. The hydraulic actuator system was chosen as the best means of achieving these requirements.

The valve stroke was increased and the valve inlet pressure decreased to a nominal 1000 psi. The increase in stroke makes the

valve less susceptible to null shift during hot firing. The load orifice was installed in the generator outlet flange to maintain a constant gas flow from the generator at the flow level required.

2.3 Injection Nozzles

Two types of secondary injection nozzles were used during the test program, sonic and supersonic. The basic design of both types was the same, the only difference being the addition of an exit cone for the supersonic nozzle.

For the initial tests in the program the nozzles were manufactured from sintered tantalum-tungsten carbide (Ta-WC).
This material was chosen to resist possible erosion of the tip of the nozzle by the 6200°F rocket motor exhaust gases. The injection nozzle is installed in such a manner that the end of the nozzle is buried approximately 0.5 inches into the motor nozzle.

From experience gained during the first two TVC motor firings the nozzle material was changed to stainless steel, to reduce both material and manufacturing costs.

2.4 Manifolds

The manifold pipes were used to transport the high temperature gas from the generator to the control valve and from the control valve

outlets to the injection nozzles.

These manifolds were sized to maintain a gas velocity of between 0.1 to 0.2 Mach Number.

Both Hastelloy C and high temperature stainless steel pipes were used.

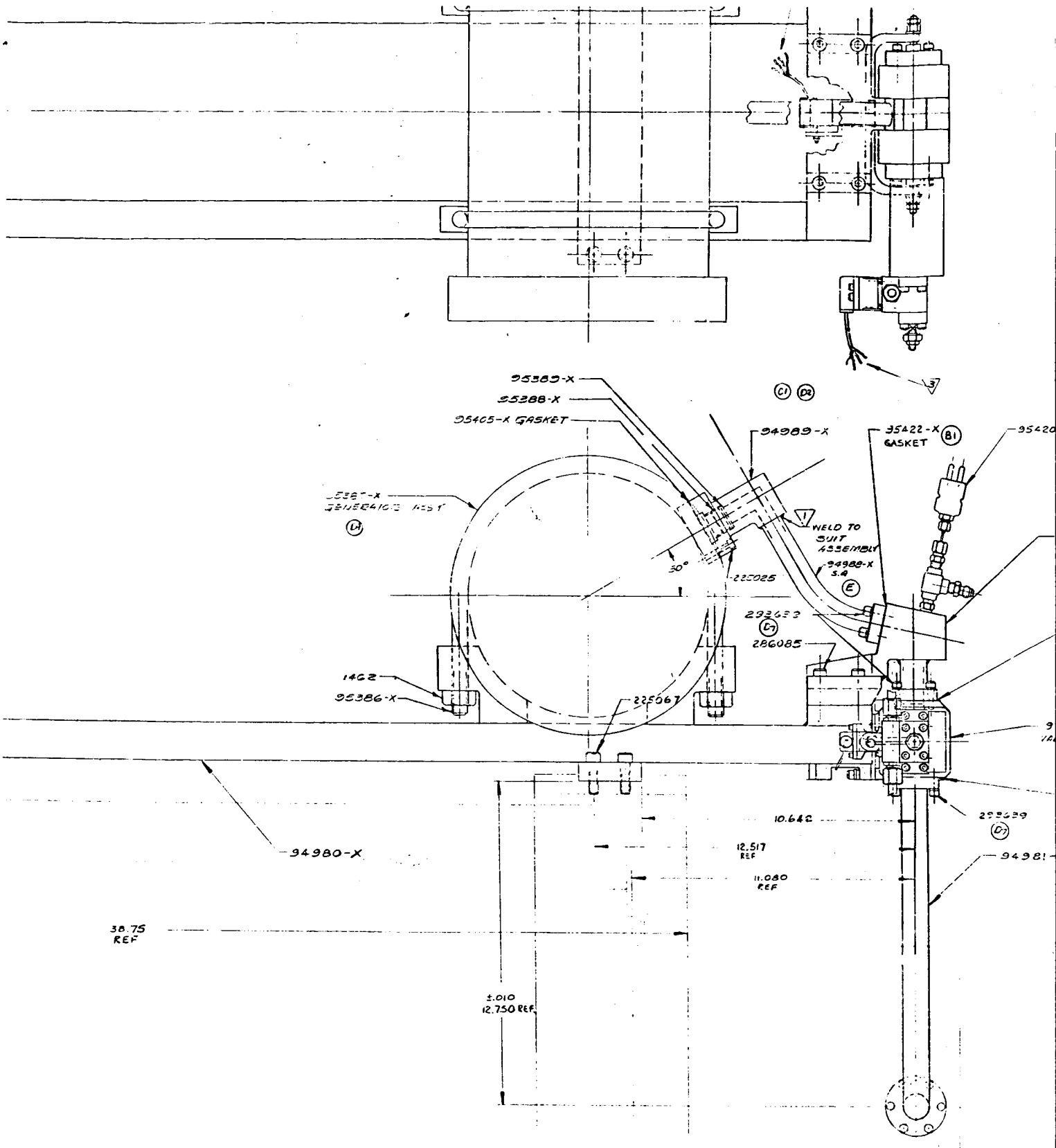

Figure 2.1 Hot Gas Seconda

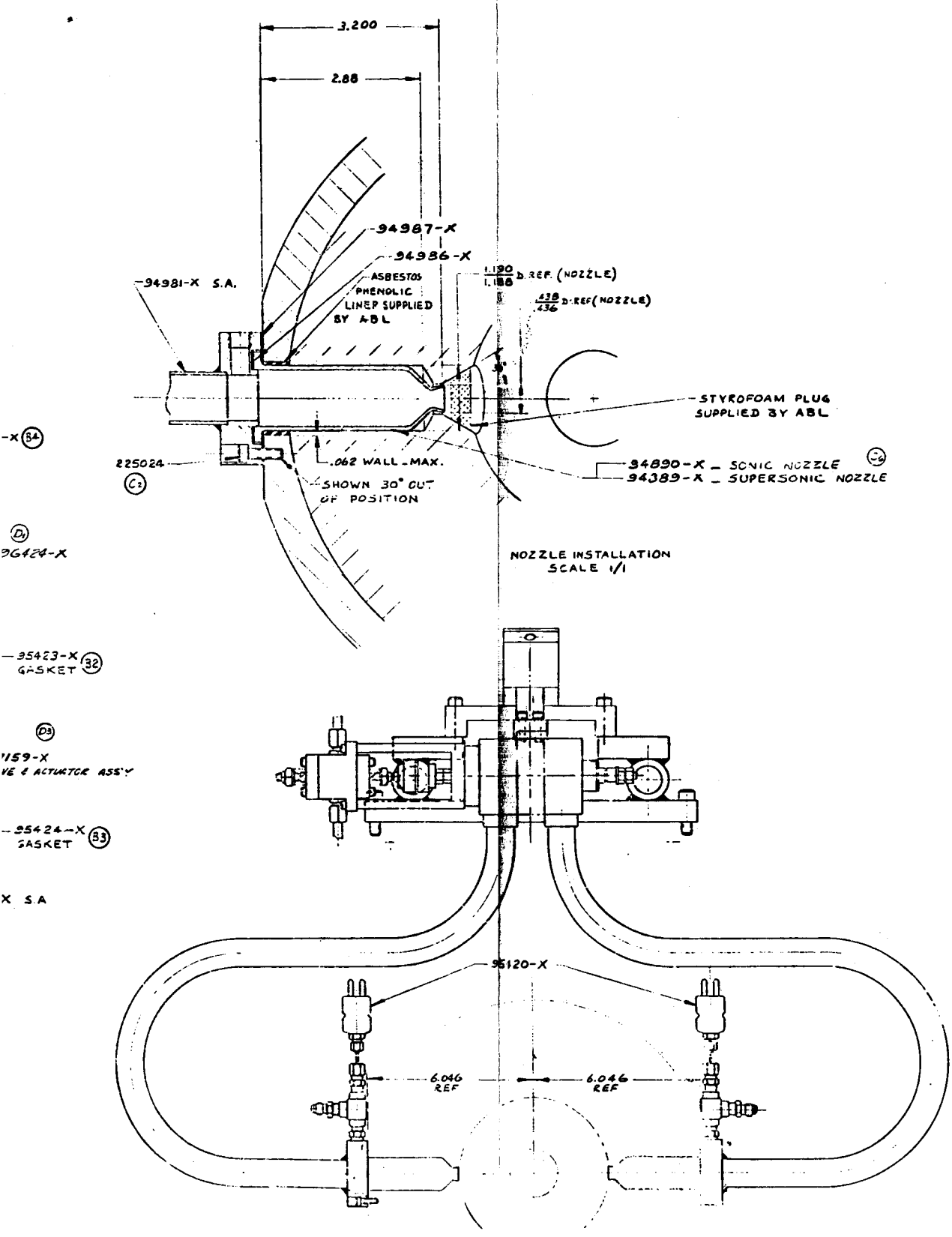

-X (34)

(D4)
3G424-X

-95423-X (32)
GASKET

(D3)
'159-X
VE & ACTUATOR ASS'Y

-95424-X (33)
GASKET

X S.A

y Injection System.

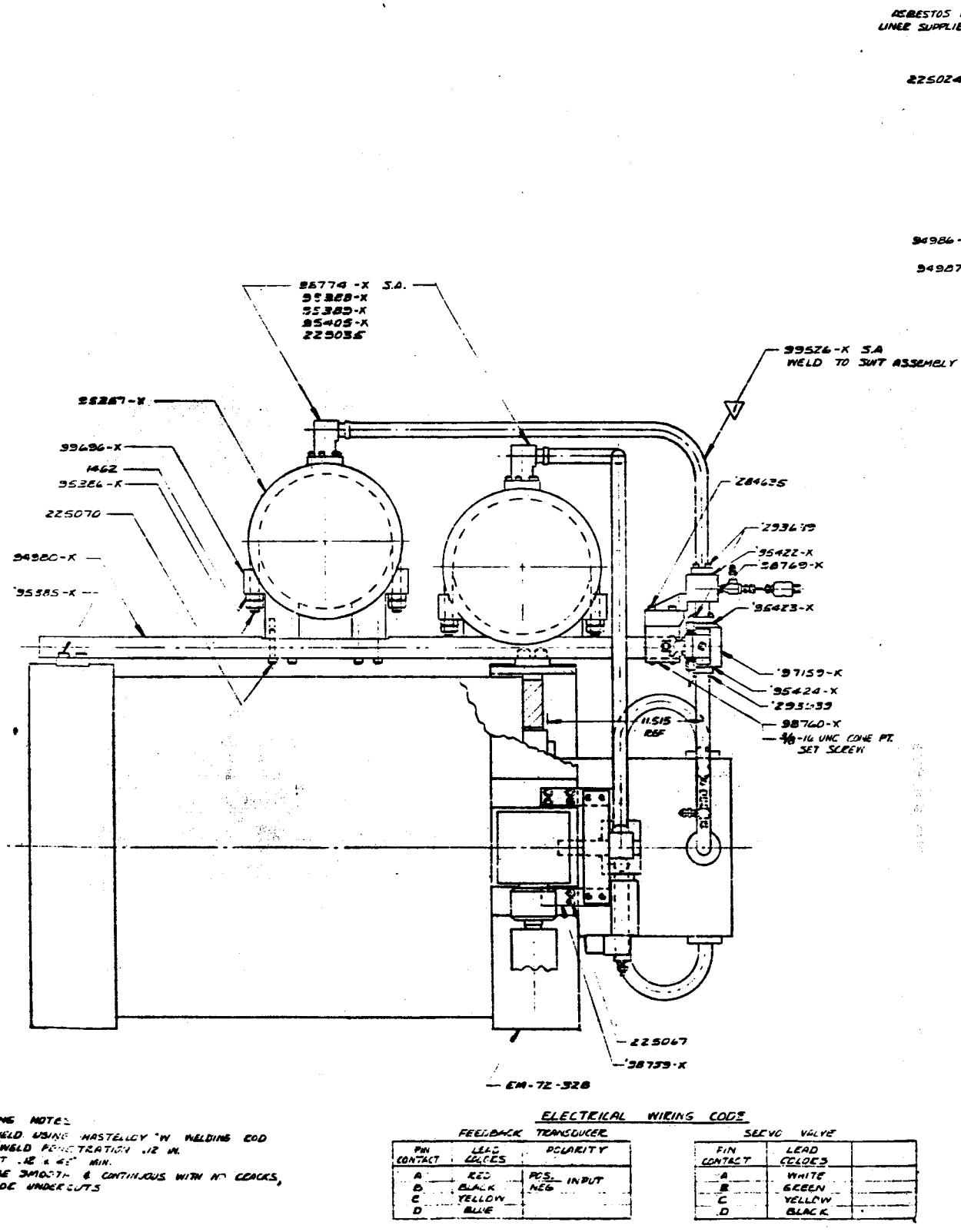

Figure 2.2 Thrust Stand Two-Axis Vertic

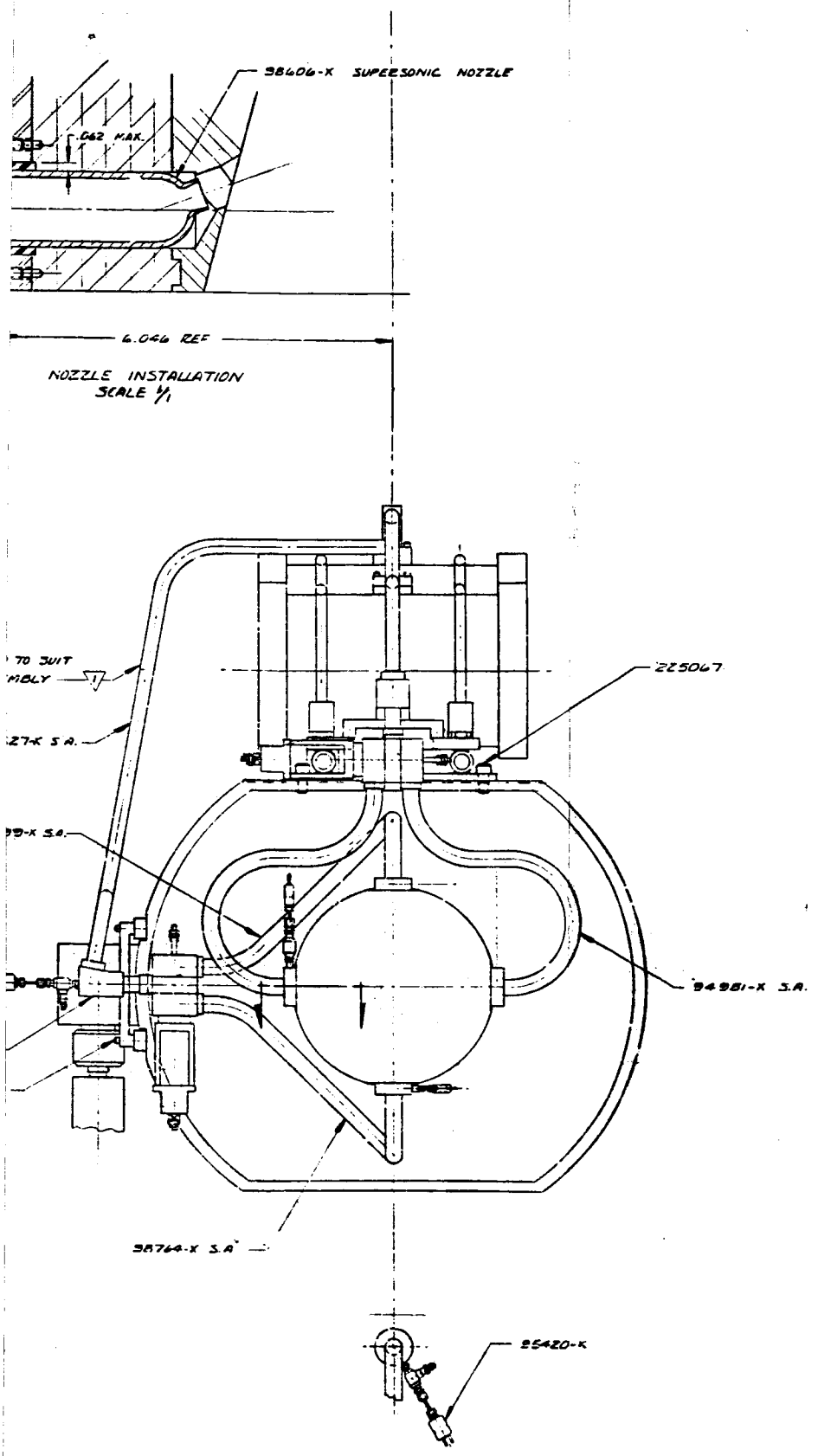
38406-X SUPERSONIC NOZZLE
.662 MAX.
6.046 REF
NOZZLE INSTALLATION
SCALE 1/1
TO SUIT
MBLY
27-K S.A.
99-X S.A.
225067
94981-X S.A.
38764-X S.A.
85420-K

al Firing.

Figure 2.3

Mass Flow Versus Generator Pressure

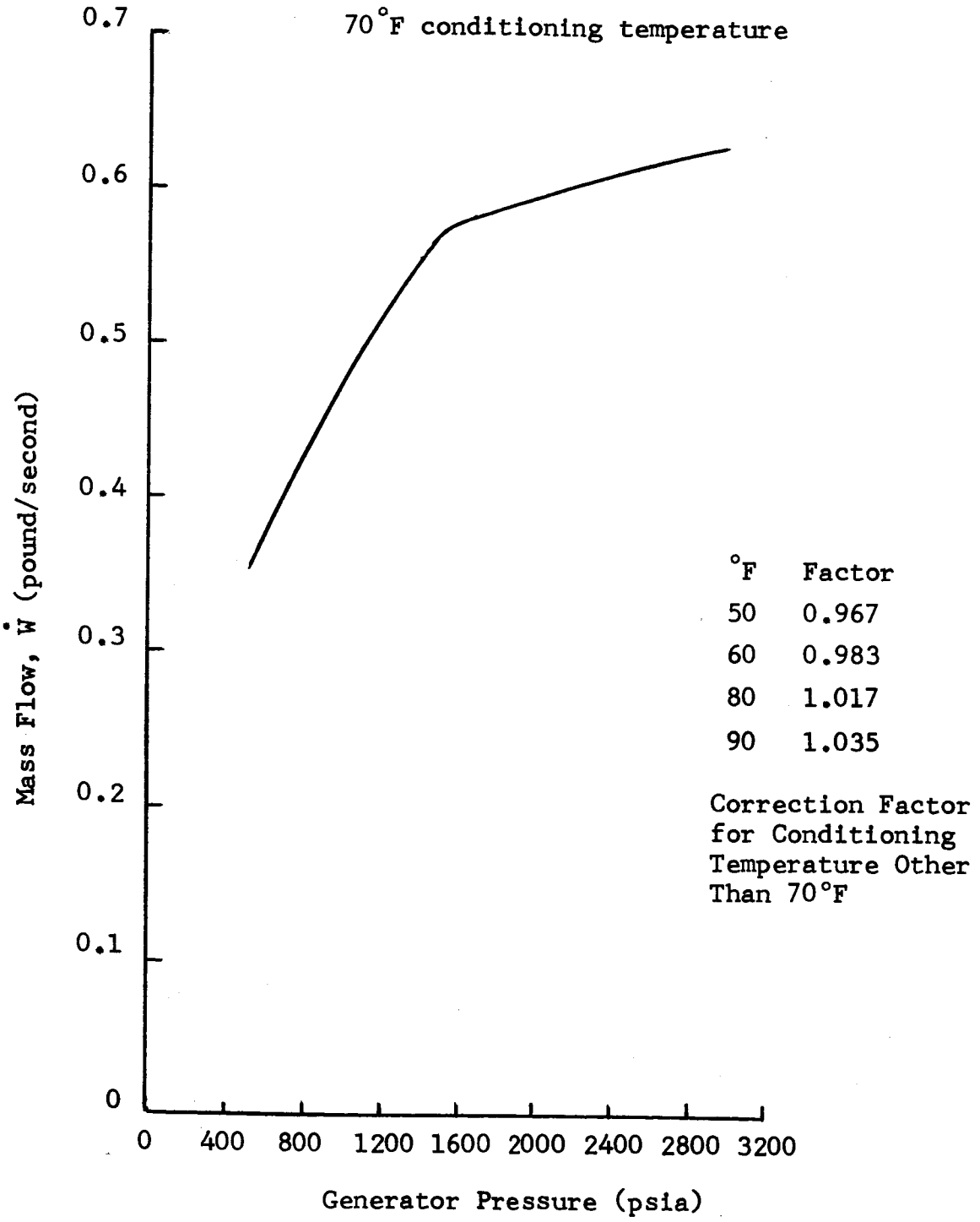

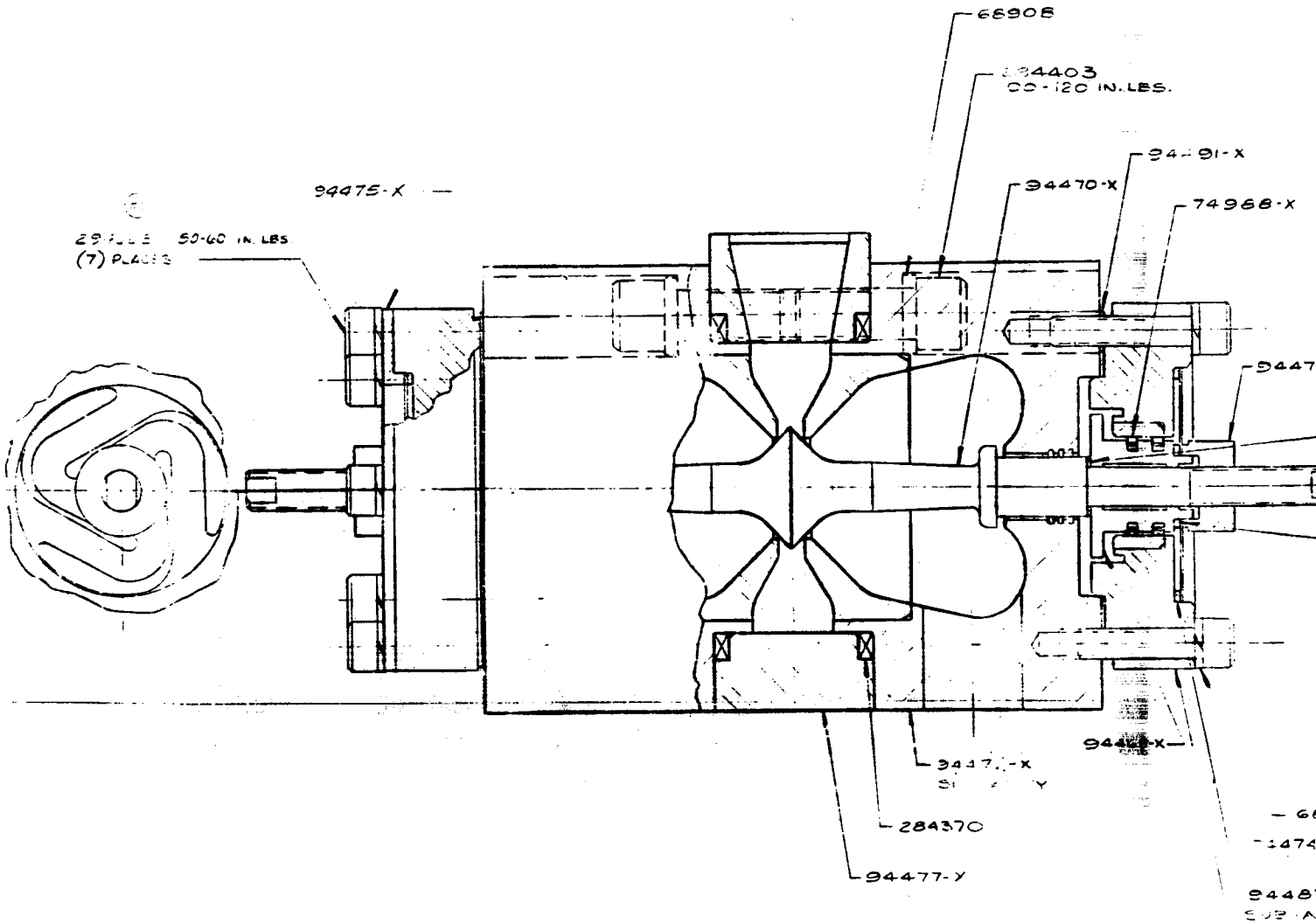

Figure 2.4 Valve Secondary Injection Hot

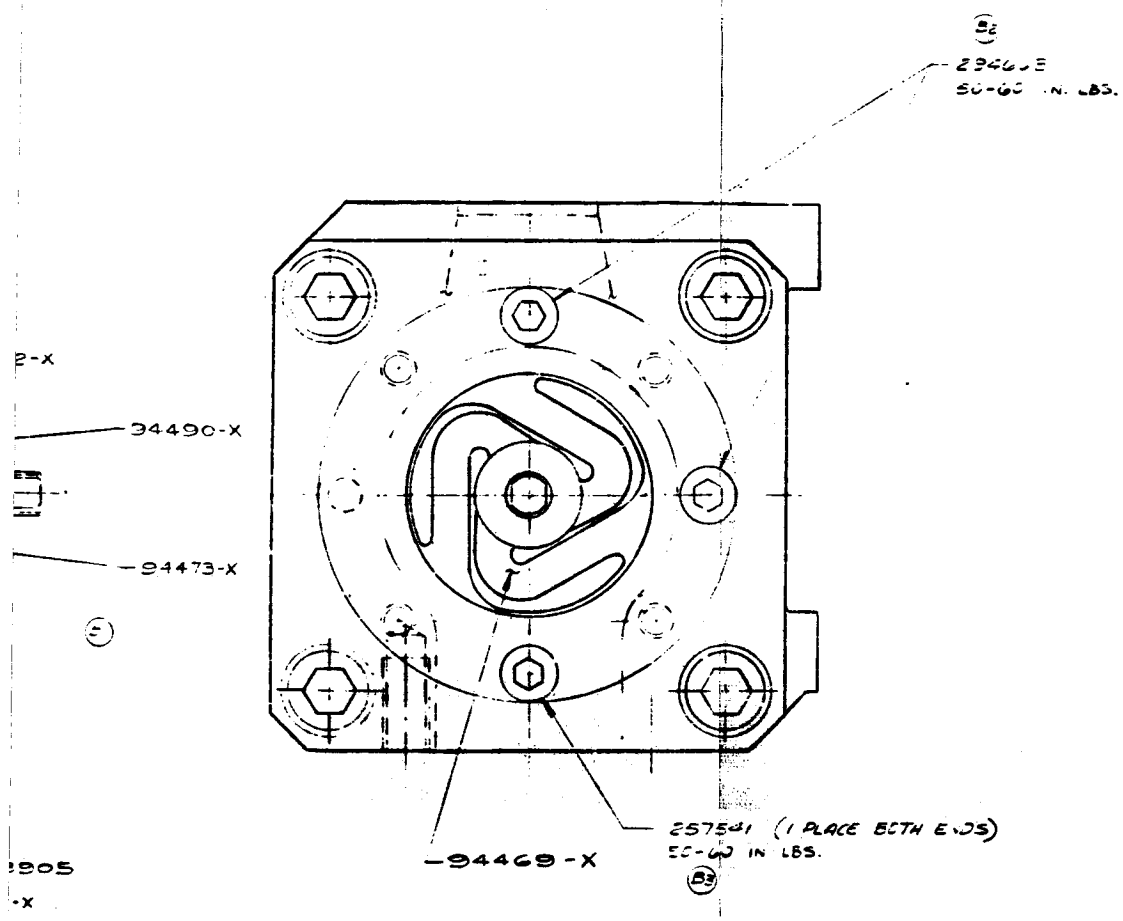

Gas Proportional Assembly.

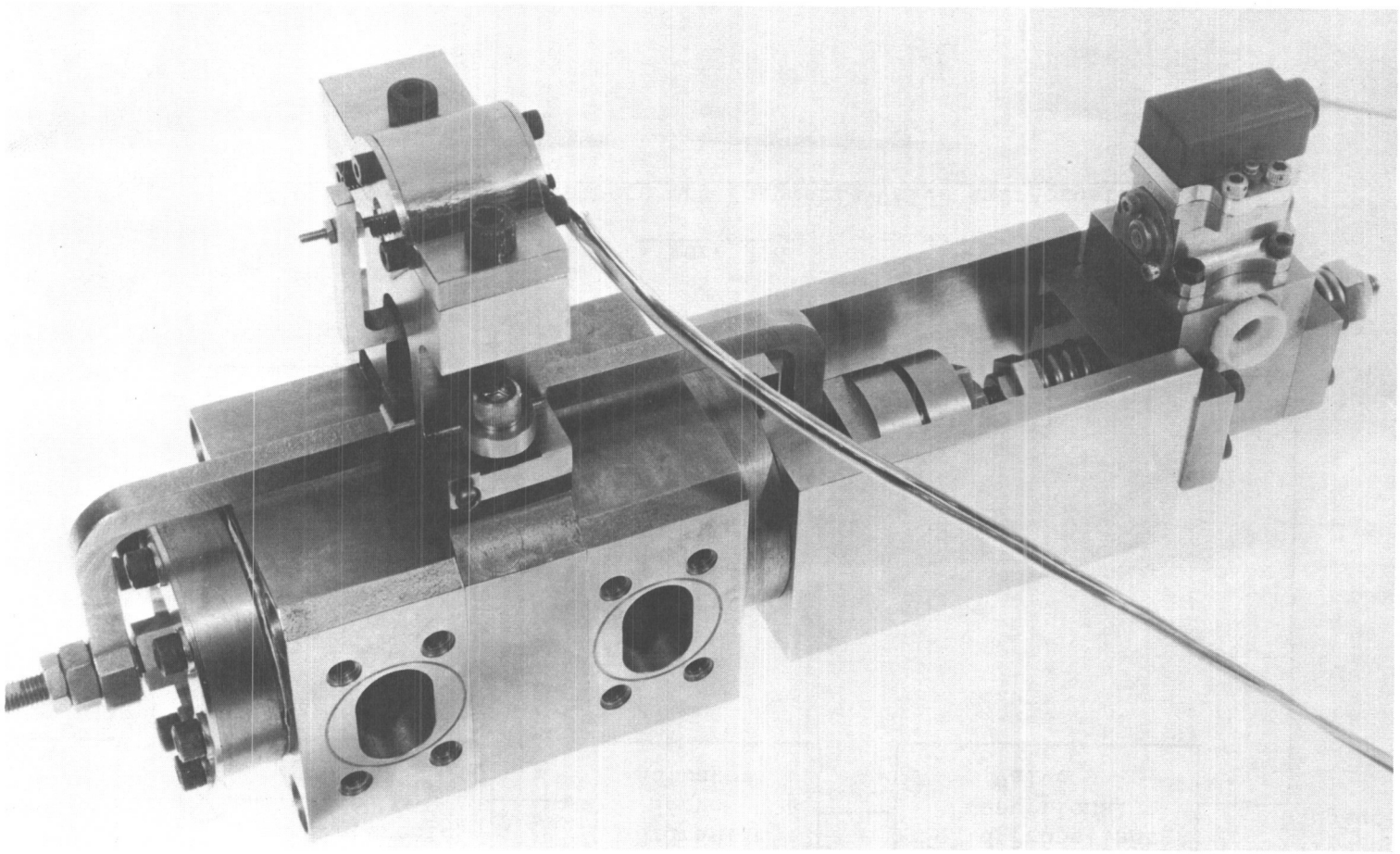

FIGURE - 2.5

HIGH TEMPERATURE PNEUMATIC VALVE

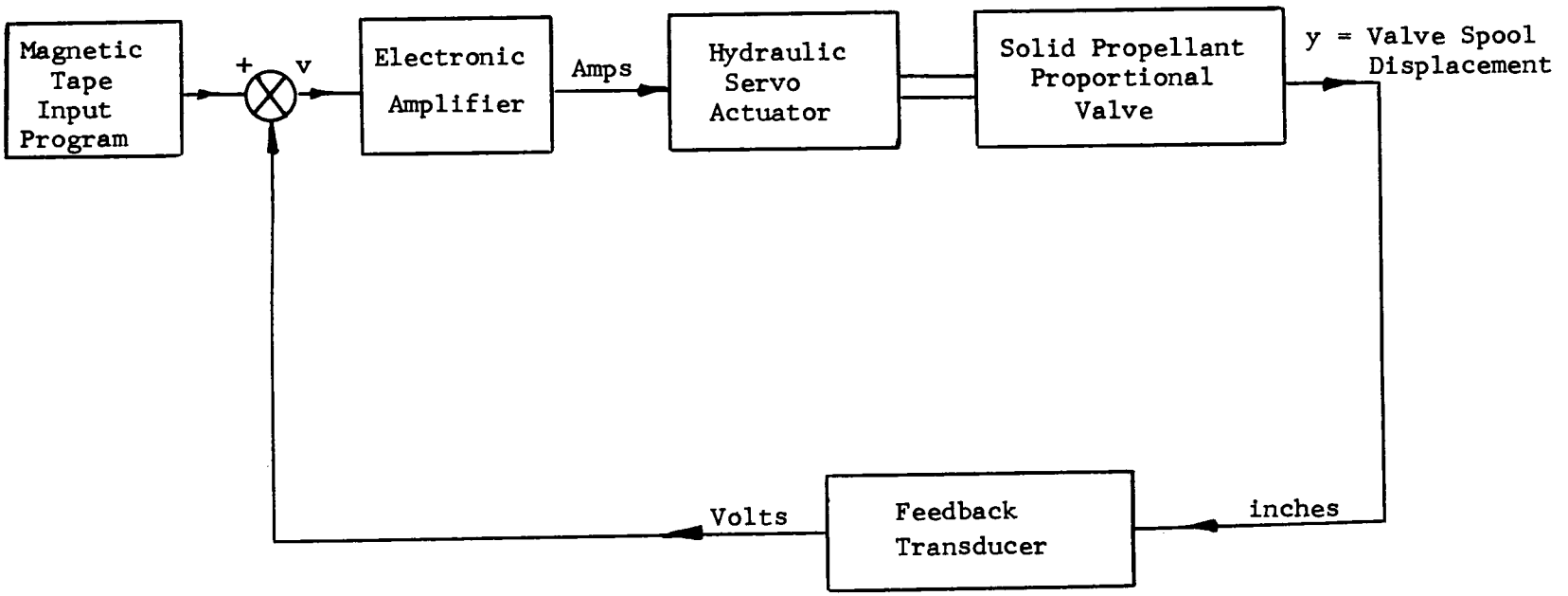

Figure 2.6

Block Diagram High Temperature Pneumatic Valve and Actuator

SECTION 3

DESCRIPTION OF ROCKET MOTOR AND TEST STAND

The TVC system test portion of this contract was conducted at the Allegany Ballistics Laboratory (ABL), Cumberland, Maryland.

In support of this program Allegany Ballistics Laboratory provided the following materials and services.

1. A rocket motor delivering a gas mass flow of 11.5 pound/second at a chamber pressure of 600 psia. Later modification achieved 12.5 to 12.9 pound/second at a chamber pressure of 550 to 590 psia. Some minor deviations to these ballistic requirements were allowed later in the program.
2. A two component thrust stand capable of measuring longitudinal and lateral forces produced by the rocket motor and TVC system to the accuracy necessary in analyzing the secondary injection phenomenon. A multi-component stand is to be used for the last TVC test which will feature control in two mutually perpendicular planes.

3. Facilities and equipment required to conduct static firings of the rocket motor TVC system assembly.

4. Reduced data from each firing along with an evaluation of the rocket motor ballistic characteristics.

3.1 Rocket Motor

The rocket motor used for this program was designed and manufactured by Allegany Ballistics Laboratory. It consisted of an end burning gas generator, designated EM72 and a heavyweight sea level nozzle. The EM72 generator was loaded with a 22 inch O.D. high impulse propellant charge containing DGV propellant.

The original design characteristics of the EM72 rocket motor were as follows:

Propellant Designation	DGV
Average Chamber Pressure	600 psia
Nozzle Exit Pressure	11 psia
Average Burning Rate	0.5 in/sec.

Burning Time	30 secs.
Throat Area	3.008 in^2
Exit Area	24.01 in^2
Nozzle Expansion Area Ratio	8:1
Propellant Surface to Throat Area Ratio	120.5:1
Propellant Mass Rate of Discharge	11.5 lb.in/sec.
Propellant O.D.	21.487 in.
Exhaust Gas Temperature	6200 $^{\circ}F$
Initial Propellant Surface Area	362.6 in^2
Average Thrust During Burning Time	2680 lb.

A summary of the EM72 motor performance is shown in Table 3.1.

The 30 second burning time was achieved by using an inert plug to fill the chamber volume not occupied by the propellant grain. Some problems were encountered in the inhibiting of the forward face of the propellant grain resulting in motor malfunctions in Test Numbers 1 and 4 (see Table 3.1). After Test 4 it was decided to completely fill the motor with the propellant grain, increasing the burning time to 42 seconds.

3.2 Test Stand

The two component thrust stand used for the first two TVC firings was manufactured by Ormond. It was capable of measuring axial thrust and lateral thrust in one plane only. It was apparent during the first TVC test that the stand was capable of only limited use for dynamic testing. During 10 cps lateral input from the secondary injection TVC system the stand approached a resonant condition producing force measurements obviously much greater than the TVC system itself could produce. Lead shot used in the stand provided sufficient damping to protect the stand from structural failure, it was necessary, however, to reduce the excitation frequency to 5 cps for the second test to obtain useful data.

Figure 3.1 shows the TVC system and EM72 motor mounted on the Ormond test stand. This stand was completely destroyed during the second TVC test when the EM72 motor exploded.

The multi-component test stand was used for the remainder of the single axis TVC tests and for the two-axis test which concluded the program. This stand designed by Allegany Ballistics Laboratory, has 6 degrees of freedom.

When mounted on the ground and fully loaded with the EM72 motor and one TVC system as shown in Figure 3.2, it has a damped natural frequency of approximately 27 cps.

During the two axis test, when the motor was fired vertically with the stand mounted on the wall as shown in Figure 3.3, the natural frequency in both the pitch and yaw axes approached 20 cps.

A detailed discussion of the test stand dynamics as applied to the analysis of the TVC system is given in Section 12.

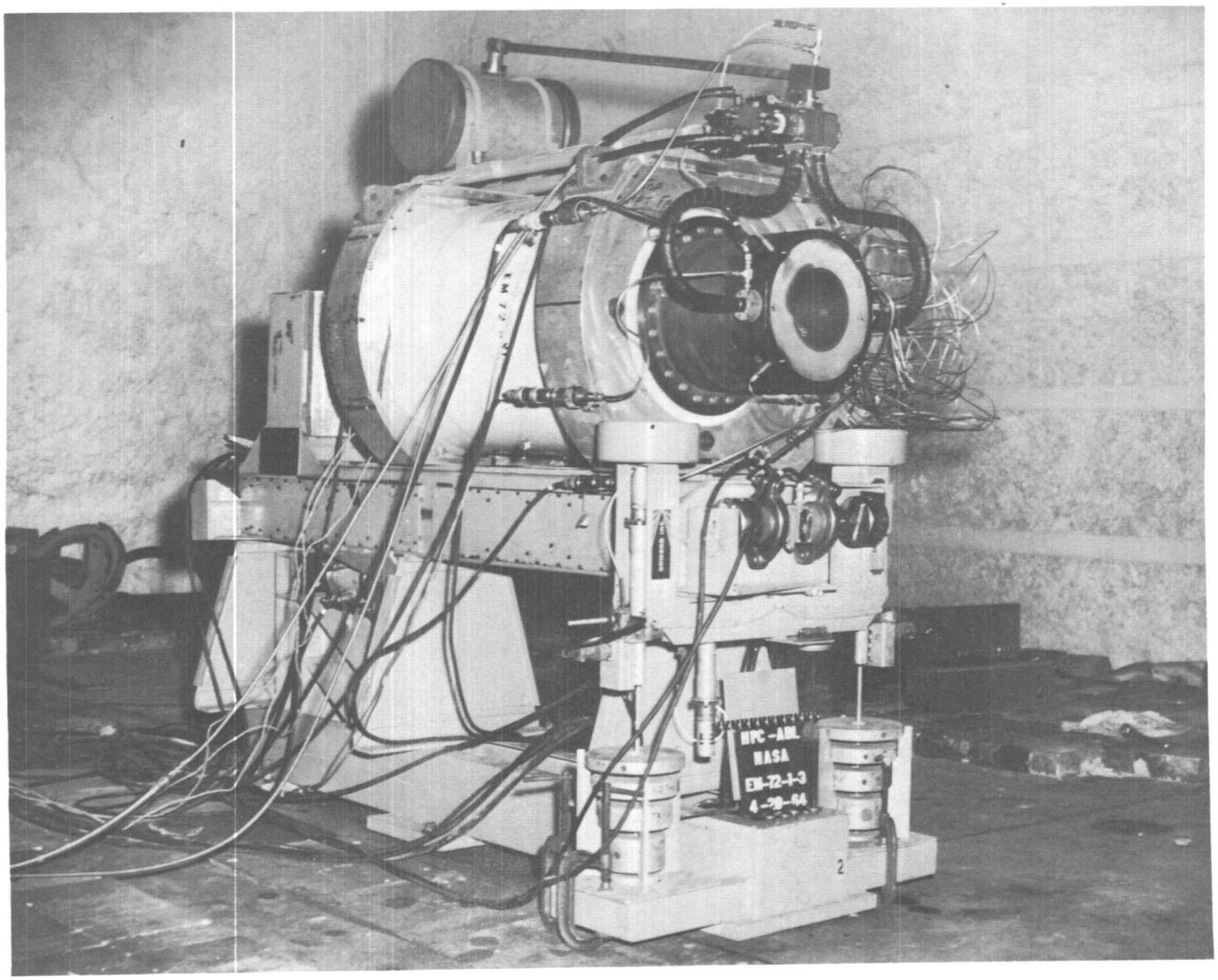

FIGURE - 3.1

VICKERS' SITVC SYSTEM AND EM72 ROCKET MOTOR
MOUNTED ON ORMOND TEST STAND

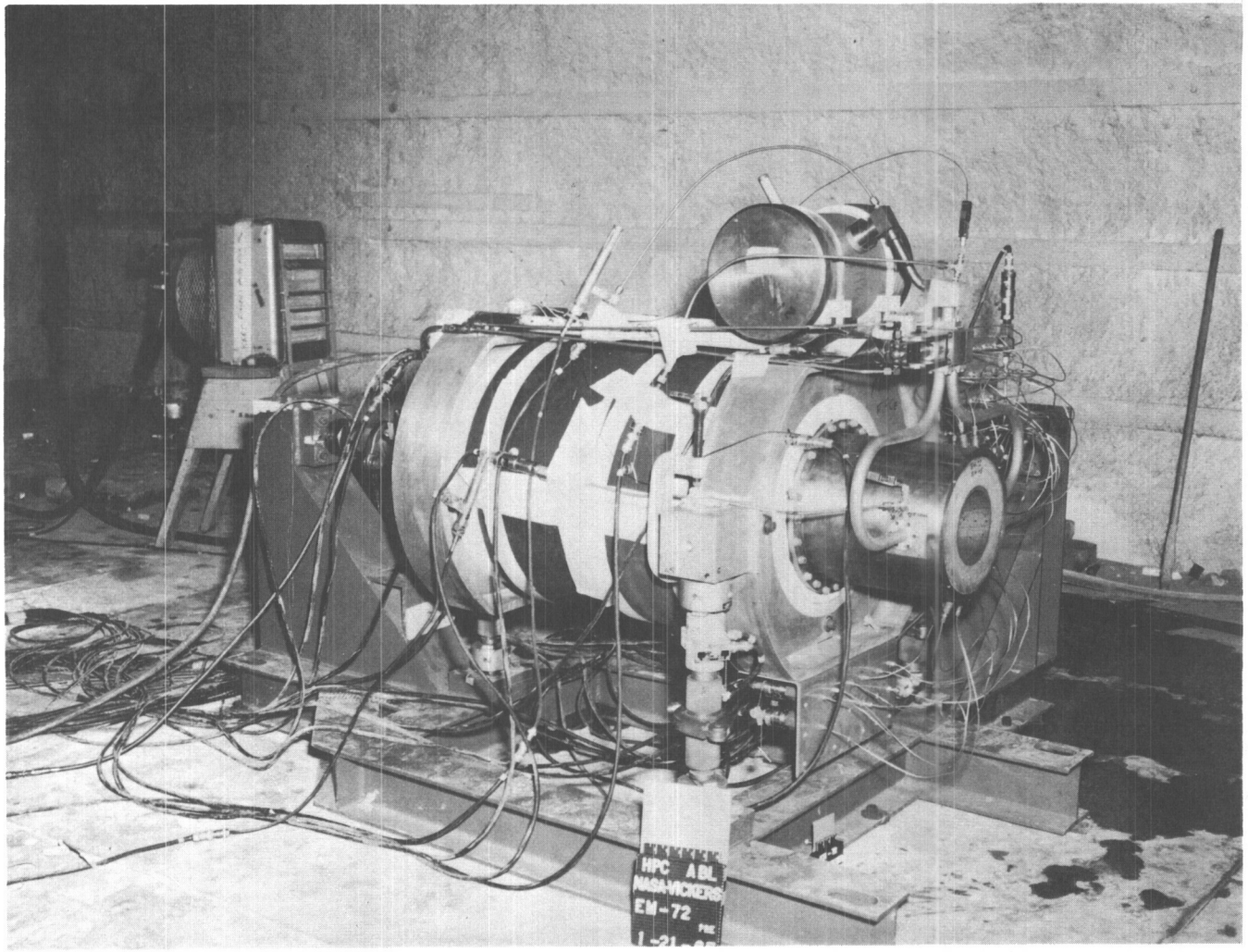

FIGURE - 3.2

VICKERS' SITVC SYSTEM AND EM72 ROCKET MOTOR MOUNTED HORIZONTALLY ON MULTI-COMPONENT TEST STAND

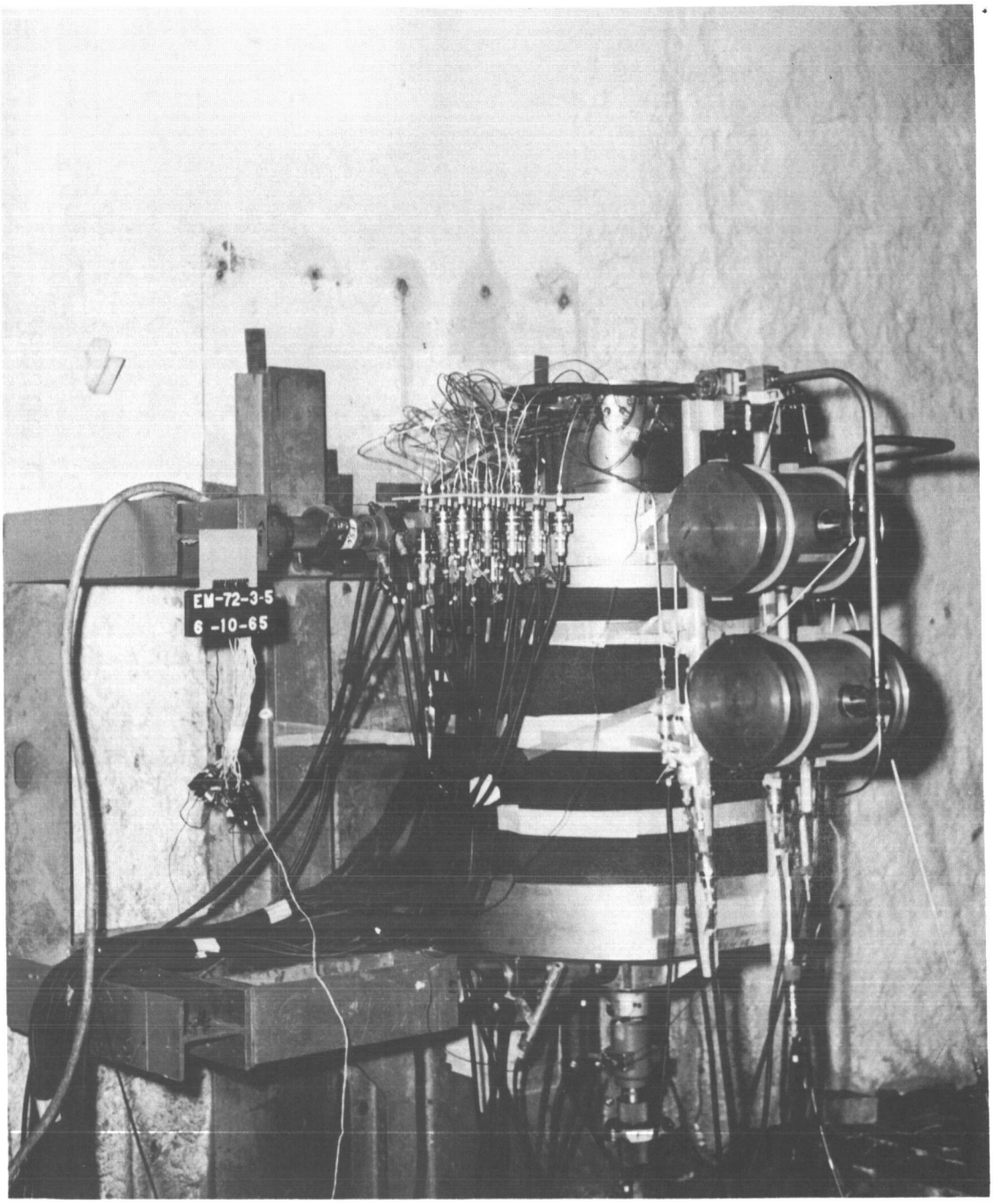

FIGURE - 3.3

TWO VICKERS' SITVC SYSTEMS AND EM72 ROCKET MOTOR MOUNTED VERTICALLY ON MULTI-COMPONENT TEST STAND

	Throat Dia. (In.)	Propellant Weight (lb)	Burning Time (sec)	Average Chamber Pressure (psia)	Average Thrust (lb)	Mass Rate of Discharge (lbm/sec)	Remarks
Contract NOrd 16640 (L-3471)	--	--	30 min.	600	--	11.5 ± .3	Design Goals
Test No. 1	1.955	355	3.960*	714*	--	--	EM-72 Malfunction
Test No. 2	2.065	323	25.650	554	2780	12.6	Successful Firing
Contract NAS 1-3555	--	--	30 min.	550-590	--	12.5-12.6	Contract Requirem't
Test No. 3	2.050	319	25.257	590	2873	12.6	Successful Firing
Test No. 4	2.048	318	9.959*	585*	2603*	--	EM-72 Malfunction
Revised Contract NAS 1-3555	--	--	40 min.	550-590	--	12.5-12.6	Contract Requirem't
Test No. 5	2.051	523	43.622	548	2621	11.9	Successful Firing
Test No. 6	2.052	520	45.458	523	2506	11.4	Successful Firing
Test No. 7	2.047	520	44.804	533	2557	11.6	Successful Firing
Test No. 8	2.046	496	42.905	534	2582	11.5	Successful Firing
Test No. 9	2.079	523	42.316	554	--	12.4	Successful Firing

* These ballistic data were computed for that portion of the firing during which the motor burned neutrally (before malfunctioning).

Table 3.1

Summary of EM-72 Rocket Motor Performance

SECTION 4

INITIAL THEORETICAL ANALYSIS

The design of the secondary injection parameters is based on a theoretical model of the interaction of primary stream boundary layer and the oblique shock induced by the secondary stream. After a review of the literature on the subject, a report by Wu, Chapkis, and Mager was chosen as the basis for initial parameter design[1]. Much of the nomenclature used in that report is retained in the following presentation of the theoretical model.

4.1 Shock Analysis

When the injected gas enters the primary nozzle, the viscous boundary layer separates from the nozzle wall and forces the main flow to proceed along an inclined slope to produce a shock wave. The gas downstream of the shock imposes a large pressure gradient on the boundary layer and distorts it even further. See Figure 4.1. The shock quickly reaches an equilibrium position in which the boundary layer separation angle, δ, the shock angle, θ, and the pressure ratio across the shock must be related to the upstream Mach number, M_o, by gas dynamic

[1] See List of References

relations. Figure 4.2 presents these relations for a specific heat ratio of 1.17. This information was extrapolated from the appendix to Reference 1 and is based on the pressure ratio required across a conical shock to cause the boundary layer to separate [2,3,4]. Figure 4.3 defines some of the system variables. Figure 4.4 provides the primary nozzle area ratio and pressure ratio as a function of Mach number.

With any given set of injection parameters, the shock location may be calculated according to the following procedure:

1) assume an M_o

2) obtain D_o and P_o from Figure 4.4

3) calculate L_s; $L_s = \dfrac{D_e - D_o}{2 \tan \alpha}$

4) obtain δ, θ, $\dfrac{\bar{P}_2}{P_o}$, and $\dfrac{P_s}{P_o}$ from Figure 4.2

5) calculate $\bar{P}_s$; $\bar{P}_s = \dfrac{1}{3} (2 P_s + P_j)$

6) calculate h ; $h = \left\{ \dfrac{.811 (A_{j*} P_{jc} \Gamma)^2}{(\bar{P}_s - P_o)[(\gamma_j+1)P_o + (\gamma_j-1)\bar{P}_s]} \right\}^{\frac{1}{4}}$

where

$$\Gamma = \gamma \left(\frac{2}{\gamma+1}\right)^{\frac{\gamma+1}{2(\gamma-1)}} \quad ; \text{ and for } \gamma_j = 1.3,\ \Gamma = 0.761$$

7) calculate X; $X = h\,[\cot \delta + \tan(\alpha+\varepsilon)]$

8) test for L_s ; $L_s = L_j + X \cos \alpha$

If the L_s obtained in step 8 matches that of step 3, the solution is correct. Otherwise, another M_o must be assumed at step 1; and the process must be repeated until the solution is obtained.

If the injection parameters have not yet been determined, the above procedure may also be used to design the injector nozzles. At step 5, the injector exit pressure P_j is set equal to P_s. Since injector throat area A_{j*} and chamber pressure P_{jc} are designed to suit the secondary system, the other steps remain unchanged. When a $P_j (P_j = P_s = \bar{P}_s)$ is found that gives a correct solution, the injector exit area A_j and Mach number M_j may be determined from isentropic flow relations.

If the secondary flow is variable, it is best to design the injector parameters at a point half way between full flow and no flow conditions. This design setting retains much of the secondary injection efficiency at full flow while assuring

sufficient injection pressure to support the shock with moderate secondary flow rate.

4.2 Side Force Calculations

After the shock location is established for a given flow condition, the side force produced by that flow through an injector nozzle can be calculated directly. The side force has four components:

1. $\left[\left(\frac{\bar{P}_2}{P_o} - 1\right)\left(X^2 \tan\theta - Xh\right)\right] P_o \cos\alpha$ — pressure increase between shock and separated region

2. $\left[\left(\frac{P_s}{P_o} - 1\right)\left(Xh - \frac{A_j}{2}\right)\right] P_o \cos\alpha$ — pressure increase in separated region

3. $(P_j - P_o) A_j \cos\varepsilon$ — pressure difference $P_j - P_o$ acting on injection nozzle area

4. $\frac{\dot{w}_j v_j}{g} \cos\varepsilon$ — momentum effect of injected gas

The full equation for side force from a single injection port is the sum of the above components:

$$F_s = \left[\left(\frac{\bar{P}_2}{P_o} - 1\right)\left(X^2 \tan\theta - Xh\right) + \left(\frac{P_s}{P_o} - 1\right)\left(Xh - \frac{A_j}{2}\right)\right] P_o \cos\alpha + \left[\left(P_j - P_o\right) A_j + \frac{\dot{w}_j v_j}{g}\right] \cos\varepsilon$$

Tests 5 and 6 used supersonic injection at a 20^{o} upstream angle. As an example of shock location and side force calculations, the results of calculations for $\frac{1}{4}$, $\frac{1}{2}$, $\frac{3}{4}$, and full flow conditions for the theoretical model applicable to these two tests are presented in Table 4.1. Curves of theoretical side force per injector versus injector chamber pressure for each test appear in Figure 4.5.

4.3 Thrust Augmentation Analysis

The above analysis may be extended to predict the amount of augmentation of primary thrust and exit pressure produced by secondary injection. Figure 4.6 shows a two-axes secondary injection system. Equal injection flows from the four ports are indicated. It is assumed that the secondary streams do not mix with the primary stream in the short distance between injection port and primary nozzle exit. At the exit plane, however, primary and secondary pressures should be nearly equal ($P_3 = P_4$). Table 4.2 lists the nomenclature used for the following analysis.

The flow equation for the primary stream in terms of exit conditions is

$$\dot{w} = \dot{w}_3 = M_3 A_3 P_3 \sqrt{\frac{\gamma g}{RT_c}\left[1 + \frac{1}{2}(\gamma-1)M_3^2\right]} \qquad (4.1)$$

If the average pressure between the shock apex plane and the exit plane may be approximated by $\frac{1}{3}(P_o + 2P_3)$, then the momentum equation is

$$\frac{1}{3}(P_o+2P_3)(A_3-A_o)+P_oA_o(1+\gamma M_o^2) = P_3A_3(1+\gamma M_3^2) + 4P_s A_4 \qquad (4.2)$$

Rearrange equation 4.2 to get

$$P_3 = \frac{P_oA_o(1+\gamma M_o^2) - 4\bar{P}_s A_4 + \frac{1}{3}P_o(A_3-A_o)}{A_3(1+\gamma M_3^2) - \frac{2}{3}(A_3-A_o)} \qquad (4.3)$$

$$\text{Define } K = [P_oA_o(1+\gamma M_o^2)-4\bar{P}_s A_4 + \frac{1}{3}P_o(A_3-A_o)]\sqrt{\frac{\gamma g}{RT_c}} \qquad (4.4$$

Combining equation 4.1, 4.3, and 4.4 and rearranging:

$$M_3^4\left[\frac{\gamma-1}{2}\frac{K^2}{\dot{w}^2} - \gamma^2\right] + M_3^2\left[\frac{K^2}{\dot{w}^2} - \frac{2\gamma}{3}\left(1+\frac{2A_o}{A^3}\right)\right] - \frac{1}{9}\left[1+\frac{2A_o}{A^3}\right]^2 = 0 \qquad (4.5$$

Equation 4.5 may be solved for M_3 which can be substituted into equation 4.3 to provide P_3.

The flow equation for each secondary stream is

$$\dot{w}_j = A_4 M_4 P_4 \sqrt{\frac{\gamma_j g}{R_j T_{jc}} \left[1 + \frac{\gamma_2 - 1}{2} M_4^2\right]} \qquad (4.6)$$

Assuming P_4 and P_3 are equal and rearranging equation 4.6:

$$M_4^4 \left(\frac{\gamma_j - 1}{2}\right) + M_4^2 - \left(\frac{\dot{w}_j}{A_4 P_3}\right)^2 \frac{R_j T_{jc}}{\gamma_j g} = 0 \qquad (4.7)$$

Solve equation 4.7 for M_4.

then $F_3 = A_3 (M_3^2 \gamma P_3 + P_3 - P_a)$

$F_4 = 4A_4 (M_4^2 \gamma_j P_3 + P_3 - P_a)$

$F = F_3 + F_4$ where F is the augmented thrust

This analysis may be applied to the two-axes system used in Test 6. For P_c = 550 psia and $\dot{w}$ = 11.5 lb/sec., the calculated values at null flow ($\dot{w}_j$ = 0.31) appearing in Table 4.1 produce these results:

K = 30.4 lbm/sec

M_3 = 2.62

P_3 = 13.4 psia

M_4 = 2.21

F_3 = 2590 lb.

F_4 = 180 lb.

F = 2770 lb.

Calculations for primary flow without secondary injection show 10.0 psia exit pressure and 2750 lb. thrust. The pressure increase is naturally expected because of the increase in flow. Thrust augmentation occurs when the positive effects of flow addition and exit pressure increase are greater than the effect of the disturbances in the primary nozzle. The theoretical calculations indicate an increase in thrust of 20 lbs. or 0.7% for this system.

4.4 Alternate Approaches to Secondary Injection Analysis

In Section 9 of this report, experimental results are compared with the theoretical calculations. During the testing period, comparisons between test data and other types of secondary injection analysis were made. Some results with respect to the blast wave analogy technique can be found in Section 10. The available literature did not provide any approach that showed acceptable quantitative correlation with all aspects of the data. For this reason, no detailed summaries are included in this report. A review of the literature in this area may be found in reference 5.

Calculated Injector Parameters	
A_{j*} = 0.1124 sq. in. A_j = 0.1386 sq. in. v_j = 3440 fps	$\frac{P_j}{P_{jc}}$ = 0.261 M_j = 1.556

P_{jc} (psia)	150	300	450	600
$\dot{w}_j$ (lb/sec)	0.155	0.31	0.465	0.62
M_o	2.60	2.54	2.50	2.47
D_o (in)	4.16	3.99	3.88	3.80
P_o (psia)	24.0	27.1	29.3	31.1
L_s (in)	3.06	3.38	3.59	3.73
δ (deg)	24.4	24.3	24.2	24.2
θ (deg)	35.0	35.4	35.7	35.9
$\bar{P}_2/P_o$	2.77	2.69	2.69	2.60
P_s/P_o	3.00	2.92	2.86	2.82
$\bar{P}_s$ (psia)	61.0	78.4	94.4	109.8
h (in)	0.468	0.585	0.658	0.708
X (in)	1.357	1.702	1.921	2.07
Force component #1 (lb)	27	47	64	79
Force component #2 (lb)	26	47	63	76
Force component #3 (lb)	2	6	11	16
Force component #4 (lb)	16	31	47	62
F_s (lb)	71	131	185	233

Table 4.1 Results of Theoretical Shock and Side Force Calculations for System Used in Tests 5 and 6

A_3	area of zone 3 = $A_e - 4A_4$	(sq. in)
F_3	axial thrust contribution of primary stream	(lb.)
M_3	primary stream Mach number at exit plane	
P_3	primary stream pressure at exit plane	(psia)
A_4	area of each zone $\simeq \frac{1}{2} \pi h^2$	(sq. in)
F_4	total axial thrust contribution of secondary streams	(lb.)
M_4	secondary stream Mach number at exit plane	
P_4	secondary stream pressure at exit plane	(psia)
K	defined by equation 4.4	(lbm/sec)
F	axial thrust of system	

Table 4.2 Additional Nomenclature Used for Thrust Augmentation Analysis

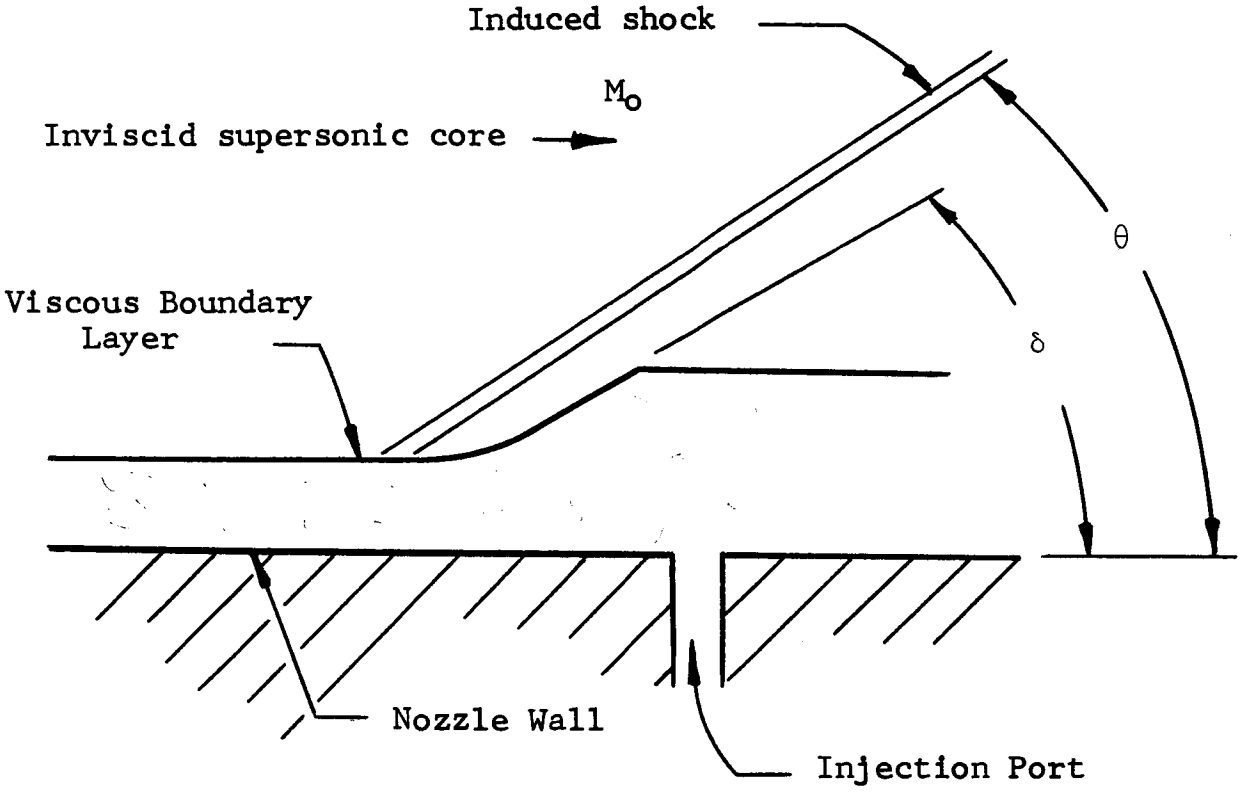

Figure 4.1 Formation of Shock Due to Separation of Boundary Layer

Figure 4.2

Shock Angle, Separation Angle and

Pressure Ratios vs Primary Mach No.

at Shock Apex

$\gamma = 1.17$

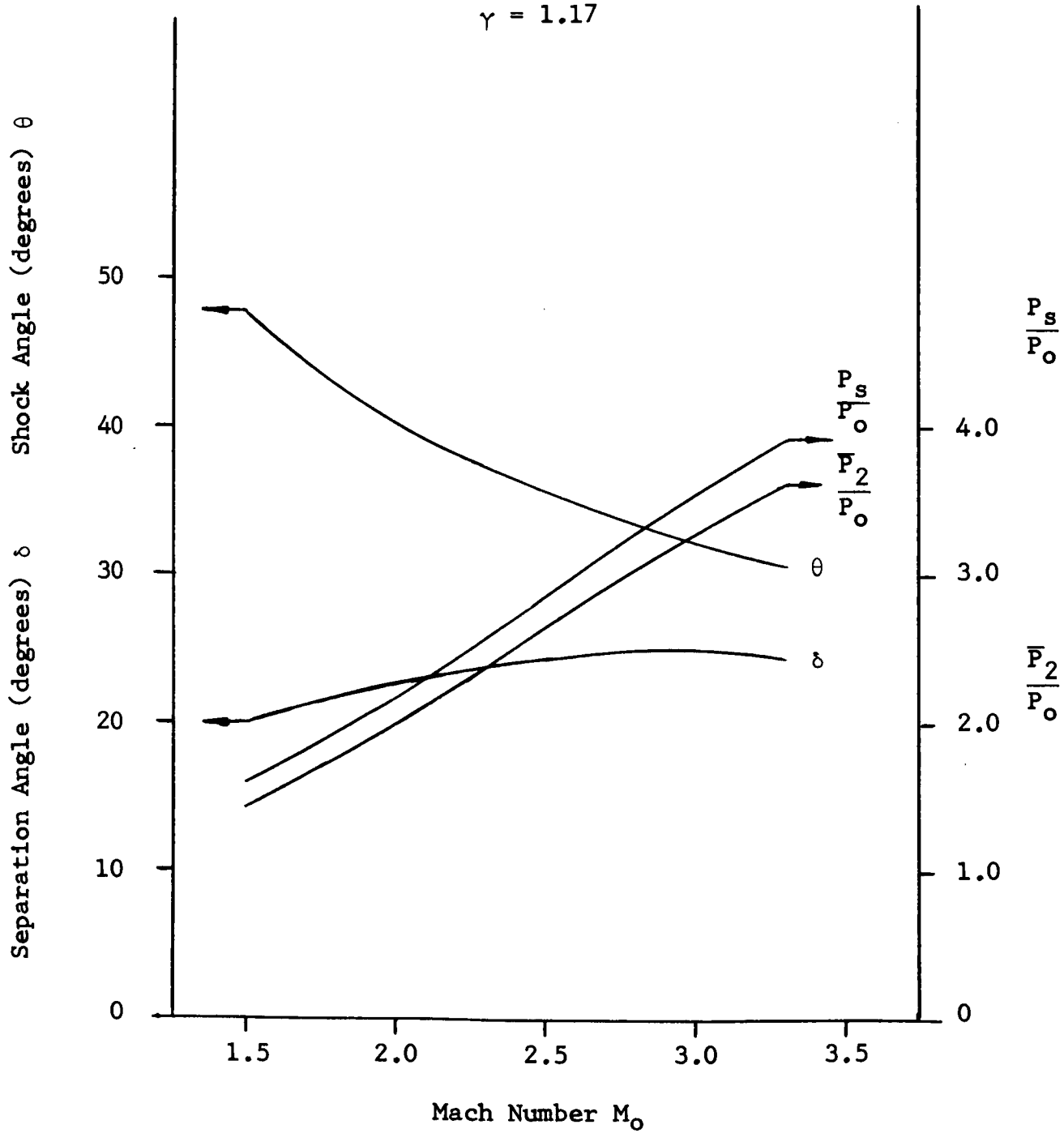

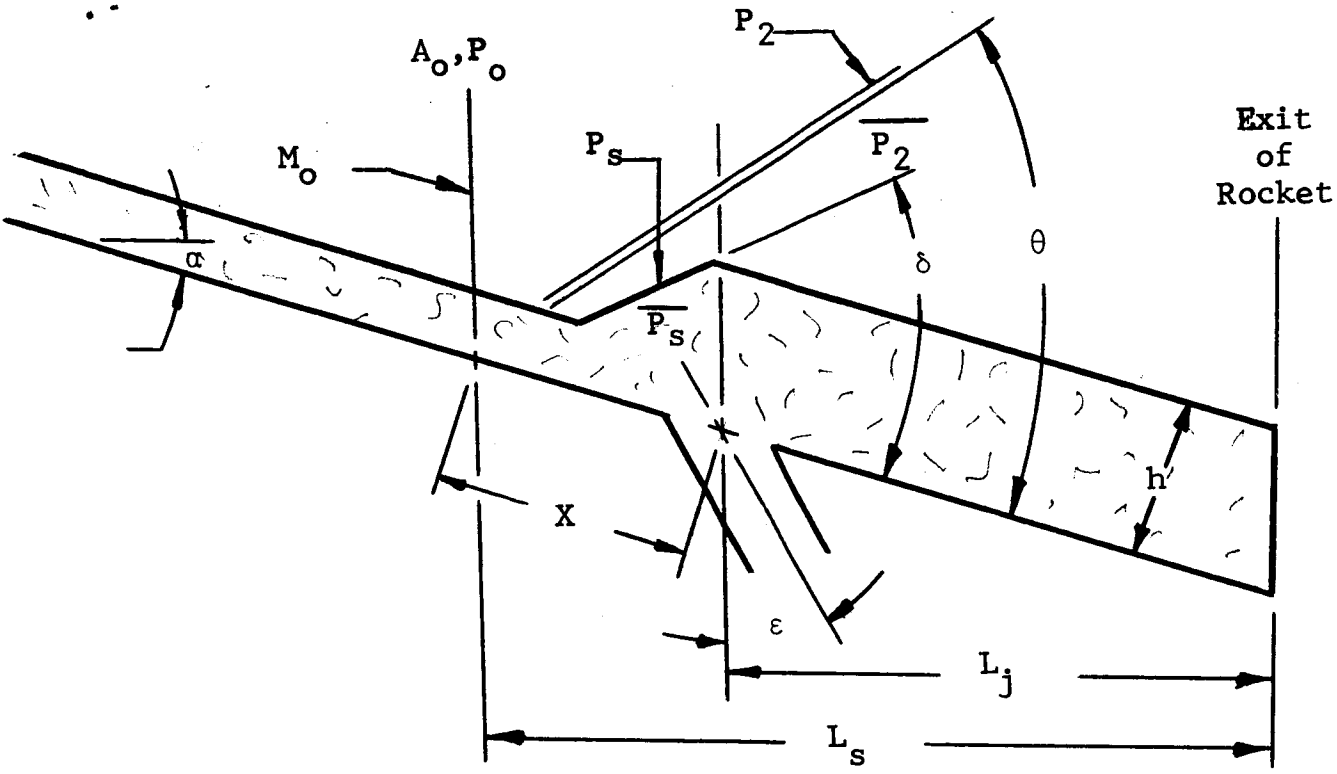

P_o	Primary Stream Pressure at Shock Apex
P_2	Pressure Along Shock
$\overline{P_2}$	Average Pressure in Shock Region
P_s	Pressure on the Separated Boundary Layer
$\overline{P_s}$	Average Pressure in Separated Region
h	Accomodation Height
L_j	Distance Between Injection Point and Exit
L_s	Distance Between Shock Apex and Exit
X	Distance Between Shock Apex and Injection Point
ε	Injection Angle
α	Nozzle Half-Angle

Figure 4.3 System Parameters and Variables

Figure 4.4

Area Ratio, Pressure Ratio

vs

Primary Mach Number

$\gamma = 1.17$

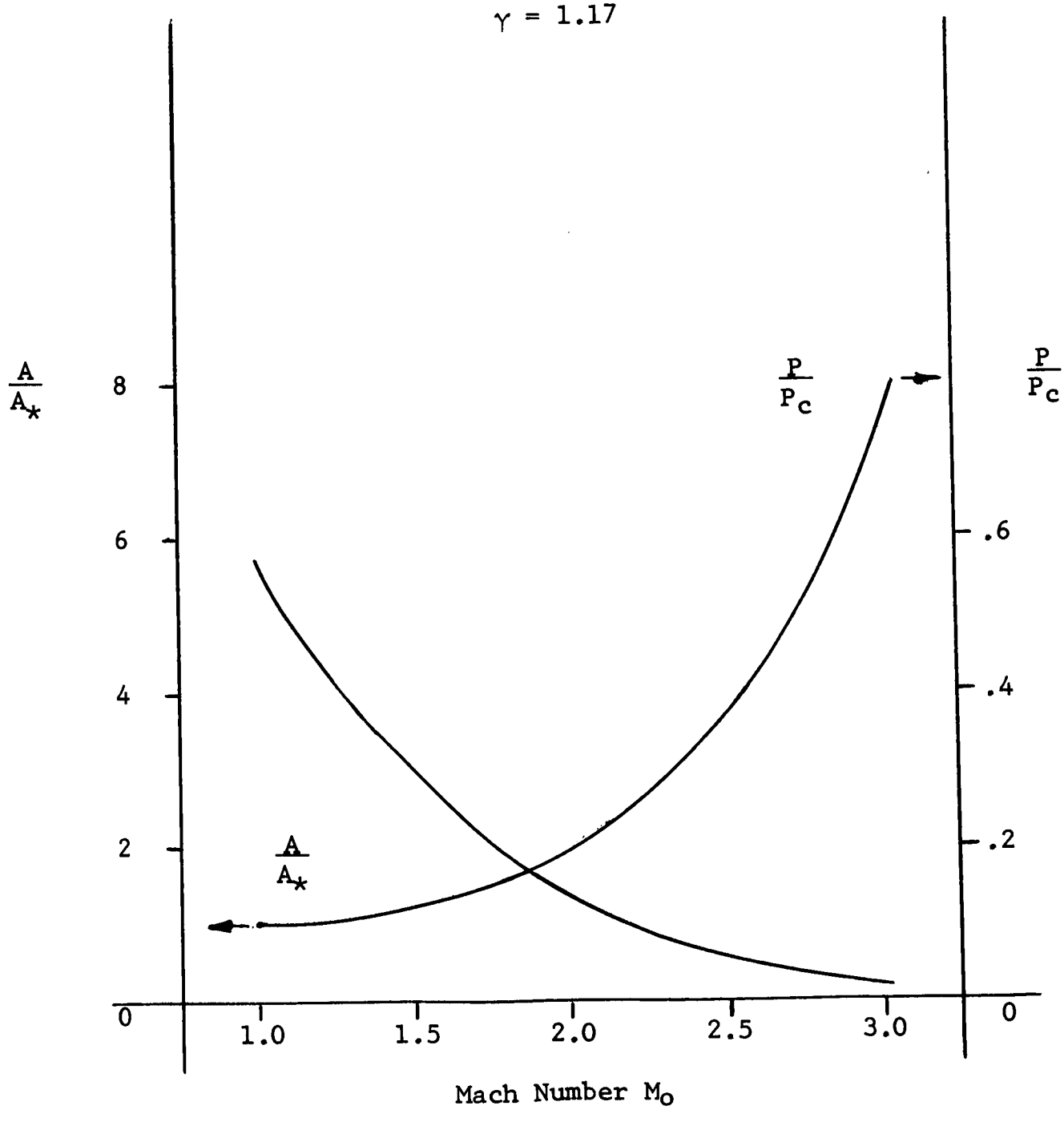

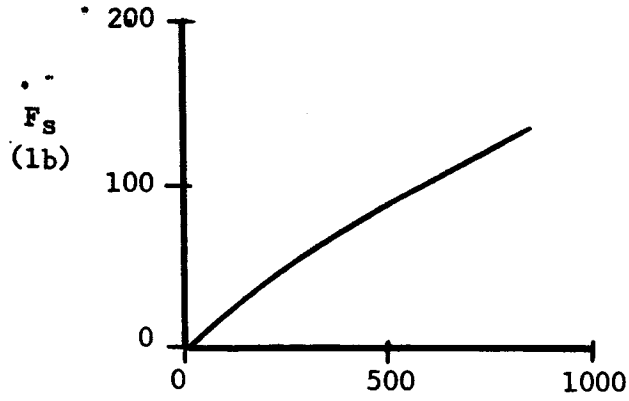

Test 1
Sonic Injection
$\varepsilon = 0 \quad \frac{X}{L} = 75\%$

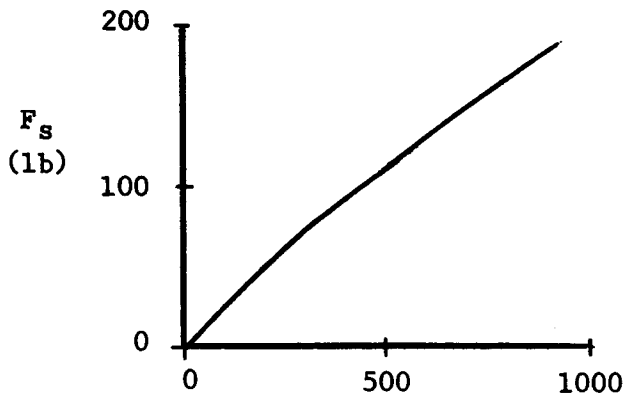

Test 2
Supersonic Injection
$\varepsilon = 0 \quad \frac{X}{L} = 75\%$

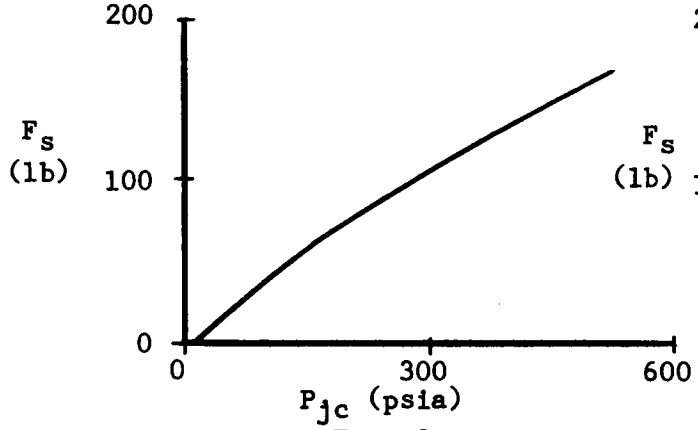

Test 3
Sonic Injection
$\varepsilon = 0 \quad \frac{X}{L} = 75\%$

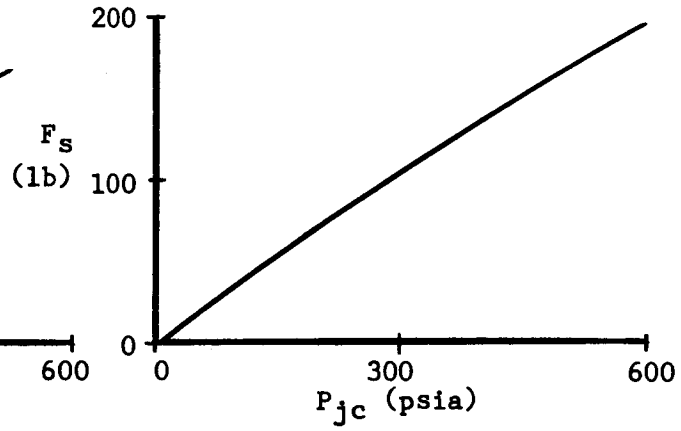

Test 4
Supersonic Injection
$\varepsilon = 0 \quad \frac{X}{L} = 60\%$

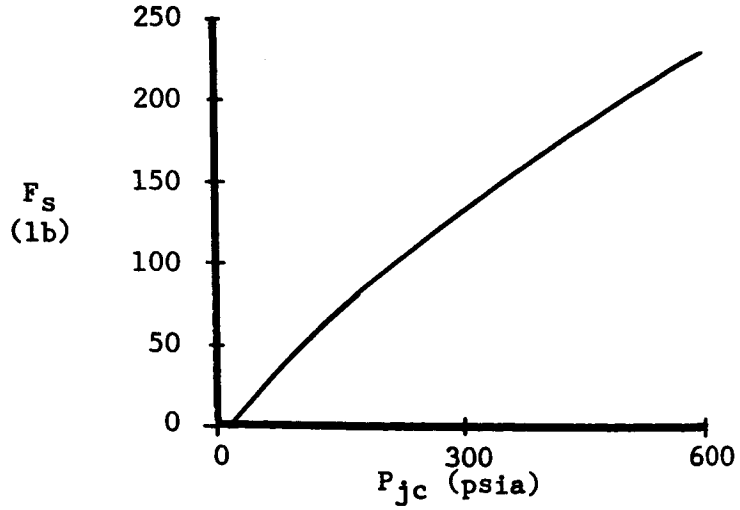

Tests 5 & 6 Supersonic Injection
$\varepsilon = 0 \quad \frac{X}{L} = 75\%$

Figure 4.5

Theoretical Side Force Per Injector Versus Injector Chamber Pressure

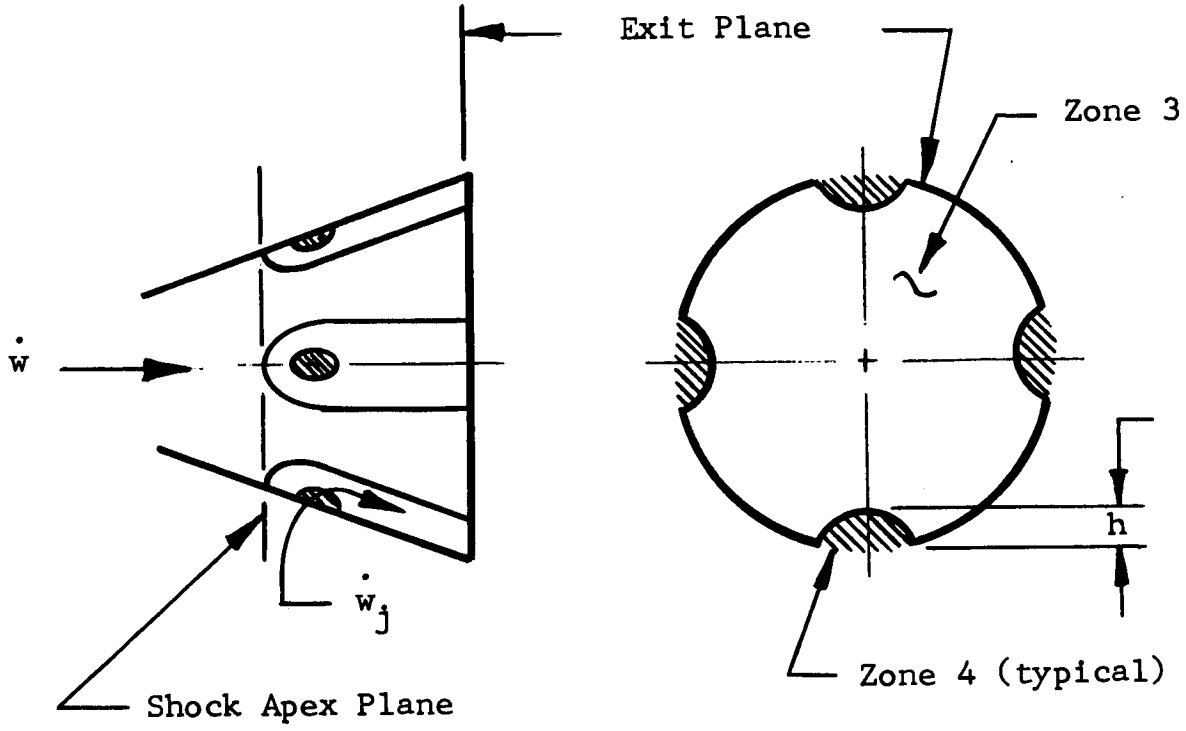

Figure 4.6 Two-Axes Secondary Injection System

SECTION 5

INSTRUMENTATION AND DATA ACQUISITION SYSTEM (DAS)

5.1 Data Acquisition System

5.1.1 Digital

At the start of the test program the DAS capabilities of the Allegany Ballistics Laboratory (ABL) consisted of the following:

1. 30 high speed channels
   - nominal 300 samples per second.
2. 28 low speed channels
   - nominal 30 samples per second.
3. 30 thermocouple channels
   - 2 samples per second.

Later in the program an additional 50 channels capable of 400 sps acquisition rate were added. The input to these channels could not be filtered, and more important the information recorded could not be automatically cross plotted with data from 1 and 2 above. At this stage in the program it was decided not to increase the amount of data to be recorded but to use the additional 40 channels as back up.

An example of the allocation of the various parameters to the DAS is shown in Appendix 1, along with the required output information. The output information was presented in both digital print outs of the DAS information from the magnetic tape storage and as time plots made with an automatic plotter using the stored data. The analytical shock display was made as a digital print out with the pressures at the nozzle pressure taps in their correct relative location with respect to the injector port. This method of presentation allowed for a rapid analysis of the shock location.

5.1.2 Analogue

In addition to the use of the digital system all parameters were also recorded on FM and on Visicorder traces. This gave complete back up of recording in case of failure of any system. The Visicorder traces were run at 4 inches per second. They are useful in obtaining an overall view of the test, for determining which parts of the test require more detailed analysis by use of the digital system, and for direct analysis in the case of the investigation of the system dynamic response.

The FM tapes can be played back onto a Visicorder readout when required. The recording speed of the Visicorder tape can be varied depending upon the type of data being analyzed. This is particularly useful for dynamic analysis since speeds of 20 inches per second or higher can be used for the analysis of step response and phase angle shift of sinusoidal inputs.

5.2 Input Signal Preparation

The required input program for each test was prepared by Vickers Incorporated and transmitted to the Allegany Ballistics Laboratory. There the program was transferred to magnetic tape as a frequency modulated signal.

During system operation the frequency modulated tape output was converted to a voltage level by a discriminator unit. A bias of 12 volts was used to maintain a null level in the circuit, the discriminator output modulating this null level in a positive or negative sense in response to an increase or decrease in signal frequency from the null frequency value.

The input programs used in the six test firings are shown in Section 6.

5.3 Camera Coverage

All tests were thoroughly documented by still and motion pictures.

Still shots were taken from all angles prior to and after completion of the test firing.

Movie films were taken at both fast speed (400 fps) and slow speed (64 fps) from at least three locations for each test.

SECTION 6

TEST PROGRAM

The basic contract and its amendment 1 called for six TVC firings to be performed by Vickers Incorporated at the Allegany Ballistics Laboratory facility. Table 6.1 lists these firings with their proposed objectives.

As the development of the secondary injection system and the EM72 motor progressed it was necessary to modify the objectives of some of the tests to obtain the most useful information and still stay within the limit of six engine TVC firings. As a result of this, it was not possible to investigate the effect of injecting the secondary flow at an angle of 20° downstream. Table 6.2 contains a list of the tests that were performed and a summary of the major parameters for each test firing.

The following sections discuss in detail the individual tests and any modifications made between tests.

6.1 Test 1 - January 23, 1964

This was the first test of the TVC system installed on the EM72 motor. The high temperature pneumatic valve was directly driven

by an electrical torque motor. The electronic amplifier for driving the valve and the magnetic tape input program were provided by Vickers.

The equipment was installed on the motor which was mounted on the Ormond 2 component test stand as shown in Figure 6.1.

During the system "dry run" which provides the final checkout of the valve input program and the data acquisition system, some problems occurred in the automatic input program circuit. This necessitated using a manual input set-up in which the input steps were fed in by manual operation of a stepping switch and the sine wave input was taken from a frequency generator. In the automatic system the complete program is put on magnetic tape as a frequency modulated signal, which is converted to a voltage level by the discriminator; this voltage is fed into the electronic amplifier and then into the torque motor.

The input program that was actually used for this test is shown in Figure 6.2.

6.1.1 After about 10 seconds of operation the igniter wires on the secondary injection system solid propellant gas generator blew

out. A subsequent investigation indicated that this was caused by using too high a voltage level for the ignition system. For the next test the voltage was decreased to 28 volts and the circuit was opened 4 seconds after ignition. The blow out of the igniter caused the gas pressure to drop to about 1000 psi, with a resultant decrease in gas flow.

6.1.2 In addition, the pressure differentials developed between the secondary injection nozzles were much lower than anticipated; this resulted in maximum side force levels only one third of the maximum desired. A study of the test data from both this TVC test and from prior cold testing with high pressure N_2 gas showed that the valve operating forces were substantially different when using hot gas. It was decided that the secondary injection system should undergo some additional hot testing at Vickers prior to the next TVC engine firing to resolve this problem. Subsequently, two additional tests were performed. While some improvement was achieved, it was felt that a more positive method of driving the valve was necessary, one that would not require a delicate valve set-up procedure.

6.1.3 A small hydraulic actuator was designed and manufactured

to drive the valve. This actuator mounts on the end of the pneumatic valve and incorporates a miniature Vickers hydraulic valve, operating in a closed loop circuit with a position feedback transducer. This system was successfully tested in a hot firing at Vickers and was used for the second test at Allegany Ballistics Laboratory.

6.2 Test 2 - April 29, 1964

The system installation for the second TVC engine firing is shown in Figure 6.3

The electronic driving equipment for the valve input was again provided by Vickers Incorporated. The input program is shown in Figure 6.4.

The test set-up and system dry run proceeded normally.

The motor and gas generators ignited as planned, however, after 10½ seconds the EM72 motor failed, destroying the motor and the two component thrust stand.

6.2.1 Subsequent examination of the test data and components indicated that the inhibitor at the forward end of the propellant grain failed causing an increase in the burning surface area.

The motor thrust increased from 2600 to 3700 pounds during the first 10 seconds of operation, the chamber pressure then exceeded the burst level of the motor case.

6.2.2 The secondary nozzle pressures followed the input program closely for the first 9 seconds. At this time the program called for a null valve position. The nozzle pressures did not return to null but were biased in a direction corresponding to a valve spool poppet bias away from the hydraulic actuator connection. An examination of the trace of feedback voltage made during the test showed that the electrical characteristics of the feedback transducer had not changed.

The feedback transducer for the closed loop hydraulic actuation system is driven from a yoke attached to each end of the valve spool. The transducer is physically located over the center of the high temperature valve in the same plane as the metering poppet. As the spool expands during firing the poppet moves away from the point of connection of the valve spool and the hydraulic actuator. To maintain the valve null position, the feedback transducer must be moved by the yoke the same distance as the spool poppet. A series of bench tests were conducted at

Vickers on the yoke and spool assembly and it was found that the relative movement between the poppet and transducer is dependent on the method of fixing the yoke to the spool. With the assembly that was used during the second TVC test the transducer moved .0025 inches when the poppet moved .010 inches, that is a ratio of 4:1 instead of the required 1:1. New attaching methods were investigated and a new technique was developed that allowed equal movement of the transducer and poppet as the spool expanded.

6.2.3 To overcome the problem of inhibiting the EM72 grain, NASA and Allegany Ballistics Laboratory decided to load the motor with a full length grain, hence removing the inert plug from the head end. This would increase the burning time from 26 to 42 seconds. A successful verification firing of the EM72 motor was carried out at Allegany Ballistics Laboratory on September 17, 1964, and the motor was then prepared for the next TVC firing.

6.2.4 The two component thrust stand was destroyed when the EM72 motor failed, so all future tests were conducted using the six component stand. At this stage in the program the new stand

had been completed and shipped to NASA Langley Research Center for preliminary calibration checks prior to the next TVC firing.

6.2.5 In preparation for the next TVC firing using sonic injection, a review of published experimental data on sonic injection was conducted. This data (Reference 5) showed an increase in side force with a decrease in secondary injection chamber pressure for the same injected mass flow rate. The relationship of chamber pressure to side force for sonic and supersonic injection for our system was then investigated using the analysis and calculation procedure detailed in Section 4 of this report. The results indicated that the side force for sonic injection increased with decreasing injection nozzle chamber pressure.

The possibility of adapting the system hardware to sonic injection at a lower pressure was then investigated. A nominal chamber pressure of 250 psia at null flow was selected, and the valve inlet pressure was reduced to 1000 psi. The required increase in valve metering area was obtained by increasing the valve total stroke from .030 to .060 inches. A load orifice was installed in the generator outlet flange to maintain the gas flow at

.62 pound/second at 2700 psi for a nominal 50 seconds burning time.

6.2.6 On the first two TVC tests the gas manifold pipe between the generator and the control valve was 42 inches long. For the third TVC test this was reduced to 7 inches by moving the gas generator over the aft mounting ring of the motor. This was done to accelerate the gas temperature rise at the injection nozzles, by reducing both the mass of the system and the radiating surface area.

6.2.7 A successful verification firing of the reduced pressure secondary injection system with the shortened gas manifold was carried out at Vickers on October 8, 1964. The gas generator pressure held between 2700 and 2625 psi for the 49 second propellant burning time. The thermocouple recordings showed that the shortened manifold had the desired effect of reducing the temperature rise time at both the valve inlet and secondary injection nozzle chambers.

6.3 Test 3 - November 3, 1964

The TVC system and the EM72 motor were mounted on the six component thrust stand as shown in Figure 6.5. For this test the

electronic equipment for signal amplification, feedback power and circuit summing was provided by Allegany Ballistics Laboratory. In addition, the input program (Figure 6.6) provided by Vickers, was put on tape and played back by Allegany Ballistics Laboratory.

The valve actuation was checked and the system dry run was successfully carried out. During the continuity check on the TVC system gas generator igniter, an open circuit condition was noted. A test range operator was sent to investigate and found that the gas generator had fired prematurely. This aborted the scheduled test and the equipment was disassembled and an investigation into the cause of the premature ignition was initiated. No positive conclusions were arrived at to explain the reason for the ignition of the gas generator. Approximately 25 igniters similar to the one used were checked to ensure that their pin-to-case resistance was greater than two megohms at 500 VDC. The Range Firing Procedure for checking and connecting the igniter circuits was revised to eliminate any possible chance for inadvertant firing of the gas generator in the future.

6.3.1 Test 3 - Repeat - December 2, 1964

The system was set-up to repeat the aborted test of November 3, 1964.

The system dry run was performed and the TVC firing carried through to a successful conclusion.

6.4 Test 4 - January 21, 1965

The TVC system and EM72 motor were mounted on the six component thrust stand as shown in Figure 6.7.

The system dry run was carried out and the installation prepared for the TVC firing.

A successful engine firing was performed without incident using the input program of Figure 6.8.

6.5 Test 5 - March 10, 1965

Figure 6.9 shows the system installation for Test Number 5.

The dry run and TVC firing were carried out using the input program shown in Figure 6.10.

6.5.1 A small crack developed in the valve center section during the firing. This caused an estimated 10 percent loss in mass flow to the secondary injection nozzles. There was no indication on the test traces of exactly when this occurred. As a result of the leakage the valve feedback transducer was burnt

out approximately 40 seconds after motor ignition, that is 2 seconds before motor burn out.

A metallurgical analysis of the part gave no indication of the cause of the failure.

6.5.2 To reduce the possibility of this reoccurring all similar parts for future tests were thoroughly re-examined for surface cracks, and stress relieved to remove any residual internal machining stresses.

6.5.3 The failure was of a minor nature and 90 percent of the test objectives were met.

6.6 Test 6 - June 10, 1965

This was the last test of the series and featured secondary injection and control in two mutually perpendicular planes. The system installation is shown in Figure 6.11. The input programs are shown in Figure 6.12 on the same time scale. These programs were sequenced to investigate the interaction effect between the flows from adjacent secondary injection nozzles.

The TVC system firing was very successful. Both of the secondary injection systems and the EM72 motor performed perfectly.

Table 6.1

Test Program - Contract Requirements
NAS 1-2962 Amendment 1

Test No.	Secondary Injection System Characteristics			General Remarks
	Nozzle Axial Location % Throat to Exit Plane of Rocket Motor Nozzle	Injection Angle	Injection Type	
1	75	Perpendicular to motor axis	Sonic	Single axis injection and control
2	75	Perpendicular to motor axis	Super-sonic	Single axis injection and control
3	Moved towards nozzle throat from 75% plane	Perpendicular to motor axis	Sonic or Super-sonic	Single axis injection and control. Type of injection to be determined from results of Tests 1 and 2
4	Best location determined from Tests 1, 2, and 3	20° Downstream	Sonic or Super-sonic	Single axis injection and control; type of injection determined from Tests 1, 2, and 3
5	Best location determined from Tests 1, 2, and 3	15° Downstream	Sonic or Super-sonic	Single axis injection and control; type of injection determined from Tests 1, 2, and 3
6	Best location determined from Tests 1, 2, and 3	Best angle as determined from Tests 1 thru 5	Sonic or Super-sonic	2 axis injection and control; type of injection determined from Tests 1 thru 5

Table 6.2

Summary of TVC Static Tests

Test No.	Rocket Motor Characteristics					Secondary Injection System Characteristics									Remarks
						Injection Nozzle Description					Gas Generator Ballistic Data			Injection Nozzles Ballistic Data		
	Mass Flow	Average Thrust	Average Chamber Pressure P_c	Specific Impulse $P_c \rightarrow 14.7$ psia	Burning Time	Type	Axial * Location	Injection* Angle	Throat Area	Exit Area	Average Pressure	Mass Flow	Total Gas Temp.	Maximum Chamber Pressure	Gas Total Temp.	
	lb/sec	lbsf	psia	secs	secs		X/L	ε	in^2	in^2	psia	lb/sec	°F	psia	°F	
1	12.6	2873	590	228	25.26	sonic	0.75	0	.0738	.0738	2300	.608	1620	519	1630	Single axis injection and control; gas generator igniter housing failed at 10 secs.
2	13.2	2820	645	214	9.96	super-sonic	0.75	0	.0674	.1024	2690	.615	1380	857	1560	Single axis injection and control; EM72 motor malfunction at 10 secs.
3	11.4	2506	523	220	45.46	sonic	0.75	0	.1353	.1353	2650	.606	2000	510	1885	Single axis injection and control; successful firing
4	11.6	2557	533	222	44.80	super-sonic	0.60	0	.1124	.1261	2670	.617	2015	575	1915	Single axis injection and control; successful firing
5	11.5	2582	534	224	42.91	super-sonic	0.75	20° upstream	.1128	.1385	2700	.619	--	544	1915	Single axis injection and control; successful firing
6	12.4	2770	554	223	42.32	super-sonic	0.75	20° upstream	.1128	.1385	2600	.625	1980	572	1880	Yaw axis } Two axes injection and control; successful firing
						super-sonic	0.75	20° upstream	.1128	.1385	2610	.625	1960	590	1860	Pitch Axis }

* X/L Ratio of the distance from the plane of the motor nozzle throat to the plane of the injection port to the distance from the plane of the throat to the nozzle exit plane.

Angle between a perpendicular to the centerline of the motor nozzle and the centerline of the injection nozzle.

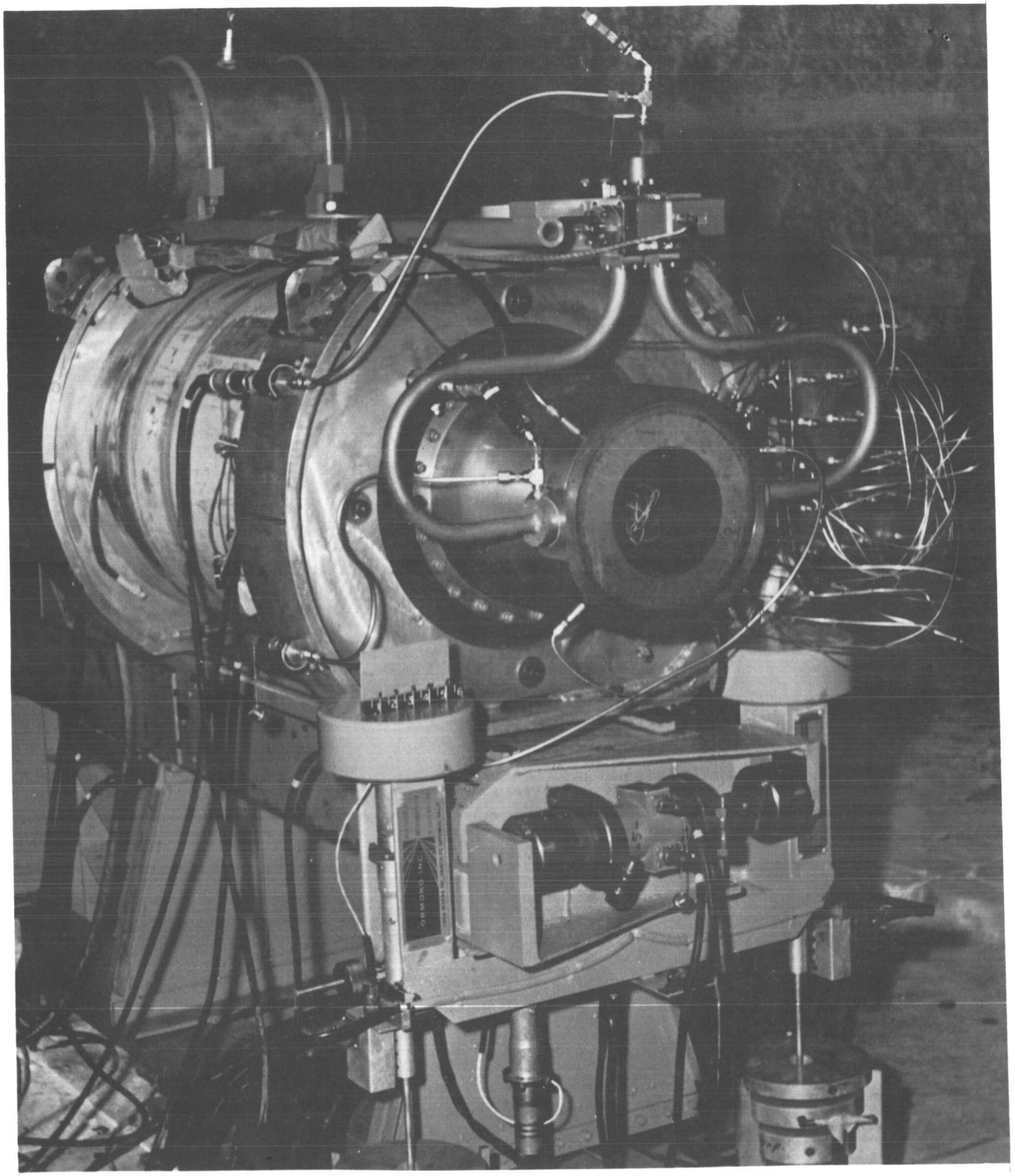

FIGURE - 6.1

SYSTEM INSTALLATION FOR TEST NO. 1

Figure 6.2

TVC Input Program Test No. 1

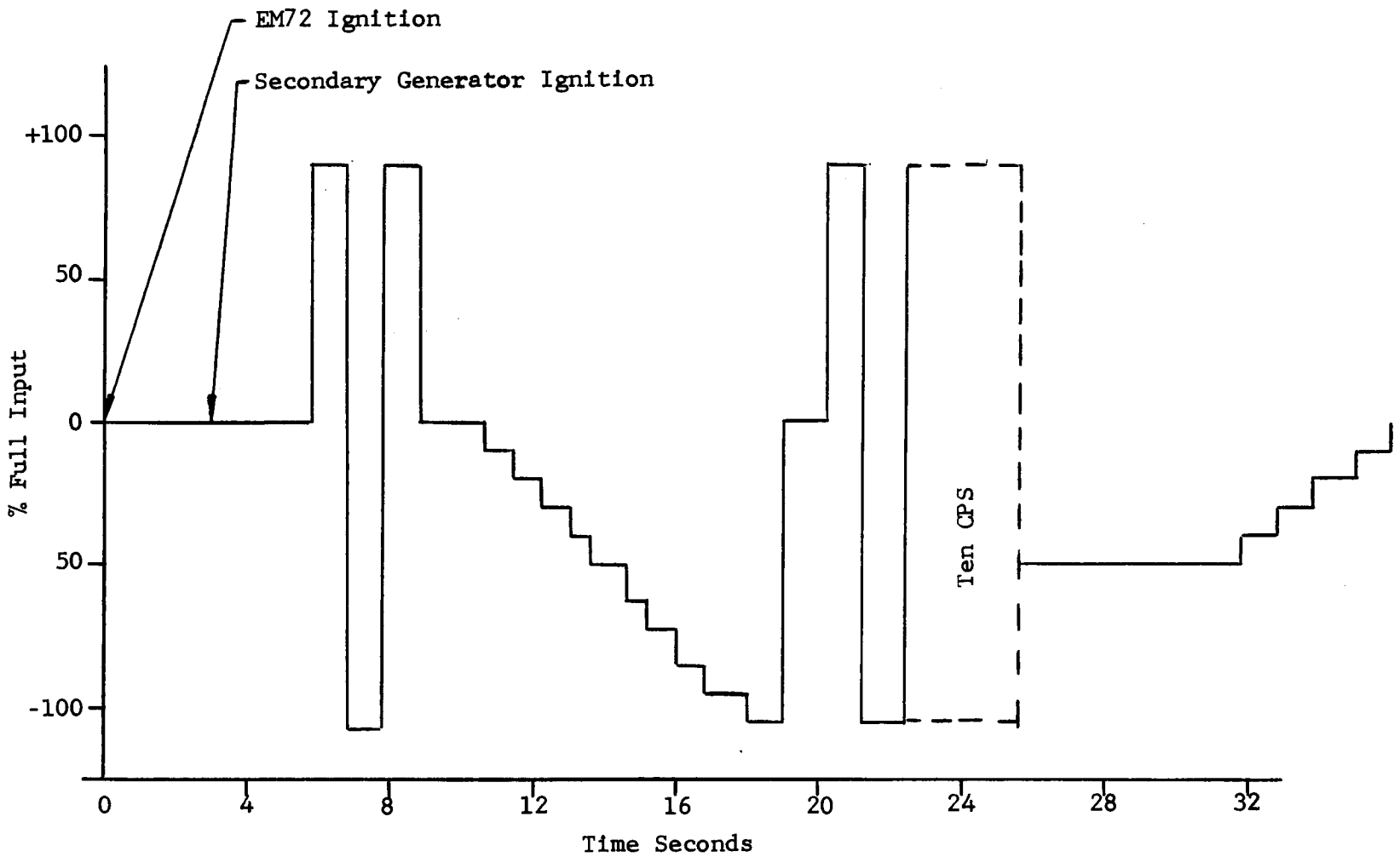

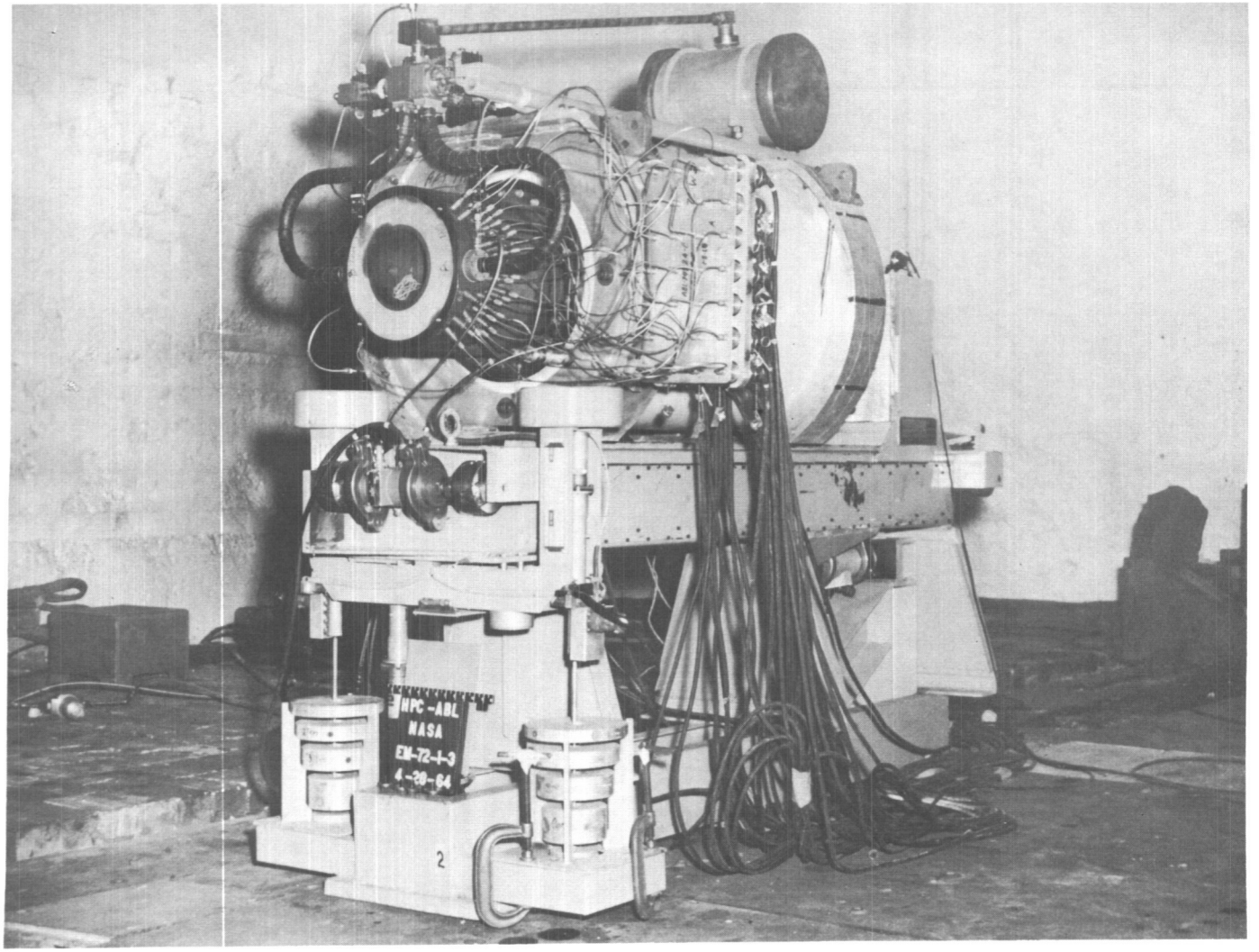

FIGURE - 6.3

SYSTEM INSTALLATION FOR TEST NO. 2

Figure 6.4

TVC Input Program Test No. 2

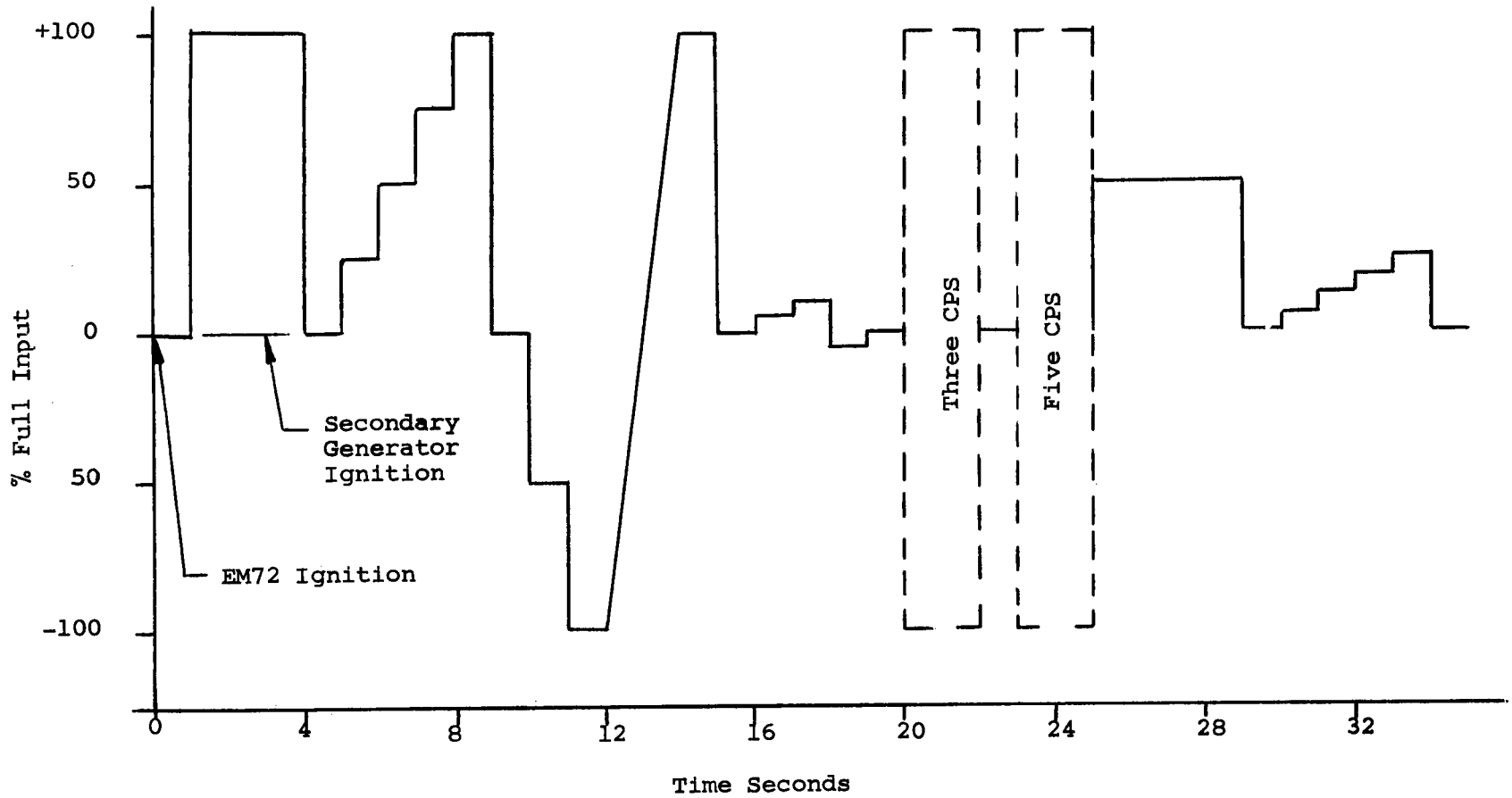

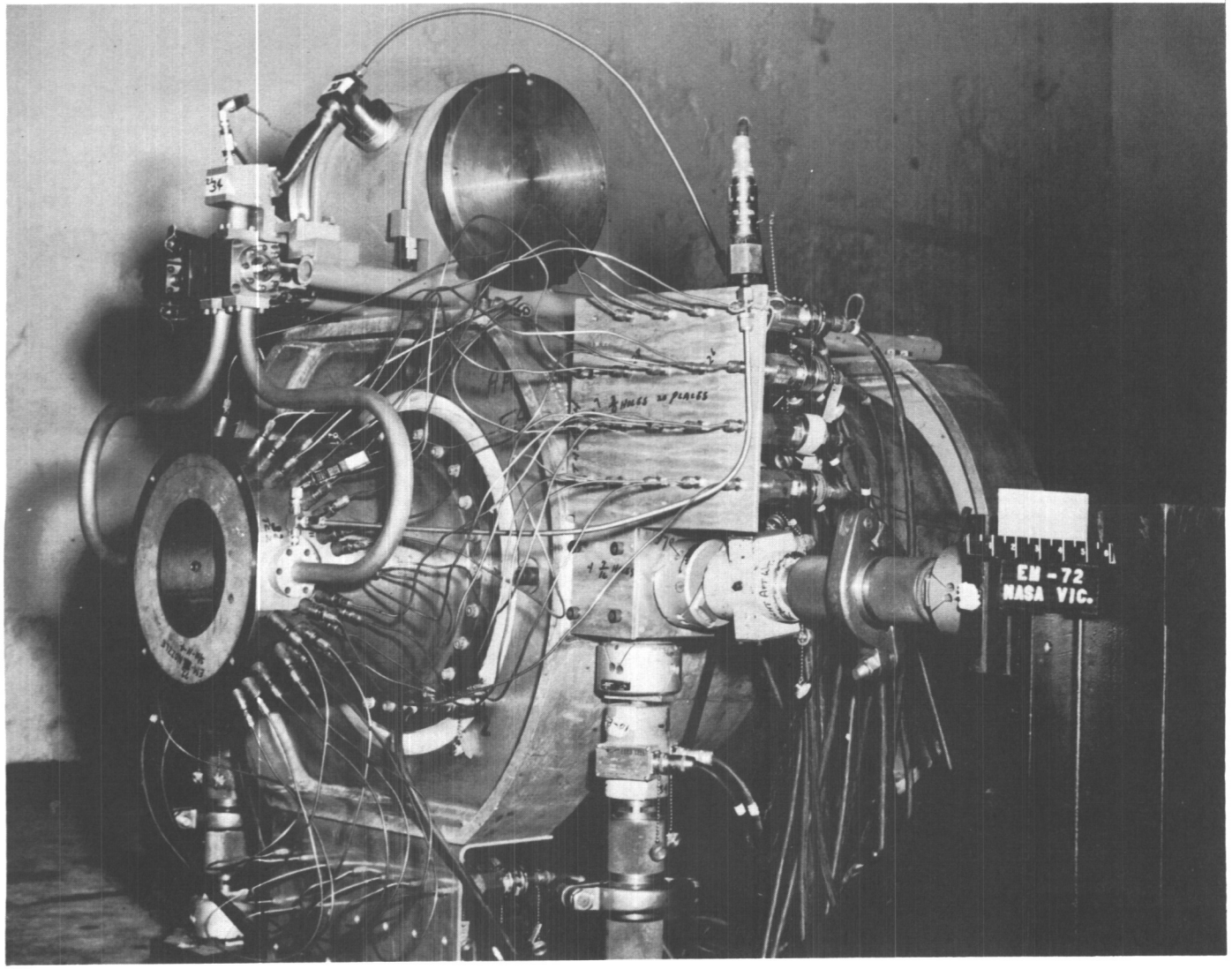

FIGURE - 6.5

SYSTEM INSTALLATION FOR TEST NO. 3

Figure 6.6

TVC Input Program Test No. 3

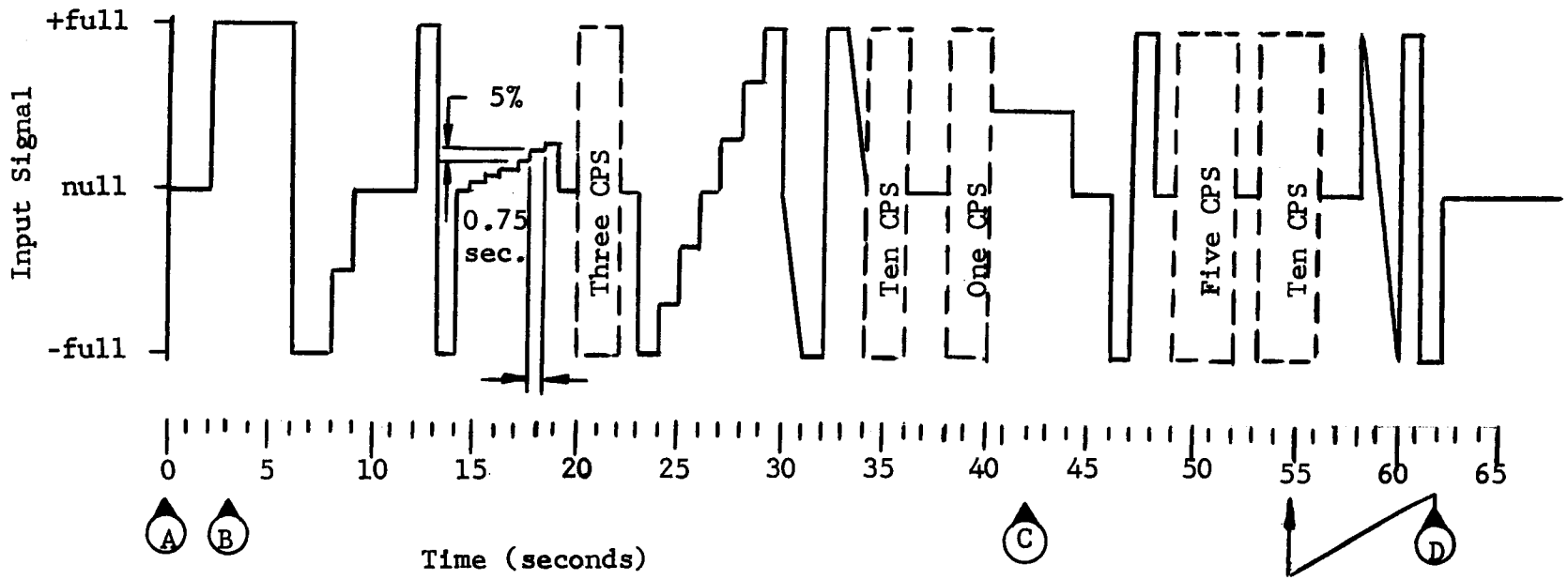

Events:
- (A) Motor ignition
- (B) Generator ignition
- (C) Motor cut-off
- (D) Generator cut-off

Note: Positive input signal indicates greater secondary flow on instrumented side of primary nozzle.

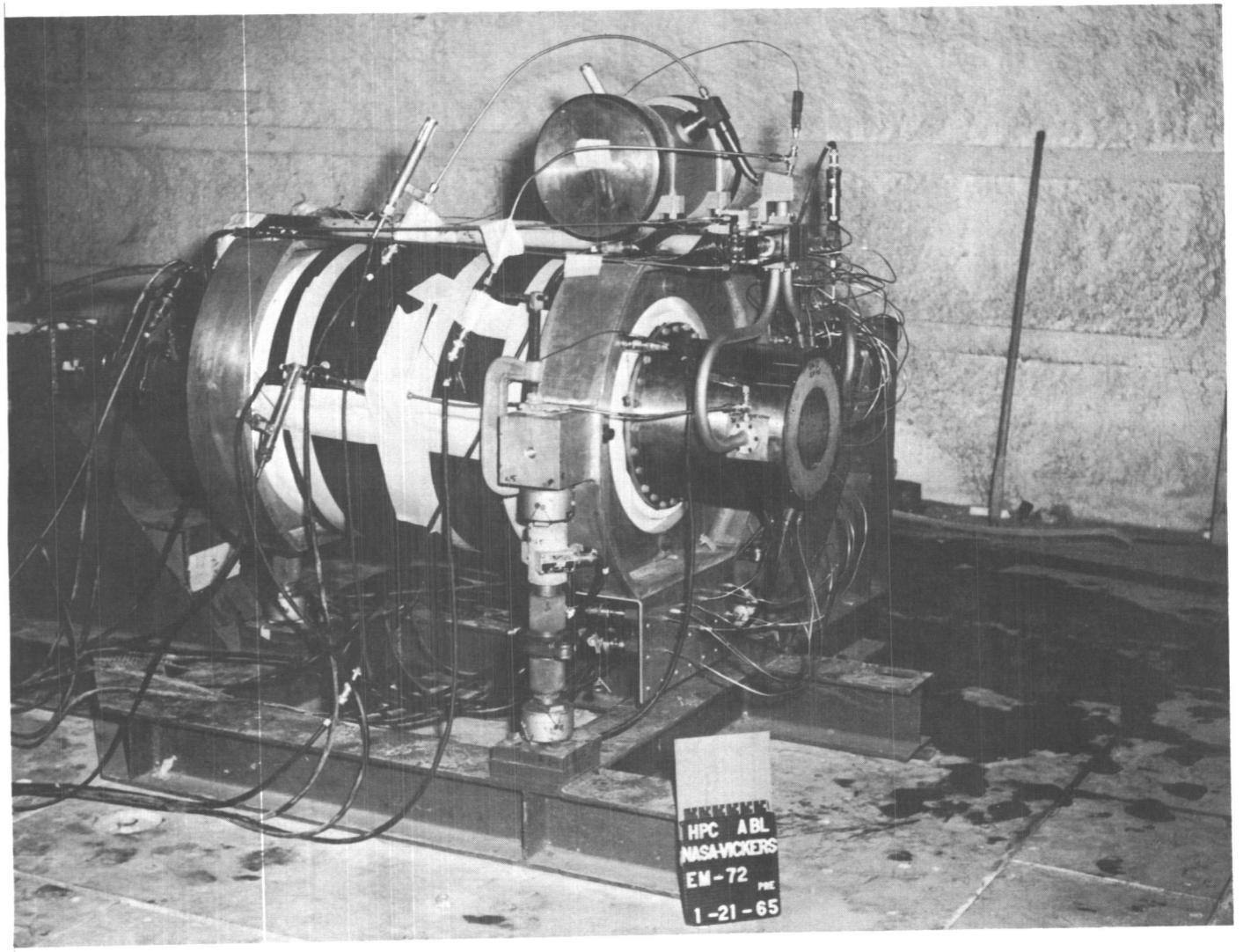

FIGURE - 6.7

SYSTEM INSTALLATION FOR TEST NO. 4

Figure 6.8

TVC Input Program Test No. 4

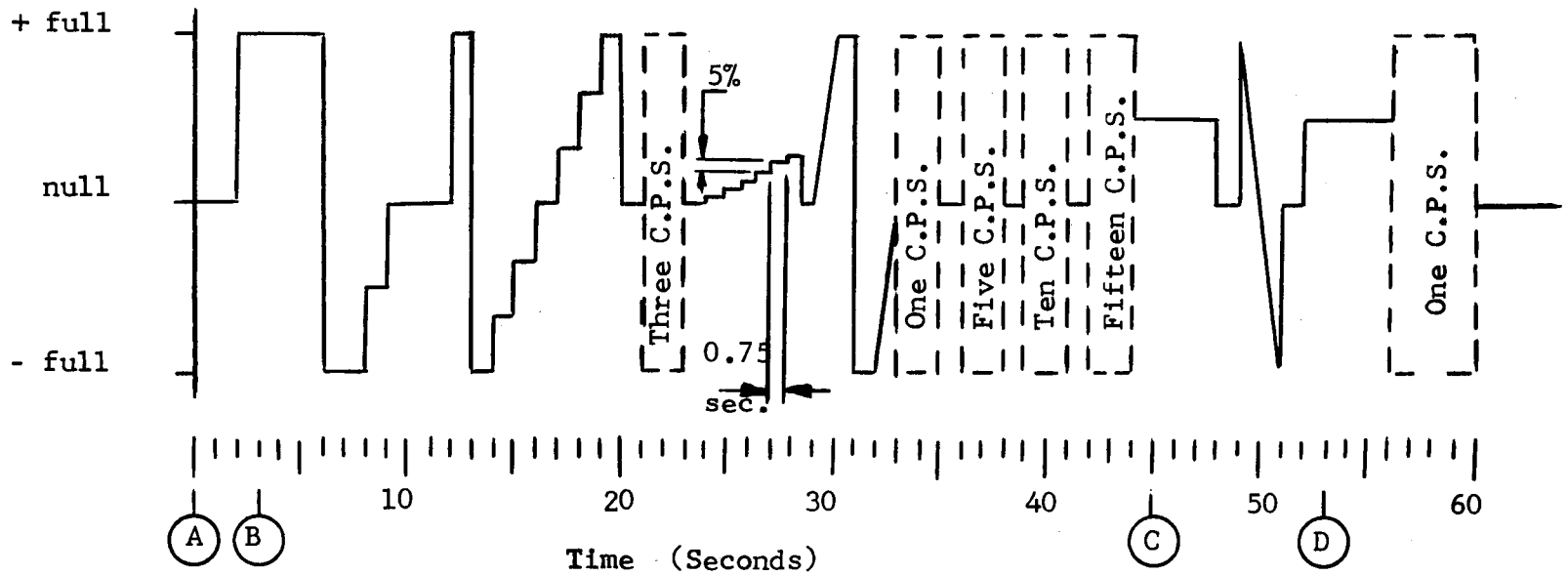

Events:

- (A) Motor Ignition
- (B) Generator Ignition
- (C) Motor Cut-Off
- (D) Generator Cut-Off

Note: Positive input signal indicates greater secondary flow on instrumented side of primary nozzle.

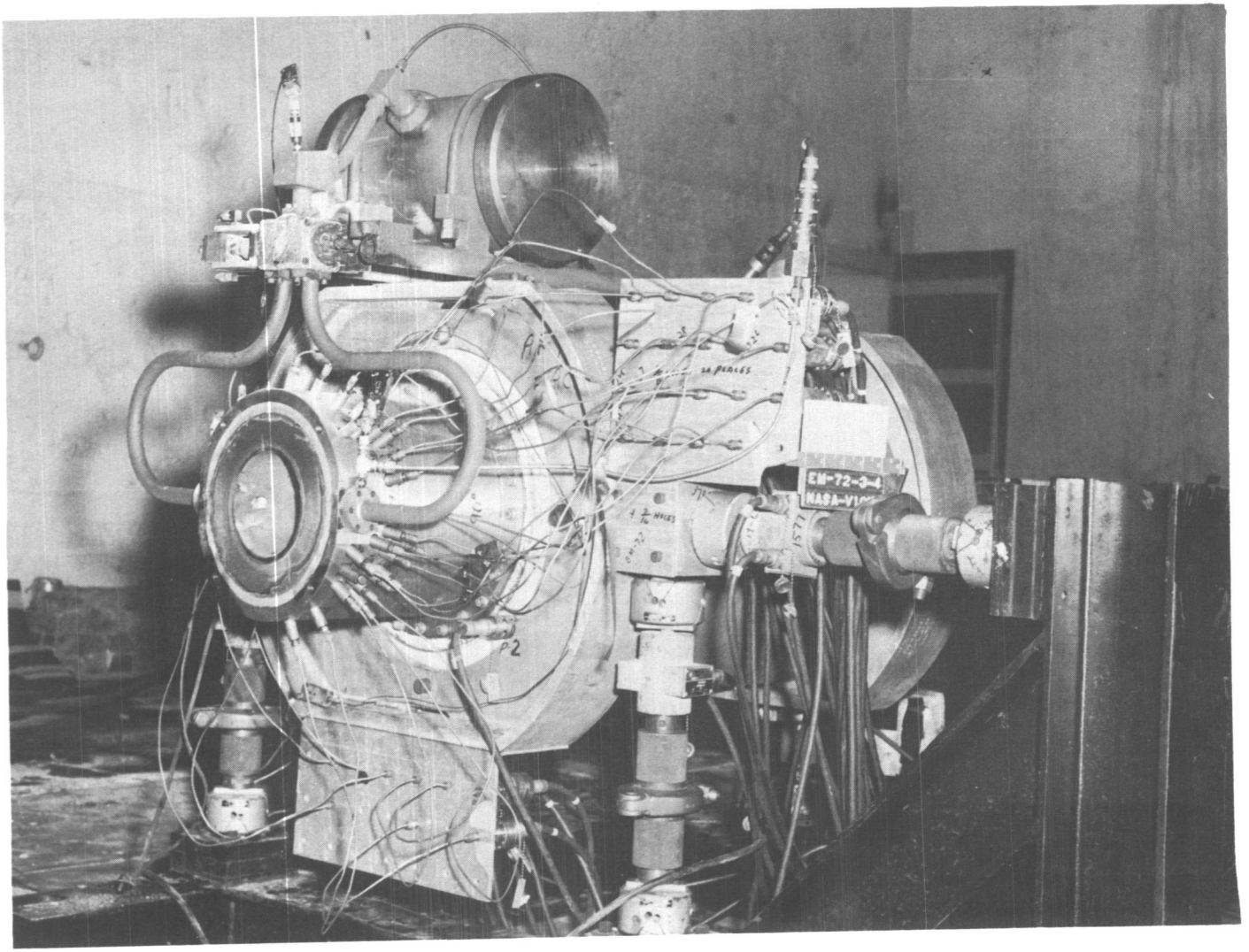

FIGURE - 6.9

SYSTEM INSTALLATION FOR TEST NO. 5

Figure 6.10

TVC Input Program Test No. 5

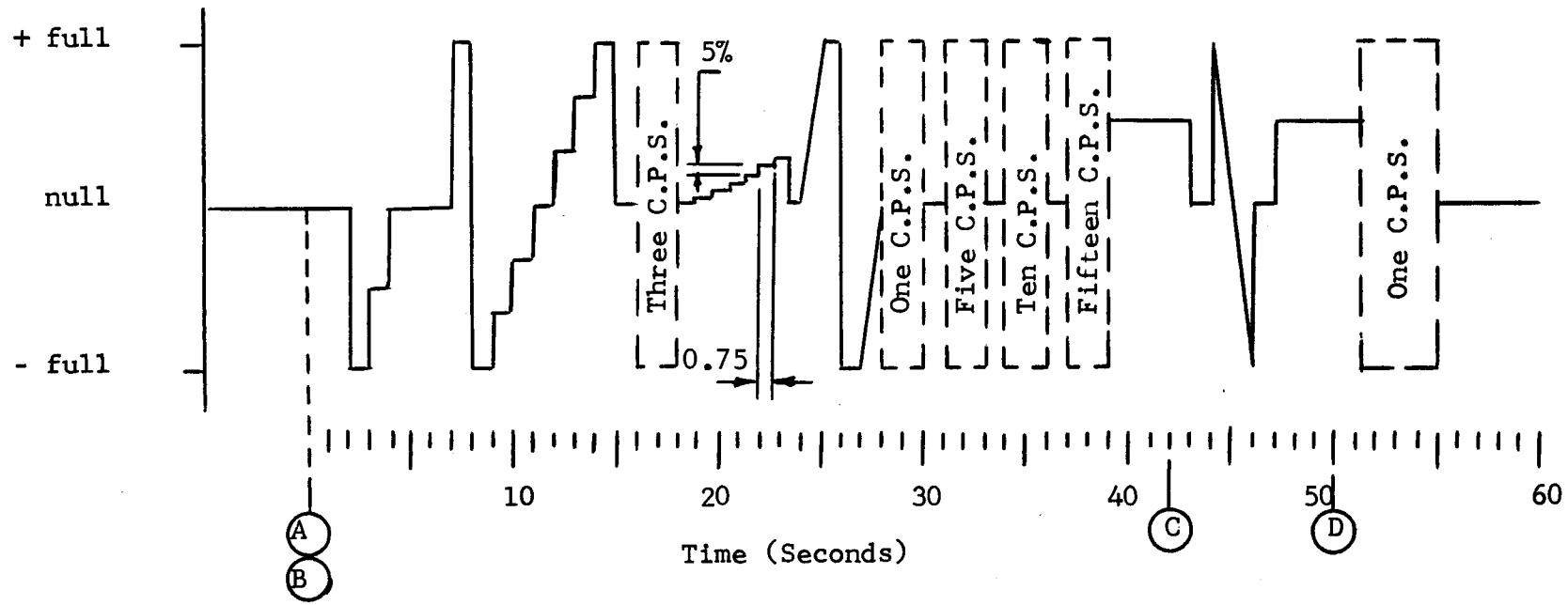

Events:
- (A) Motor Ignition
- (B) Generator Ignition
- (C) Motor Cut-Off
- (D) Generator Cut-Off

Note: Positive input signal indicates greater secondary flow on instrumented side of primary nozzle.

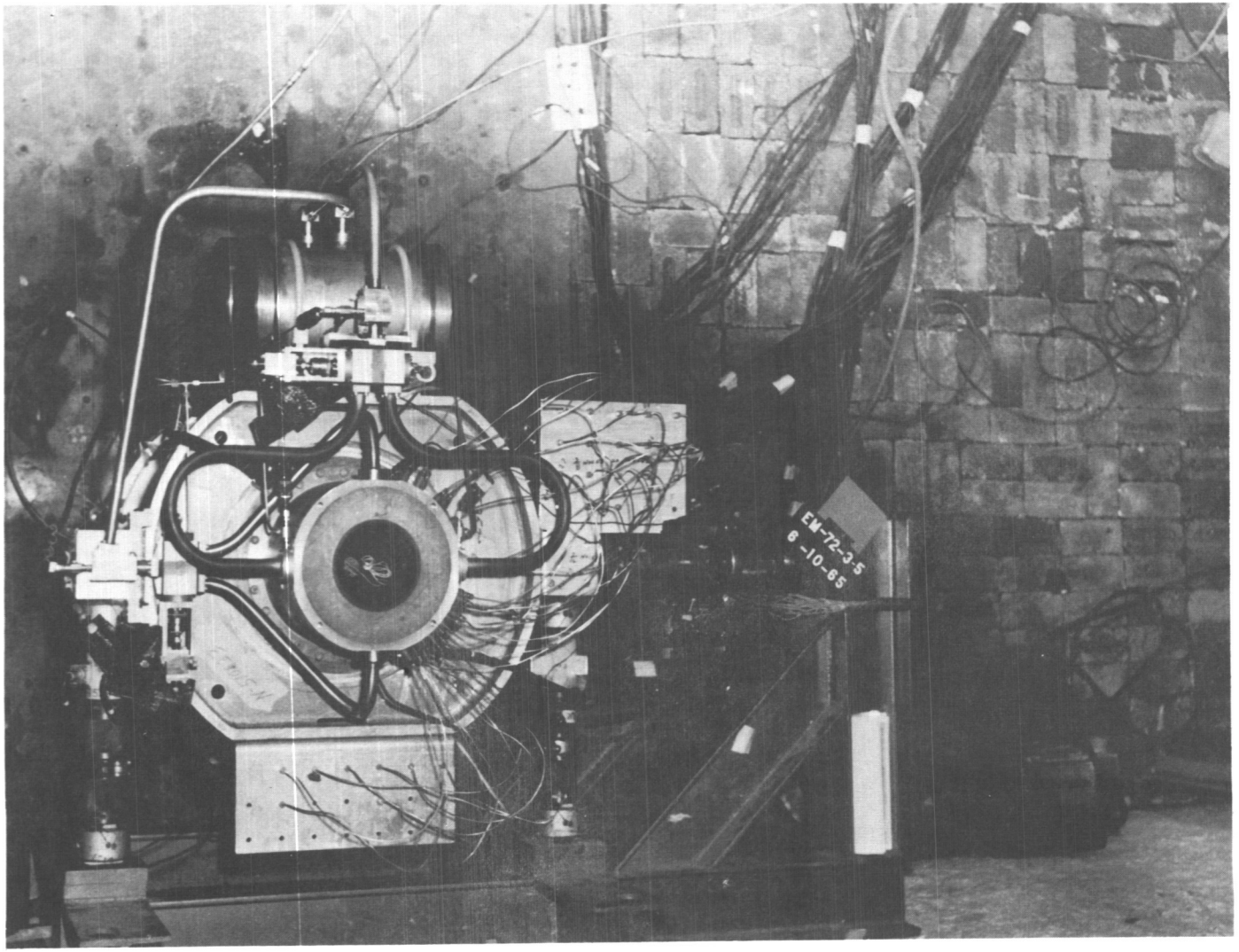

FIGURE - 6.11

SYSTEM INSTALLATION FOR TEST NO. 6

Figure 6.12

TVC Input Program Test No. 6

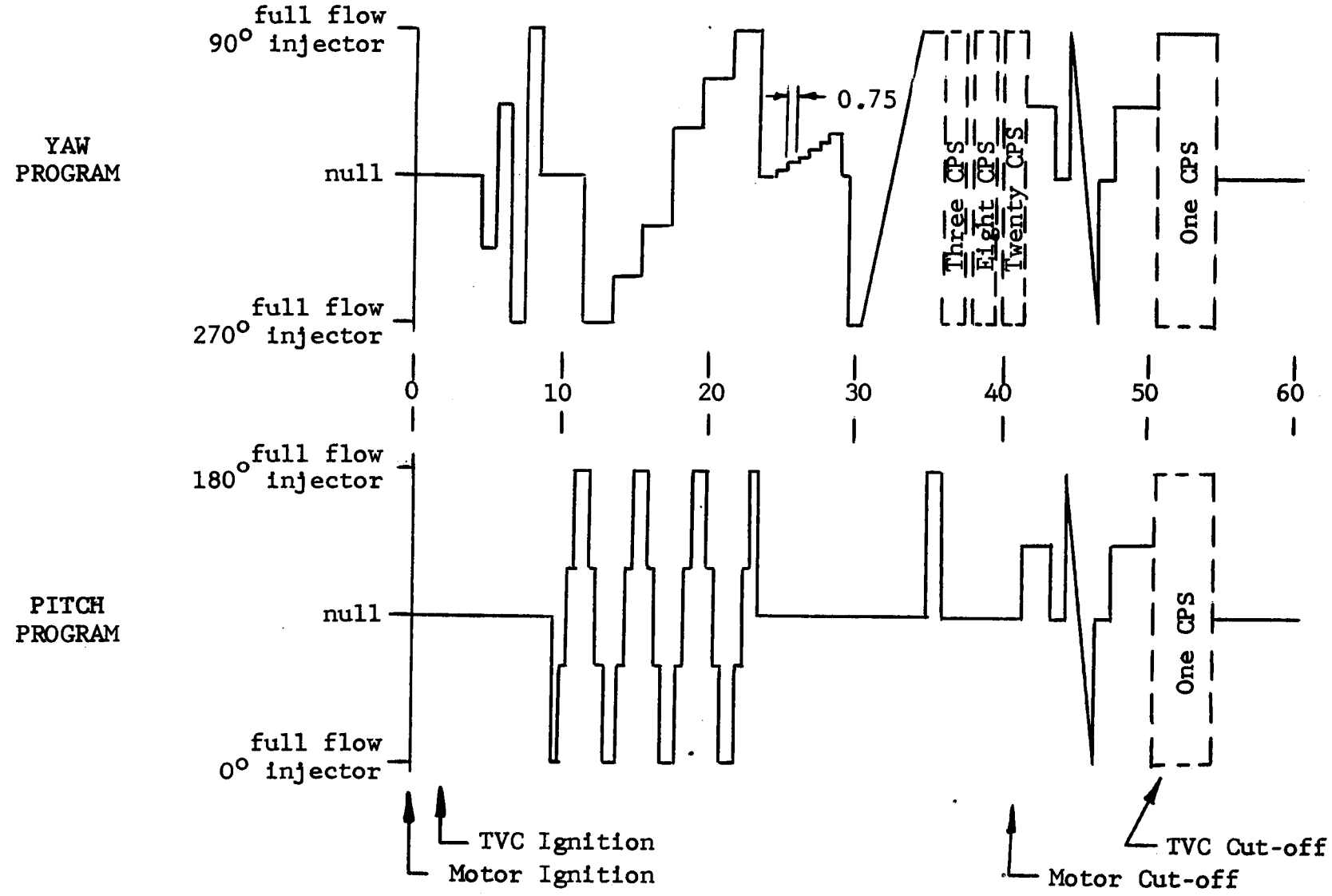

SECTION 7

TEST RESULTS - SIDE FORCE AND THRUST AUGMENTATION

Side force measurements are obtained from tabulated digital data. A printed sampling rate of 100 samples per second appears to be most convenient. The algebraic sum of the two load cells readings is averaged over 15 or 20 samples in a time period after the initial transients have settled. Some of the side force results (for each test) are tabulated in this Section. The conventional plots used for comparison with other types of secondary injection thrust vector control systems are also included.

7.1 Tabulated Results

Table 7.1 gives the average flow rate, thrust, and specific impulse of the rocket motor for each test. With the exception of Test 2, the motor performance is steady enough so that the measured values are always within a few percent of average. In any calculations involving these values, the actual readings at the given time are used.

Representative data points from Tests 1 through 5 are given in Table 7.2. Magnification factor is defined and derived in Section 7.2. Theoretical side force for each test is based on

the curves in Figure 4.5. From these curves, a side force for each injector corresponding to the chamber pressure of that injection nozzle can be found. Theoretical side force is the difference between the two side force values of opposing injector nozzles.

Thrust vector control is applied to two planes of injection in Test 6. A relatively large number of data points are presented in Table 7.3 in order to show the independence of side force in one plane to side force activities in the other plane. It may also be seen that there is no difference in results between yaw and pitch injection planes.

7.2 Magnification Factor

One standard by which a secondary injection system is evaluated is the magnification factor, MF. The magnification factor is the ratio of the side force obtained by the injection of a secondary gas stream into the exhaust cone of a supersonic nozzle to the side force obtainable from a simple vernier rocket with the same nozzle geometry and flow conditions. For single-axis injection from opposed ports, the measured side force should

be compared to the difference between the thrusts generated by two vernier rockets. In the following equations, a method for determining this thrust difference for vernier rockets is derived.

$$F_1 - F_2 = \dot{m}_1 v_1 + A_{e_1} (p_{e_1} - p_{a_1}) - [\dot{m}_2 v_2 + A_{e_2} (p_{e_2} - p_{a_2})]$$

where $A_{e_1} = A_{e_2} = A_e$ and $p_{a_1} = p_{a_2}$.

$$\therefore \quad F_1 - F_2 = \dot{m}_1 v_1 - \dot{m}_2 v_2 + A_e (p_{e_1} - p_{e_2}) \tag{7.1}$$

The $(\dot{m}\ v)$ terms in equation 7.1 may be expanded as follows:

$$mv = \left\{ \zeta_d A_* p_c \sqrt{\frac{\gamma}{gRT_c} \left(\frac{2}{\gamma+1}\right)^{\frac{\gamma+1}{\gamma-1}}} \right\} \left\{ \zeta_v \sqrt{\frac{2\gamma gRT_c}{\gamma-1} \left[1 - \left(\frac{P_e}{P_c}\right)^{\frac{\gamma-1}{\gamma}} \right]} \right\}$$

where $\frac{P_e}{P_c}$ = ratio of exit pressure to chamber pressure, a constant for any given nozzle configuration.

$$mv = \zeta_d \zeta_v A_* p_c \gamma \sqrt{\frac{2}{\gamma-1} \left(\frac{2}{\gamma+1}\right)^{\frac{\gamma+1}{\gamma-1}} \left[1 - \left(\frac{P_e}{P_c}\right)^{\frac{\gamma-1}{\gamma}} \right]} \tag{7.2}$$

where ζ_d and ζ_v are discharge and velocity correction factors respectively. Substituting equation 7.2 into equation 7.1 produces

$$F_1 - F_2 = \left[\zeta_d \zeta_v A_* \gamma \sqrt{\frac{2}{\gamma-1}\left(\frac{2}{\gamma+1}\right)^{\frac{\gamma+1}{\gamma-1}}\left[1 - \left(\frac{P_e}{P_c}\right)^{\frac{\gamma-1}{\gamma}}\right]} + A_e \frac{P_e}{P_c}\right]\left(P_{c_1} - P_{c_2}\right) \tag{7.3}$$

The only variables in equation 7.3 are p_{c_1} and p_{c_2}. The value of ζ_d can be determined experimentally; an approximate value for ζ_v is 0.92. The rest of the equation can be evaluated from the parameters for the individual tests. With this derivation, (F_1-F_2) can be calculated as a function of chamber pressures alone even though chamber pressure itself is dependent on temperature and mass flow.

Magnification factor is then obtained as the quotient of measured side force divided by (F_1-F_2). Table 7.4 lists the average magnification factor for each test. The entry $\left(\frac{F_1-F_2}{P_{c_1}-P_{c_2}}\right)$ is the constant term of equation 7.3.

7.3 Other Results and Discussion

Probably the most common means of comparison for secondary injection systems is the graph of side force to axial thrust ratio versus differential injectant flow to primary flow ratio. These results for the six tests are given in Figures 7.1 through 7.6 and

summarized in Figure 7.7. In Figure 7.8, the range of test results given in Figure 7.7 is superimposed on a force ratio versus flow ratio curve that shows the areas usually associated with hot gas injection and with cold gas or inert liquid secondary injection. The slopes of the force ratio lines on Figure 7.7 are equal to the specific impulse ratio, $\frac{I_j}{I}$, for each test. These specific impulse ratios are listed in Table 7.4.

At this point, some discussion of the results shown in Figure 7.7 and Table 7.4 is in order. In both Tests 1 and 5, there was a leak in the secondary injection system. Any leak makes calculation of ζ_d, the discharge correction factor, impossible. When an average value for ζ_d is placed into the equation for choked flow

$$\dot{w} = \zeta_d A^* p_c \sqrt{\frac{g\gamma}{RT_c}} \left(\frac{2}{\gamma+1}\right)^{\frac{\gamma+1}{2(\gamma-1)}},$$

the mass flow calculated for each injection nozzle varies from the true mass flow in a test in which the true ζ_d is higher or lower than the average value used. An error in this calculation is reflected in the differential injectant flow term, $\Delta\dot{w}_j$. The correlation of results between Tests 5 and 6 indicates that the

average ζ_d used for Test 5 is acceptable. Correlation of Test 1 with Test 3 is not as good. It is expected that slightly better results are obtainable with the lower chamber pressures of Test 3 (see Sections 9 and 11), but some of the large difference in the two tests may be caused by the actual ζ_d of Test 1 being lower than the average value used.

One other test appears to be affected by imperfect test conditions. In Test 3, the rocket motor burned at a steadily increasing rate until its failure in the tenth second of the run. The conditions in the primary nozzle were, of course, different from those to which the secondary system was sized. In addition, the secondary system was not at its proper operating temperature for all the data points used in that shortened test. It is fairly certain, therefore, that the specific impulse ratio and magnification factor calculated for Test 2 are somewhat lower than they should be.

7.4 Thrust Augmentation

In each test, the rocket motor is ignited before the TVC system. The analog traces of axial thrust show a slight increase when

the gas generator(s) is started. Since the size of the thrust augmentation is small compared to the unaugmented thrust and since some stand vibration due to motor and TVC system ignition is present, it is difficult to obtain an accurate reading on thrust augmentation. Estimated values for each test are:

Test	1	2	3	4	5	6
Thrust Augmentation (lb)	60	20	30	40	40	70

Another effect on motor characteristics by the addition of secondary flow is the increase in pressure at the primary nozzle exit plane. Some indication of that increase is obtained by comparing the pressure readings in the row of taps closest to the exit plane before and after TVC system ignition. Some increase can be seen in each test, but the amount of pressure increase is small (one psi or less).

Test No.	Average Primary Flow $\dot{w}$ (lb/sec)	Average Primary Thrust F (lb)	Average Primary Specific Impulse I (sec)
1	12.4	2870	230
2	14	3000	210
3	11.5	2550	220
4	11.6	2600	220
5	11.5	2570	220
6	12.4	2760	220

Table 7.1 Averaged Test Results for Rocket Motor

Test No.	Time after Motor Ignition (sec)	Injection Chamber Pressure p_{jc_1} (psia)	Injection Chamber Pressure p_{jc_2} (psia)	Differential Injection Flow $\Delta\dot{w}_j$ (lb/sec)	Measured Side Force F_j (lb)	Secondary Specific Impulse I_j (sec)	Magnification Factor MF	Theoretical Side Force F_{th} (lb)
1	8.6	499	351	0.107	25	234	1.83	21
1	15.0	136	233	0.072	16	222	1.79	15
1	16.5	114	257	0.106	22	208	1.67	23
1	17.9	71	303	0.170	36	212	1.68	39
1	20.6	291	81	0.158	36	228	1.86	35
1	21.7	53	325	0.196	45	230	1.79	47
2	6.5	702	79	0.504	105	208	1.80	122
2	7.0	748	64	0.533	115	216	1.80	133
2	7.5	798	36	0.584	130	223	1.82	154
2	8.0	825	35	0.583	135	232	1.83	160
2	8.5	843	32	0.591	139	235	1.83	165
2	9.0	857	33	0.589	142	241	1.84	166
3	12.0	15	493	0.607	159	262	2.01	158
3	27.3	509	15	0.605	162	268	1.98	162
3	31.0	94	415	0.386	96	248	1.80	99
3	32.6	495	26	0.575	152	264	1.95	152
3	38.4	282	220	0.072	20	278	1.94	18
3	42.0	377	125	0.301	79	262	1.89	76
4	10.0	75	469	0.448	106	237	1.86	133
4	14.2	395	175	0.226	57	252	1.78	74
4	17.2	100	476	0.399	98	246	1.78	127
4	23.0	353	239	0.114	28	246	1.65	38
4	30.0	600	29	0.604	156	258	1.84	189
4	43.2	206	396	0.194	50	258	1.79	63
5	11.2	20	544	0.559	179	320	2.32	214
5	13.2	172	363	0.181	62	343	2.21	71
5	16.3	488	45	0.456	152	333	2.33	176
5	17.4	227	296	0.067	22	328	2.18	26
5	27.8	496	21	0.504	164	325	2.35	198
5	28.9	106	393	0.289	93	322	2.20	110

Table 7.2 Secondary Injection Results for Tests 1 through 5

Plane of Injection	Time after Motor Ignition (sec)	Injector Chamber Pressure p_{jc_1} (psia)	Injector Chamber Pressure p_{jc_2} (psia)	Differential Injection Flow $\dot{\Delta w}_j$ (lb/sec)	Measured Side Force F_j (lb)	Secondary Specific Impulse I_j (sec)	Magnification Factor MF	Theoretical Side Force F_{th} (lb)	Side Force, Other Plane (lb)
Yaw	10.0	236	312	0.080	25	312	2.18	28	-182
Yaw	10.5	258	292	0.033	11	333	2.16	13	-84
Yaw	11.0	264	291	0.027	7	259	1.71	9	89
Yaw	11.5	271	287	0.015	5	333	2.08	6	186
Yaw	12.0	24	563	0.605	180	298	2.21	217	187
Yaw	12.5	24	566	0.605	186	307	2.27	218	94
Yaw	13.0	24	570	0.605	185	306	2.24	219	-71
Yaw	13.5	24	572	0.607	185	305	2.23	220	-191
Yaw	14.0	54	532	0.501	159	317	2.20	185	-190
Yaw	14.5	57	528	0.495	159	321	2.24	182	-73
Yaw	15.0	58	525	0.491	157	320	2.22	181	88
Yaw	15.5	58	527	0.492	154	313	2.18	182	193
Yaw	16.0	156	422	0.272	87	320	2.16	98	193
Yaw	16.5	159	421	0.269	87	323	2.20	97	96
Yaw	17.0	161	419	0.265	85	321	2.18	95	-60
Yaw	17.5	164	416	0.261	81	310	2.12	93	-188
Yaw	18.0	377	196	0.201	61	303	2.22	67	-187
Yaw	18.5	382	191	0.208	62	298	2.14	71	-58
Yaw	19.0	386	191	0.210	62	295	2.10	72	82
Yaw	19.5	386	193	0.207	63	304	2.19	70	194
Yaw	20.0	496	79	0.450	141	313	2.23	159	195
Yaw	20.5	500	76	0.457	144	315	2.24	161	95
Yaw	21.0	504	75	0.458	145	317	2.24	164	-49
Yaw	21.5	507	72	0.466	146	313	2.22	167	-186
Yaw	22.0	566	28	0.579	183	316	2.25	215	-187
Yaw	22.5	565	27	0.575	181	315	2.23	214	-50
Yaw	23.0	567	27	0.582	184	316	2.26	215	80
Yaw	23.5	569	27	0.582	183	314	2.23	216	199
Pitch	16.5	437	148	0.302	96	318	2.20	106	-87
Pitch	22.5	209	377	0.174	50	288	1.97	61	181
Pitch	23.5	589	21	0.616	199	323	2.32	228	183
Pitch	29.0	309	289	0.020	7	350	2.33	7	61
Pitch	36.0	579	31	0.585	183	313	2.21	216	181

Table 7.3 Secondary Injection Results for Test 6

Test No.	Injection Type	Location of Injectors	Angle of Injection	$\frac{F_1-F_2}{P_{c_1}-P_{c_2}}$	Magnification Factor, MF	Specific Impulse Ratio, $\frac{I_j}{I}$
1	sonic	75%	motor axis	0.0936	1.78	0.96
2	supersonic	75%	motor axis	0.0923	1.82	1.13
3	sonic	75%	motor axis	0.1660	1.90	1.19
4	supersonic	60%	motor axis	0.1451	1.79	1.09
5	supersonic	75%	20° upstream	0.1470	2.29	1.45
6	supersonic	75%	20° upstream	0.1512	2.22	1.44

Table 7.4 Average Magnification Factors for Tests 1 through 6

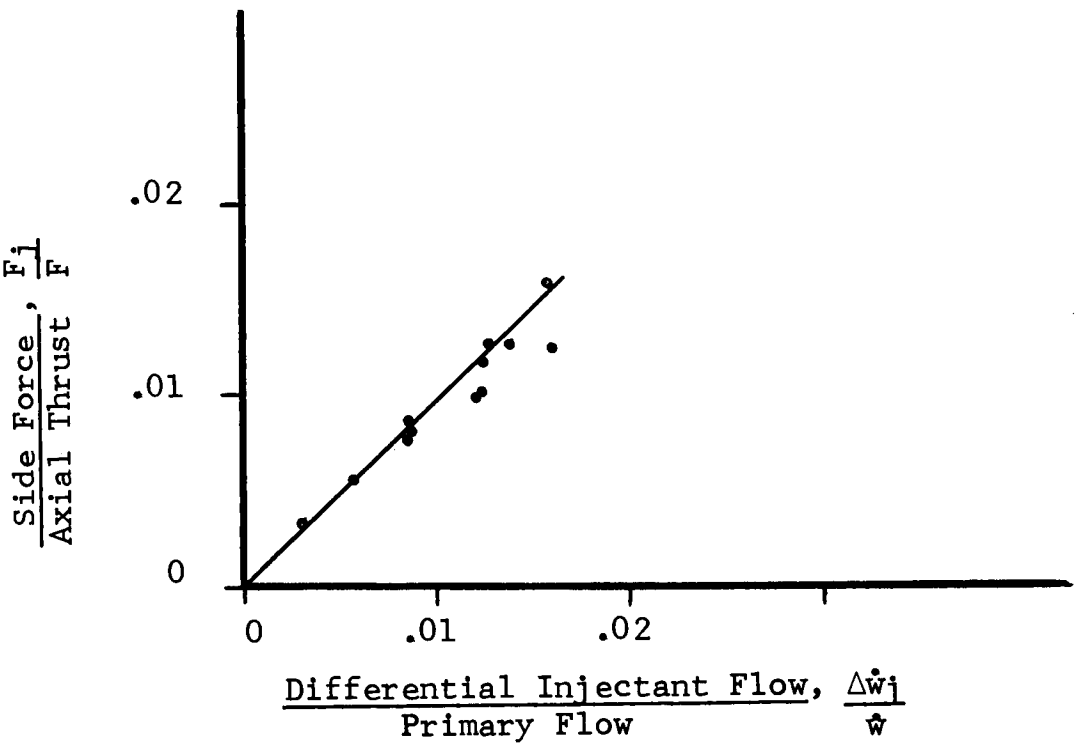

Figure 7.1 Force Ratio Versus Flow Ratio - Test 1

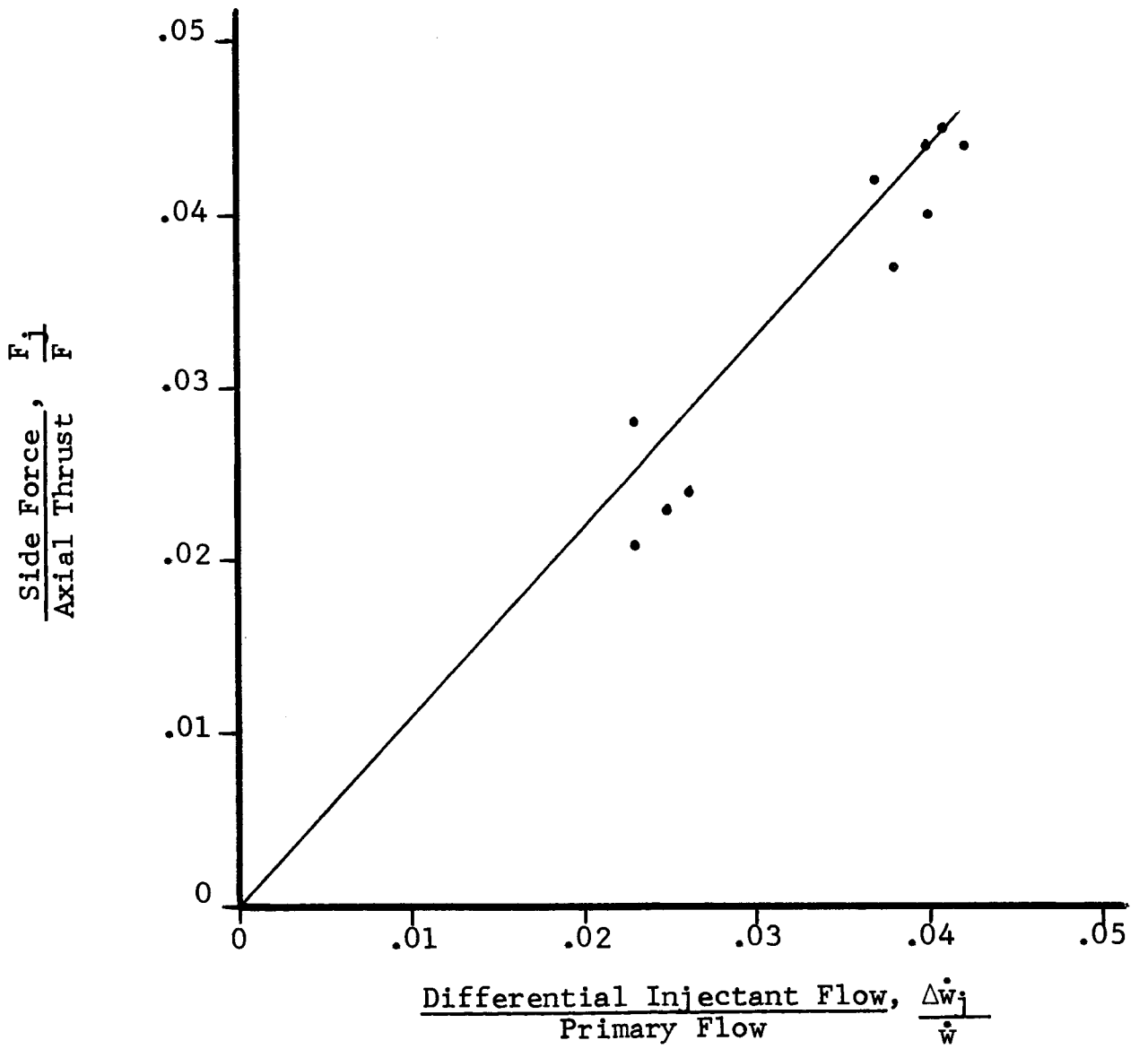

Figure 7.2 Force Ratio Versus Flow Ratio - Test 2

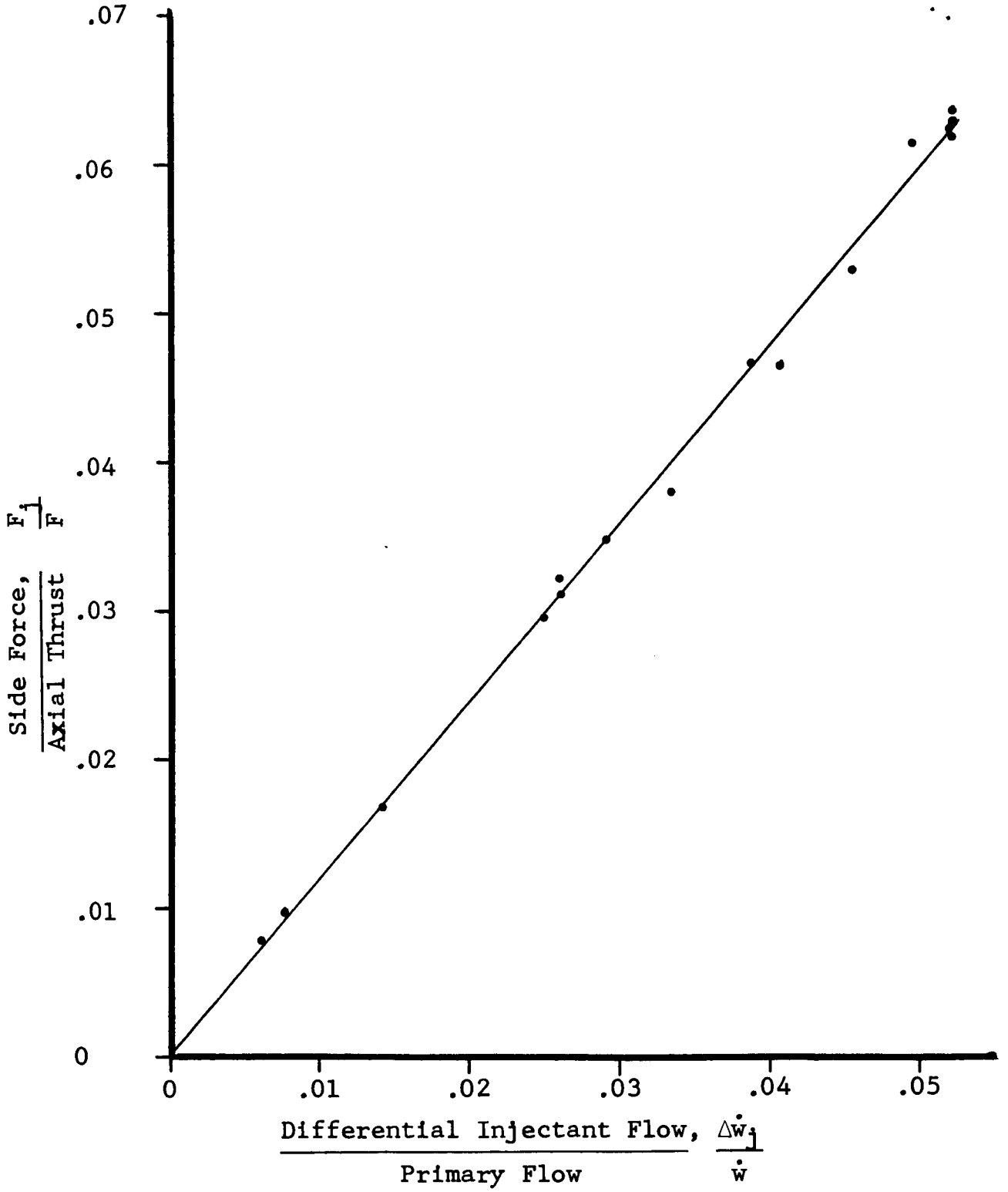

Figure 7.3 Force Ratio versus Flow Ratio - Test 3

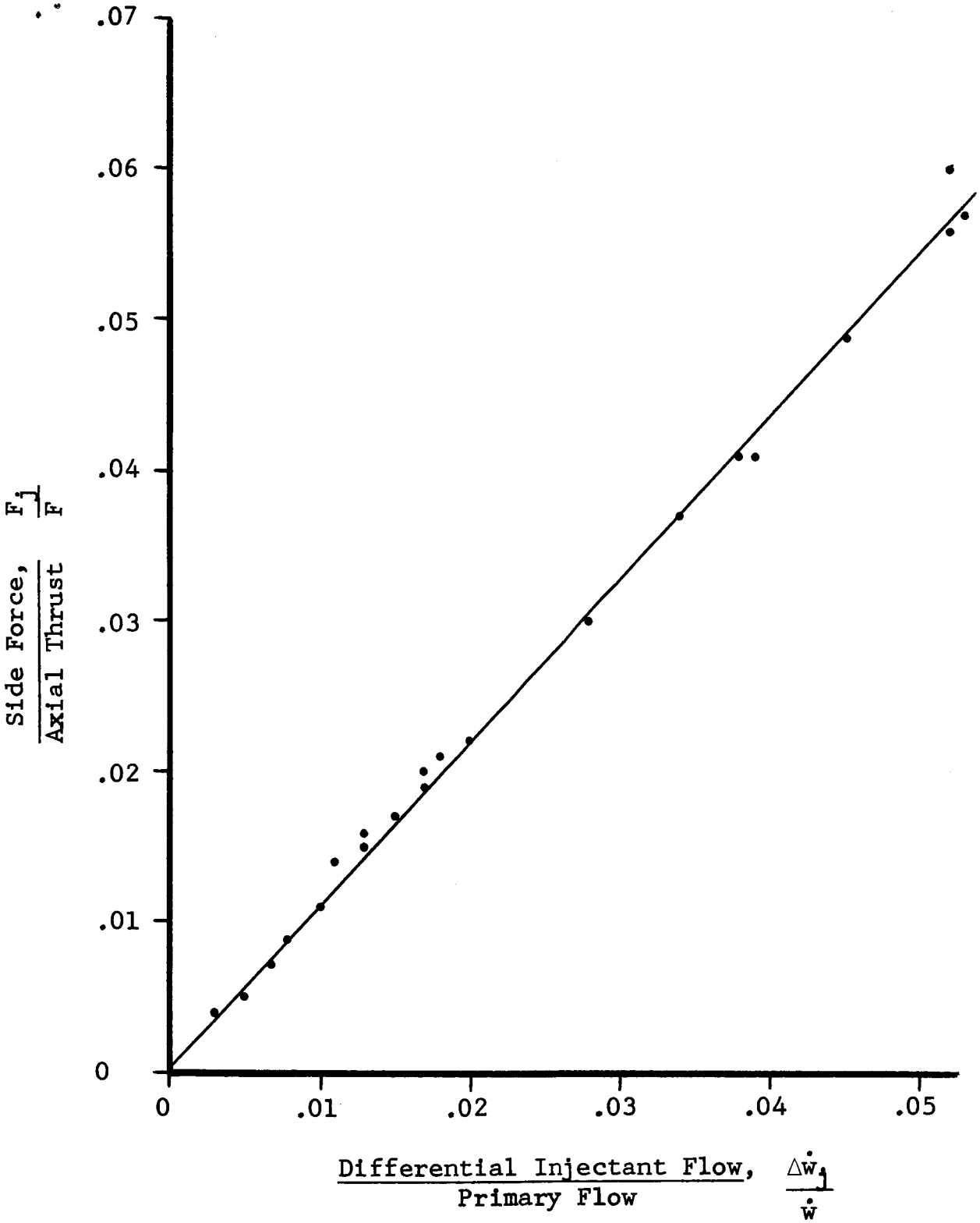

Figure 7.4 Force Ratio Versus Flow Ratio - Test 4

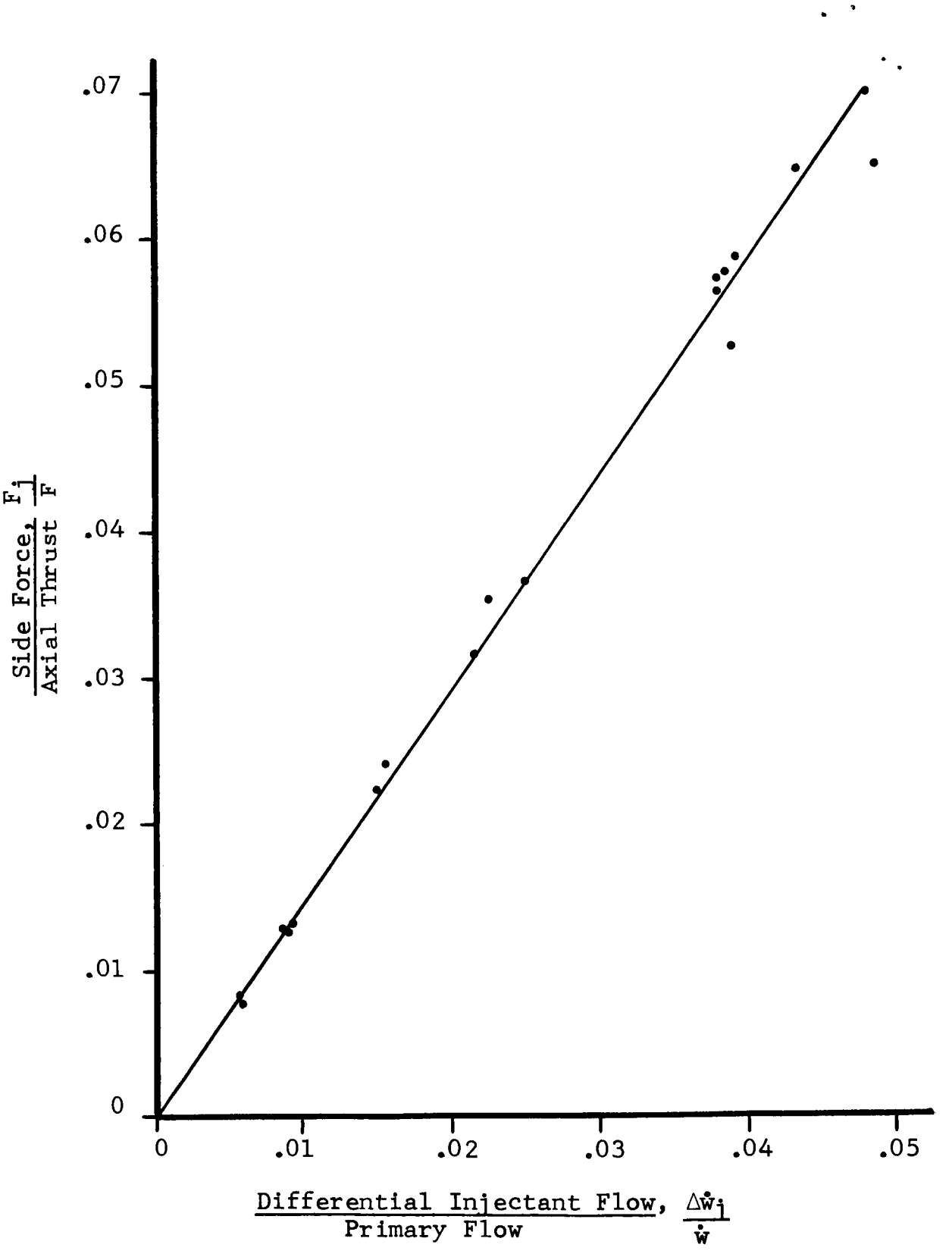

Figure 7.5 Force Ratio Versus Flow Ratio - Test 5

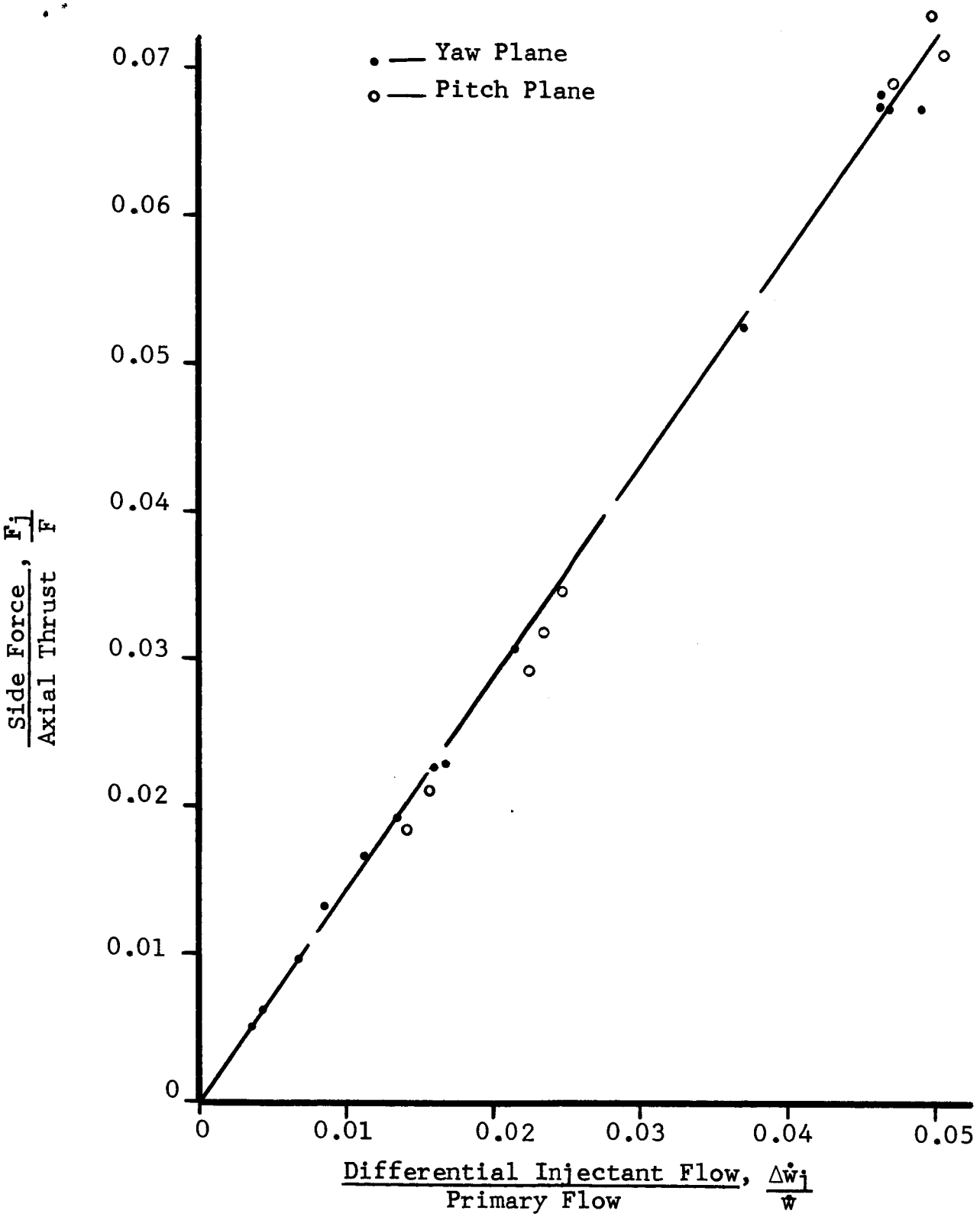

Figure 7.6 Force Ratio Versus Flow Ratio - Test 6

	Injection Type	Location of injector	Angle of Injection
1	Sonic	75%	⊥ Motor Axis
2	Supersonic	75%	⊥ Motor Axis
3	Sonic	75%	⊥ Motor Axis
4	Supersonic	60%	⊥ Motor Axis
5	Supersonic	75%	20° Upstream
6	Supersonic	75%	20° Upstream

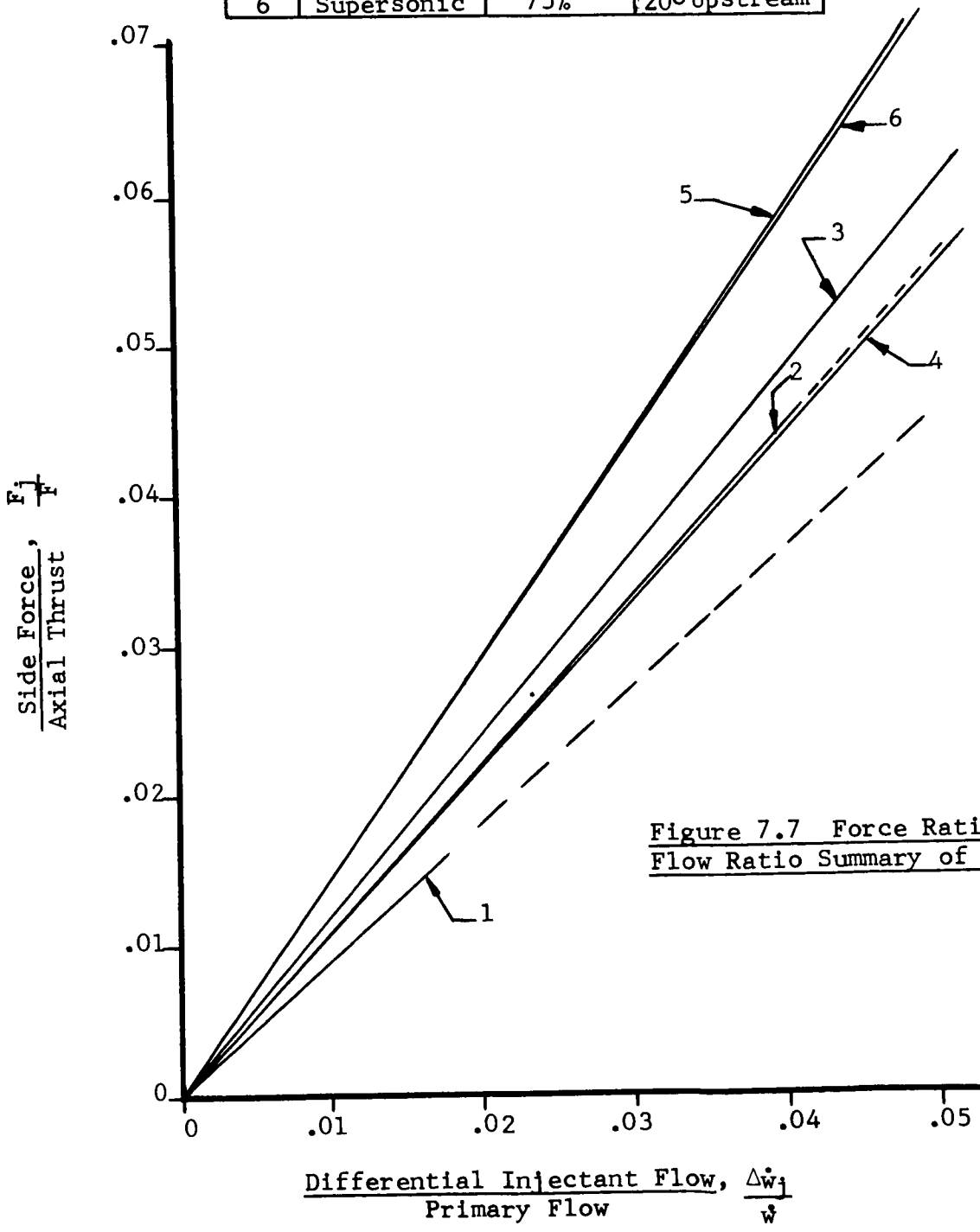

Figure 7.7 Force Ratio Versus Flow Ratio Summary of Six Tests

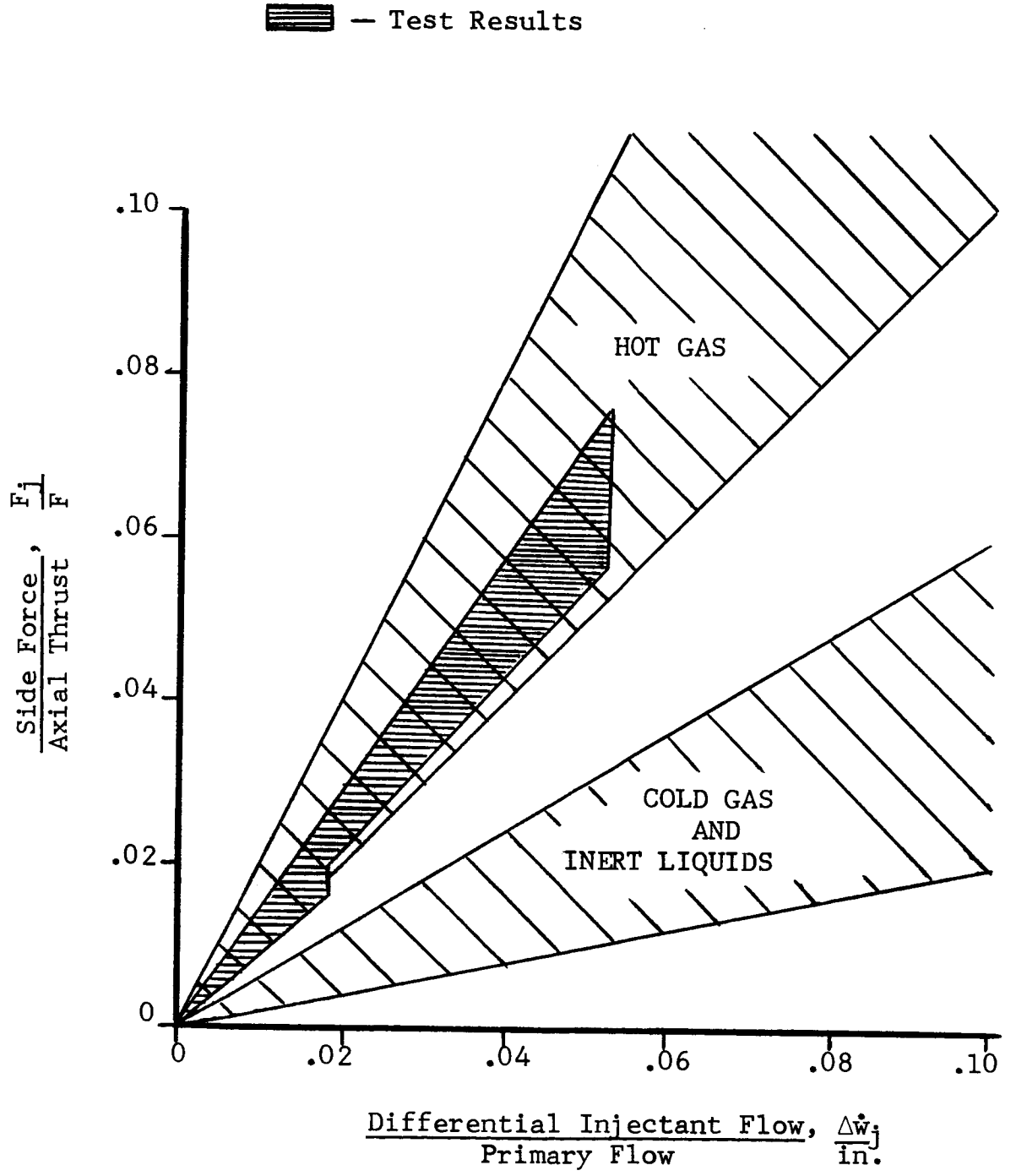

Figure 7.8 Relative Effectiveness of Various Secondary Injectants

SECTION 8

TEST RESULTS-SHOCK WAVE PATTERNS

As part of the effort in correlating the theoretical analysis with the experimental results, a series of pressure taps were installed in the rocket motor nozzle exit cone to record static pressure during the test firings. The number of taps was limited to 28 by the instrumentation available to record the pressure readings during the tests.

In Paragraph 8.1 a series of shock wave locations are shown for each of the six tests; the location of the shocks being determined by the variation in the static pressure readings from the nominal values.

Some additional analysis is performed on the shock pattern results of Tests 3, 4, and 5. Paragraph 8.2 gives the percent contribution to side force upstream and downstream of the injection port as determined by wall pressure integration techniques. Paragraph 8.3 shows the location of channels cut into the nozzle wall by the gas flow near the injection ports.

8.1 Shock Locations

In the following Figures 8.1 through 8.76, the location of the

shock as determined by the static pressure readings is shown on a developed layout of the nozzle cone. On each layout are grid lines of azimuth angles from the injection port and axial locations of the pressure tap lines measured along the nozzle wall from the exit plane. The dots identifying the tap locations are placed as close as possible to their actual location in the nozzle after machining, so that they do not always fall exactly on the grid line.

Figure 8.1 is the legend explaining the information to be found on the subsequent figures. For each test the development of the shock is shown as the injection nozzle chamber pressure increases. For Tests 1 through 5 the gas is injected in one plane only and the majority of the pressure taps were arranged around one injection port to obtain as much information as possible. Each plot is identified by test number and the time after motor ignition, and contains the injection nozzle chamber pressure, P_j (psia); the injected gas total temperature, T_j ($^\circ$F); the ratio of injected gas pressure to the motor chamber pressure, P_j/P_c; and the ratio of injected gas flow to the motor flow, $\dot{w}_j/\dot{w}$. In this case $\dot{w}_j$ is the gas flow from the one nozzle and not the differential flow between the two injection nozzles.

For Test Number 6 with two-axis injection two series of curves are presented; the first with the pitch injection at null, that is equal flow from each pitch injection nozzle, with varying flow from the one yaw injector as shown. The second series is with maximum flow from one pitch injector and varying flow from the yaw port. On these figures the parameters of the yaw injector are identified by the subscript 32.

8.1.1 Figures 8.77 through 8.83 summarize the static pressure levels in the nozzle as a function of injector nozzle pressure for the six test firings. Test Number 6 is represented by Figures 8.82 and 8.83; the first showing the effects of a variation in yaw injector pressure with the pitch valve at null and the latter with one pitch injector at maximum flow conditions.

The nominal pressure at each tap is denoted by the tap pressure for zero injector chamber pressure.

8.2 Excess Pressure Contributions to Side Force

The amount of side force contribution due to excess wall pressures upstream and downstream of the injection port can be determined by the following method. For a given test, a shock pattern for a condition of high secondary flow rate on the instrumented side

of the nozzle is selected. For the time at which that shock pattern is obtained, the total side force produced by secondary injection through the port on that side of the nozzle is determined from the test stand load cell readout. When there is no flow through the opposite port, the required side force value is simply the total measured side force; if there is opposing flow, the side force produced on the instrumented side of the nozzle can be calculated from the data on side force versus flow rate obtained for the entire test. Next, the momentum force produced by the injection nozzle on the instrumented side of the motor nozzle is calculated and subtracted from the total side force produced at that port. The remaining force is that produced by the pressures within the shock structure acting on the wall of the nozzle.

The selected shock pattern is divided into a number of sectors. Judging by the pressure readings of the pressure taps within each of these sectors and in adjacent sectors, an average value of pressure in excess of the pressure level in that sector when it is not enclosed by the shock structure is chosen. Next, the area of each sector normal to direction of side force is calculated. To do this, the 15° half-angle of the motor nozzle and

the azimuth of the individual sectors must be taken into account. Multiplying the area normal to the side force by the average excess pressure level produces the side force contribution for each sector. The sum of the contributions from all sectors enclosed by the shock should be equal to the force value calculated previously as total side force minus momentum force of injector. If the two force levels are not equal, adjustments are made in choosing the average excess pressure levels for the individual sectors. After a short trial-and-error process, a set of excess pressure levels for the sectors can be found which produce the proper side force value while remaining consistent with the pressure tap readings in the sectors.

The results of application of this method to shock patterns from Tests 3, 4, and 5 are given in Table 8.1. In the Table, the contribution from sectors upstream and downstream of the injection point are added separately. Contributions from upstream and downstream are given as percentages of the total excess pressure force and of the side force from the instrumented side of the nozzle.

Some observations may be made regarding the results in Table 8.1. Having the shock azimuth at the primary nozzle exit plane exceed

90° in Test 4 imposed a large penalty on the downstream excess pressure contribution to side force. As a result, the total side force is lower than it should have been, and the percentages associated with the upstream excess pressure contribution are higher.

It seems that the downstream contribution to side force is about 25 percent for a properly designed system. The upstream contribution varies with the type and angle of injection. Sonic injection perpendicular to the motor axis produces an upstream force contribution equal to 23 percent of the side force, while 20° upstream supersonic injection increases the upstream contribution to 35 percent. These figures are reflected in the increase from 48 percent to 60 percent in the total excess pressure contribution to side force.

8.3 Erosion Patterns

Post-firing examination of the primary nozzle after each test always revealed an erosion pattern starting near the injection ports and running down to the exit plane. NASA Langley examined the nozzles from Tests 3, 4, and 5, and drew contour maps of the erosion patterns about each injection port. The erosion "channels"

have a certain width which is probably created by the variations in flow coming from the injection ports. There is, however, a definite center for the channels which may be assumed to correspond to the average flow conditions from each injector over the entire test. For each test, the position of the center of the channels for the two nozzles is averaged and presented in Figures 8.84, 8.85, and 8.86. The significance of the erosion patterns is discussed in Section 10.

Figure 8.87 is a photograph showing the erosion pattern in the nozzle after Test 5, which corresponds to the channel location shown in Figure 8.86.

Test	3	4	5
Type of injection	sonic	supersonic	supersonic
Injection nozzle location	75%	60%	75%
Angle of injection	⊥ motor axis	⊥ motor axis	20° upstream
Time after motor ignition (sec.)	28.5	28.9	27.8
Shock azimuth at exit plane	74°	98°	76°
Injector chamber pressure, instrumented side (psia)	510	458	496
Injector chamber pressure, opposite side (psia)	16	145	21
Measured side force (lb)	158	85	164
Side force, instrumented side (lb)	158	124½	166
Injector momentum force (lb)	82	65	66
Excess pressure force (lb)	76	59½	100
Upstream excess pressure contribution (lb)	36	37½	58
Downstream excess pressure contribution (lb)	40	22¼	42
Upstream percent of excess pressure force	47%	63%	58%
Downstream percent of excess pressure force	53%	37%	42%
Upstream percent of side force	23%	30%	35%
Downstream percent of side force	25%	18%	25%
Excess pressure percent of side force	48%	48%	60%

Table 8.1 Results of Shock Pattern Analysis

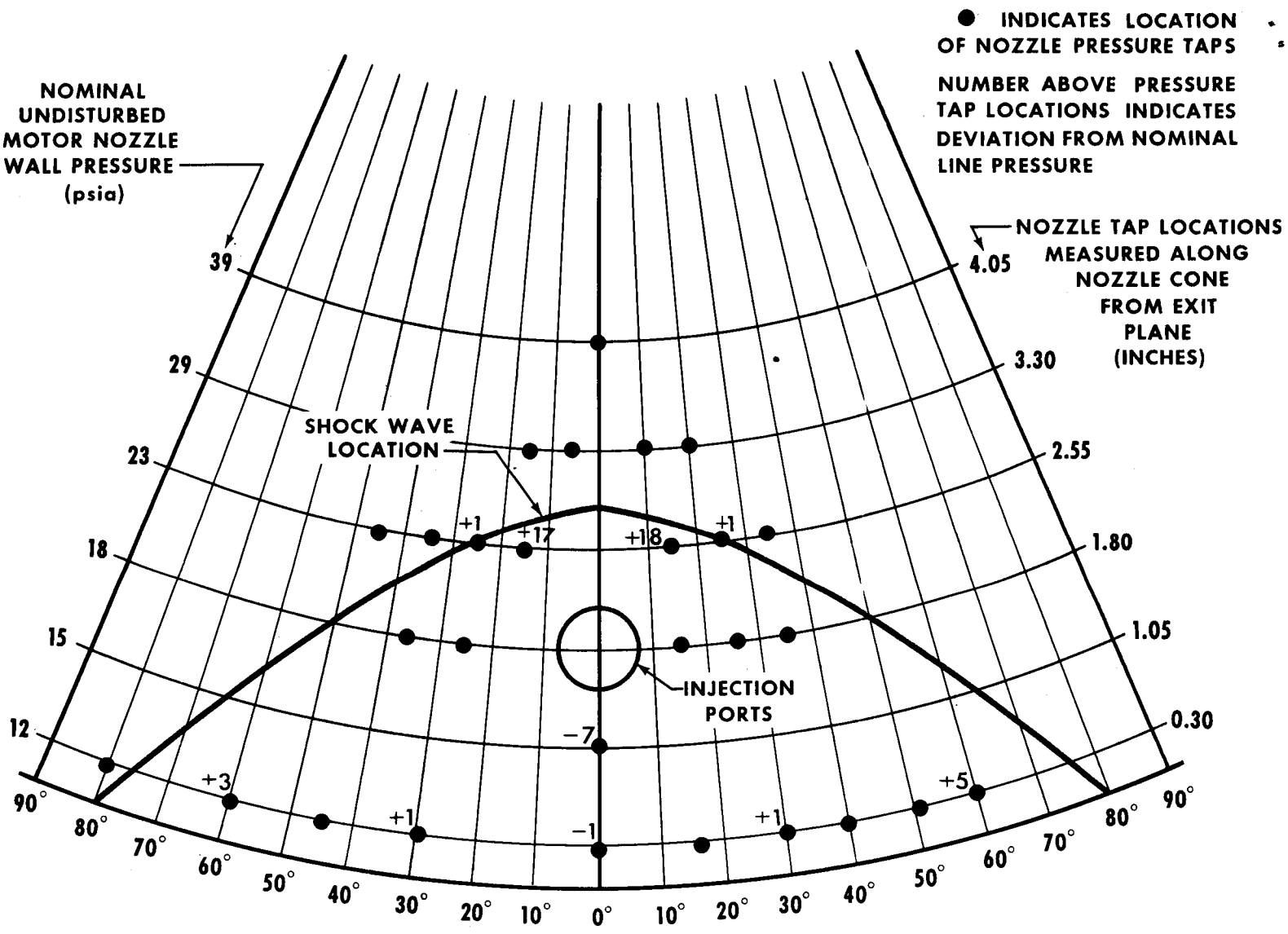
● INDICATES LOCATION OF NOZZLE PRESSURE TAPS
NUMBER ABOVE PRESSURE TAP LOCATIONS INDICATES DEVIATION FROM NOMINAL LINE PRESSURE
NOMINAL UNDISTURBED MOTOR NOZZLE WALL PRESSURE (psia)
NOZZLE TAP LOCATIONS MEASURED ALONG NOZZLE CONE FROM EXIT PLANE (INCHES)
39
29
23
18
15
12
4.05
3.30
2.55
1.80
1.05
0.30
SHOCK WAVE LOCATION
INJECTION PORTS
+1
+17
+18
+1
+3
+1
−7
−1
+1
+5
90°
80°
70°
60°
50°
40°
30°
20°
10°
0°
10°
20°
30°
40°
50°
60°
70°
80°
90°

Figure 8.1

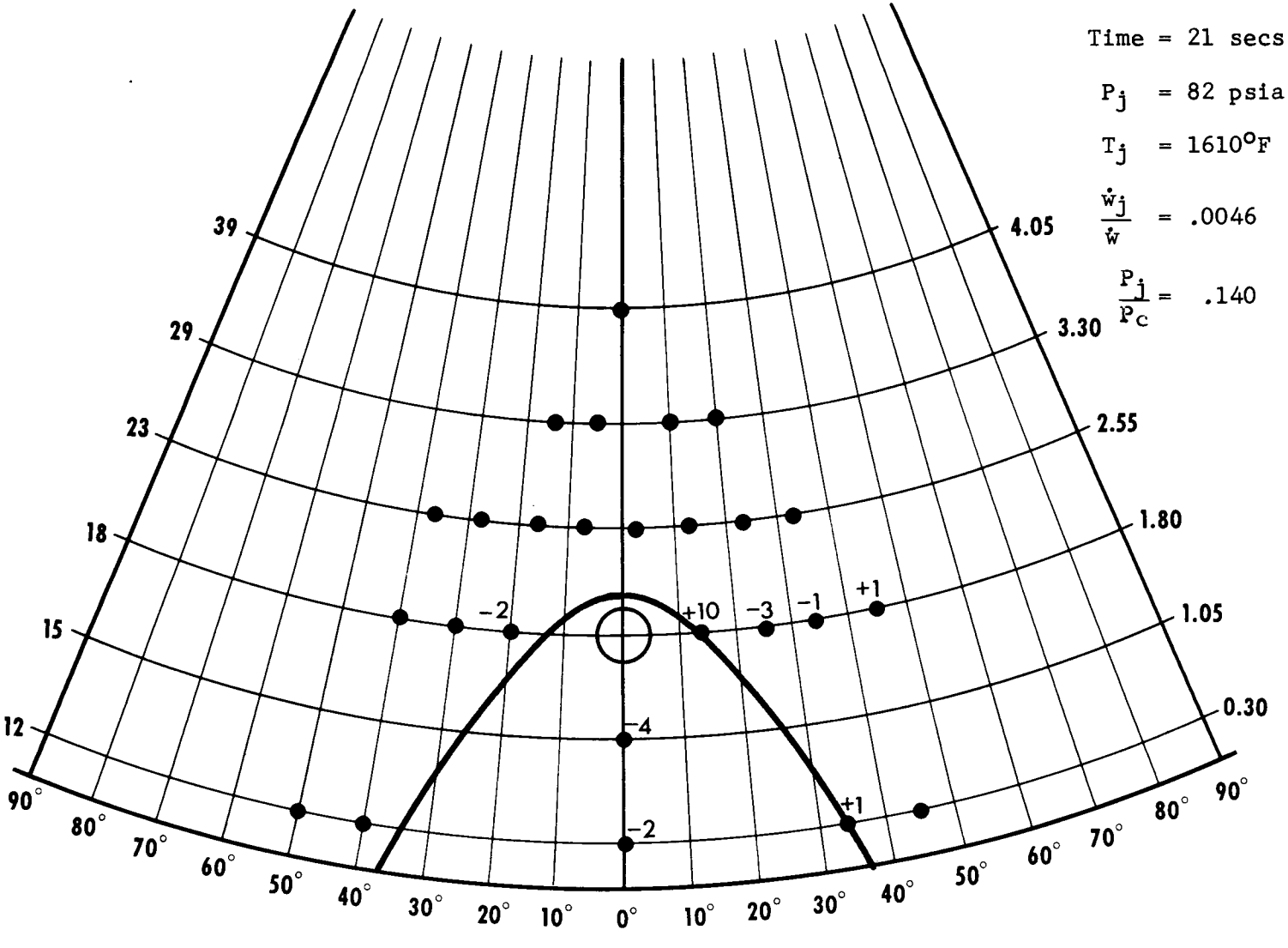
Test No. 1
Time = 21 secs.
P_j = 82 psia
T_j = 1610°F
$\frac{\dot{w}_j}{\dot{w}}$ = .0046
$\frac{P_j}{P_c}$ = .140
39
29
23
18
15
12
4.05
3.30
2.55
1.80
1.05
0.30
90°
80°
70°
60°
50°
40°
30°
20°
10°
0°
10°
20°
30°
40°
50°
60°
70°
80°
90°
-2
+10
-3
-1
+1
-4
-2
+1

Figure 8.2

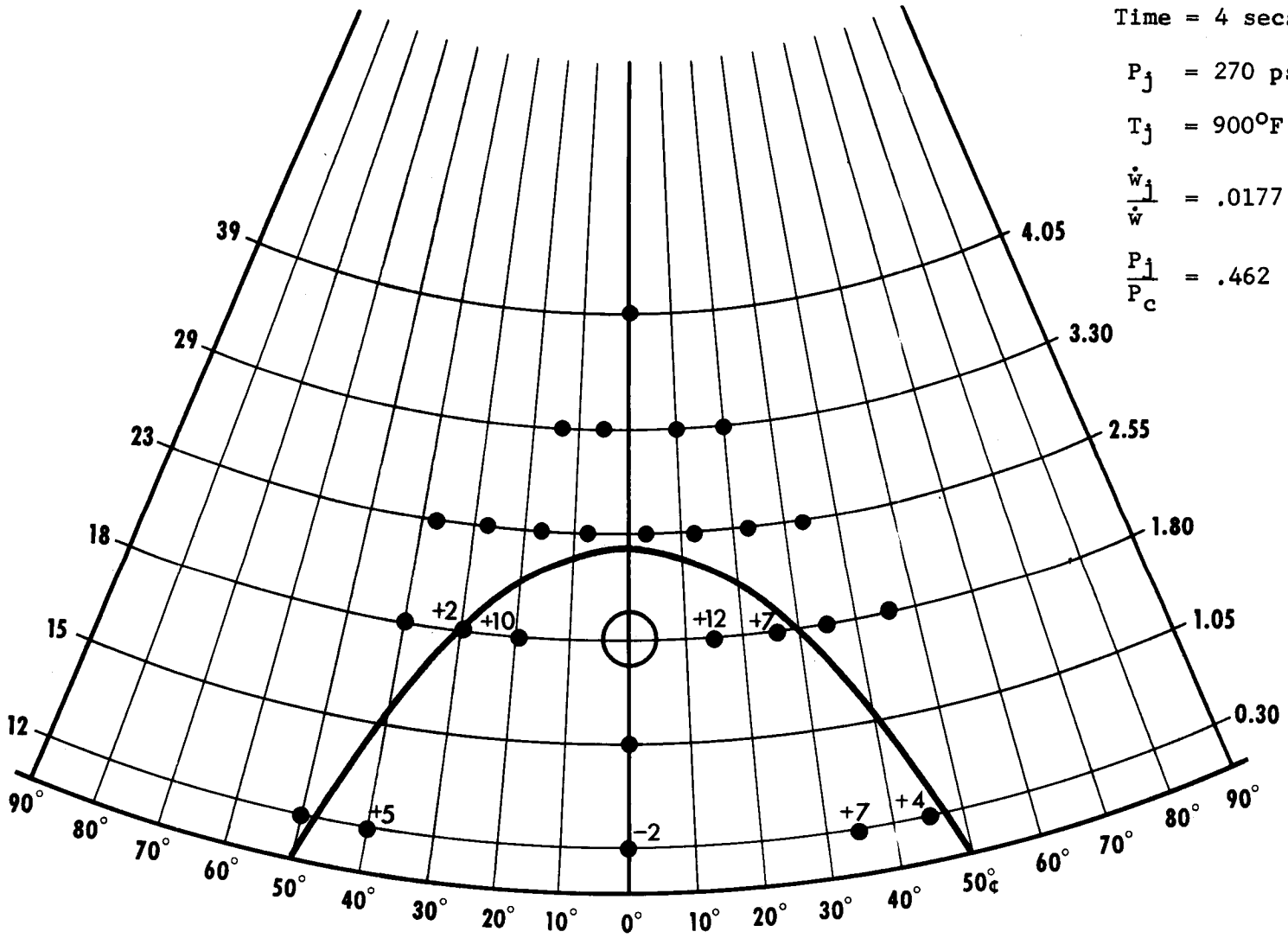
Test No. 1
Time = 4 secs.
P_j = 270 psia
T_j = 900°F
$\frac{\dot{w}_j}{\dot{w}}$ = .0177
$\frac{P_j}{P_c}$ = .462
39
29
23
18
15
12
4.05
3.30
2.55
1.80
1.05
0.30
+2
+10
+12
+7
+5
-2
+7
+4
90°
80°
70°
60°
50°
40°
30°
20°
10°
0°
10°
20°
30°
40°
50°
60°
70°
80°
90°

Figure 8.3

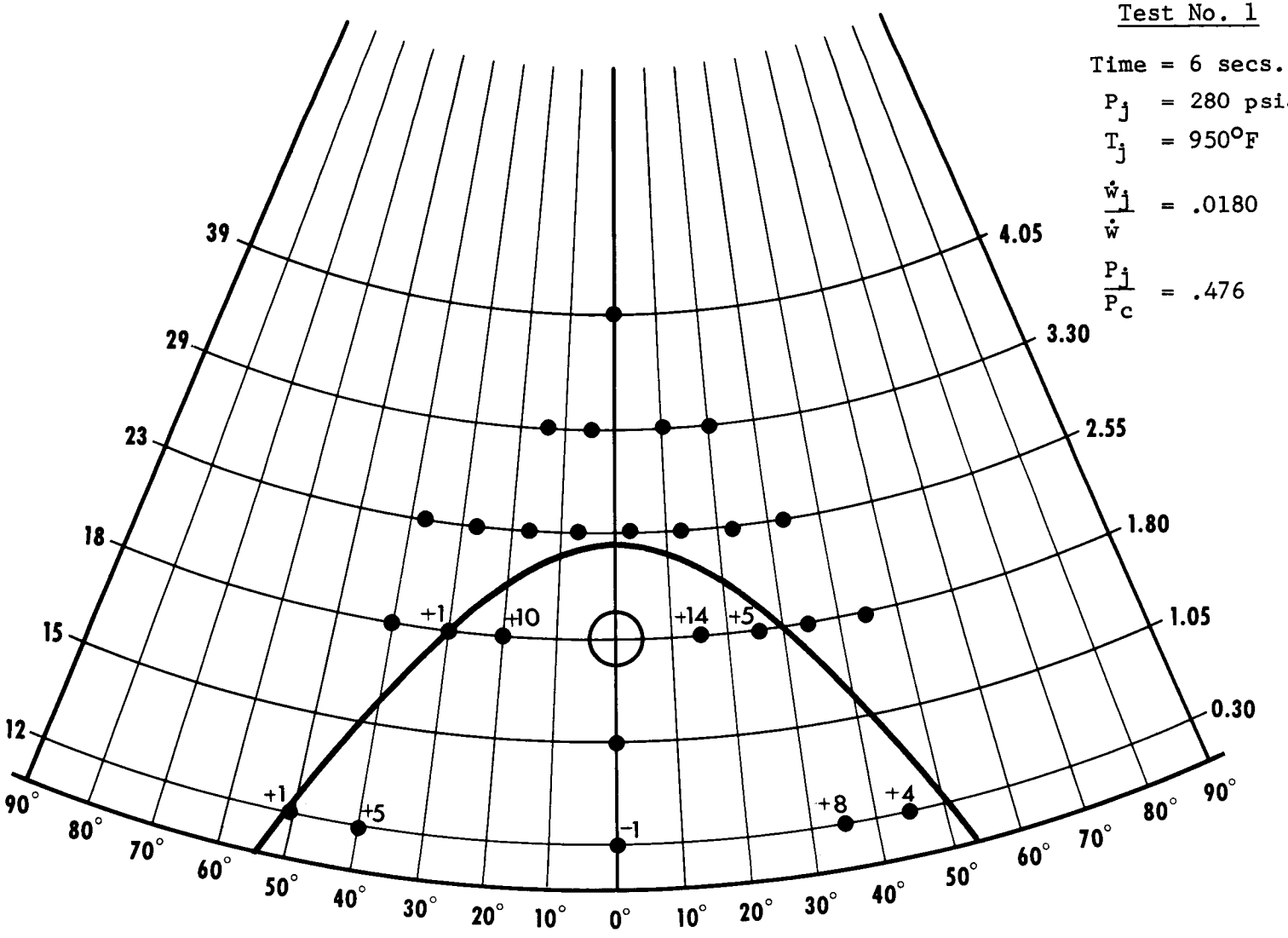
Test No. 1
Time = 6 secs.
P_j = 280 psia
T_j = 950°F
$\frac{\dot{w}_j}{\dot{w}}$ = .0180
$\frac{P_j}{P_c}$ = .476
39
29
23
18
15
12
4.05
3.30
2.55
1.80
1.05
0.30
90°
80°
70°
60°
50°
40°
30°
20°
10°
0°
+1
+10
+14
+5
+1
+5
-1
+8
+4

Figure 8.4

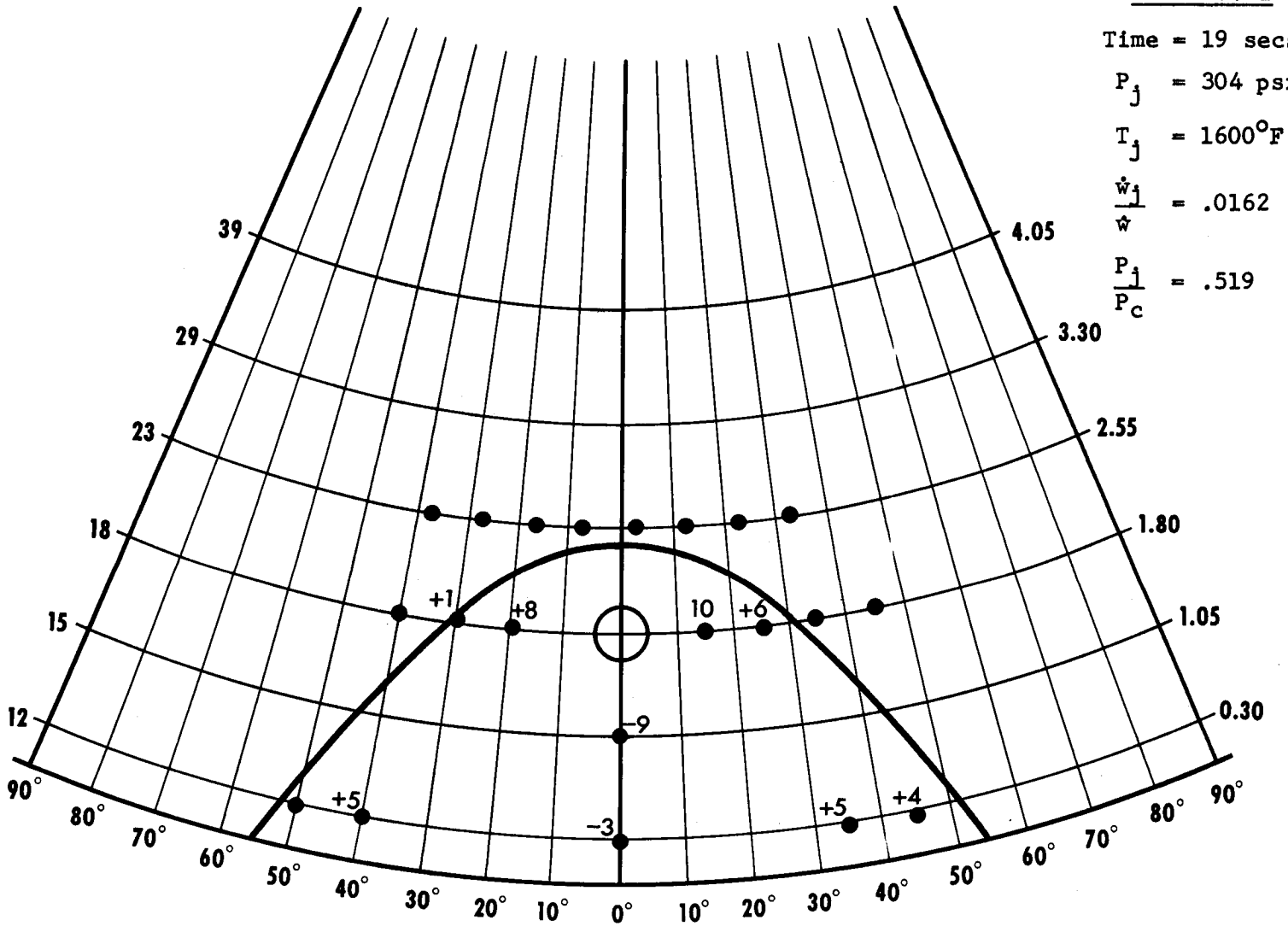
Test No. 1
Time = 19 secs.
P_j = 304 psia
T_j = 1600°F
$\frac{\dot{w}_j}{\dot{w}}$ = .0162
$\frac{P_j}{P_c}$ = .519
39
29
23
18
15
12
4.05
3.30
2.55
1.80
1.05
0.30
90°
80°
70°
60°
50°
40°
30°
20°
10°
0°
10°
20°
30°
40°
50°
60°
70°
80°
90°
+1
+8
10
+6
-9
+5
-3
+5
+4

Figure 8.5

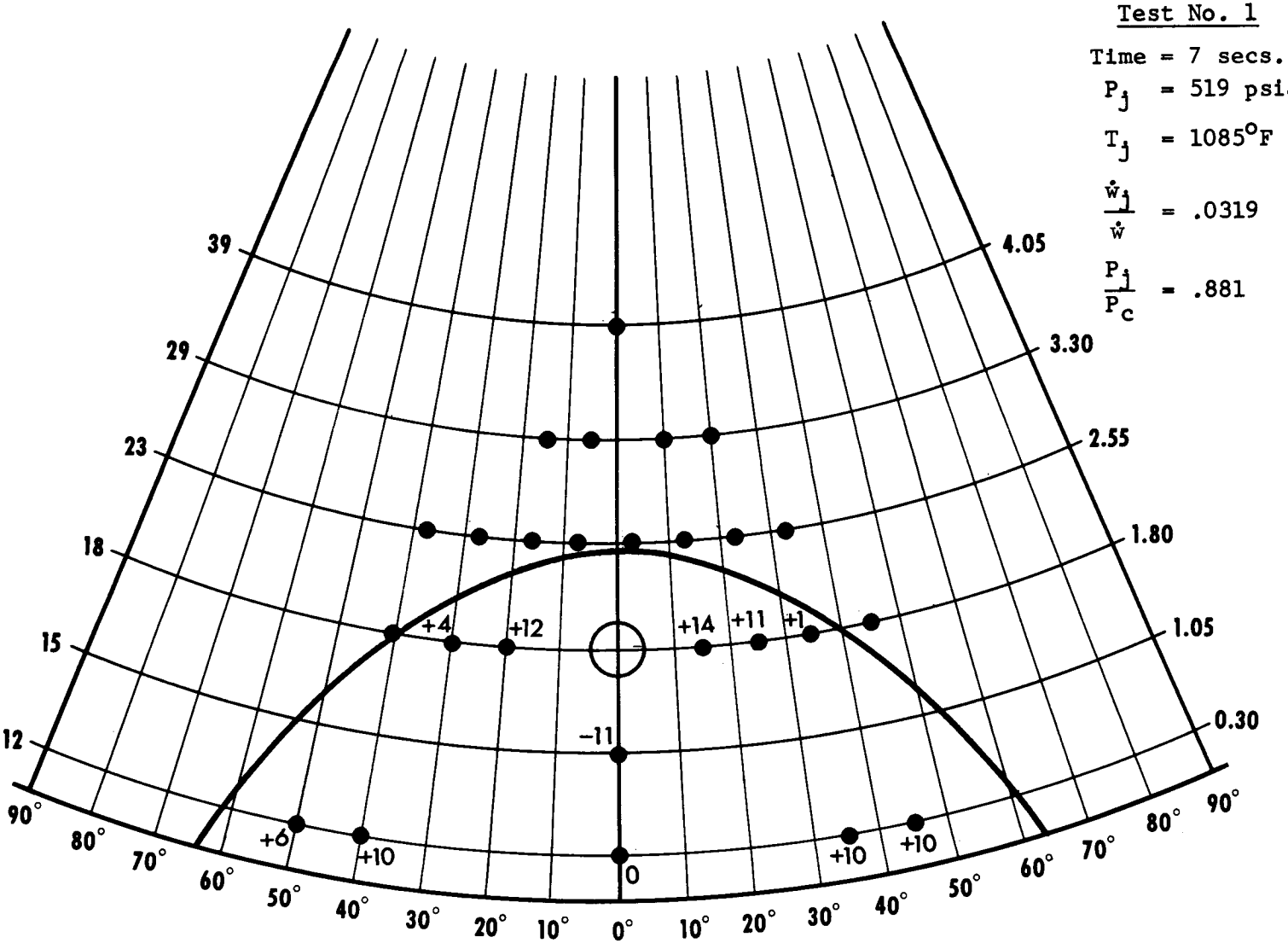
Test No. 1
Time = 7 secs.
P_j = 519 psia
T_j = 1085°F
$\frac{\dot{w}_j}{\dot{w}}$ = .0319
$\frac{P_j}{P_c}$ = .881
39
29
23
18
15
12
4.05
3.30
2.55
1.80
1.05
0.30
+4
+12
+14
+11
+1
-11
+6
+10
0
+10
+10
90°
80°
70°
60°
50°
40°
30°
20°
10°
0°
10°
20°
30°
40°
50°
60°
70°
80°
90°

Figure 8.6

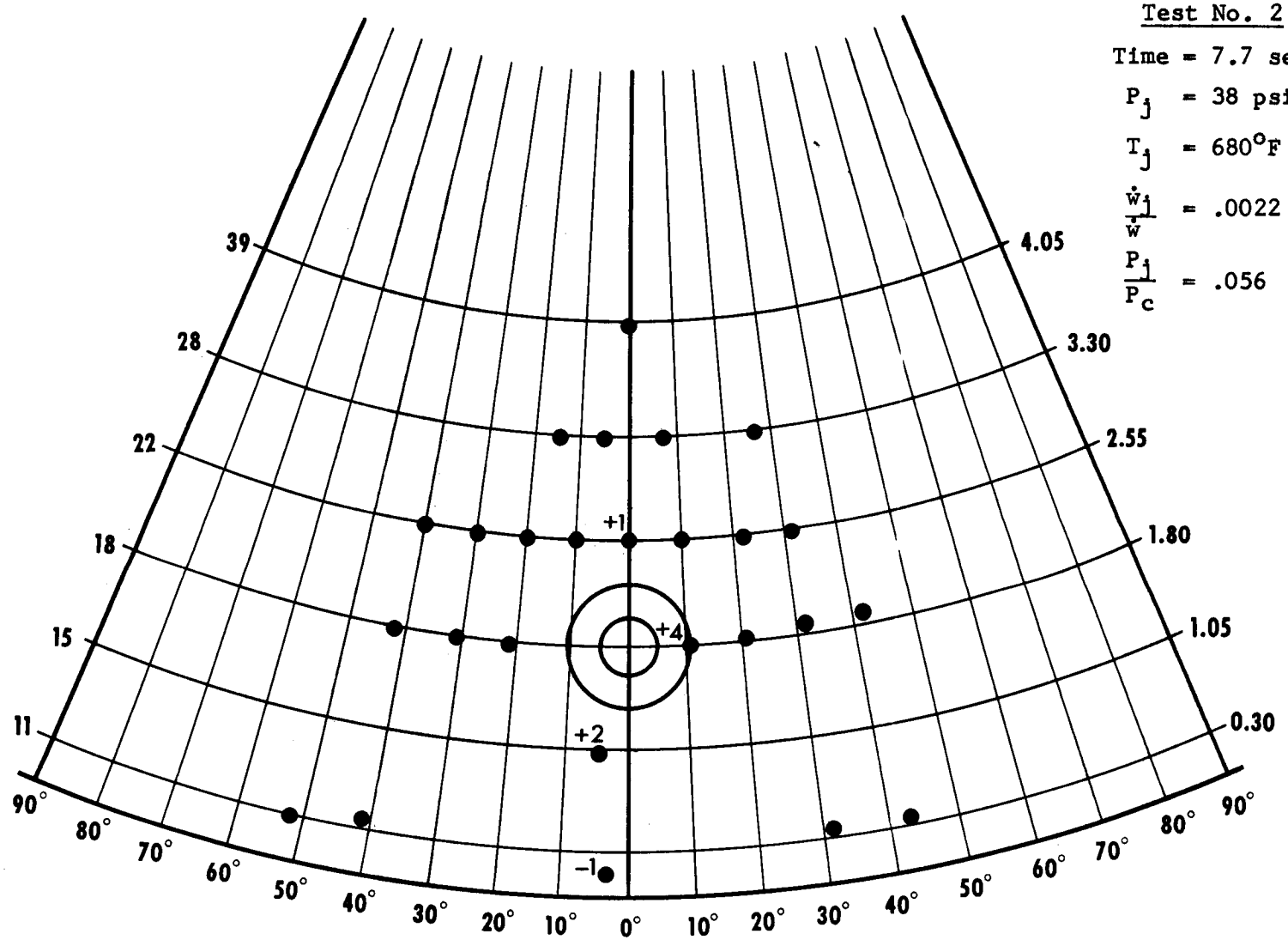
Test No. 2
Time = 7.7 secs.
P_j = 38 psia
T_j = 680°F
$\frac{\dot{w}_j}{\dot{w}}$ = .0022
$\frac{P_j}{P_c}$ = .056
39
28
22
18
15
11
4.05
3.30
2.55
1.80
1.05
0.30
+1
+4
+2
-1
90°
80°
70°
60°
50°
40°
30°
20°
10°
0°
10°
20°
30°
40°
50°
60°
70°
80°
90°

Figure 8.7

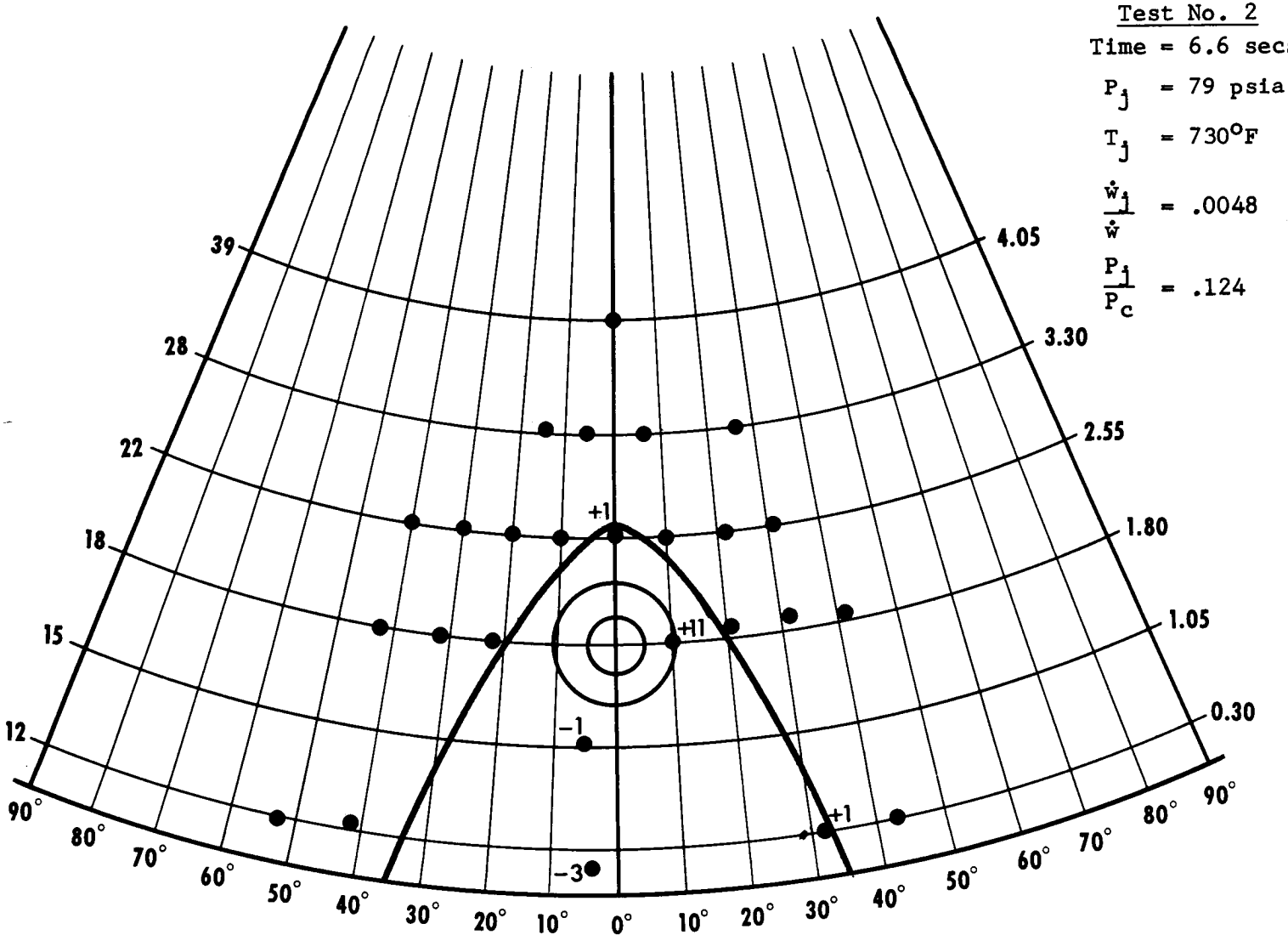
Test No. 2
Time = 6.6 secs.
P_j = 79 psia
T_j = 730°F
$\frac{\dot{w}_j}{\dot{w}}$ = .0048
$\frac{P_j}{P_c}$ = .124
39
28
22
18
15
12
4.05
3.30
2.55
1.80
1.05
0.30
+1
+11
-1
-3
+1
90°
80°
70°
60°
50°
40°
30°
20°
10°
0°
10°
20°
30°
40°
50°
60°
70°
80°
90°

Figure 8.8

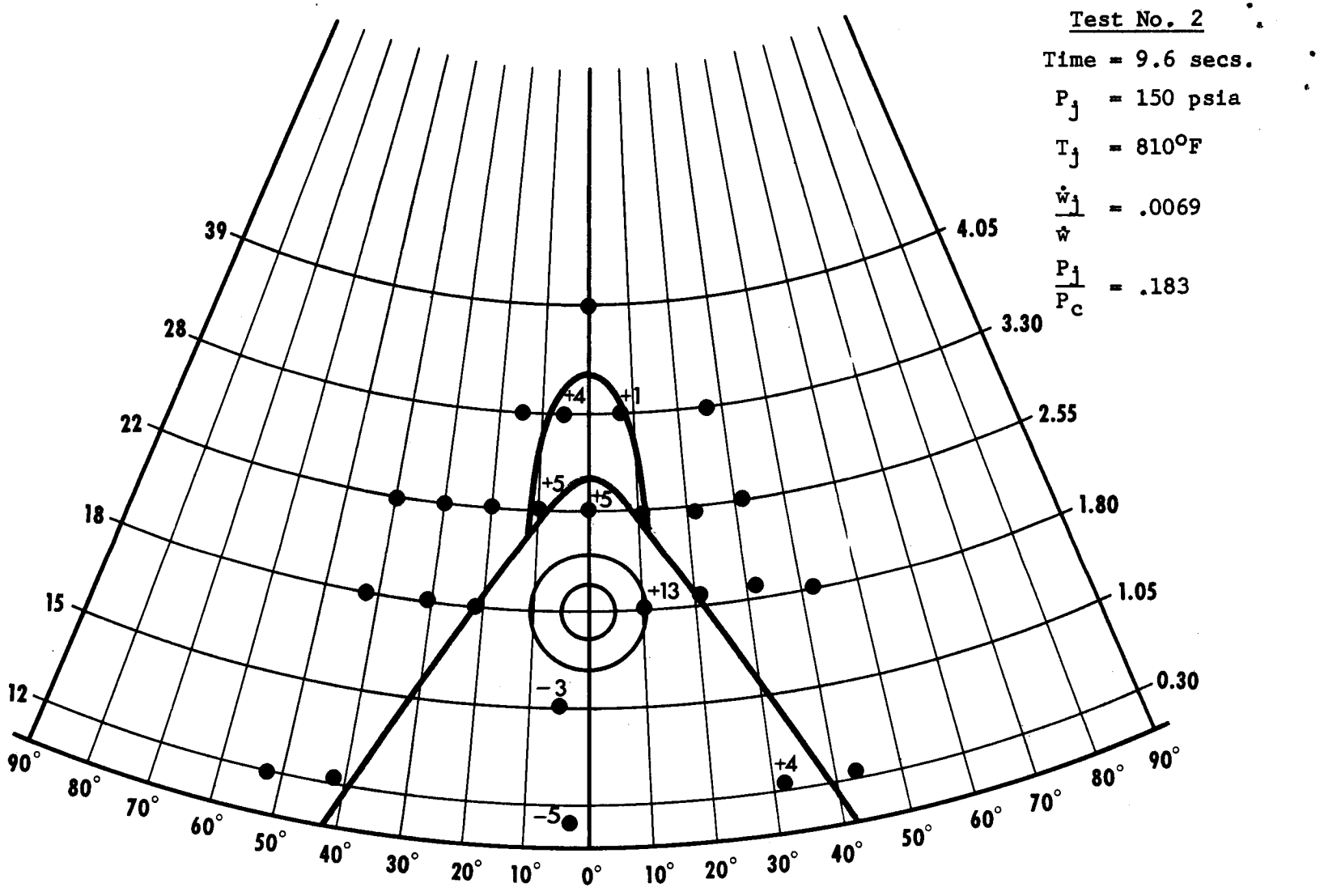
Test No. 2
Time = 9.6 secs.
P_j = 150 psia
T_j = 810°F
$\frac{\dot{w}_j}{\dot{w}}$ = .0069
$\frac{P_j}{P_c}$ = .183
39
28
22
18
15
12
4.05
3.30
2.55
1.80
1.05
0.30
+4
+1
+5
+5
+13
−3
+4
−5
90°
80°
70°
60°
50°
40°
30°
20°
10°
0°
10°
20°
30°
40°
50°
60°
70°
80°
90°

Figure 8.9

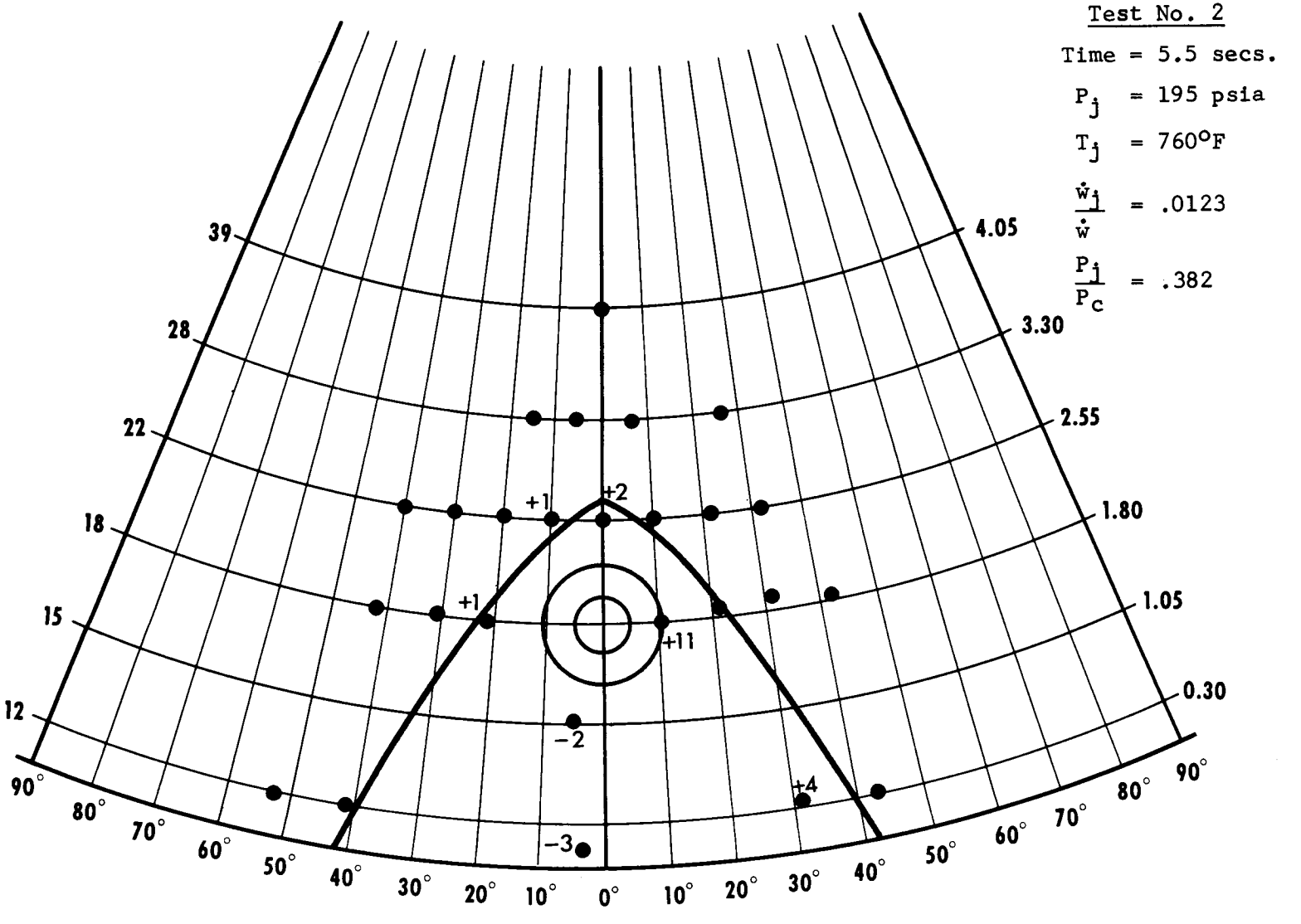
Test No. 2
Time = 5.5 secs.
P_j = 195 psia
T_j = 760°F
$\frac{\dot{w}_j}{\dot{w}}$ = .0123
$\frac{P_j}{P_c}$ = .382
39
28
22
18
15
12
4.05
3.30
2.55
1.80
1.05
0.30
+1
+2
+1
+11
−2
+4
−3
90°
80°
70°
60°
50°
40°
30°
20°
10°
0°
10°
20°
30°
40°
50°
60°
70°
80°
90°

Figure 8.10

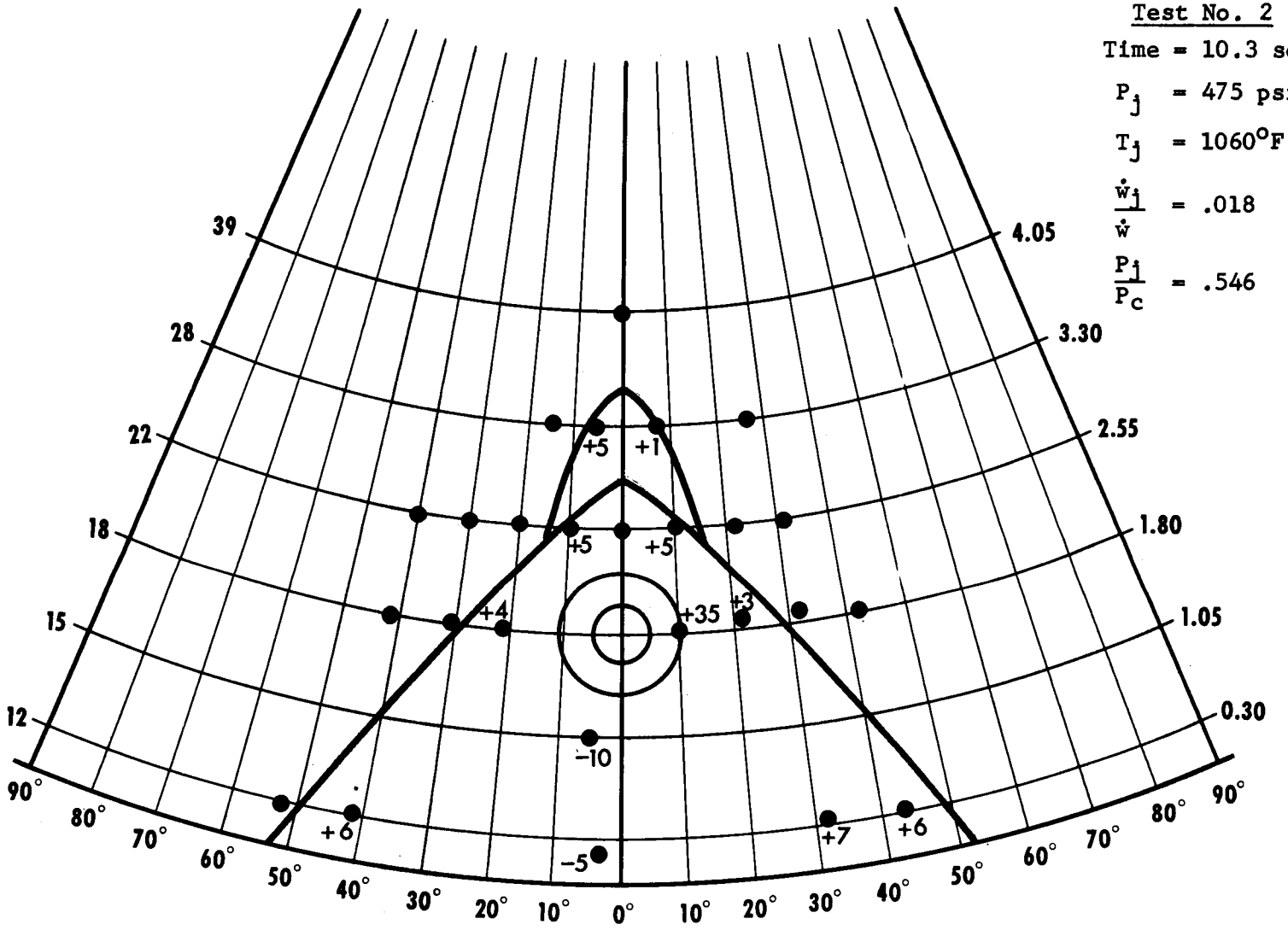
Test No. 2
Time = 10.3 secs.
P_j = 475 psia
T_j = 1060°F
$\frac{\dot{w}_j}{\dot{w}}$ = .018
$\frac{P_j}{P_c}$ = .546
39
28
22
18
15
12
4.05
3.30
2.55
1.80
1.05
0.30
90°
80°
70°
60°
50°
40°
30°
20°
10°
0°
+5
+1
+5
+5
+4
+35
+3
-10
+6
-5
+7
+6

Figure 8.11

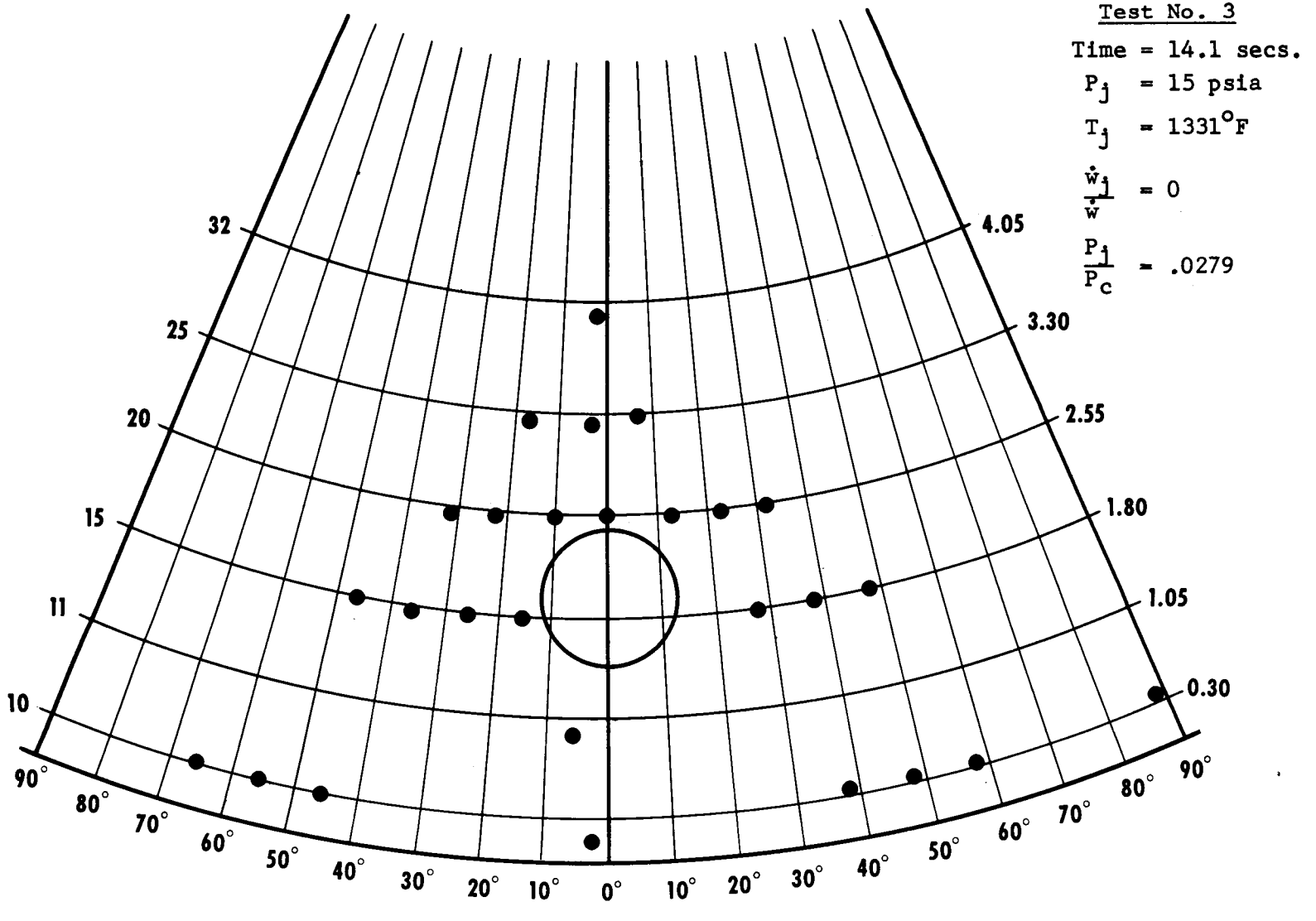
Test No. 3
Time = 14.1 secs.
P_j = 15 psia
T_j = 1331°F
$\frac{\dot{w}_j}{\dot{w}}$ = 0
$\frac{P_j}{P_c}$ = .0279
32
25
20
15
11
10
4.05
3.30
2.55
1.80
1.05
0.30
90° 80° 70° 60° 50° 40° 30° 20° 10° 0° 10° 20° 30° 40° 50° 60° 70° 80° 90°

Figure 8.12

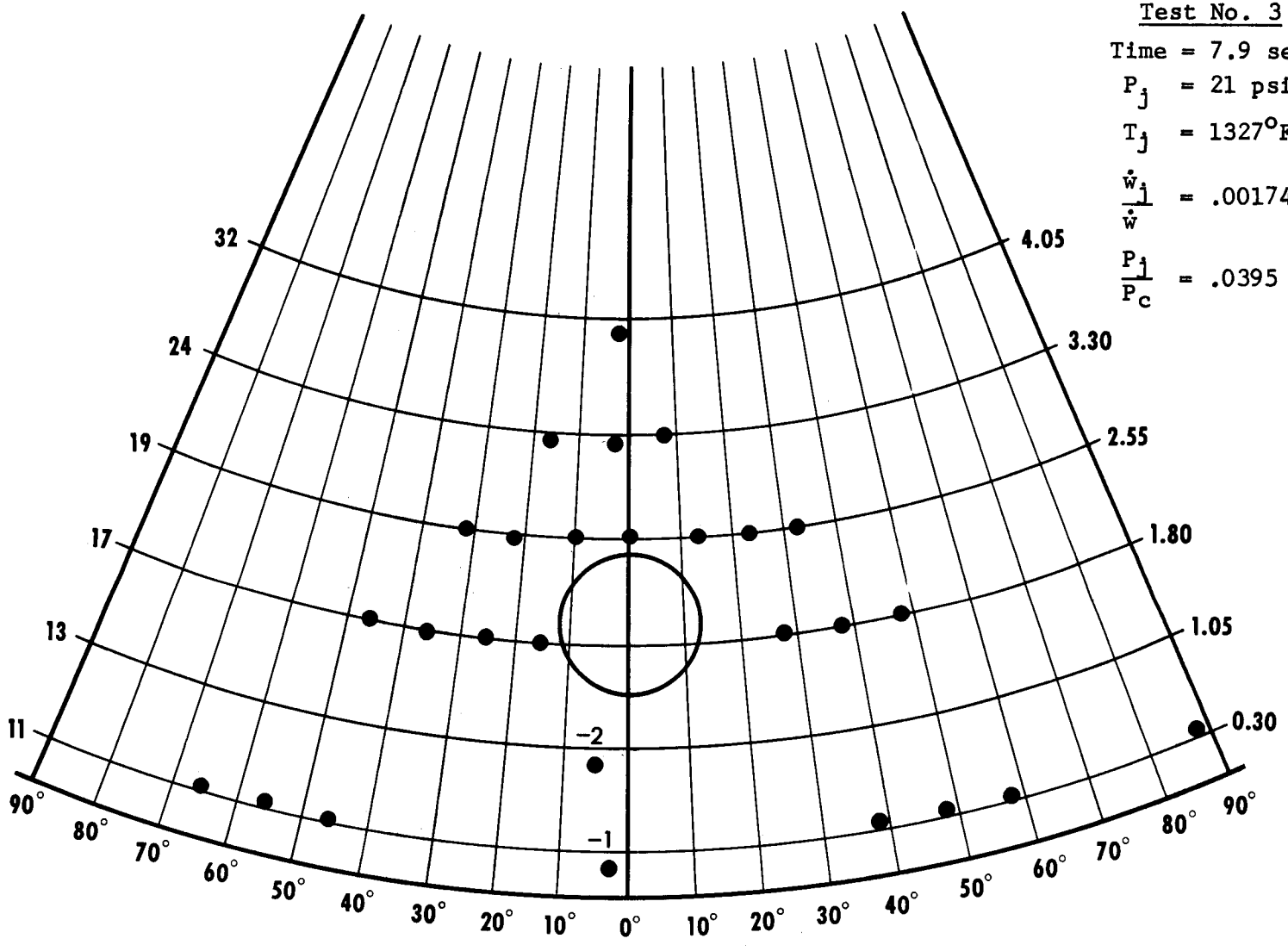
Test No. 3
Time = 7.9 secs.
P_j = 21 psia
T_j = 1327°F
$\frac{\dot{w}_j}{\dot{w}}$ = .00174
$\frac{P_j}{P_c}$ = .0395
32
24
19
17
13
11
4.05
3.30
2.55
1.80
1.05
0.30
-2
-1
90°
80°
70°
60°
50°
40°
30°
20°
10°
0°
10°
20°
30°
40°
50°
60°
70°
80°
90°

Figure 8.13

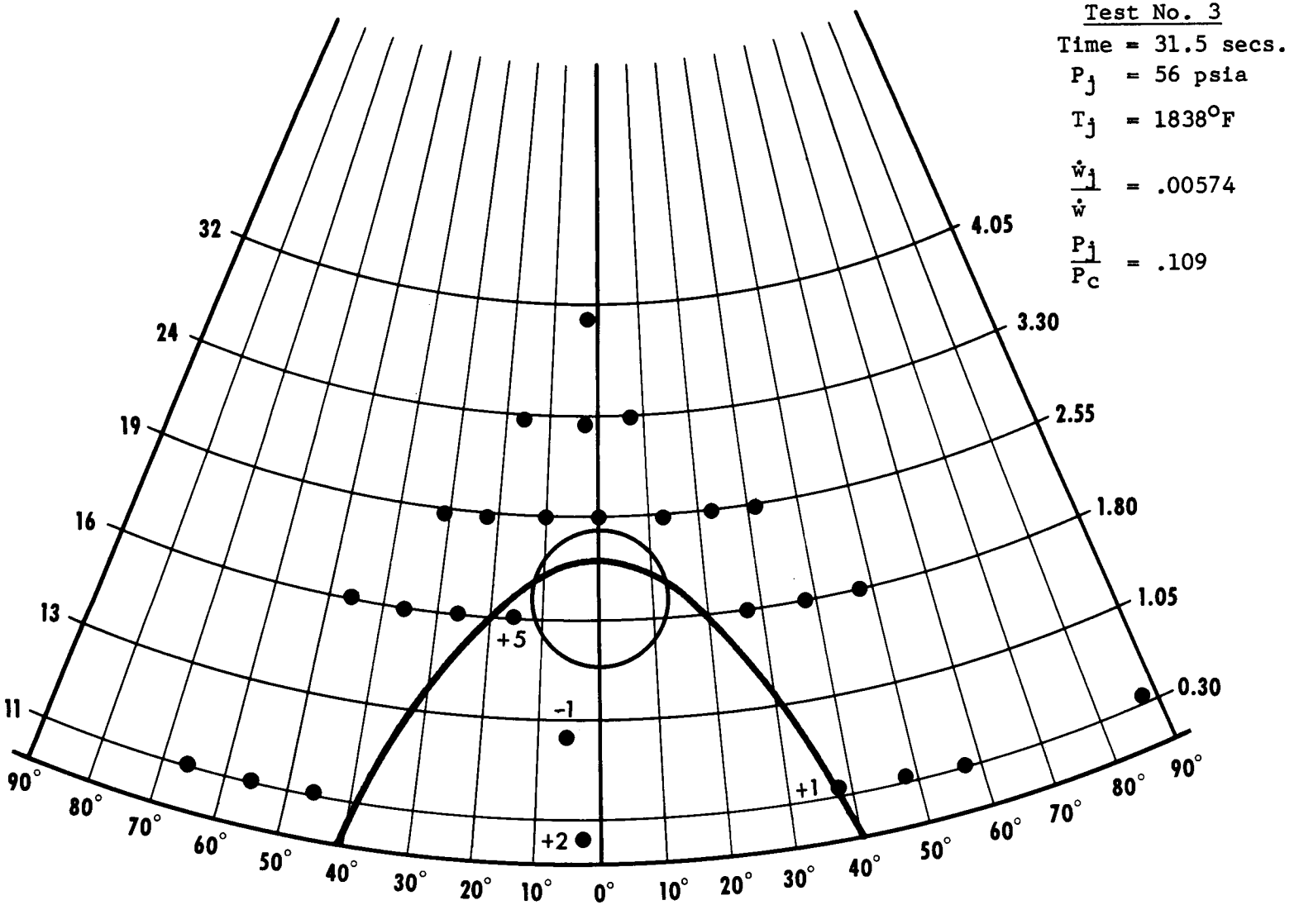
Test No. 3
Time = 31.5 secs.
P_j = 56 psia
T_j = 1838°F
$\frac{\dot{w}_j}{\dot{w}}$ = .00574
$\frac{P_j}{P_c}$ = .109
32
24
19
16
13
11
4.05
3.30
2.55
1.80
1.05
0.30
+5
-1
+1
+2
90°
80°
70°
60°
50°
40°
30°
20°
10°
0°
10°
20°
30°
40°
50°
60°
70°
80°
90°

Figure 8.14

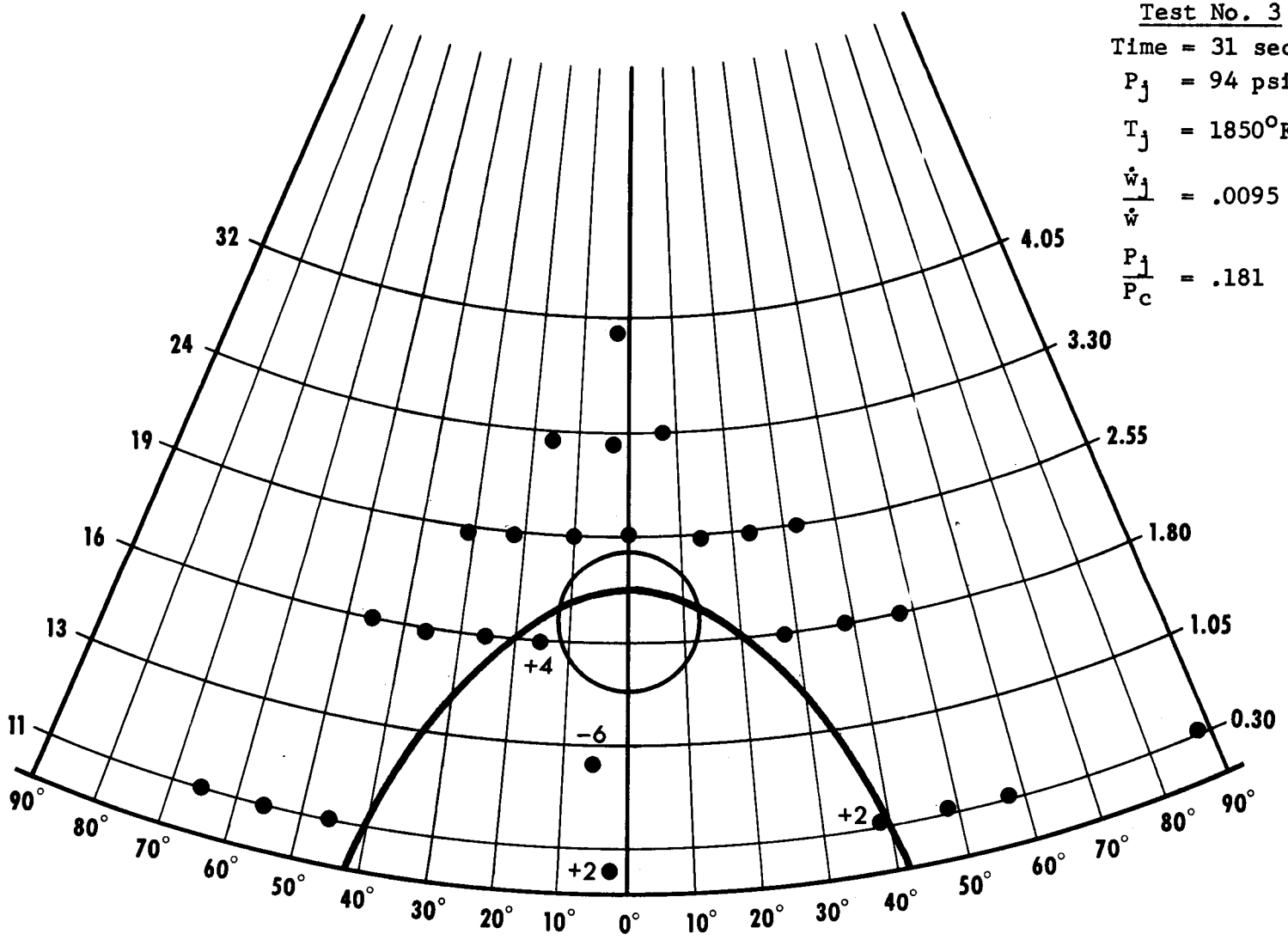
Test No. 3
Time = 31 secs.
P_j = 94 psia
T_j = 1850°F
$\frac{\dot{w}_j}{\dot{w}}$ = .0095
$\frac{P_j}{P_c}$ = .181
32
24
19
16
13
11
4.05
3.30
2.55
1.80
1.05
0.30
+4
-6
+2
+2
90°
80°
70°
60°
50°
40°
30°
20°
10°
0°
10°
20°
30°
40°
50°
60°
70°
80°
90°

Figure 8.15

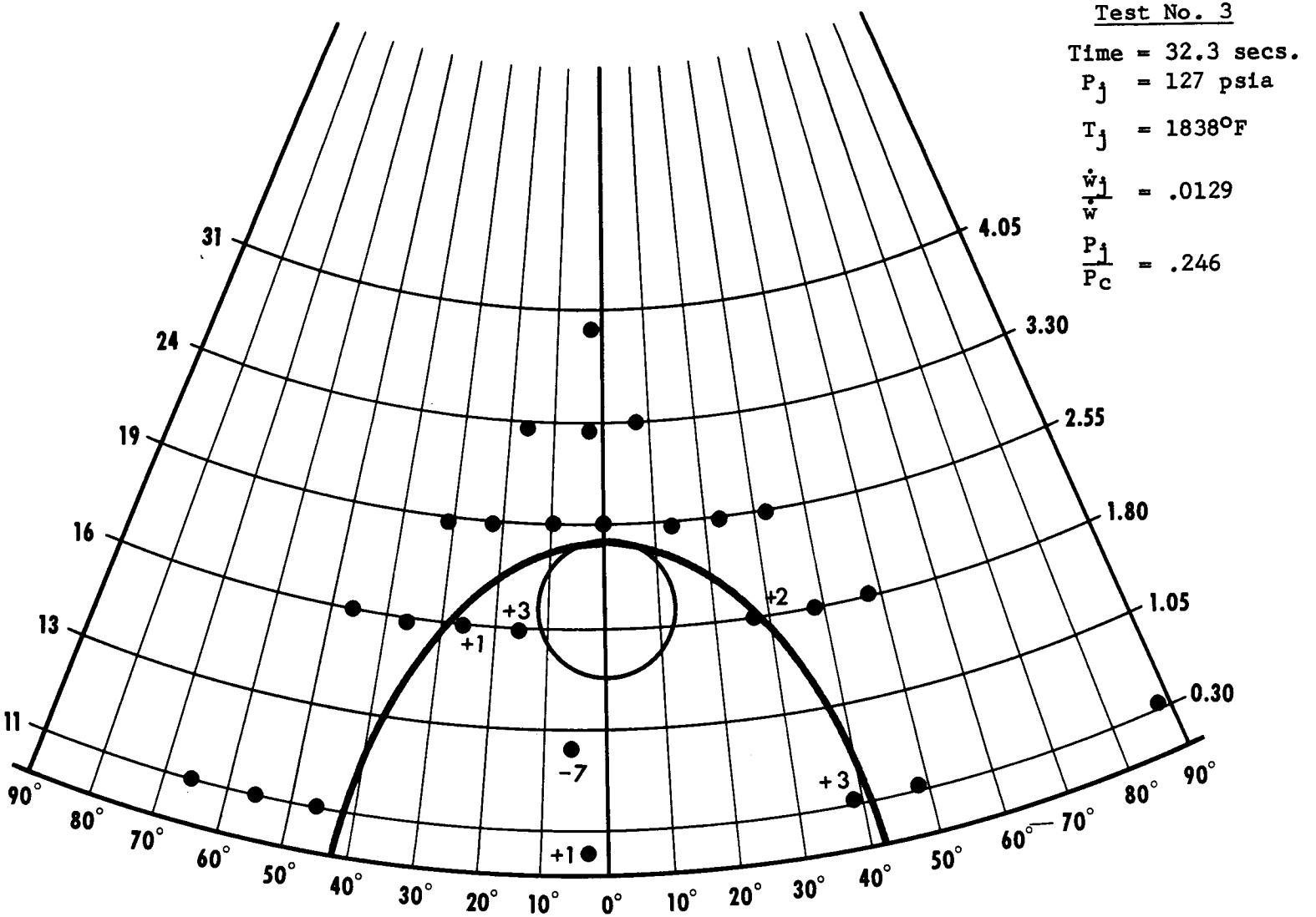
Test No. 3
Time = 32.3 secs.
P_j = 127 psia
T_j = 1838°F
$\frac{\dot{w}_j}{\dot{w}}$ = .0129
$\frac{P_j}{P_c}$ = .246
31
24
19
16
13
11
4.05
3.30
2.55
1.80
1.05
0.30
90°
80°
70°
60°
50°
40°
30°
20°
10°
0°
10°
20°
30°
40°
50°
60°
70°
80°
90°
+3
+1
+2
-7
+3
+1

Figure 8.16

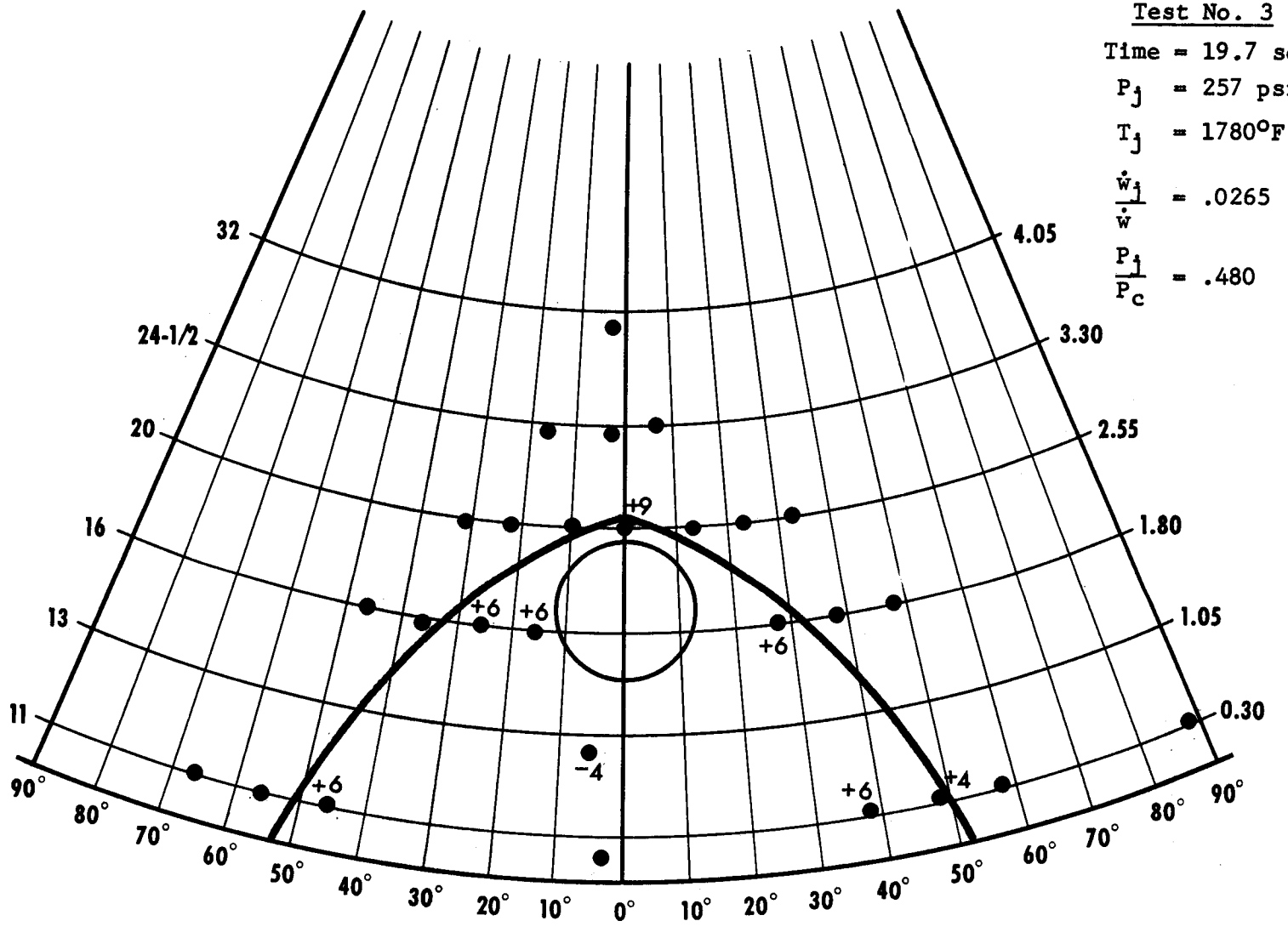
Test No. 3
Time = 19.7 secs.
P_j = 257 psia
T_j = 1780°F
$\frac{\dot{w}_j}{\dot{w}}$ = .0265
$\frac{P_j}{P_c}$ = .480
32
24-1/2
20
16
13
11
4.05
3.30
2.55
1.80
1.05
0.30
+9
+6
+6
+6
+6
+6
+4
-4
90°
80°
70°
60°
50°
40°
30°
20°
10°
0°
10°
20°
30°
40°
50°
60°
70°
80°
90°

Figure 8.17

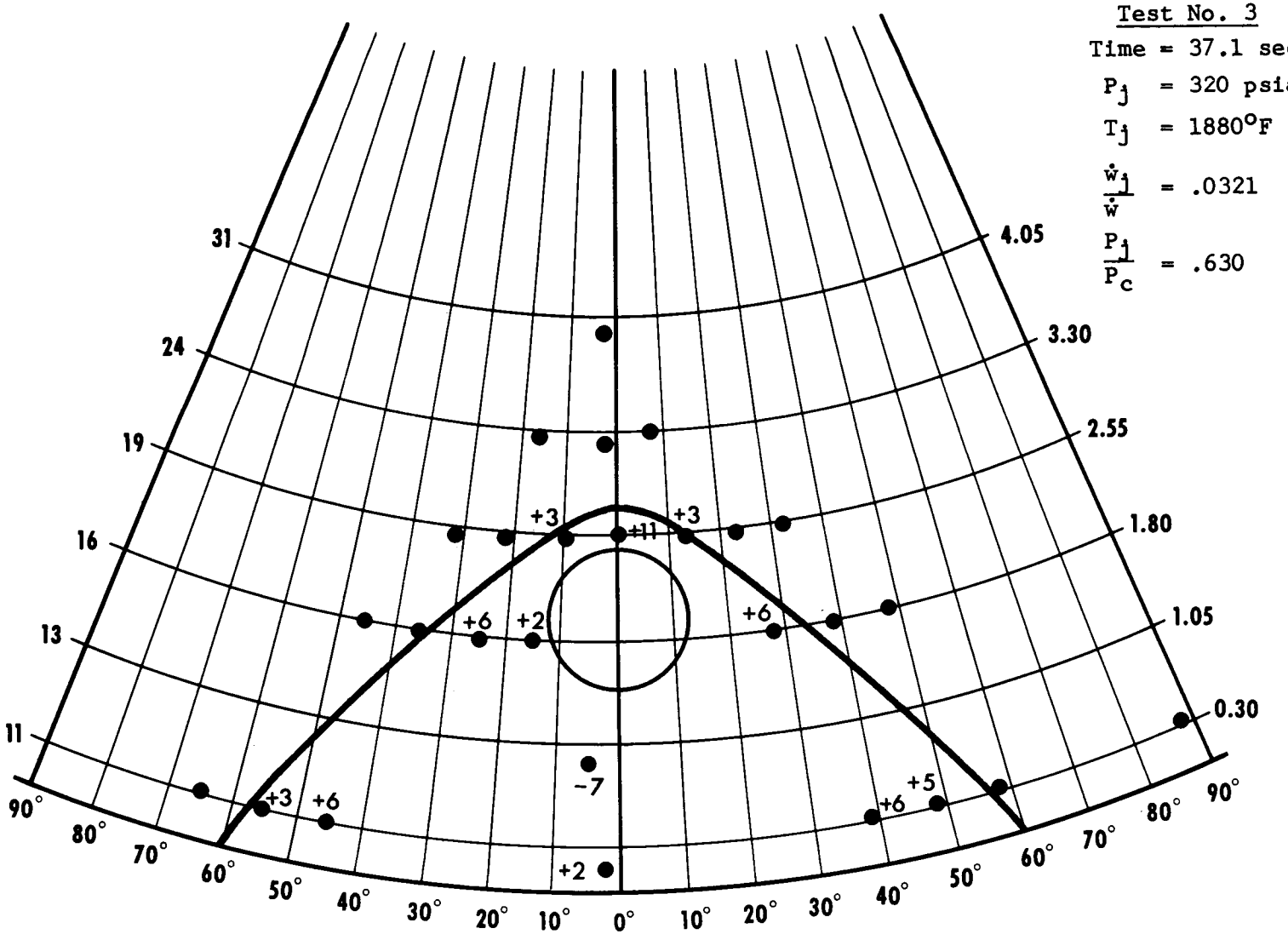
Test No. 3
Time = 37.1 secs.
P_j = 320 psia
T_j = 1880°F
$\frac{\dot{w}_j}{\dot{w}}$ = .0321
$\frac{P_j}{P_c}$ = .630
31
24
19
16
13
11
4.05
3.30
2.55
1.80
1.05
0.30
+3
+3
+11
+6
+2
+6
+3
+6
-7
+2
+6
+5
90°
80°
70°
60°
50°
40°
30°
20°
10°
0°
10°
20°
30°
40°
50°
60°
70°
80°
90°

Figure 8.18

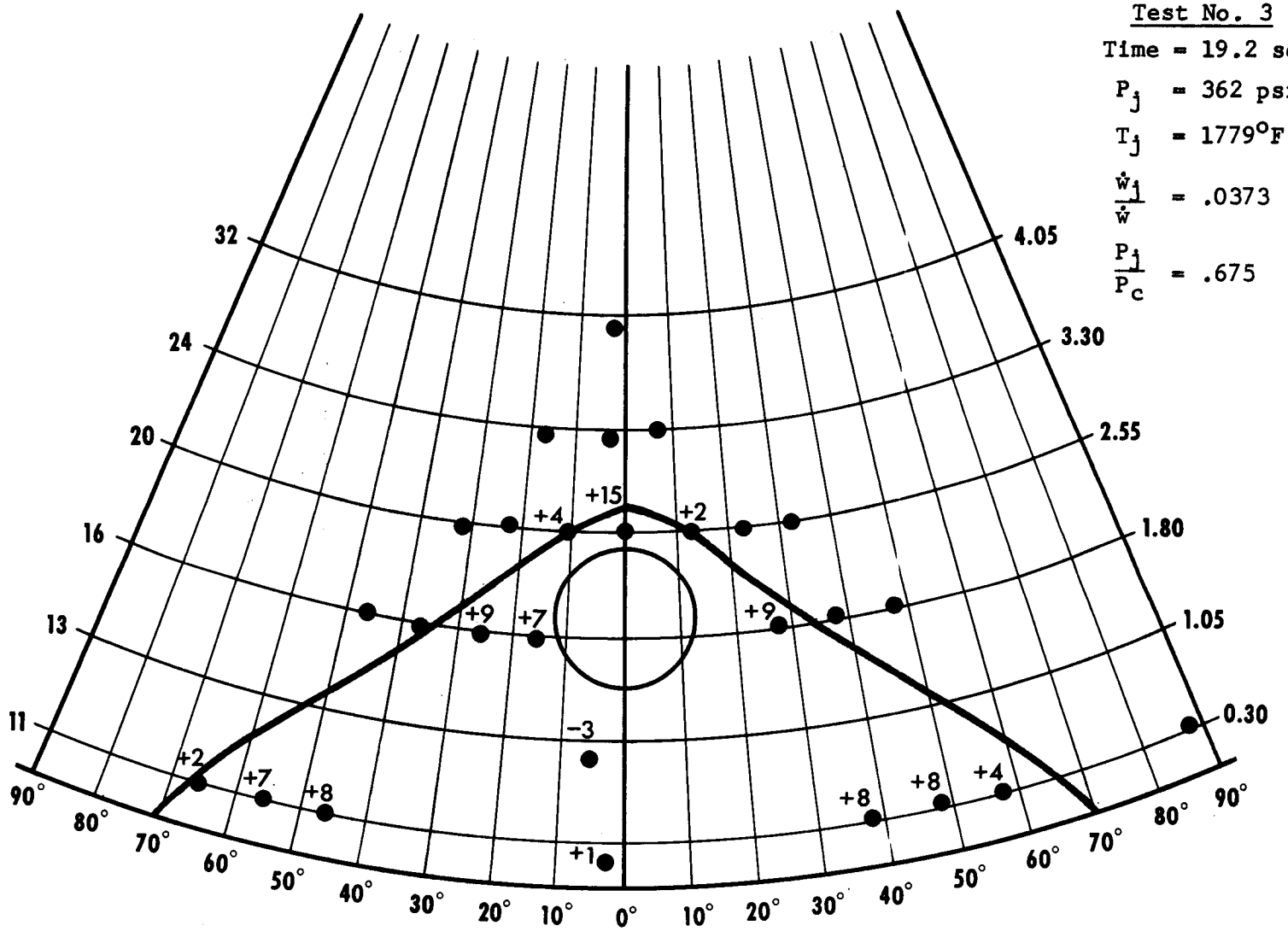
Test No. 3
Time = 19.2 secs.
P_j = 362 psia
T_j = 1779°F
$\frac{\dot{w}_j}{\dot{w}}$ = .0373
$\frac{P_j}{P_c}$ = .675
32
24
20
16
13
11
4.05
3.30
2.55
1.80
1.05
0.30
+15
+4
+2
+9
+7
+9
-3
+2
+7
+8
+8
+8
+4
+1
90°
80°
70°
60°
50°
40°
30°
20°
10°
0°
10°
20°
30°
40°
50°
60°
70°
80°
90°

Figure 8.19

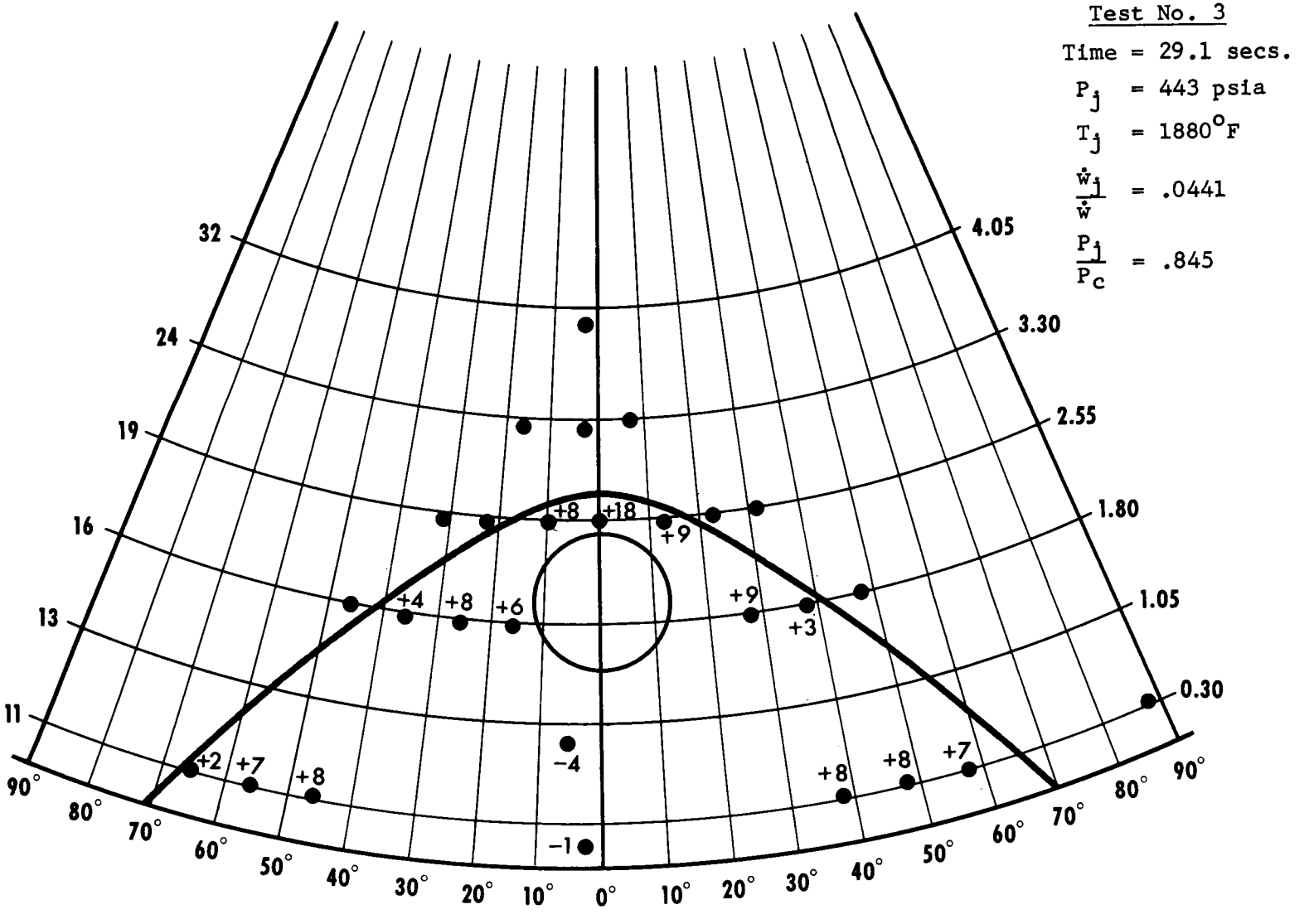
Test No. 3
Time = 29.1 secs.
P_j = 443 psia
T_j = 1880°F
$\frac{\dot{w}_j}{\dot{w}}$ = .0441
$\frac{P_j}{P_c}$ = .845
32
24
19
16
13
11
4.05
3.30
2.55
1.80
1.05
0.30
+8
+18
+9
+4
+8
+6
+9
+3
+2
+7
+8
-4
-1
+8
+8
+7
90°
80°
70°
60°
50°
40°
30°
20°
10°
0°
10°
20°
30°
40°
50°
60°
70°
80°
90°

Figure 8.20

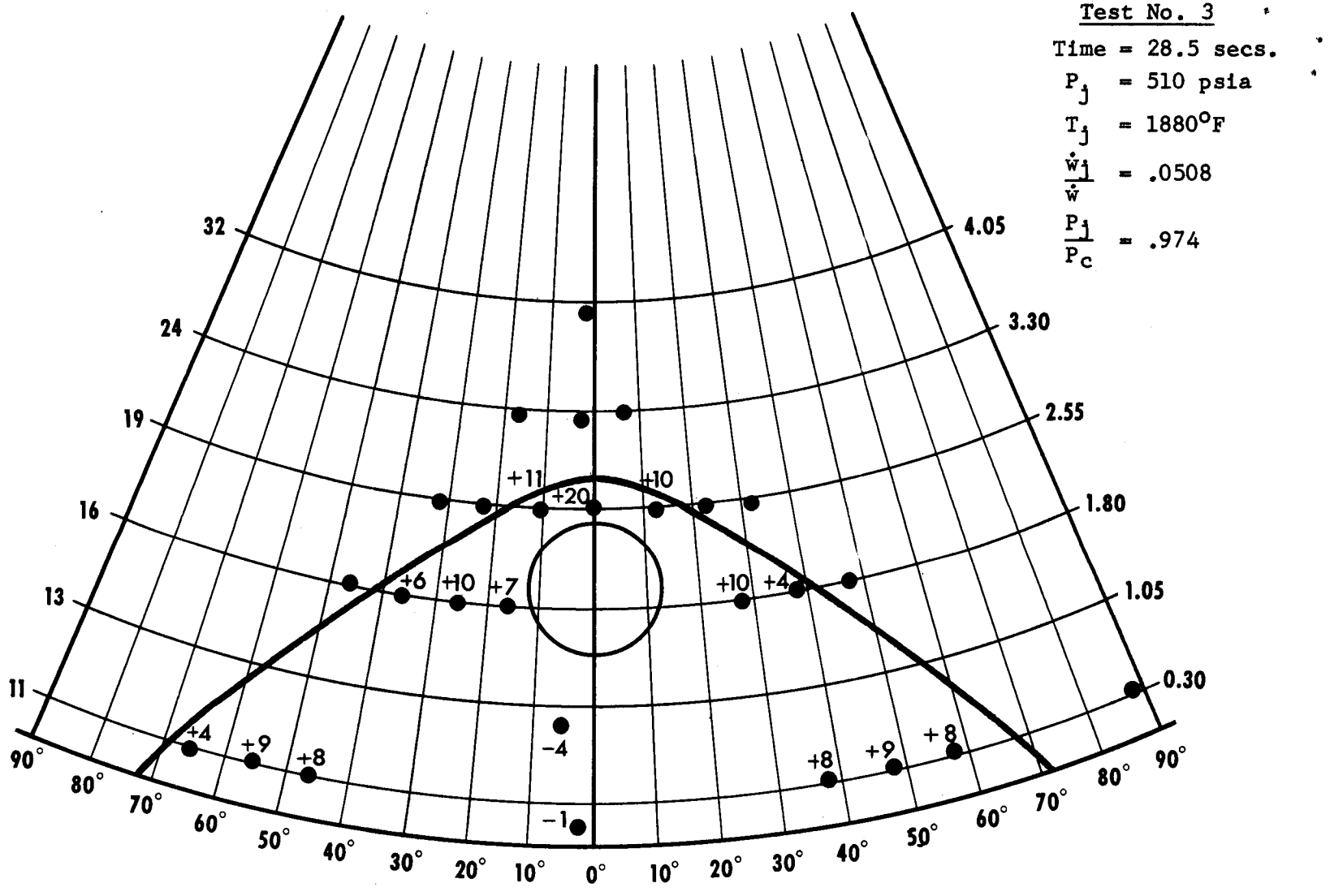
Test No. 3
Time = 28.5 secs.
P_j = 510 psia
T_j = 1880°F
$\frac{\dot{w}_j}{\dot{w}}$ = .0508
$\frac{P_j}{P_c}$ = .974
32
24
19
16
13
11
4.05
3.30
2.55
1.80
1.05
0.30
+11
+20
+10
+6
+10
+7
+10
+4
+4
+9
+8
-4
-1
+8
+9
+8
90°
80°
70°
60°
50°
40°
30°
20°
10°
0°
10°
20°
30°
40°
50°
60°
70°
80°
90°

Figure 8.21

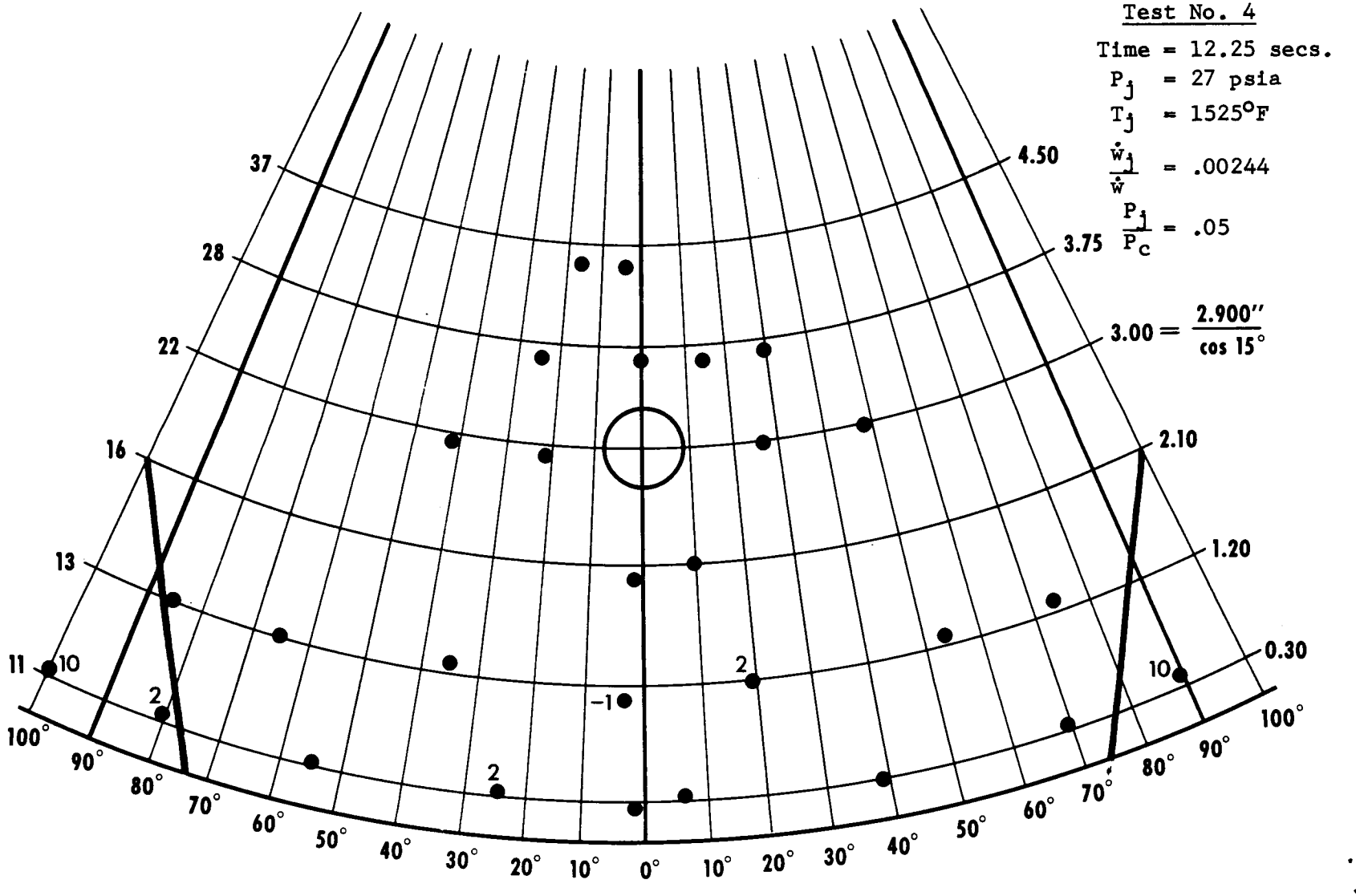
Test No. 4
Time = 12.25 secs.
P_j = 27 psia
T_j = 1525°F
$\frac{\dot{w}_j}{\dot{w}}$ = .00244
$\frac{P_j}{P_c}$ = .05
3.00 = 2.900" / cos 15°
37
28
22
16
13
11
10
2
100°
90°
80°
70°
60°
50°
40°
30°
20°
10°
0°
4.50
3.75
2.10
1.20
0.30
-1
2
2
10

Figure 8.22

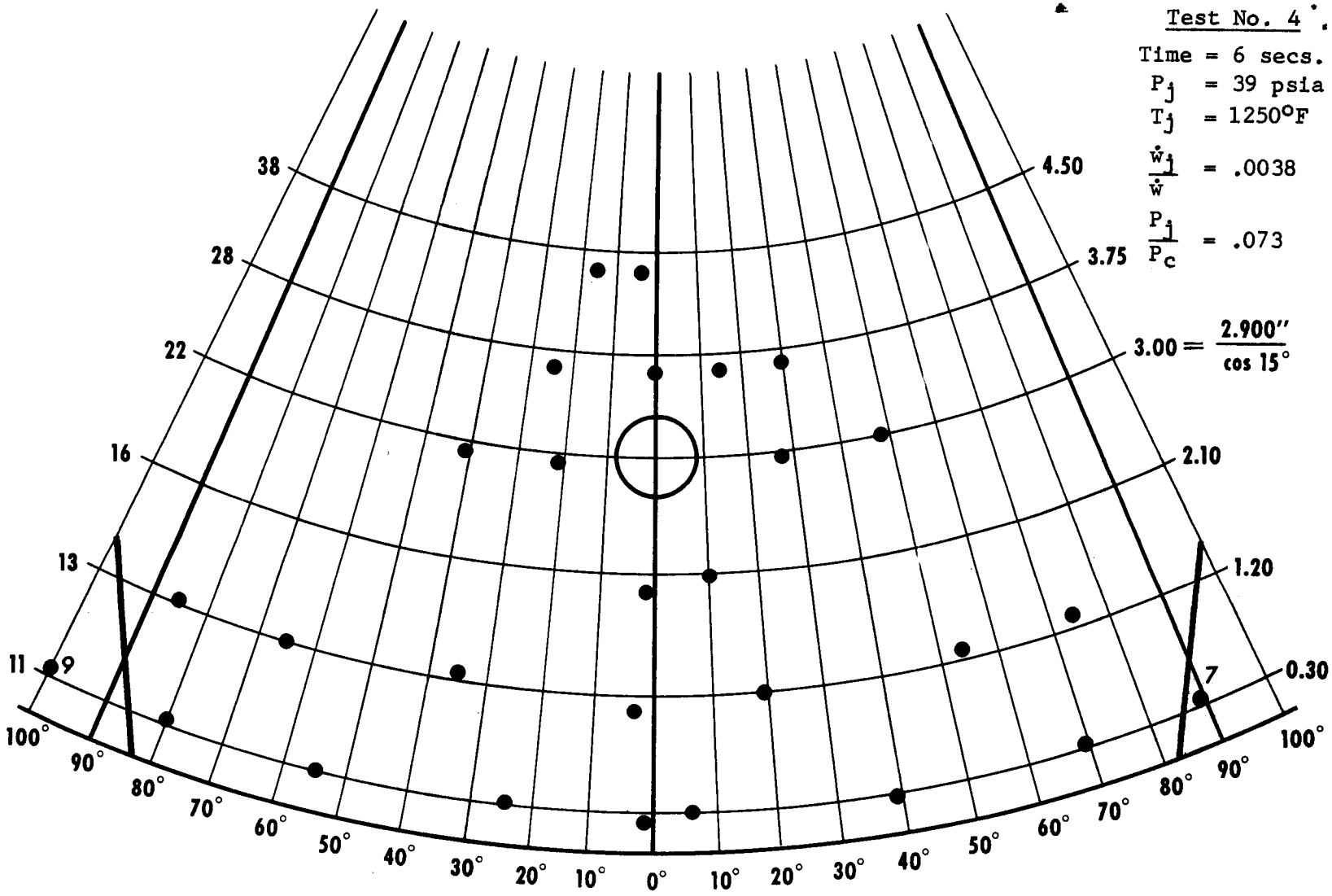
Test No. 4
Time = 6 secs.
P_j = 39 psia
T_j = 1250°F
$\frac{\dot{w}_j}{\dot{w}}$ = .0038
$\frac{P_j}{P_c}$ = .073
38
28
22
16
13
11
9
7
4.50
3.75
3.00 = 2.900" / cos 15°
2.10
1.20
0.30
100°
90°
80°
70°
60°
50°
40°
30°
20°
10°
0°
10°
20°
30°
40°
50°
60°
70°
80°
90°
100°

Figure 8.23

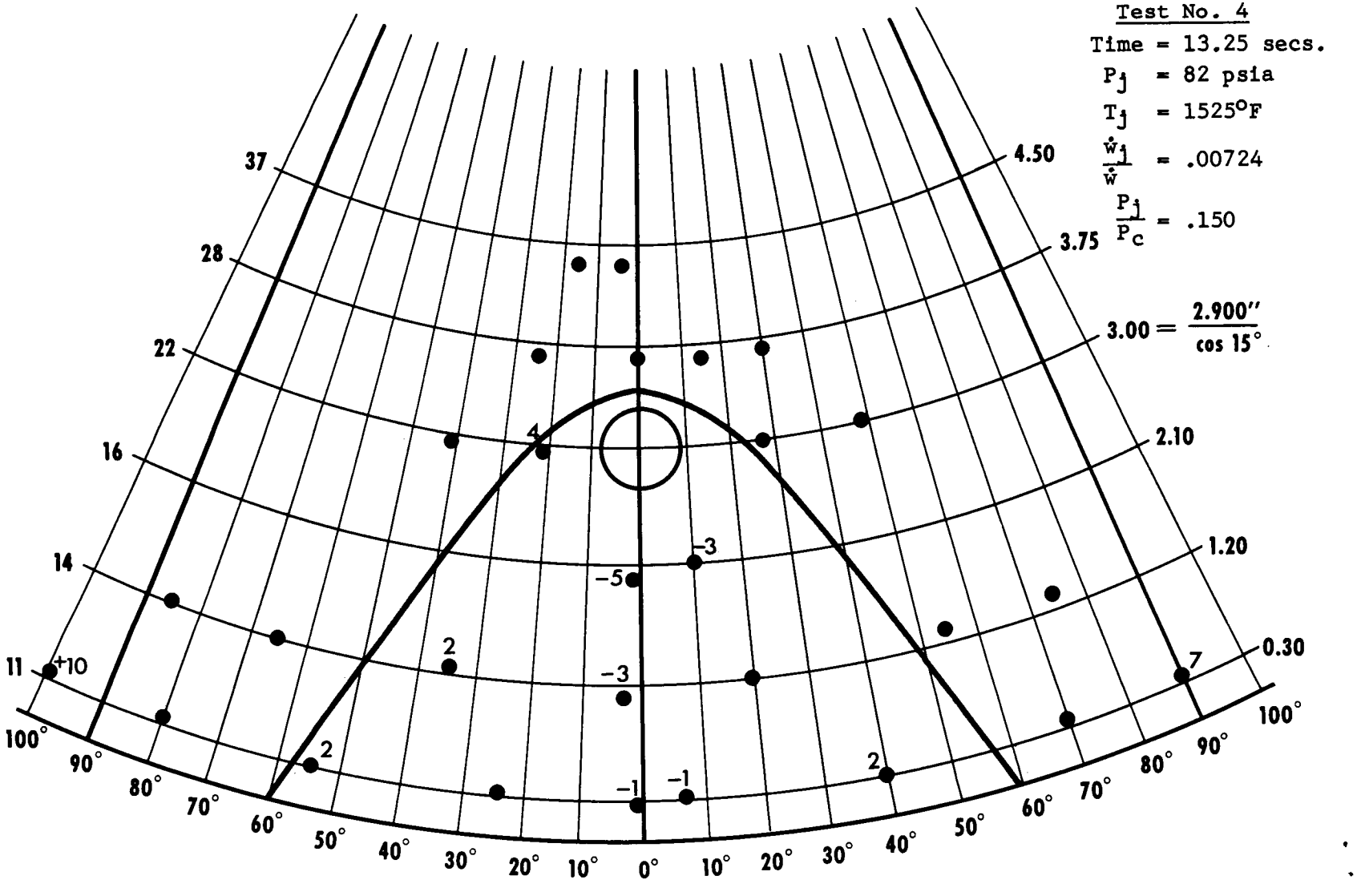
Test No. 4
Time = 13.25 secs.
P_j = 82 psia
T_j = 1525°F
$\frac{\dot{w}_j}{\dot{w}}$ = .00724
$\frac{P_j}{P_c}$ = .150
3.00 = 2.900" / cos 15°
4.50
3.75
2.10
1.20
0.30
37
28
22
16
14
11
+10
7
4
-5
-3
2
-3
2
2
-1
-1
100°
90°
80°
70°
60°
50°
40°
30°
20°
10°
0°
10°
20°
30°
40°
50°
60°
70°
80°
90°
100°

Figure 8.24

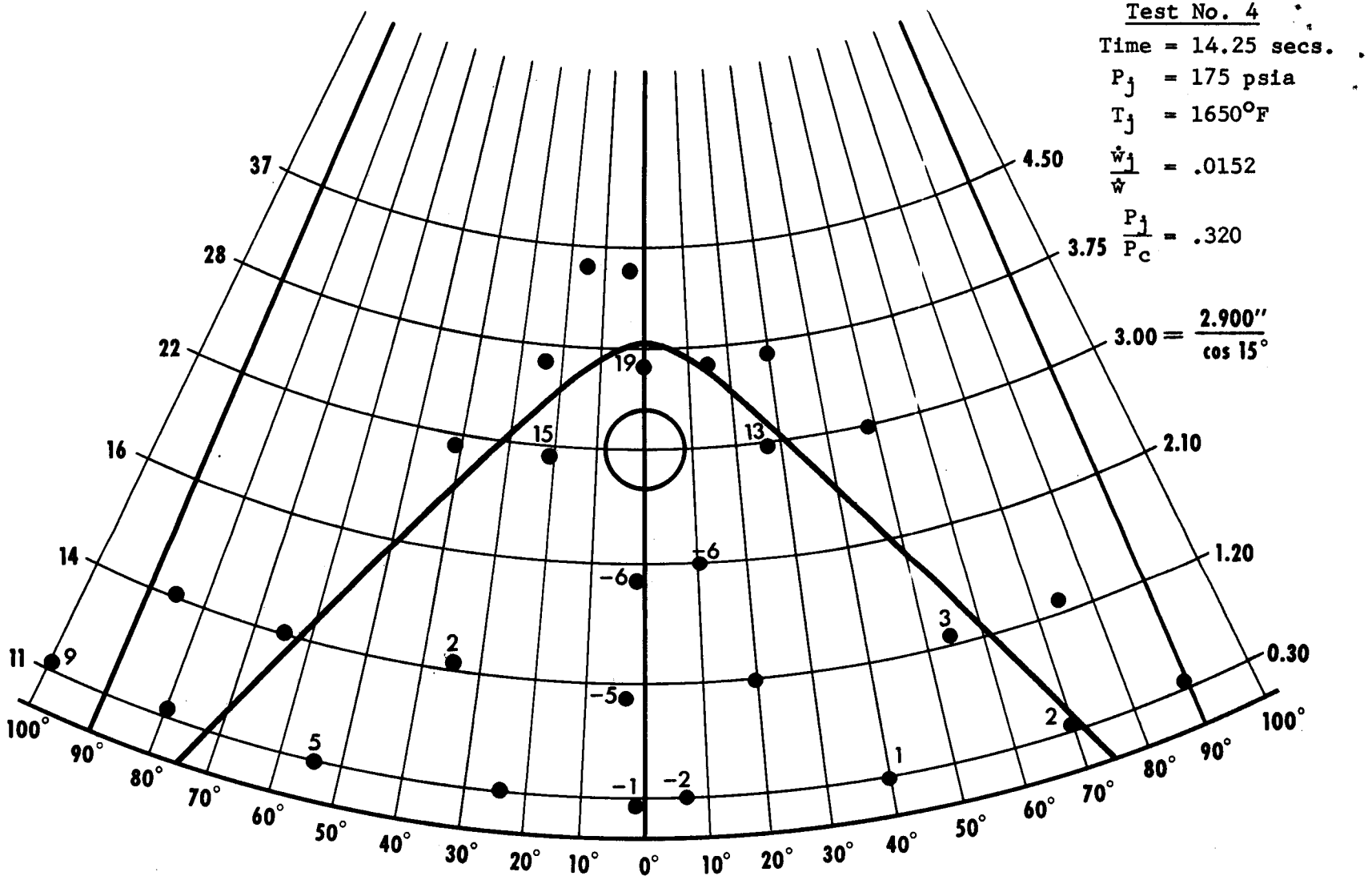
Test No. 4
Time = 14.25 secs.
P_j = 175 psia
T_j = 1650°F
$\frac{\dot{w}_j}{\dot{w}}$ = .0152
$\frac{P_j}{P_c}$ = .320
4.50
3.75
3.00 = 2.900" / cos 15°
2.10
1.20
0.30
37
28
22
16
14
11
9
19
15
13
-6
-6
3
2
-5
2
5
1
-1
-2
100°
90°
80°
70°
60°
50°
40°
30°
20°
10°
0°
10°
20°
30°
40°
50°
60°
70°
80°
90°
100°

Figure 8.25

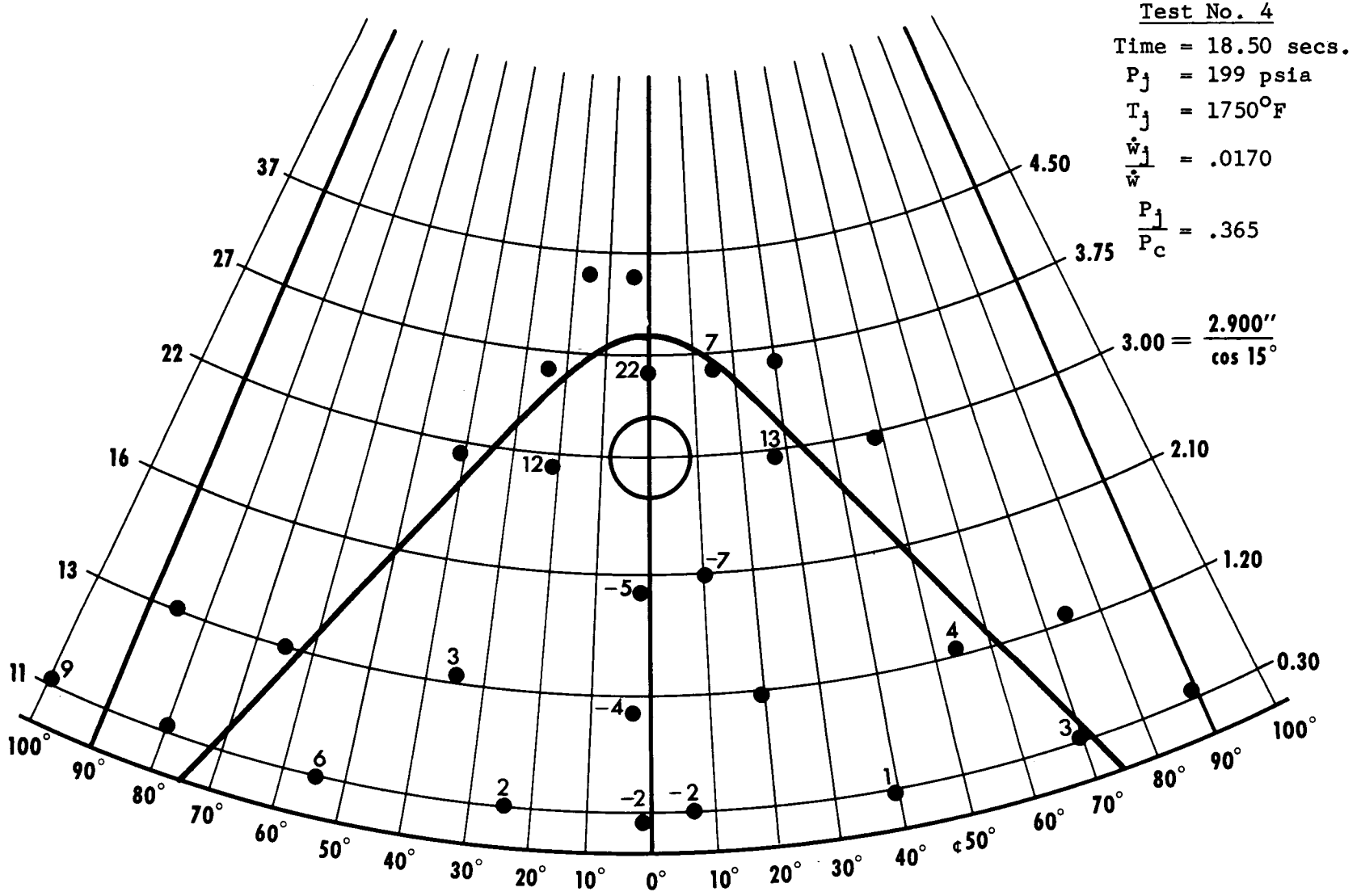
Test No. 4
Time = 18.50 secs.
P_j = 199 psia
T_j = 1750°F
$\frac{\dot{w}_j}{\dot{w}}$ = .0170
$\frac{P_j}{P_c}$ = .365
3.00 = 2.900" / cos 15°
37
27
22
16
13
11
4.50
3.75
2.10
1.20
0.30
100°
90°
80°
70°
60°
50°
40°
30°
20°
10°
0°
22
12
7
13
-7
-5
3
-4
9
6
2
-2
-2
4
3
1

Figure 8.26

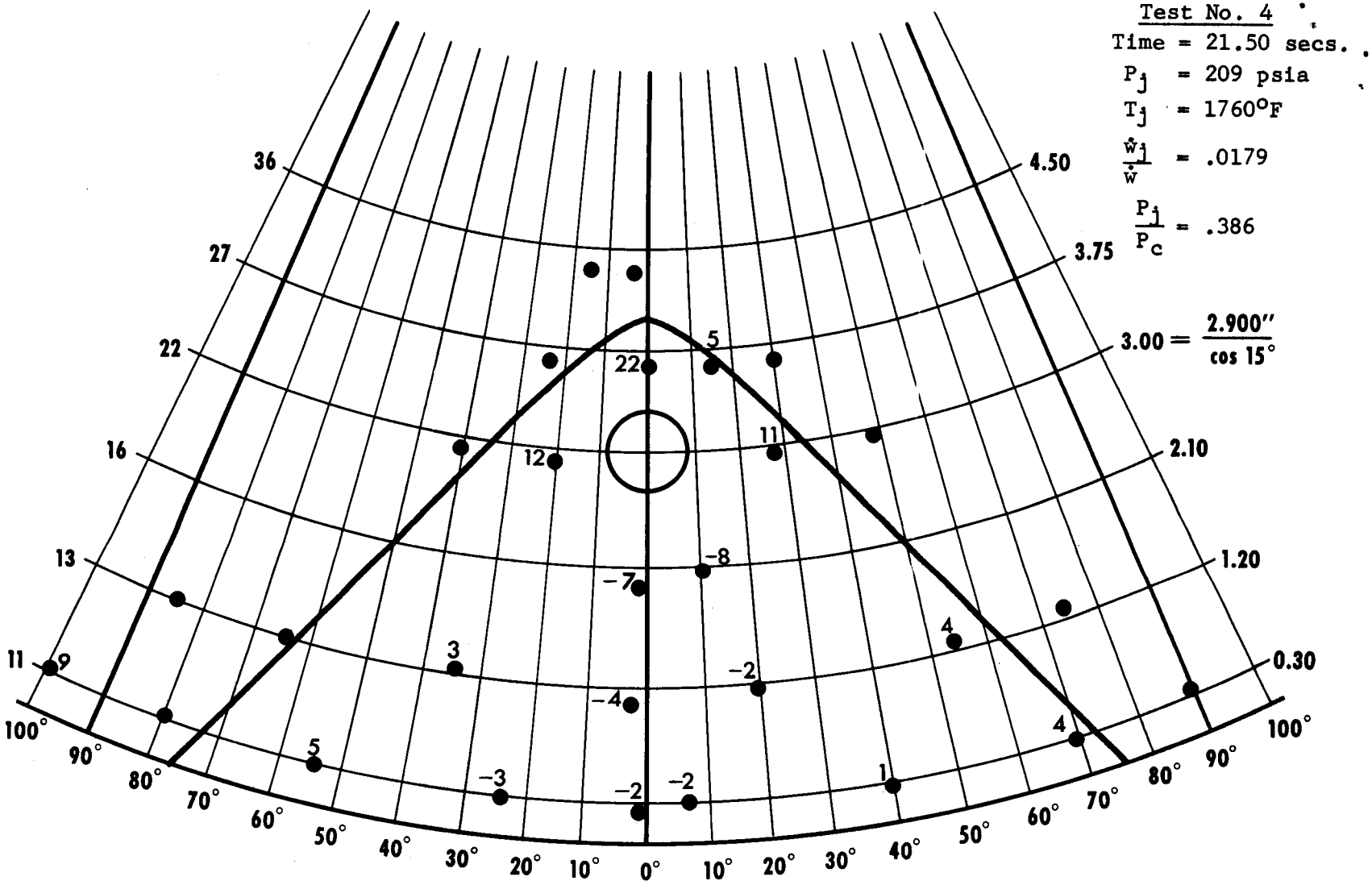
Test No. 4
Time = 21.50 secs.
P_j = 209 psia
T_j = 1760°F
$\frac{\dot{W}_j}{\dot{W}}$ = .0179
$\frac{P_j}{P_c}$ = .386
4.50
3.75
3.00 = 2.900" / cos 15°
2.10
1.20
0.30
36
27
22
16
13
11
100°
90°
80°
70°
60°
50°
40°
30°
20°
10°
0°
10°
20°
30°
40°
50°
60°
70°
80°
90°
100°
22
12
11
-8
-7
4
3
-2
-4
5
-3
-2
-2
1
4
9
5

Figure 8.27

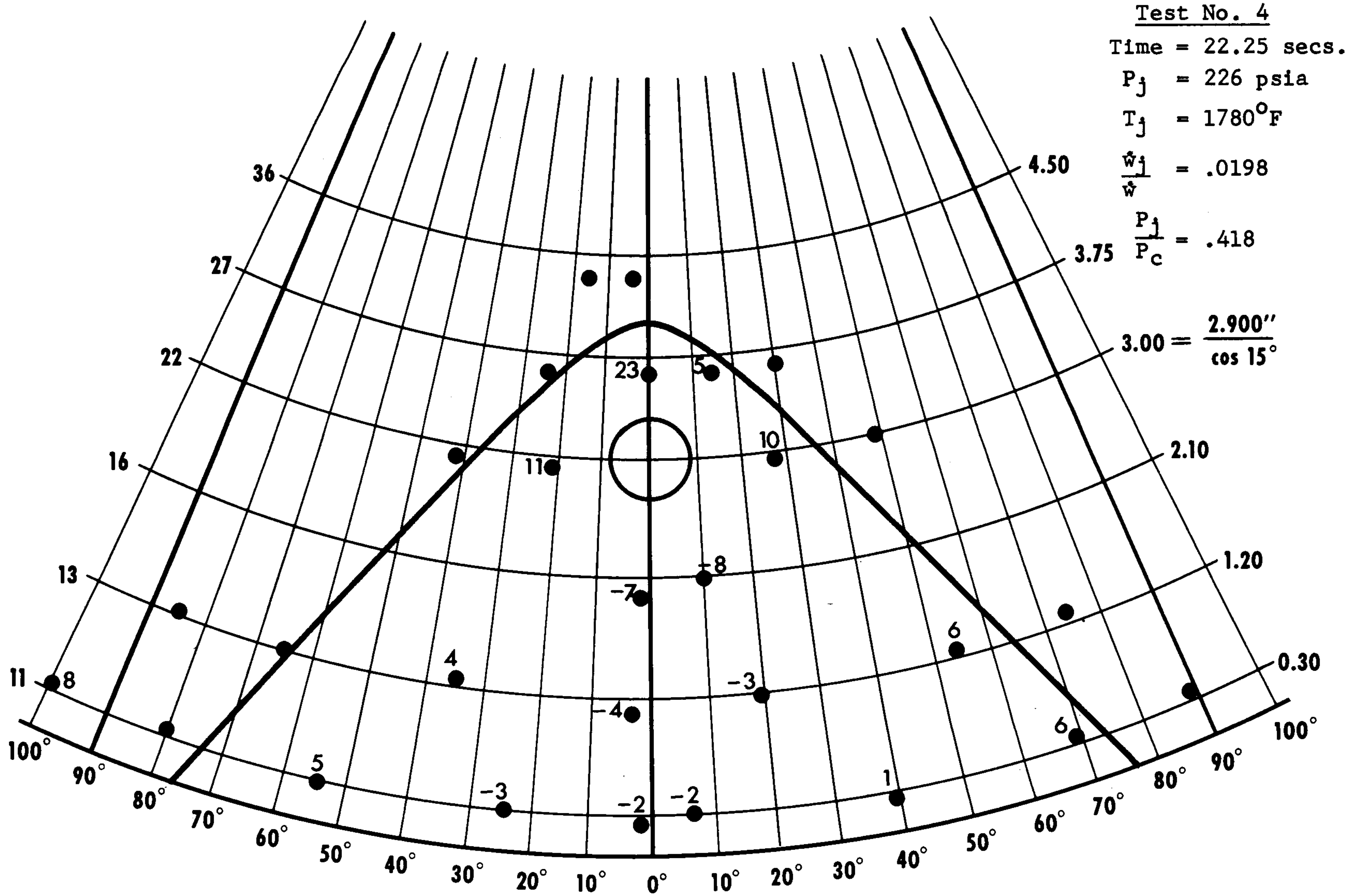

Test No. 4
Time = 22.25 secs.
P_j = 226 psia
T_j = 1780°F
$\dot{w}_j / \dot{w}$ = .0198
P_j / P_c = .418
3.00 = 2.900″ / cos 15°
4.50
3.75
2.10
1.20
0.30
36
27
22
16
13
11
100°
90°
80°
70°
60°
50°
40°
30°
20°
10°
0°

Figure 8.28

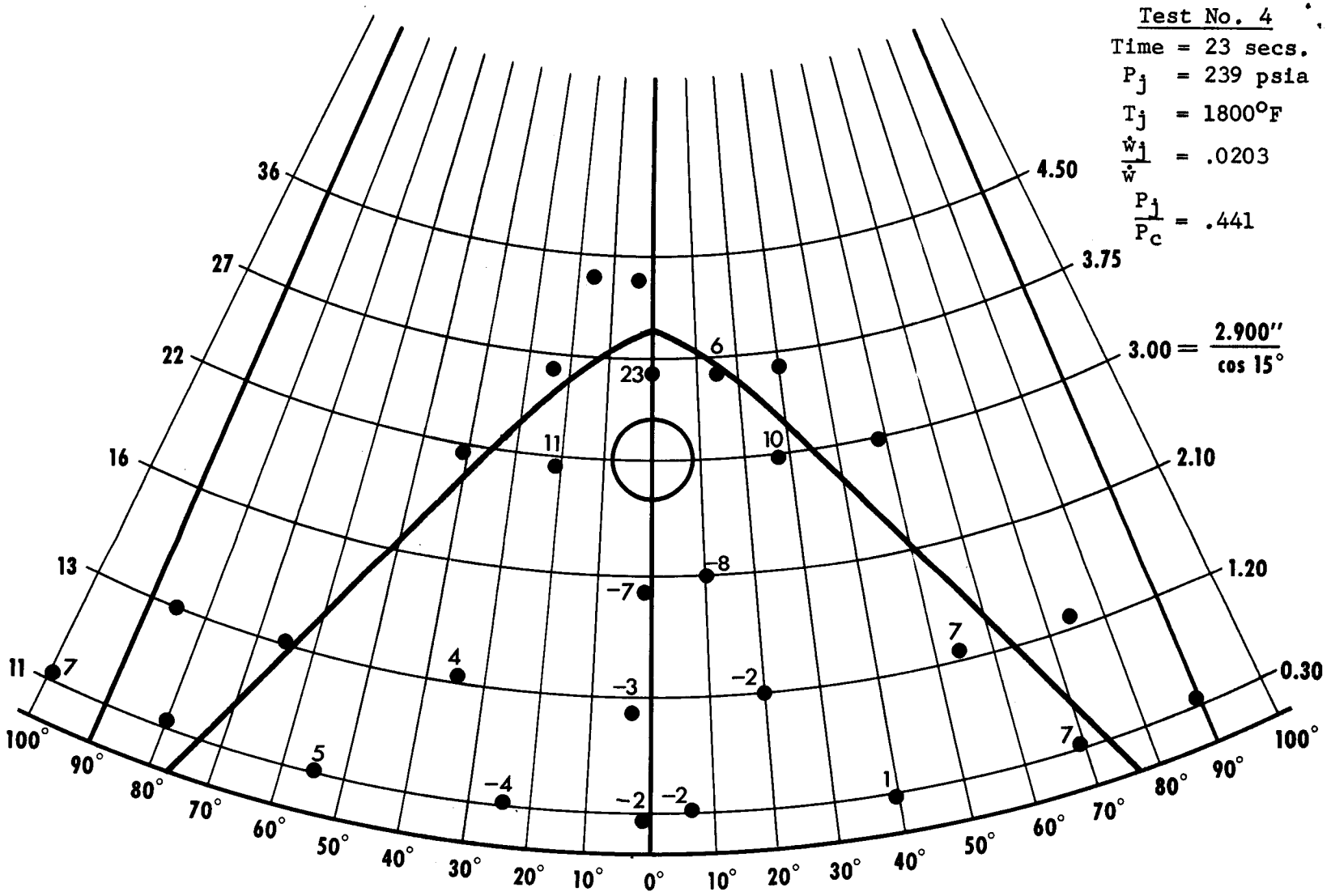
Test No. 4
Time = 23 secs.
P_j = 239 psia
T_j = 1800°F
$\frac{\dot{w}_j}{\dot{w}}$ = .0203
$\frac{P_j}{P_c}$ = .441
4.50
3.75
3.00 = 2.900" / cos 15°
2.10
1.20
0.30
36
27
22
16
13
11
100°
90°
80°
70°
60°
50°
40°
30°
20°
10°
0°
10°
20°
30°
40°
50°
60°
70°
80°
90°
100°
23
6
11
10
-7
8
4
-3
-2
7
5
-4
-2
-2
1
7
11
7

Figure 8.29

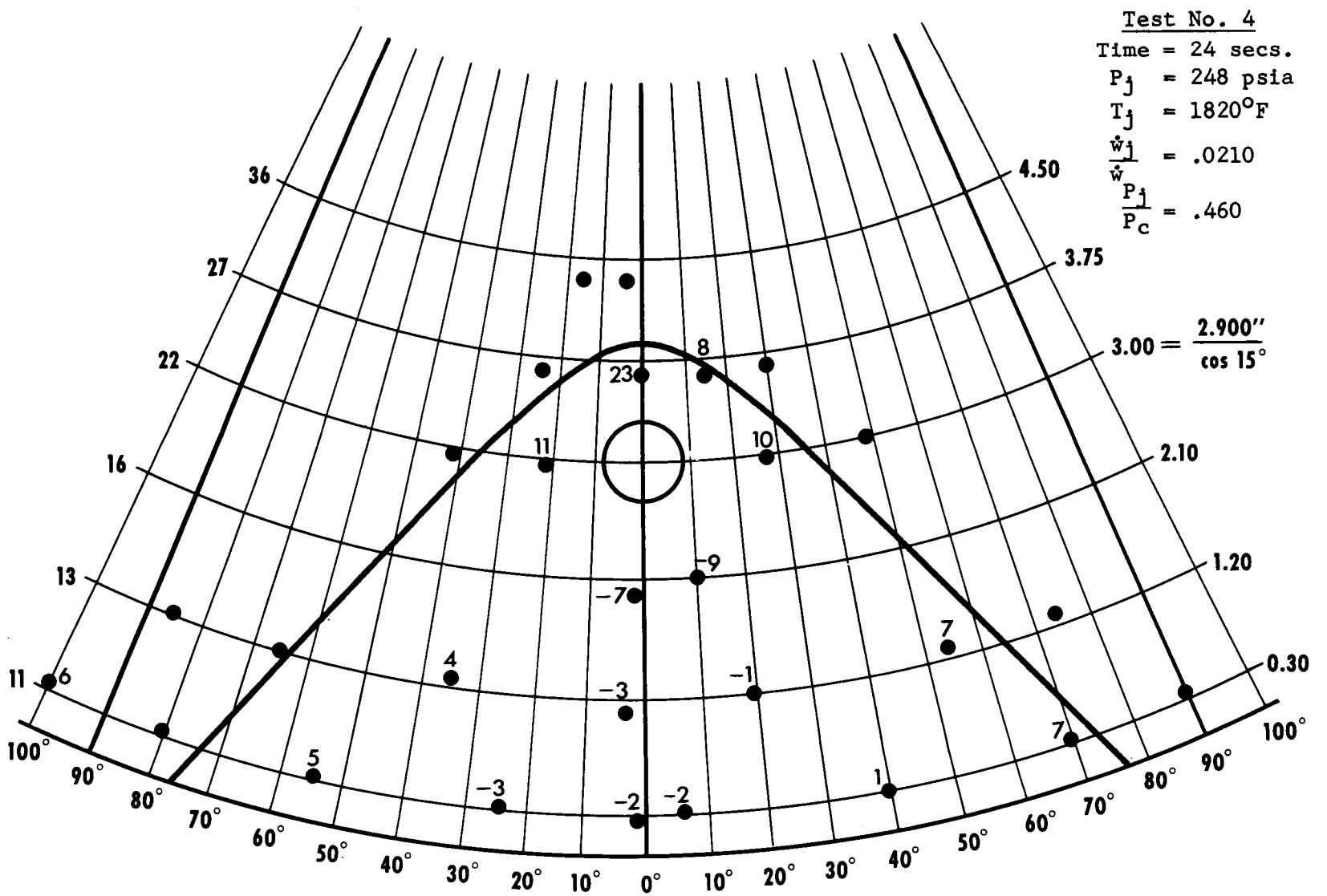
Test No. 4
Time = 24 secs.
P_j = 248 psia
T_j = 1820°F
$\frac{\dot{w}_j}{\dot{w}}$ = .0210
$\frac{P_j}{P_c}$ = .460
4.50
3.75
3.00 = 2.900" / cos 15°
2.10
1.20
0.30
36
27
22
16
13
11
100°
90°
80°
70°
60°
50°
40°
30°
20°
10°
0°
10°
20°
30°
40°
50°
60°
70°
80°
90°
100°
23
8
11
10
-9
-7
-3
-2
-2
-3
4
6
5
-1
7
1
7

Figure 8.30

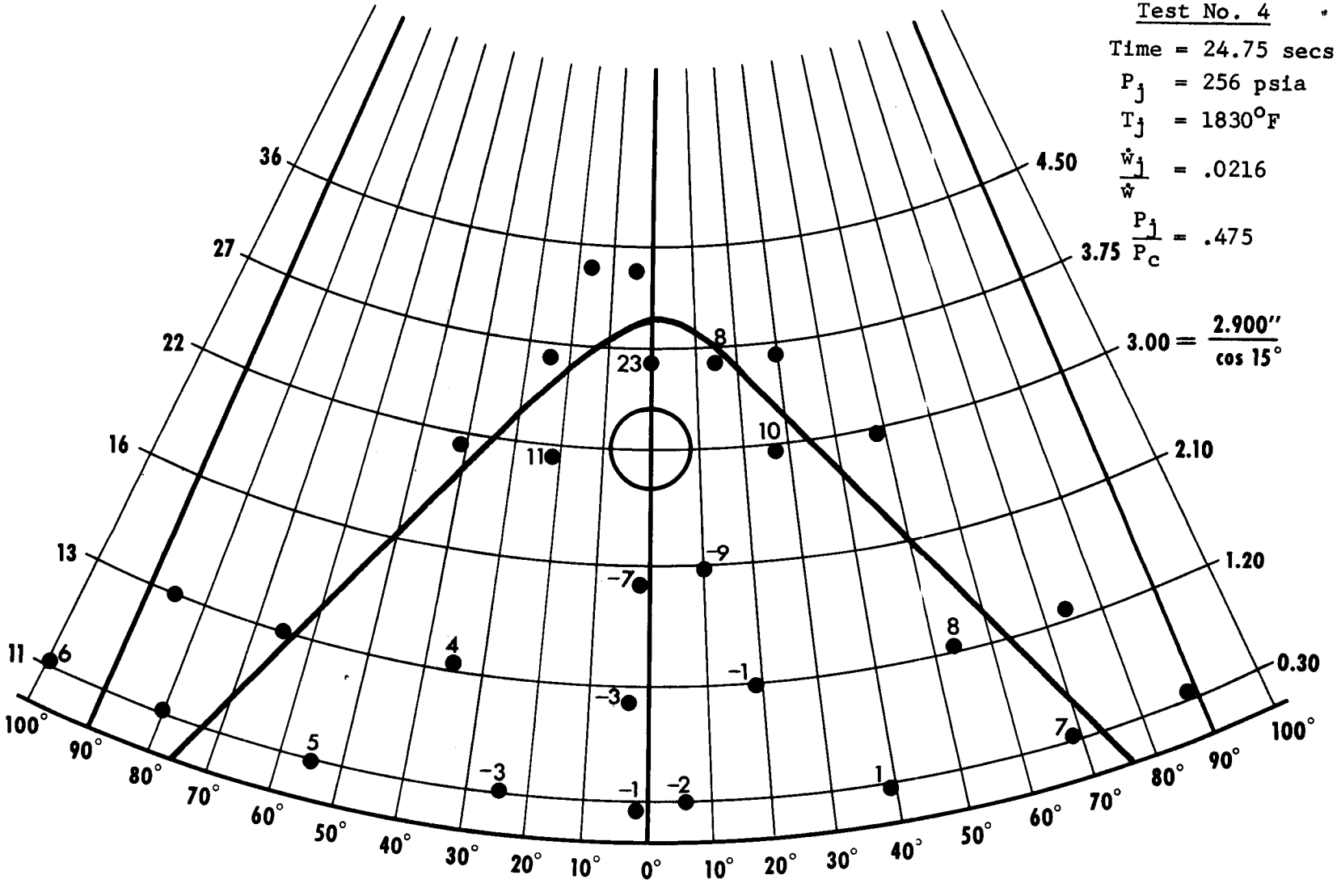
Test No. 4
Time = 24.75 secs.
P_j = 256 psia
T_j = 1830°F
$\frac{\dot{w}_j}{\dot{w}}$ = .0216
$\frac{P_j}{P_c}$ = .475
3.00 = 2.900" / cos 15°
4.50
3.75
2.10
1.20
0.30
36
27
22
16
13
11
100°
90°
80°
70°
60°
50°
40°
30°
20°
10°
0°
23
8
10
11
-9
-7
4
-1
-3
8
6
5
-3
-1
-2
1
7

Figure 8.31

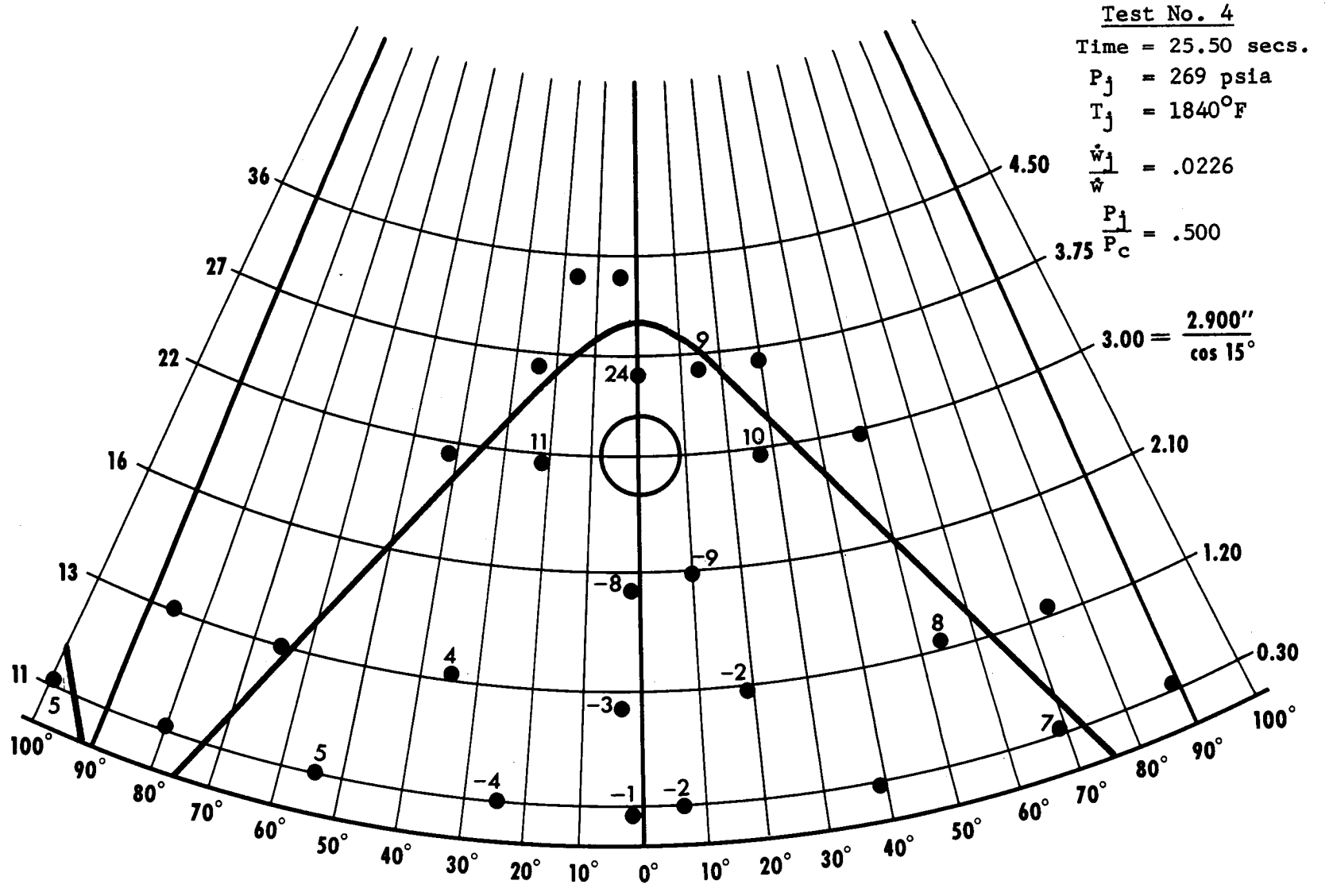
Test No. 4
Time = 25.50 secs.
P_j = 269 psia
T_j = 1840°F
$\frac{\dot{w}_j}{\dot{w}}$ = .0226
$\frac{P_j}{P_c}$ = .500
4.50
3.75
3.00 = 2.900" / cos 15°
2.10
1.20
0.30
36
27
22
16
13
11
100°
90°
80°
70°
60°
50°
40°
30°
20°
10°
0°
10°
20°
30°
40°
50°
60°
70°
80°
90°
100°
24
9
11
10
-9
-8
8
4
-2
-3
5
7
5
-4
-1
-2

Figure 8.32

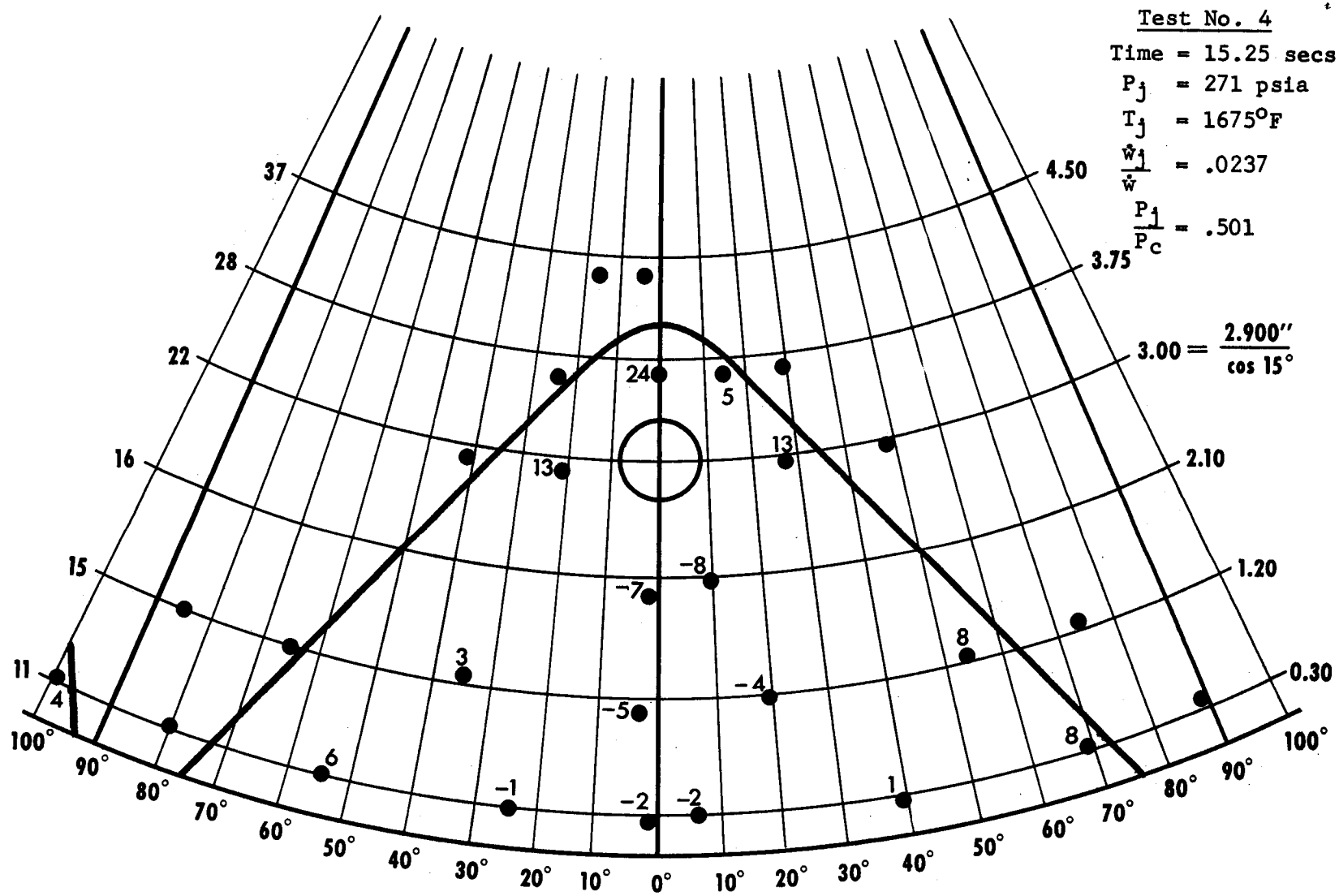
Test No. 4
Time = 15.25 secs.
P_j = 271 psia
T_j = 1675°F
$\frac{\dot{w}_j}{\dot{w}}$ = .0237
$\frac{P_j}{P_c}$ = .501
4.50
3.75
3.00 = 2.900" / cos 15°
2.10
1.20
0.30
37
28
22
16
15
11
100°
90°
80°
70°
60°
50°
40°
30°
20°
10°
0°
10°
20°
30°
40°
50°
60°
70°
80°
90°
100°
24
5
13
13
-8
-7
8
3
-4
-5
4
8
6
-1
-2
-2
1

Figure 8.33

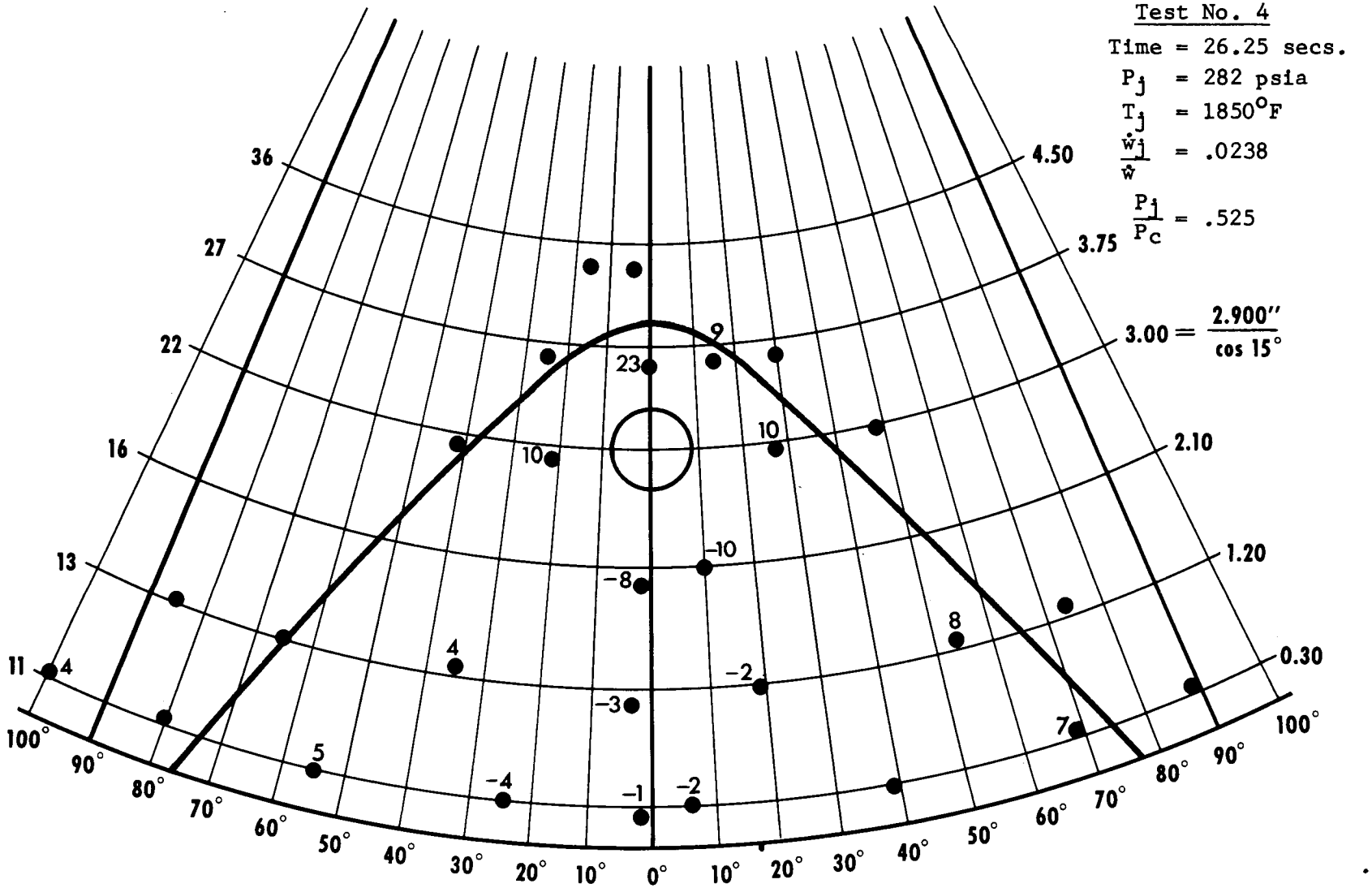
Test No. 4
Time = 26.25 secs.
P_j = 282 psia
T_j = 1850°F
$\frac{\dot{w}j}{\dot{w}}$ = .0238
$\frac{P_j}{P_c}$ = .525
3.00 = 2.900" / cos 15°
36
27
22
16
13
11
4.50
3.75
2.10
1.20
0.30
100°
90°
80°
70°
60°
50°
40°
30°
20°
10°
0°
23
9
10
10
-10
-8
-3
-2
-1
-2
-4
5
4
4
8
7
-2

Figure 8.34

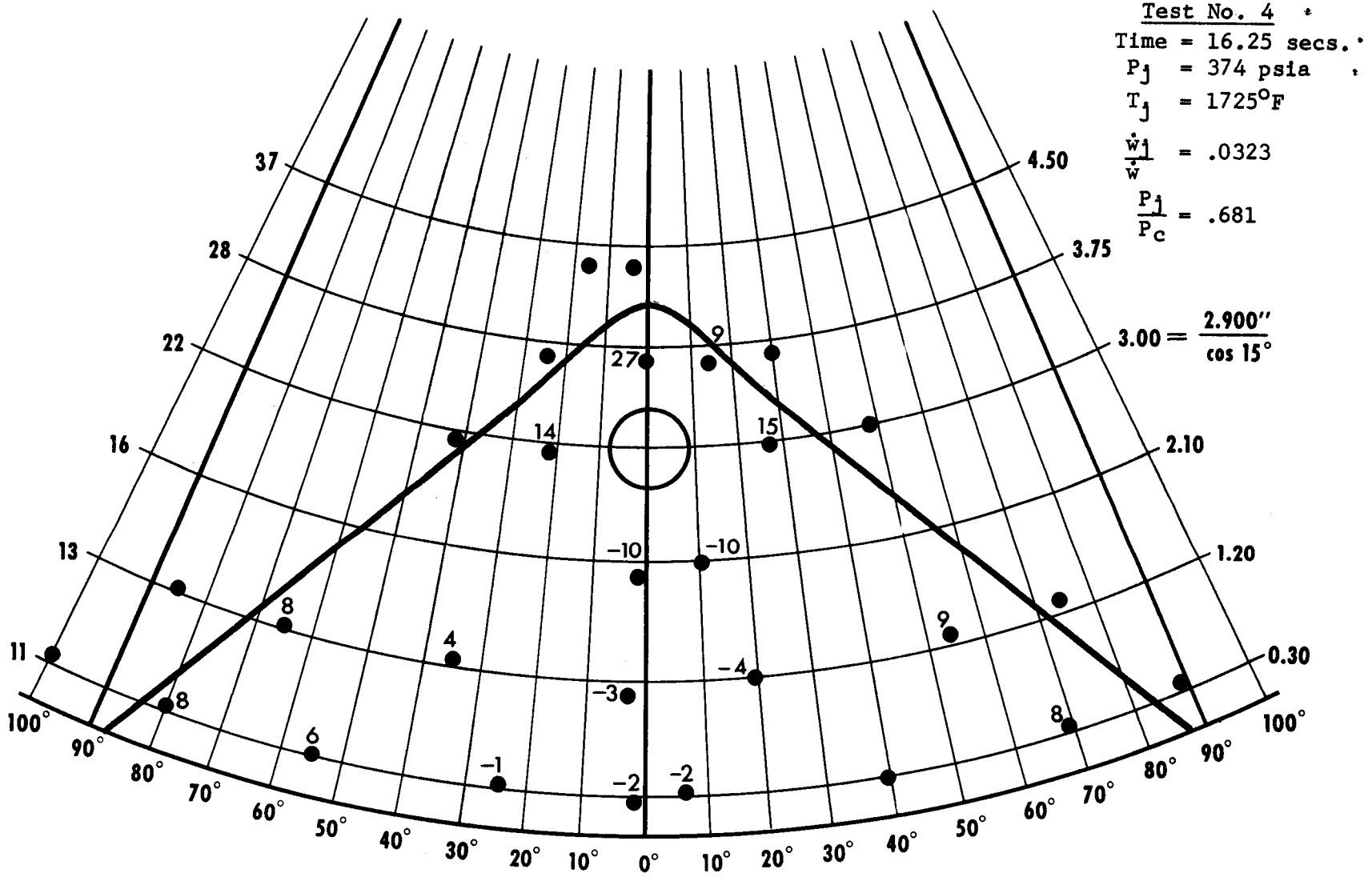
Test No. 4
Time = 16.25 secs.
P_j = 374 psia
T_j = 1725°F
$\frac{\dot{w}j}{\dot{w}}$ = .0323
$\frac{P_j}{P_c}$ = .681
4.50
3.75
3.00 = 2.900" / cos 15°
2.10
1.20
0.30
37
28
22
16
13
11
27
9
14
15
-10
-10
8
4
-4
-3
9
8
6
-1
-2
-2
8
100°
90°
80°
70°
60°
50°
40°
30°
20°
10°
0°
10°
20°
30°
40°
50°
60°
70°
80°
90°
100°

Figure 8.35

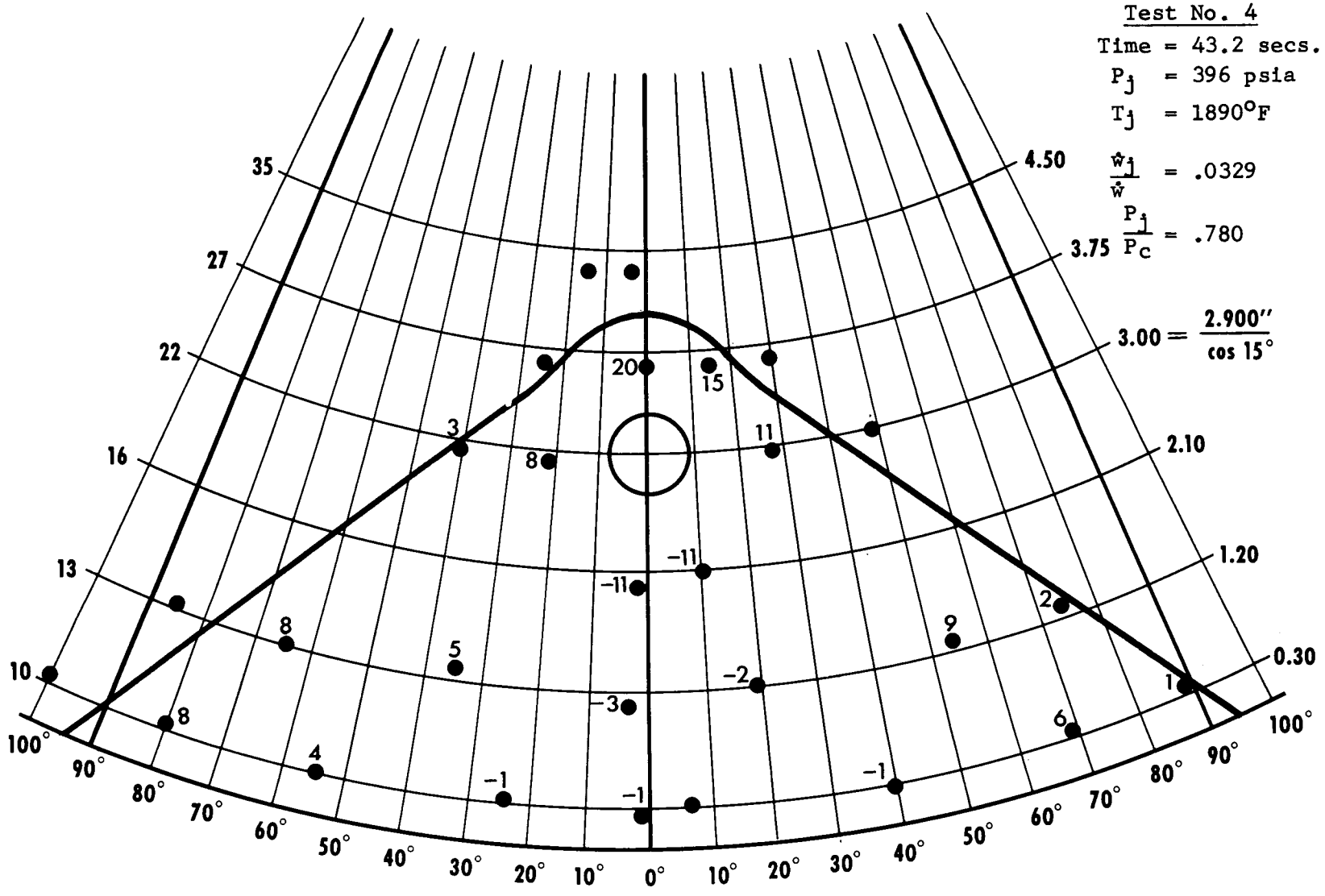
Test No. 4
Time = 43.2 secs.
P_j = 396 psia
T_j = 1890°F
$\frac{\dot{w}_j}{\dot{w}}$ = .0329
$\frac{P_j}{P_c}$ = .780
3.00 = 2.900" / cos 15°
4.50
3.75
2.10
1.20
0.30
35
27
22
16
13
10
20
15
3
8
11
-11
-11
8
5
-2
-3
9
2
1
6
8
4
-1
-1
-1
100°
90°
80°
70°
60°
50°
40°
30°
20°
10°
0°
10°
20°
30°
40°
50°
60°
70°
80°
90°
100°

Figure 8.36

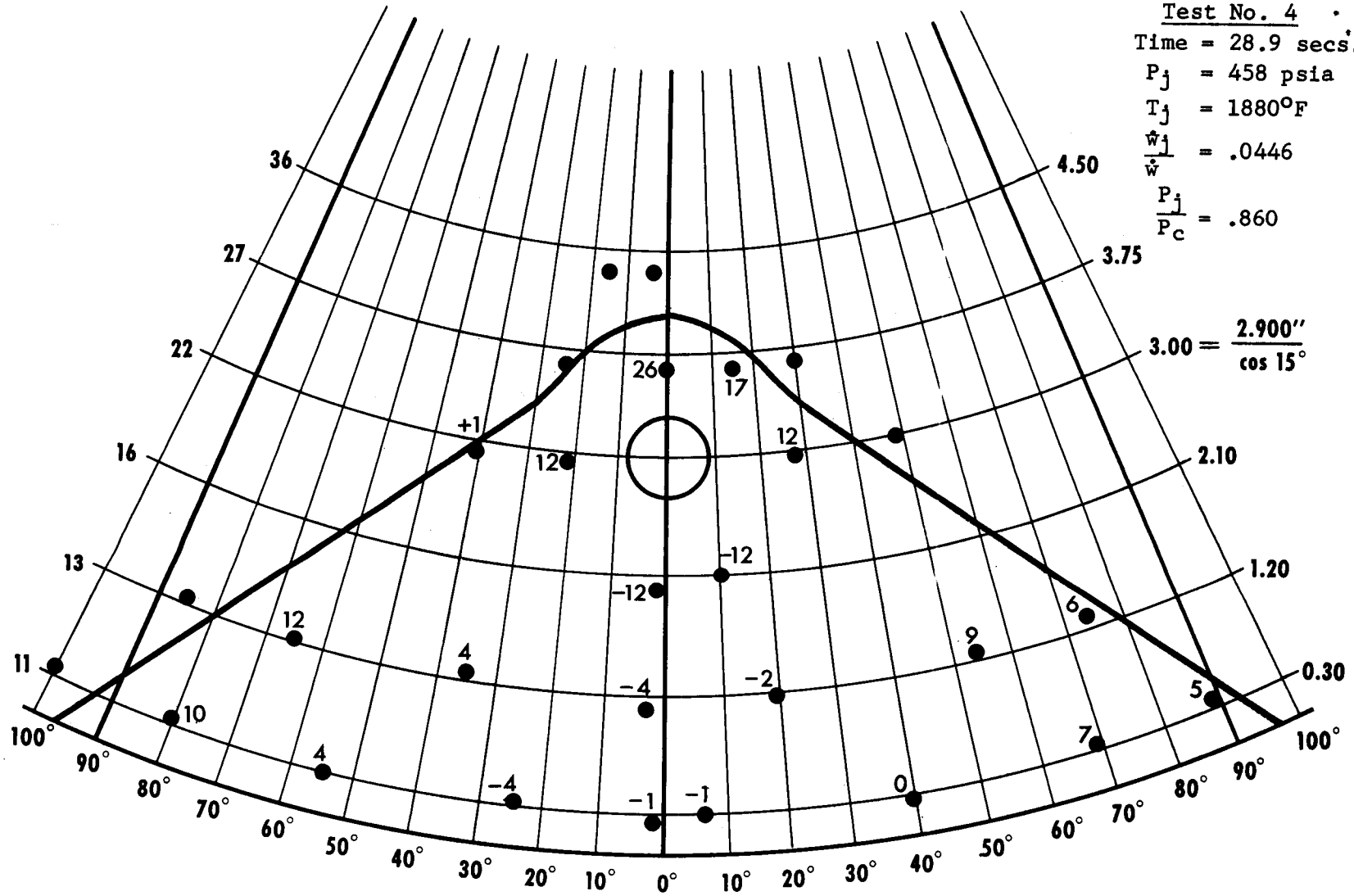
Test No. 4
Time = 28.9 secs.
P_j = 458 psia
T_j = 1880°F
$\frac{\dot{w}_j}{\dot{w}}$ = .0446
$\frac{P_j}{P_c}$ = .860
3.00 = 2.900" / cos 15°
36
27
22
16
13
11
4.50
3.75
2.10
1.20
0.30
100°
90°
80°
70°
60°
50°
40°
30°
20°
10°
0°
26
17
+1
12
-12
4
-4
-2
10
-1
6
9
5
7
0

Figure 8.37

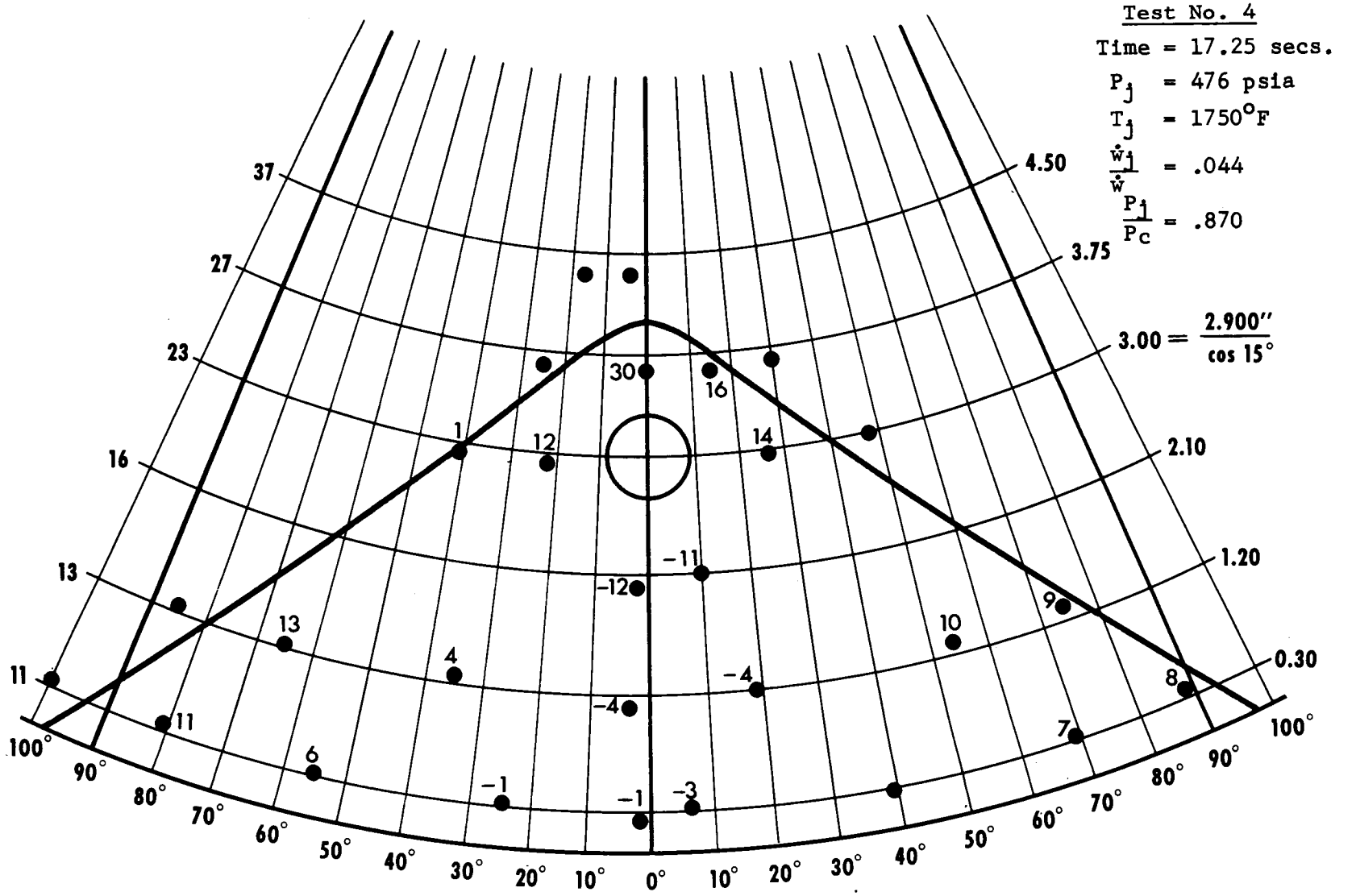
Test No. 4
Time = 17.25 secs.
P_j = 476 psia
T_j = 1750°F
$\frac{\dot{w}_j}{\dot{w}}$ = .044
$\frac{P_j}{P_c}$ = .870
3.00 = 2.900" / cos 15°
4.50
3.75
2.10
1.20
0.30
37
27
23
16
13
11
100°
90°
80°
70°
60°
50°
40°
30°
20°
10°
0°
10°
20°
30°
40°
50°
60°
70°
80°
90°
100°
30
16
1
12
14
-11
-12
13
4
-4
-4
10
9
8
7
11
6
-1
-1
-3

Figure 8.38

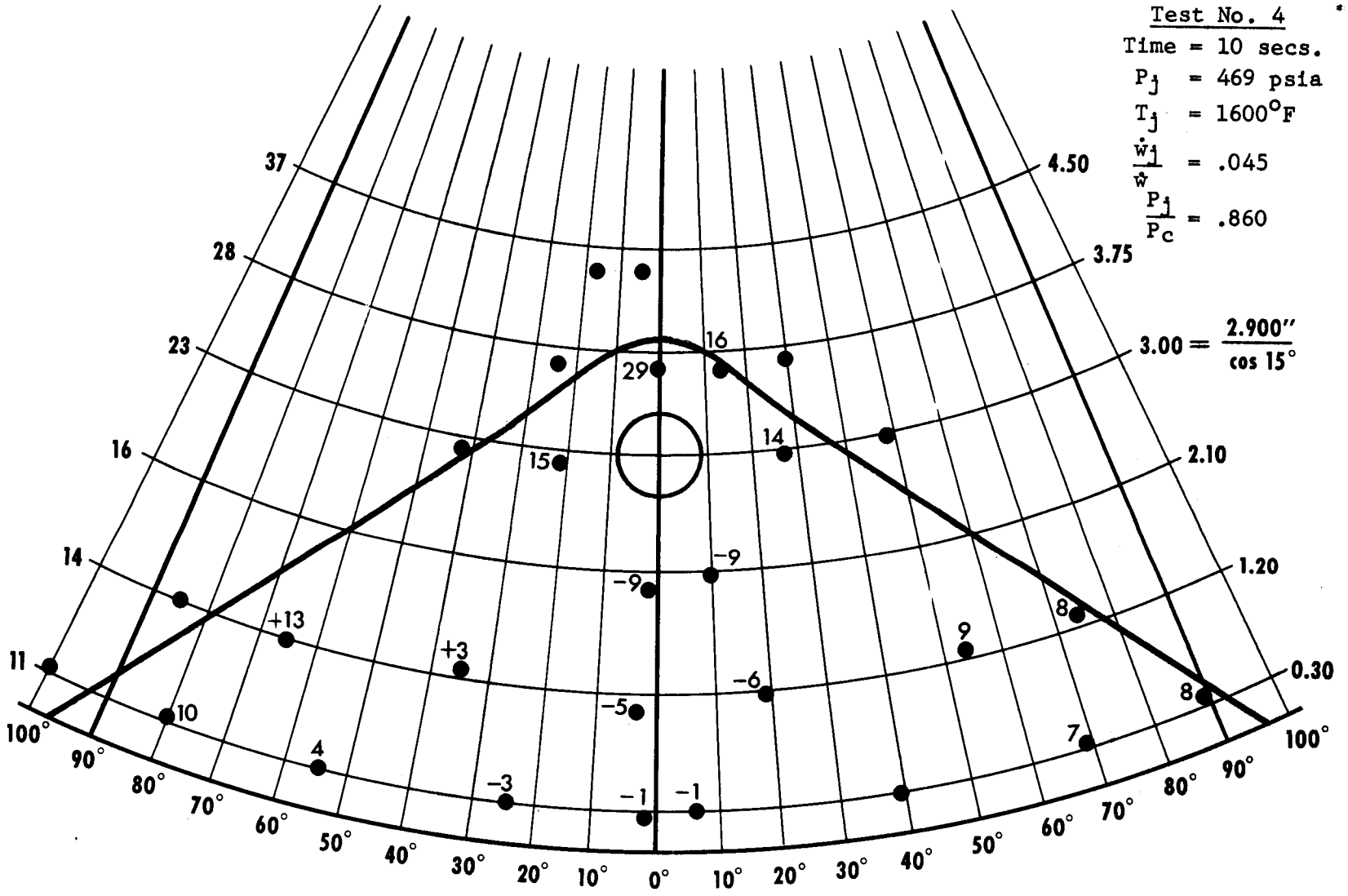
Test No. 4
Time = 10 secs.
P_j = 469 psia
T_j = 1600°F
$\frac{\dot{w}_j}{\dot{w}}$ = .045
$\frac{P_j}{P_c}$ = .860
4.50
3.75
3.00 = 2.900" / cos 15°
2.10
1.20
0.30
37
28
23
16
14
11
100°
90°
80°
70°
60°
50°
40°
30°
20°
10°
0°
10°
20°
30°
40°
50°
60°
70°
80°
90°
100°
16
29
15
14
−9
−9
+13
+3
−6
−5
9
8
8
7
10
4
−3
−1
−1

Figure 8.39

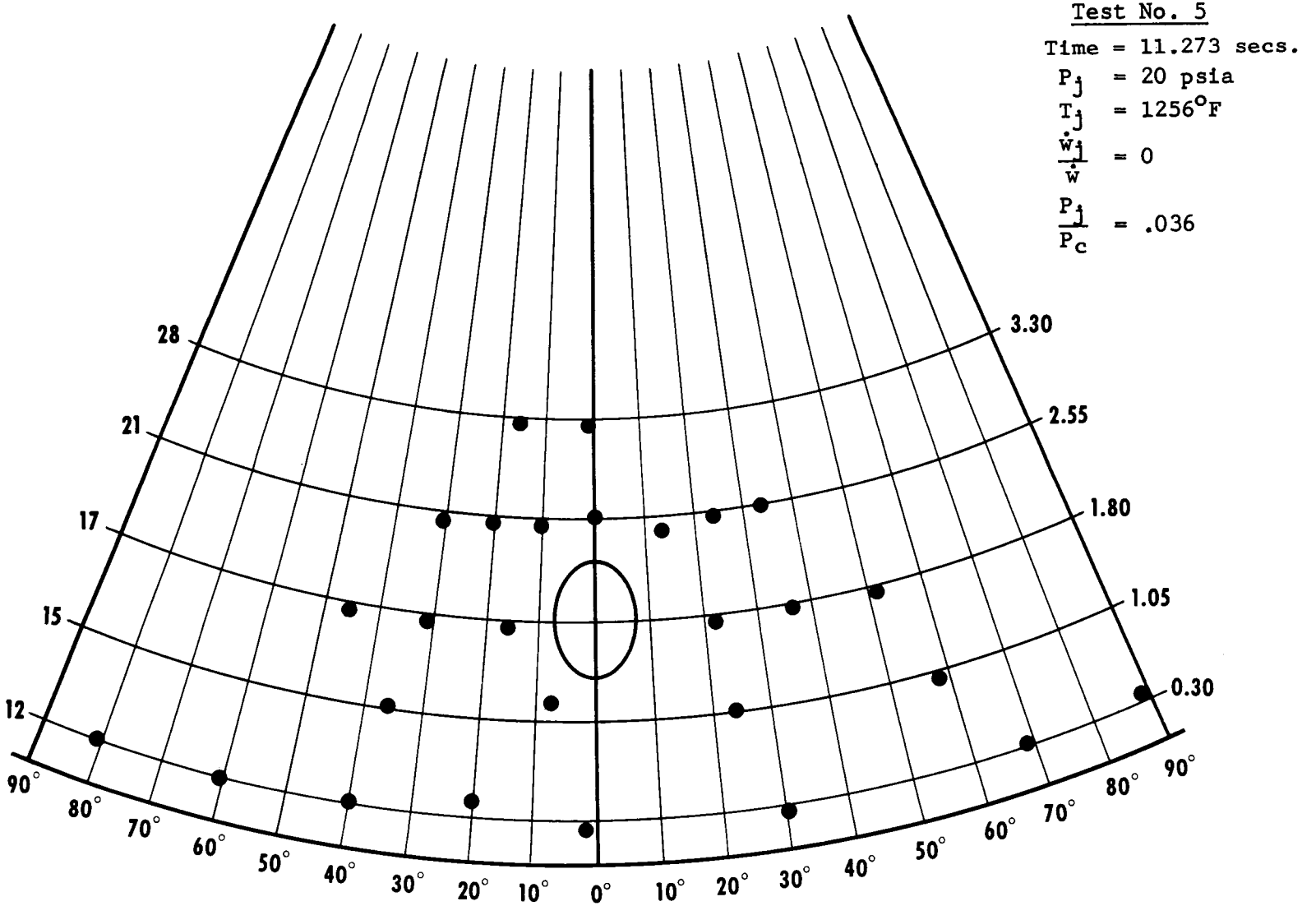
Test No. 5
Time = 11.273 secs.
P_j = 20 psia
T_j = 1256°F
$\frac{\dot{w}_j}{\dot{w}}$ = 0
$\frac{P_j}{P_c}$ = .036
28
21
17
15
12
3.30
2.55
1.80
1.05
0.30
90° 80° 70° 60° 50° 40° 30° 20° 10° 0° 10° 20° 30° 40° 50° 60° 70° 80° 90°

Figure 8.40

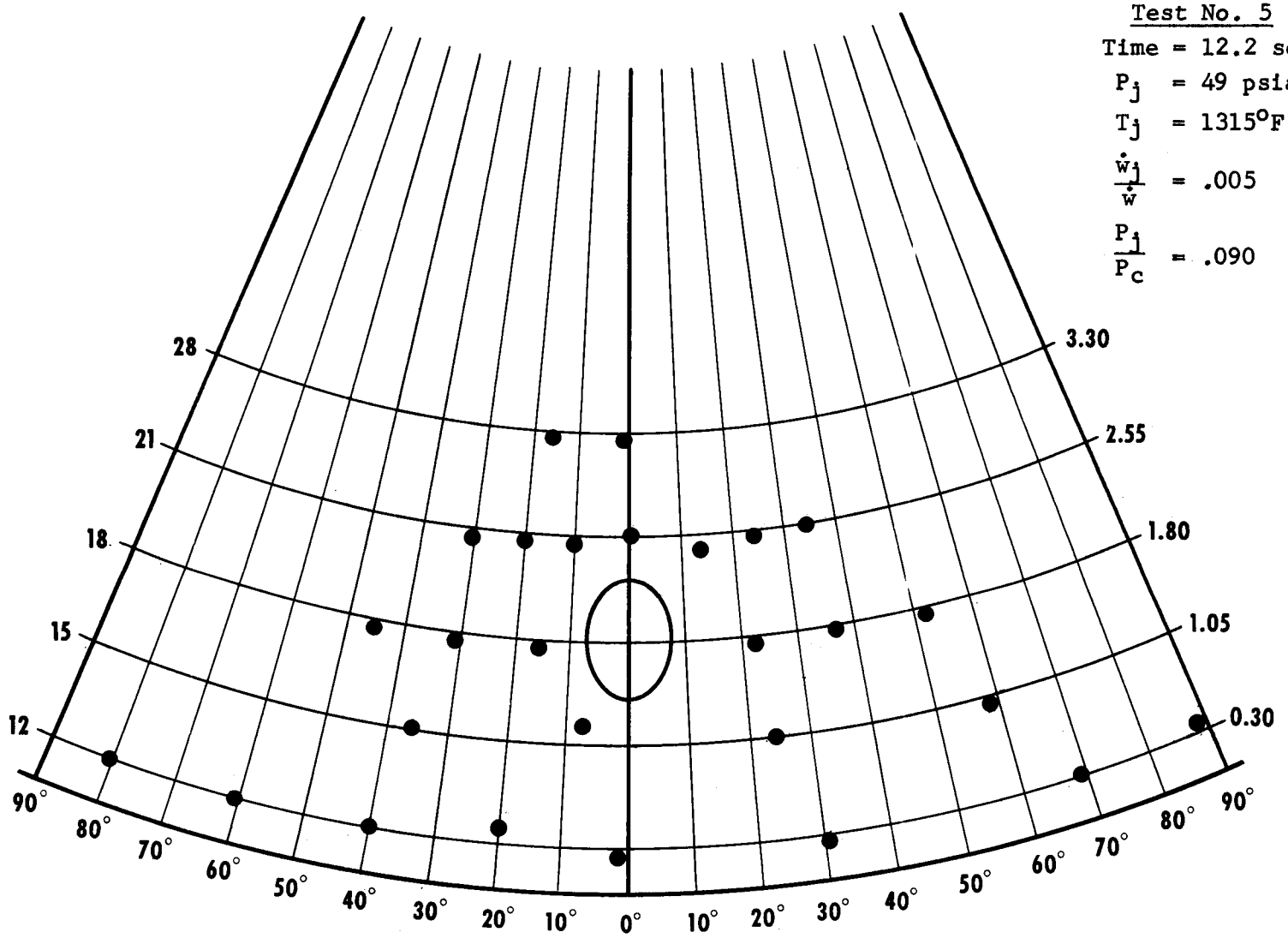
Test No. 5
Time = 12.2 secs.
P_j = 49 psia
T_j = 1315°F
$\frac{\dot{w}_j}{\dot{w}}$ = .005
$\frac{P_j}{P_c}$ = .090
28
21
18
15
12
3.30
2.55
1.80
1.05
0.30
90°
80°
70°
60°
50°
40°
30°
20°
10°
0°
10°
20°
30°
40°
50°
60°
70°
80°
90°

Figure 8.41

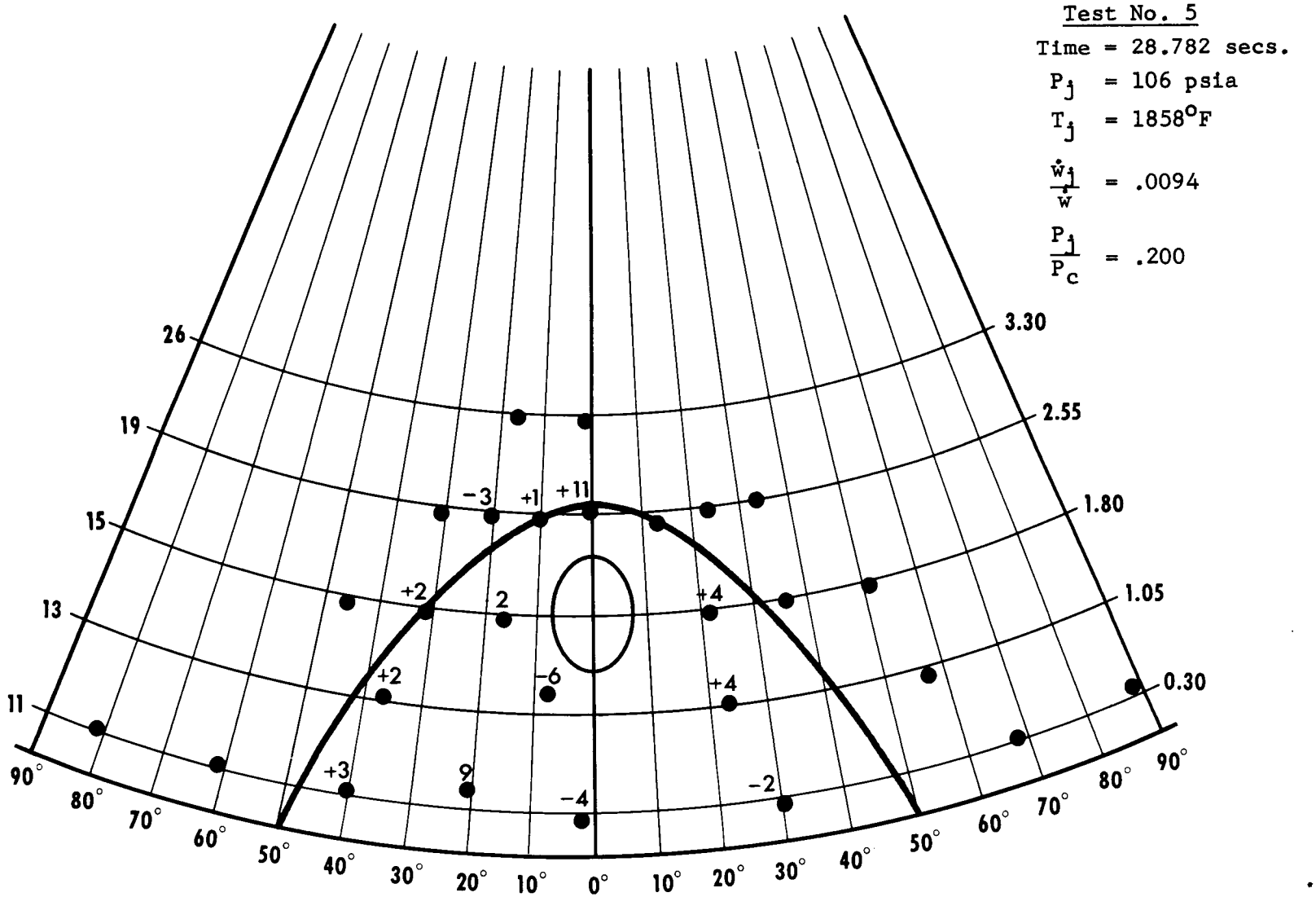
Test No. 5
Time = 28.782 secs.
P_j = 106 psia
T_j = 1858°F
$\frac{\dot{w}_j}{\dot{w}}$ = .0094
$\frac{P_j}{P_c}$ = .200
26
19
15
13
11
3.30
2.55
1.80
1.05
0.30
90°
80°
70°
60°
50°
40°
30°
20°
10°
0°
10°
20°
30°
40°
50°
60°
70°
80°
90°
-3
+1
+11
+2
2
+4
+2
-6
+4
+3
9
-4
-2

Figure 8.42

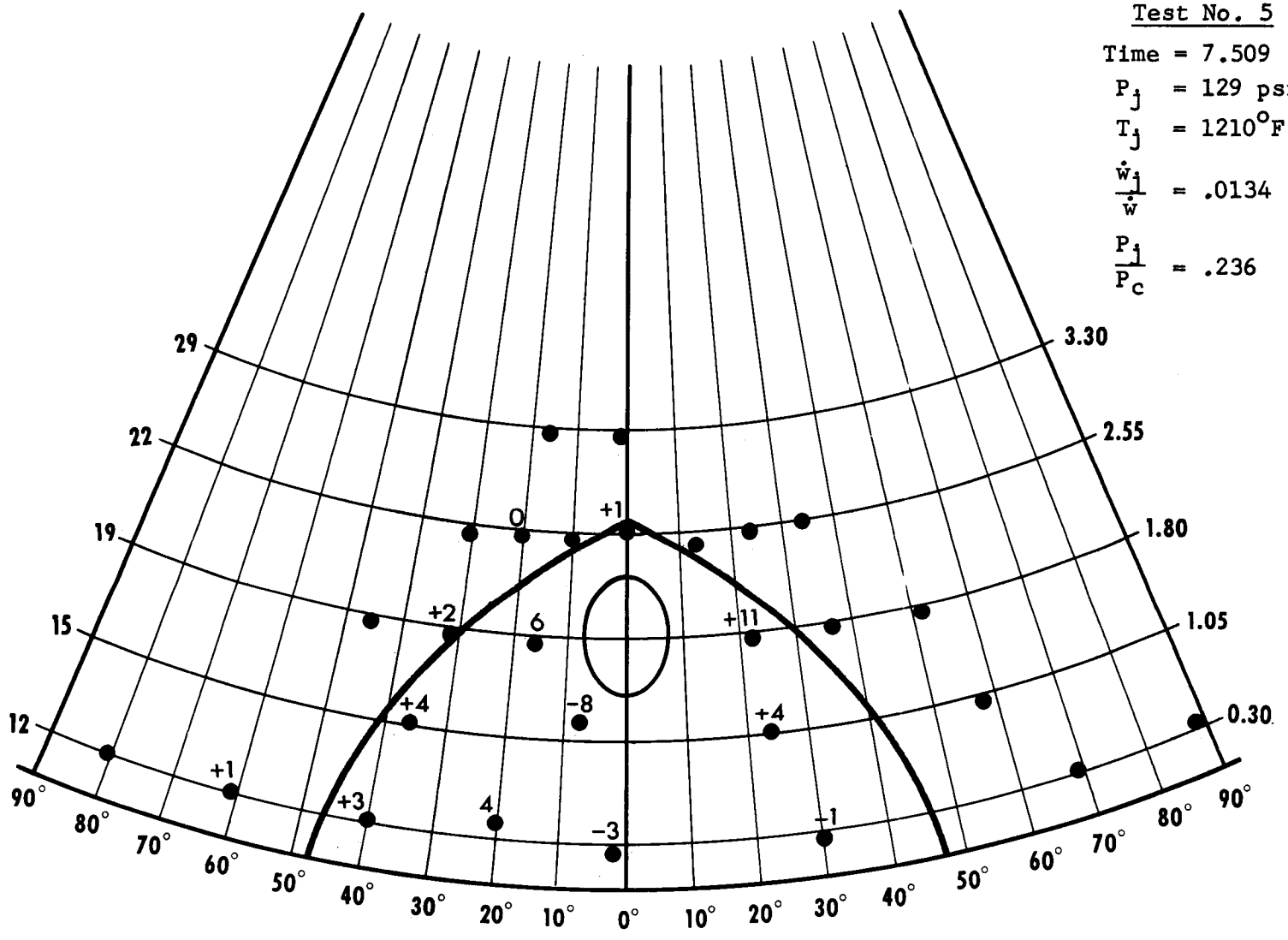
Test No. 5
Time = 7.509 secs.
P_j = 129 psia
T_j = 1210°F
$\frac{\dot{w}_j}{\dot{w}}$ = .0134
$\frac{P_j}{P_c}$ = .236
29
22
19
15
12
3.30
2.55
1.80
1.05
0.30
90°
80°
70°
60°
50°
40°
30°
20°
10°
0°
10°
20°
30°
40°
50°
60°
70°
80°
90°
0
+1
+2
6
+11
+4
-8
+4
+1
+3
4
-3
+1

Figure 8.43

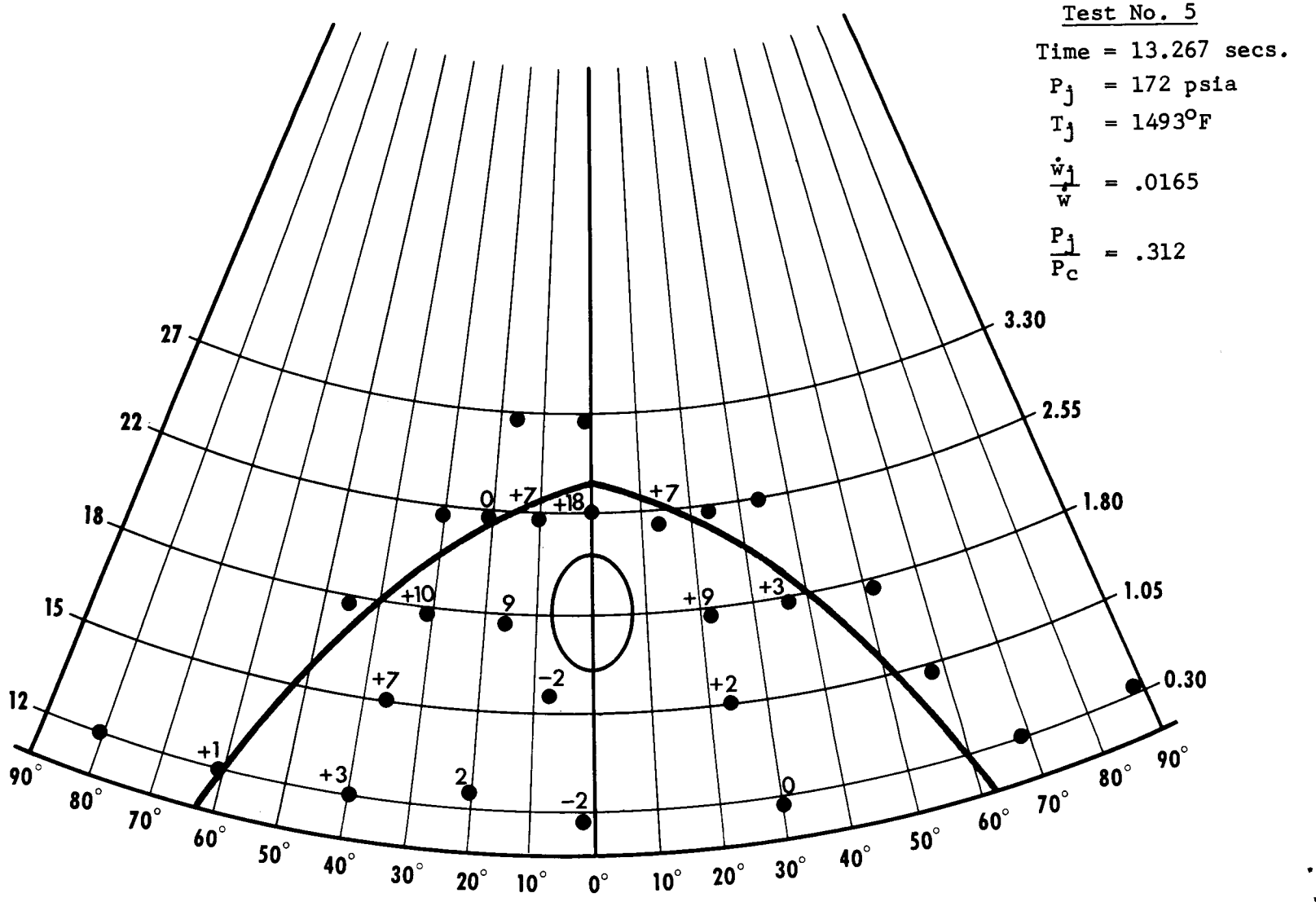
Test No. 5
Time = 13.267 secs.
P_j = 172 psia
T_j = 1493°F
$\frac{\dot{w}_j}{\dot{w}}$ = .0165
$\frac{P_j}{P_c}$ = .312
27
22
18
15
12
3.30
2.55
1.80
1.05
0.30
90°
80°
70°
60°
50°
40°
30°
20°
10°
0°
10°
20°
30°
40°
50°
60°
70°
80°
90°
0
+7
+18
+7
+10
9
+9
+3
+7
-2
+2
+1
+3
2
-2
0

Figure 8.44

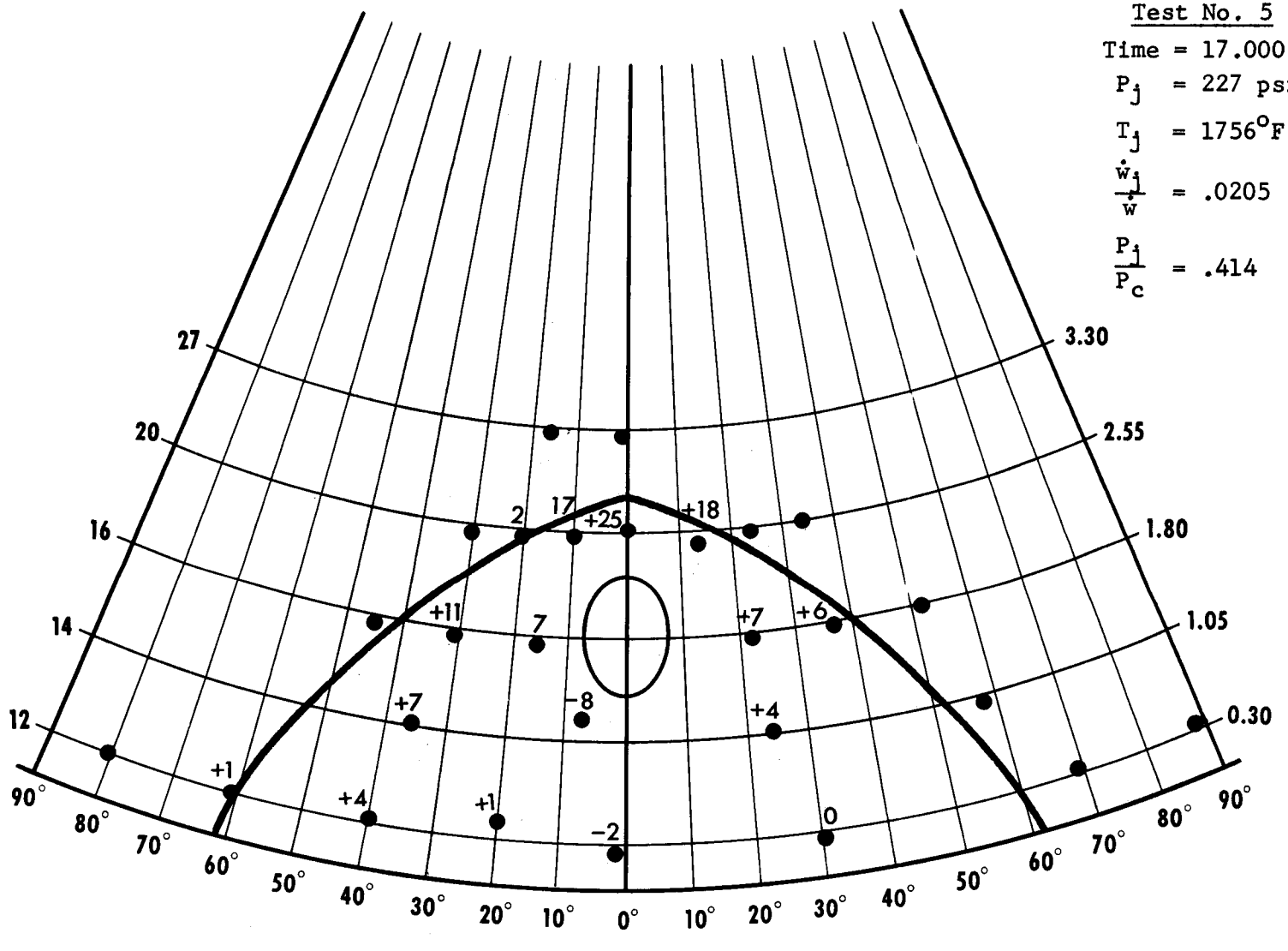
Test No. 5
Time = 17.000 secs.
P_j = 227 psia
T_j = 1756°F
$\frac{\dot{w}_j}{\dot{w}}$ = .0205
$\frac{P_j}{P_c}$ = .414
27
20
16
14
12
3.30
2.55
1.80
1.05
0.30
90°
80°
70°
60°
50°
40°
30°
20°
10°
0°
10°
20°
30°
40°
50°
60°
70°
80°
90°
+1
+4
+1
-2
0
+7
-8
+4
+11
7
+7
+6
2
17
+25
+18

Figure 8.45

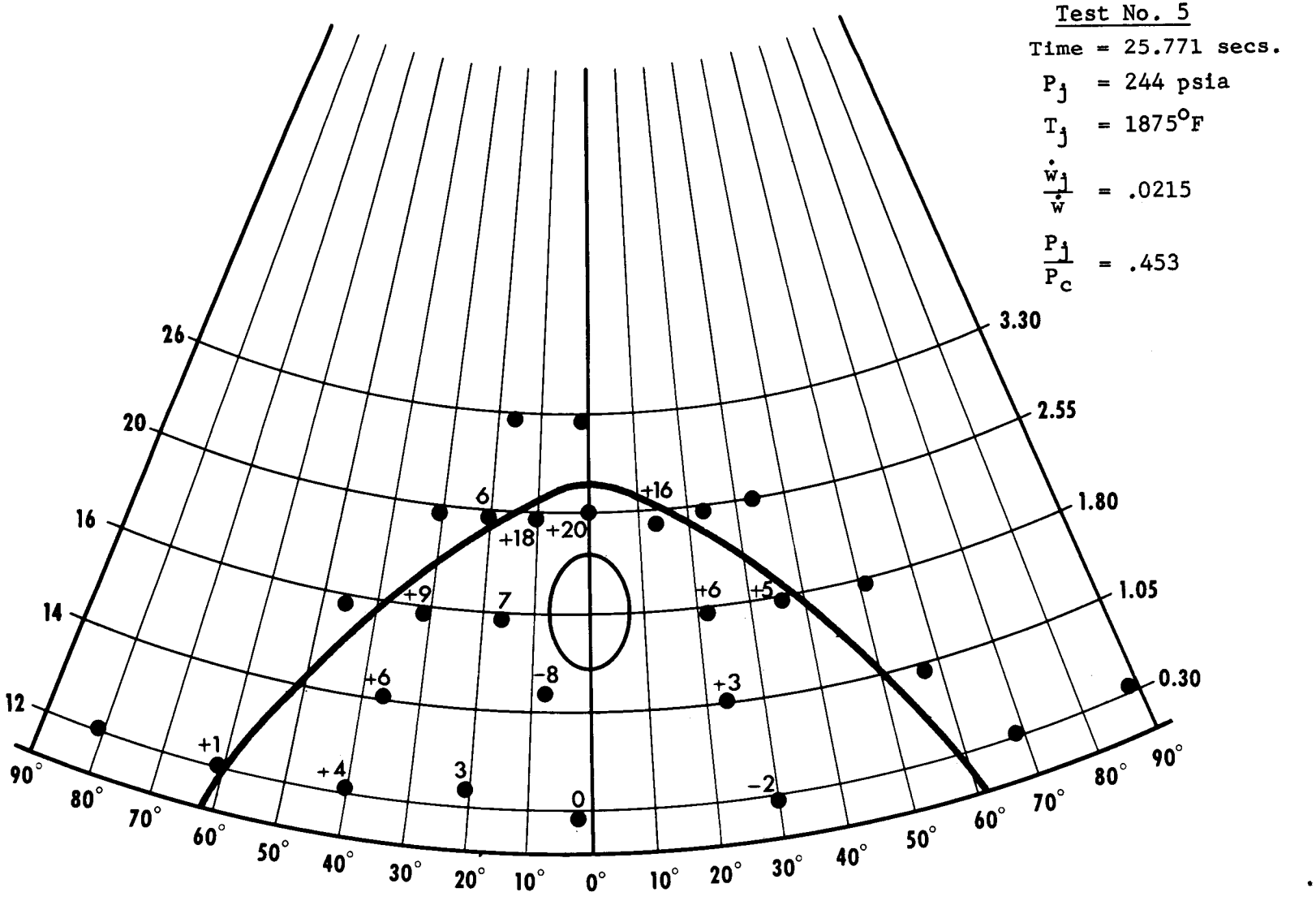
Test No. 5
Time = 25.771 secs.
P_j = 244 psia
T_j = 1875°F
$\frac{\dot{w}_j}{\dot{w}}$ = .0215
$\frac{P_j}{P_c}$ = .453
26
20
16
14
12
3.30
2.55
1.80
1.05
0.30
90°
80°
70°
60°
50°
40°
30°
20°
10°
0°
10°
20°
30°
40°
50°
60°
70°
80°
90°
+1
+4
3
0
-2
+6
-8
+3
+9
7
+6
+5
6
+18
+20
+16

Figure 8.46

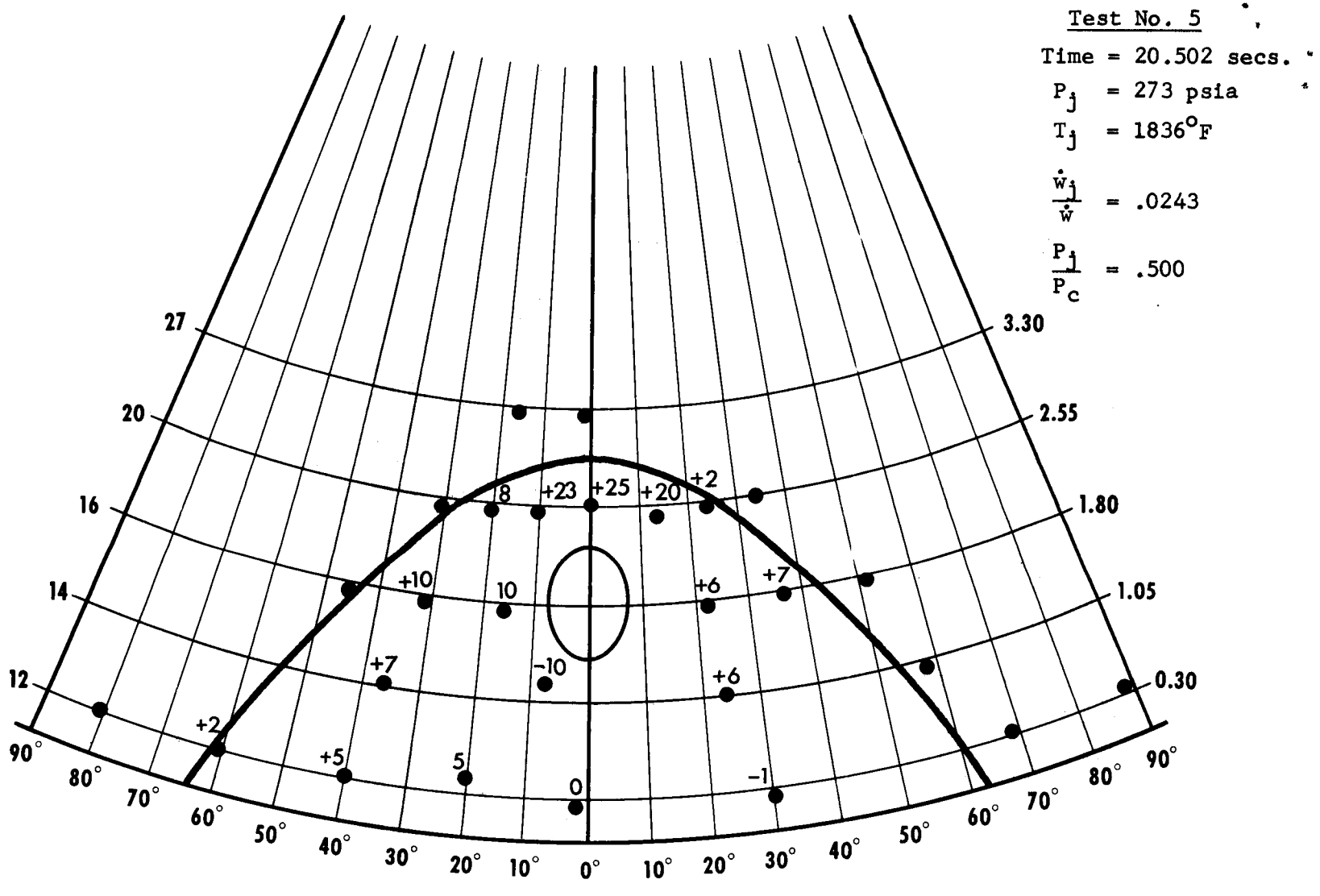
Test No. 5
Time = 20.502 secs.
P_j = 273 psia
T_j = 1836°F
$\frac{\dot{w}_j}{\dot{w}}$ = .0243
$\frac{P_j}{P_c}$ = .500
27
20
16
14
12
3.30
2.55
1.80
1.05
0.30
8
+23
+25
+20
+2
+10
10
+6
+7
+7
-10
+6
+2
+5
5
0
-1
90°
80°
70°
60°
50°
40°
30°
20°
10°
0°
10°
20°
30°
40°
50°
60°
70°
80°
90°

Figure 8.47

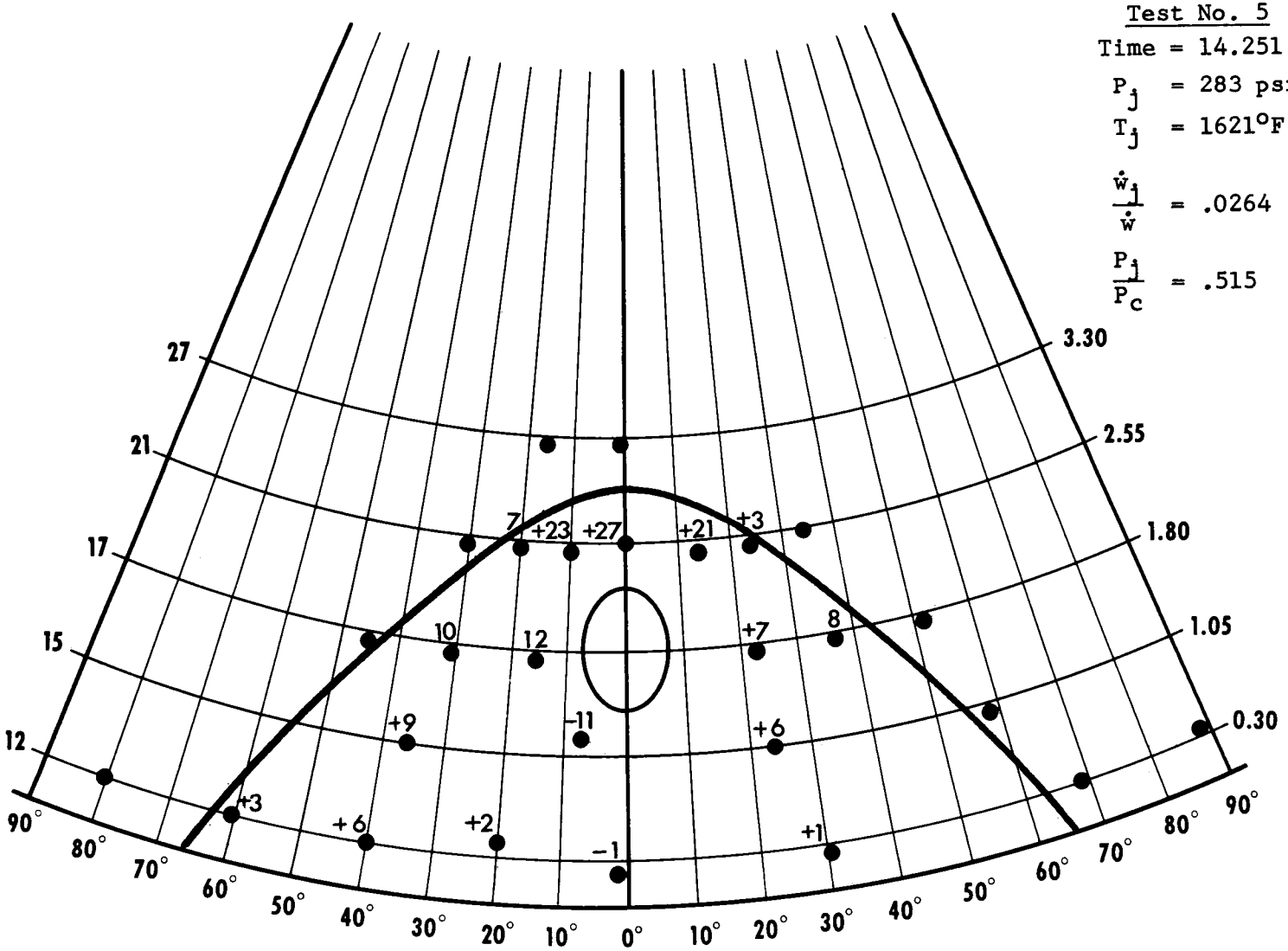
Test No. 5
Time = 14.251 secs.
P_j = 283 psia
T_j = 1621°F
$\frac{\dot{w}_j}{\dot{w}}$ = .0264
$\frac{P_j}{P_c}$ = .515
27
21
17
15
12
3.30
2.55
1.80
1.05
0.30
90°
80°
70°
60°
50°
40°
30°
20°
10°
0°
10°
20°
30°
40°
50°
60°
70°
80°
90°
7
+23
+27
+21
+3
10
12
+7
8
+9
-11
+6
+3
+6
+2
-1
+1

Figure 8.48

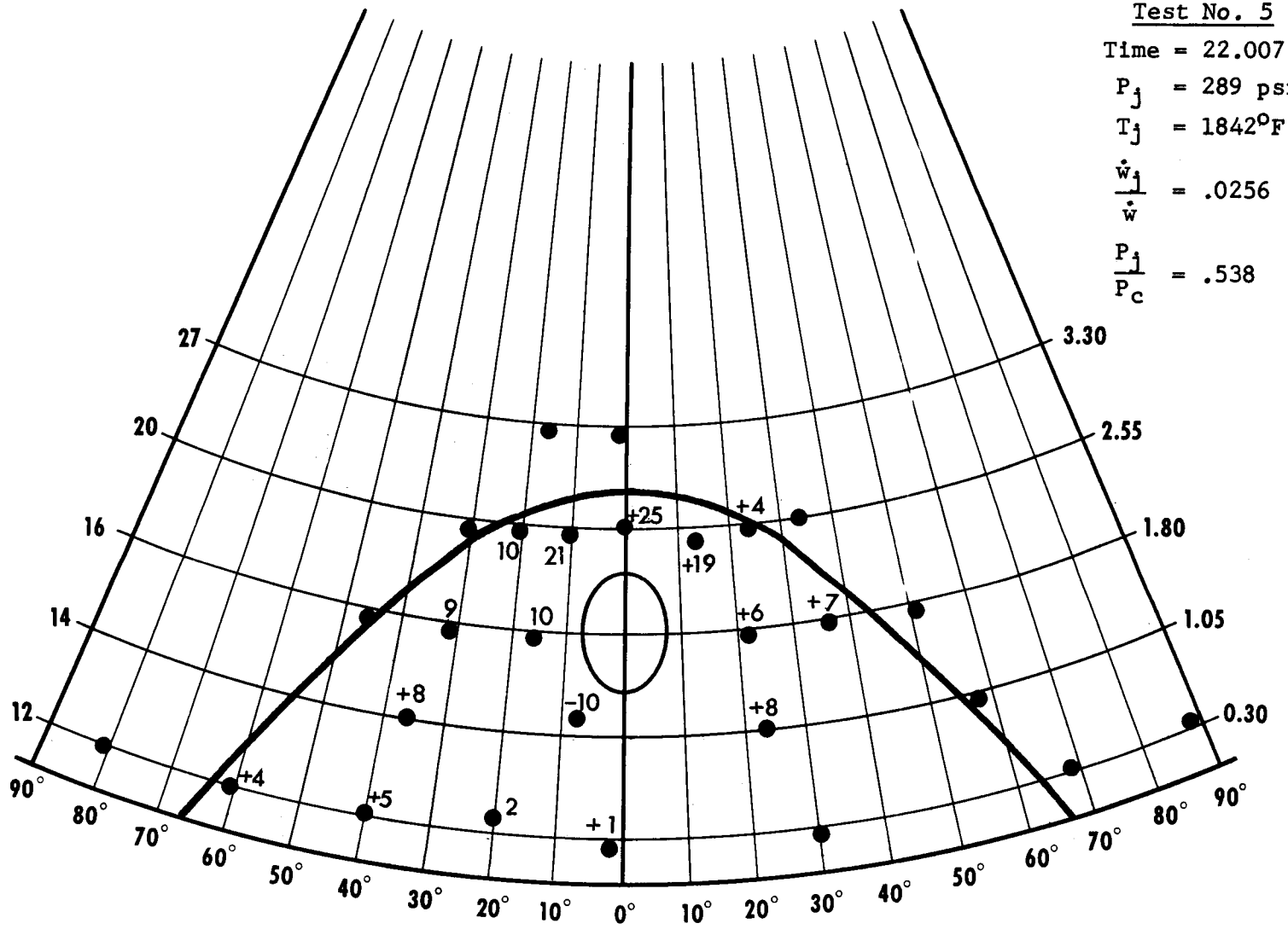
Test No. 5
Time = 22.007 secs.
P_j = 289 psia
T_j = 1842°F
$\frac{\dot{w}_j}{\dot{w}}$ = .0256
$\frac{P_j}{P_c}$ = .538
27
20
16
14
12
3.30
2.55
1.80
1.05
0.30
90°
80°
70°
60°
50°
40°
30°
20°
10°
0°
10°
20°
30°
40°
50°
60°
70°
80°
90°
+25
+4
10
21
+19
9
10
+6
+7
+8
-10
+8
+4
+5
2
+1

Figure 8.49

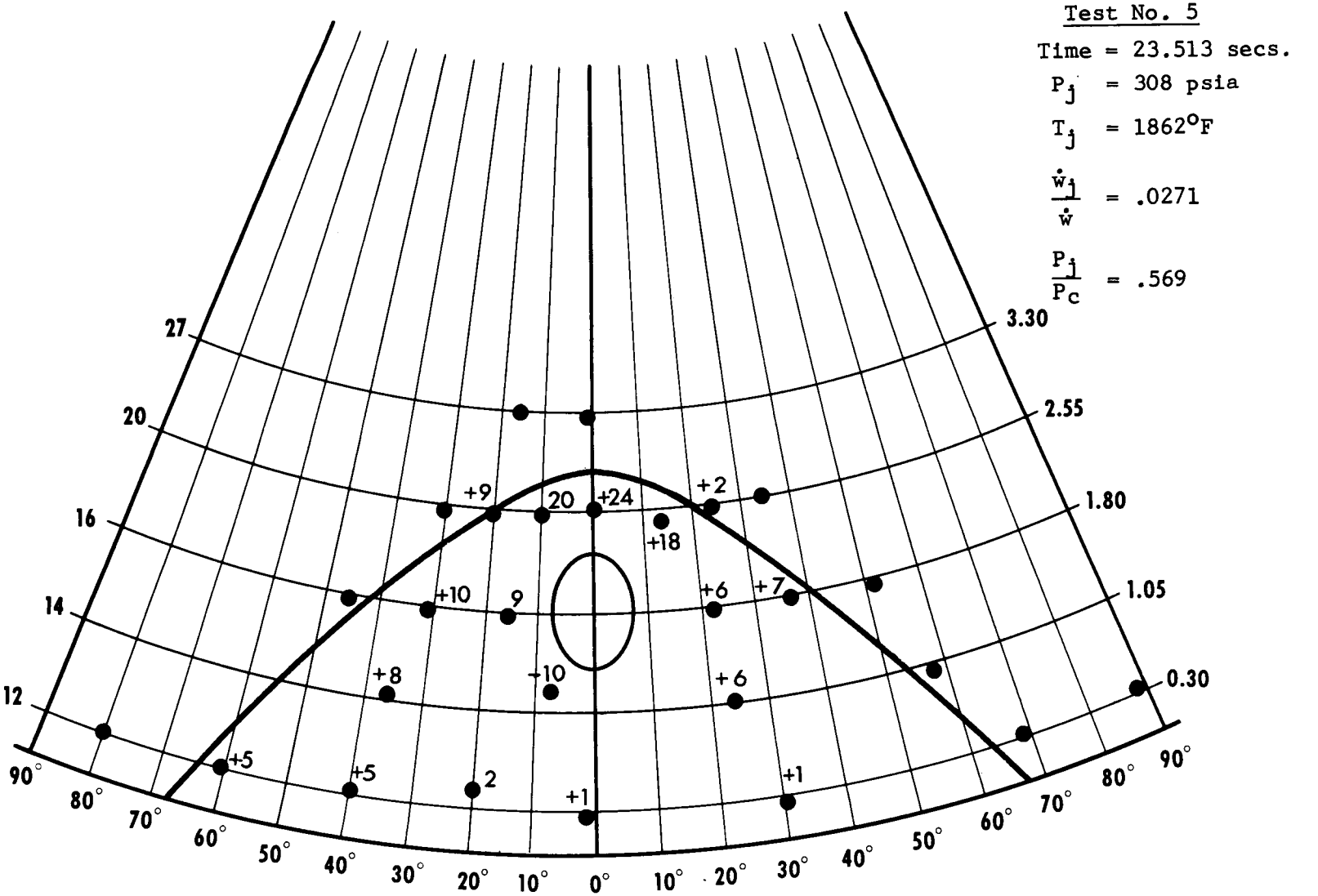
Test No. 5
Time = 23.513 secs.
P_j = 308 psia
T_j = 1862°F
$\frac{\dot{w}_j}{\dot{w}}$ = .0271
$\frac{P_j}{P_c}$ = .569
27
20
16
14
12
3.30
2.55
1.80
1.05
0.30
+9
20
+24
+2
+18
+10
9
+6
+7
+8
+10
+6
+5
+5
2
+1
+1
90°
80°
70°
60°
50°
40°
30°
20°
10°
0°
10°
20°
30°
40°
50°
60°
70°
80°
90°

Figure 8.50

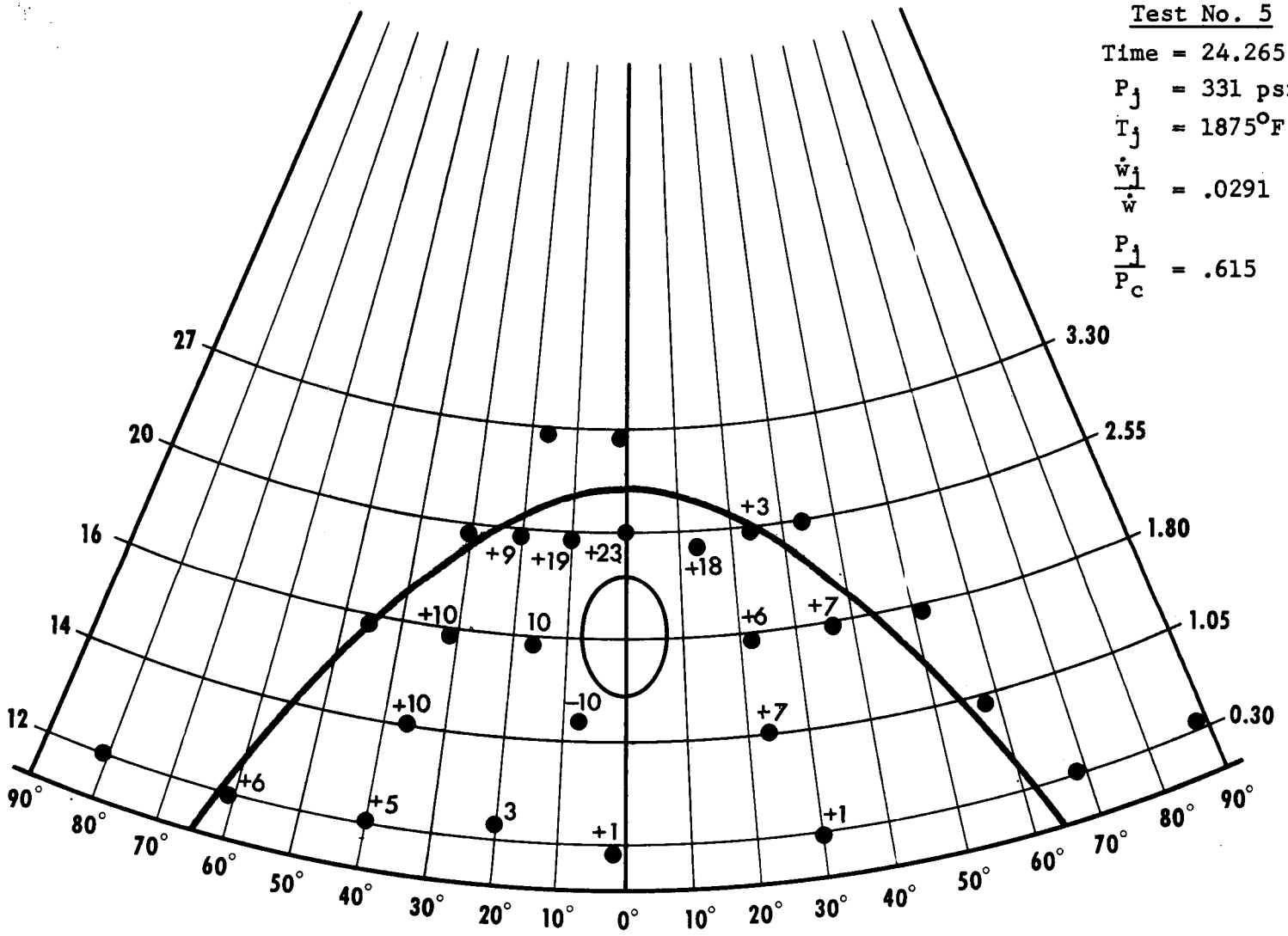
Test No. 5
Time = 24.265 secs.
P_j = 331 psia
T_j = 1875°F
$\frac{\dot{w}_j}{\dot{w}}$ = .0291
$\frac{P_j}{P_c}$ = .615
27
20
16
14
12
3.30
2.55
1.80
1.05
0.30
+3
+9
+19
+23
+18
+10
10
+6
+7
+10
-10
+7
+6
+5
3
+1
+1
90°
80°
70°
60°
50°
40°
30°
20°
10°
0°
10°
20°
30°
40°
50°
60°
70°
80°
90°

Figure 8.51

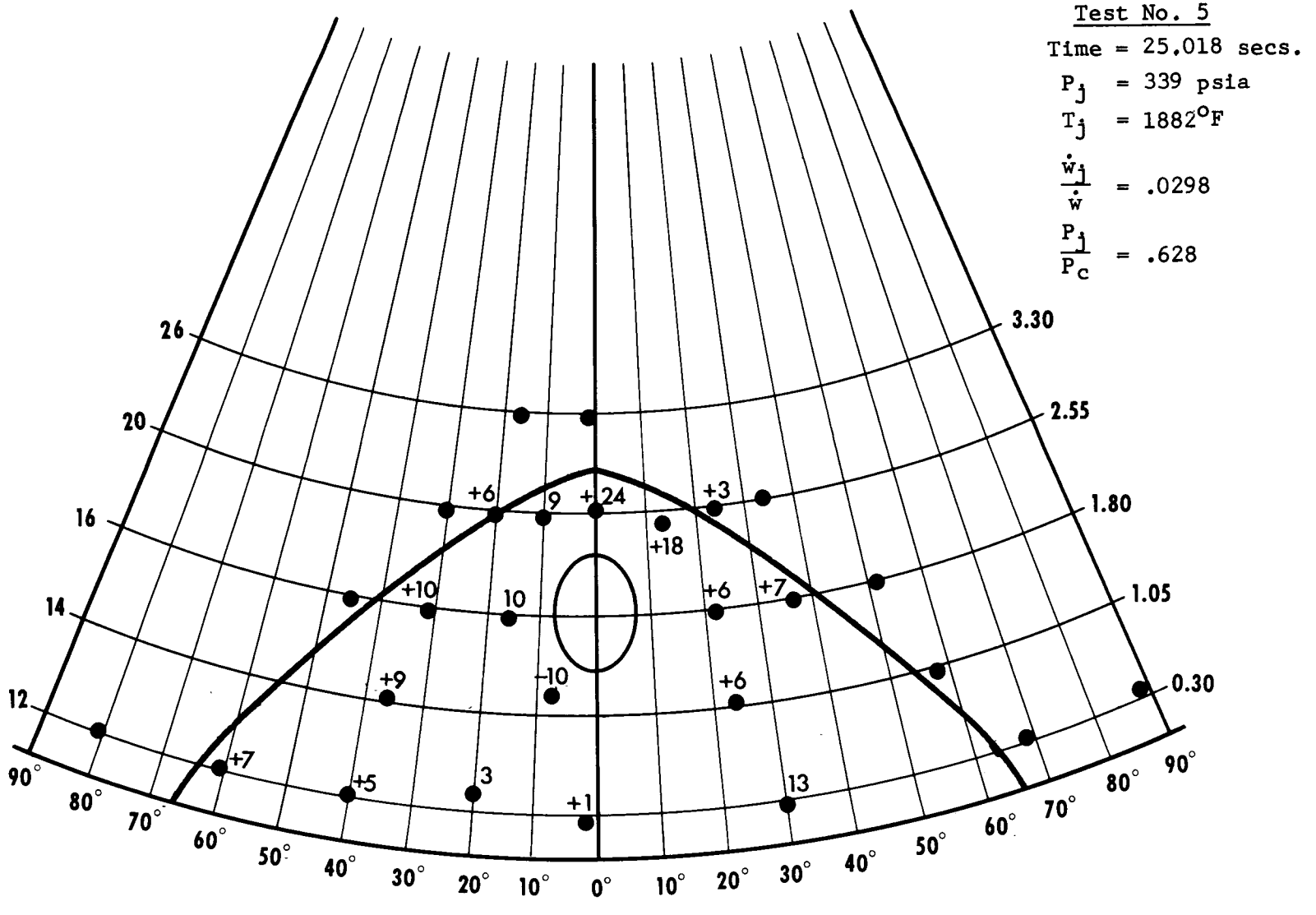
Test No. 5
Time = 25.018 secs.
P_j = 339 psia
T_j = 1882°F
$\frac{\dot{w}_j}{\dot{w}}$ = .0298
$\frac{P_j}{P_c}$ = .628
26
20
16
14
12
3.30
2.55
1.80
1.05
0.30
+6
9
+24
+3
+18
+10
10
+6
+7
+9
-10
+6
+7
+5
3
+1
13
90°
80°
70°
60°
50°
40°
30°
20°
10°
0°
10°
20°
30°
40°
50°
60°
70°
80°
90°

Figure 8.52

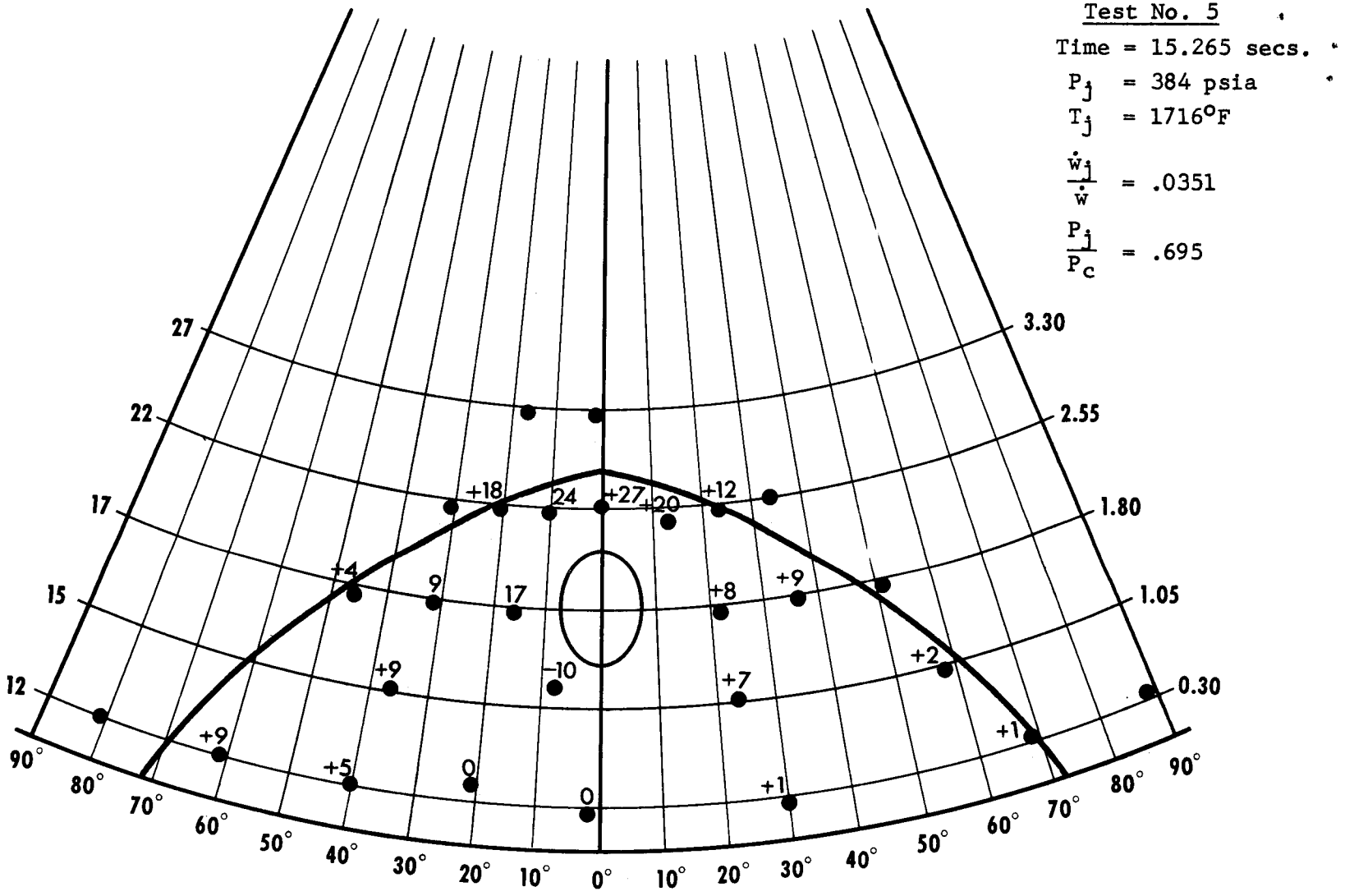
Test No. 5
Time = 15.265 secs.
P_j = 384 psia
T_j = 1716°F
$\frac{\dot{w}_j}{\dot{w}}$ = .0351
$\frac{P_j}{P_c}$ = .695
27
22
17
15
12
3.30
2.55
1.80
1.05
0.30
+18
24
+27
+20
+12
+4
9
17
+8
+9
+9
-10
+7
+2
+9
+5
0
0
+1
+1
90°
80°
70°
60°
50°
40°
30°
20°
10°
0°
10°
20°
30°
40°
50°
60°
70°
80°
90°

Figure 8.53

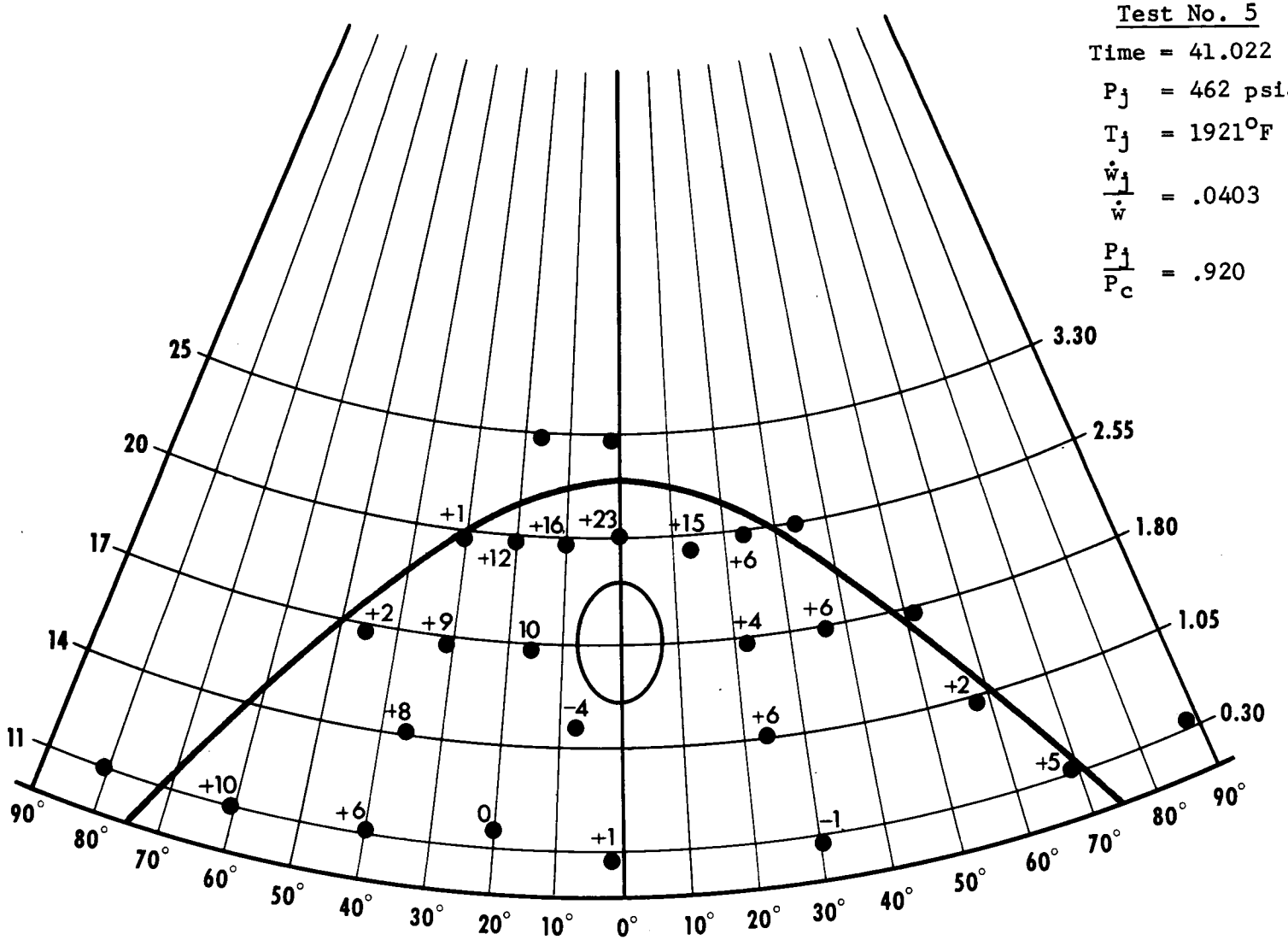
Test No. 5
Time = 41.022 secs.
P_j = 462 psia
T_j = 1921°F
$\frac{\dot{w}_j}{\dot{w}}$ = .0403
$\frac{P_j}{P_c}$ = .920
25
20
17
14
11
3.30
2.55
1.80
1.05
0.30
90°
80°
70°
60°
50°
40°
30°
20°
10°
0°
+1
+16
+23
+15
+12
+6
+2
+9
10
+4
+6
+8
-4
+6
+2
+10
+6
0
+1
-1
+5

Figure 8.54

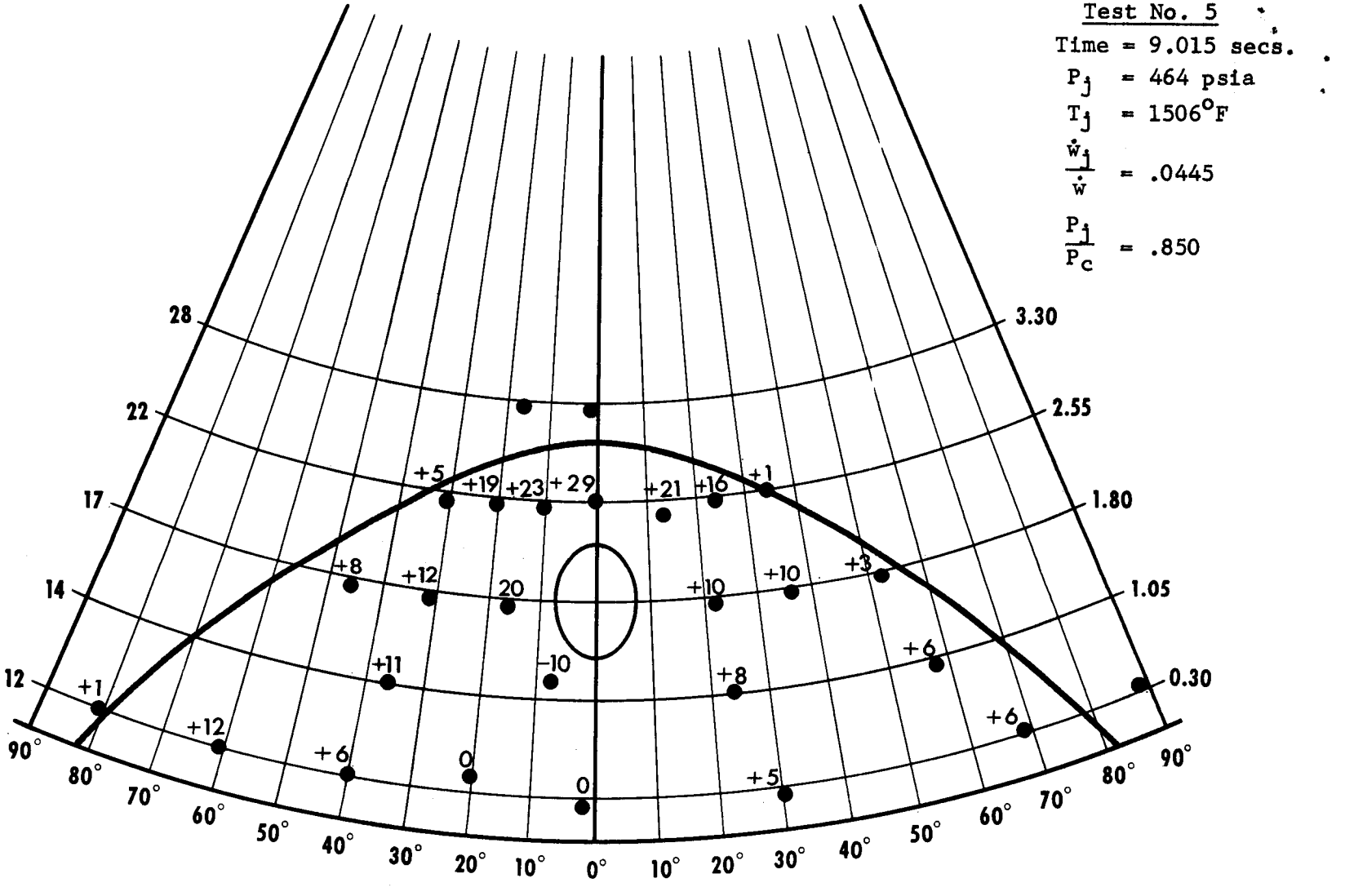
Test No. 5
Time = 9.015 secs.
P_j = 464 psia
T_j = 1506°F
$\frac{\dot{w}_j}{\dot{w}}$ = .0445
$\frac{P_j}{P_c}$ = .850
28
22
17
14
12
3.30
2.55
1.80
1.05
0.30
+5
+19
+23
+29
+21
+16
+1
+8
+12
20
+10
+10
+3
+11
-10
+8
+6
+1
+12
+6
0
0
+5
+6
90°
80°
70°
60°
50°
40°
30°
20°
10°
0°
10°
20°
30°
40°
50°
60°
70°
80°
90°

Figure 8.55

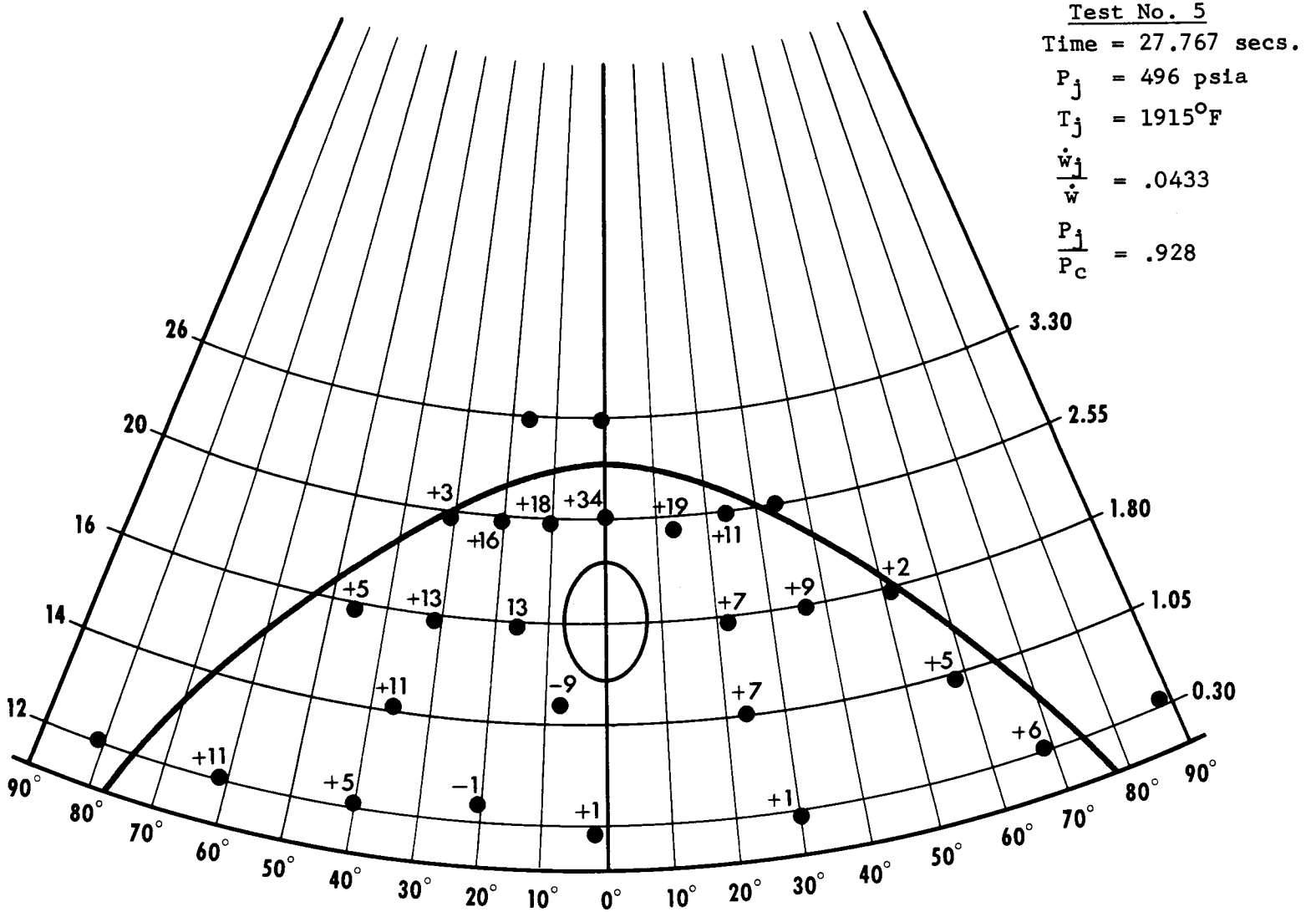
Test No. 5
Time = 27.767 secs.
P_j = 496 psia
T_j = 1915°F
$\frac{\dot{w}_j}{\dot{w}}$ = .0433
$\frac{P_j}{P_c}$ = .928
26
20
16
14
12
3.30
2.55
1.80
1.05
0.30
+3
+18
+34
+19
+11
+16
+5
+13
13
+7
+9
+2
+11
-9
+7
+5
+11
+5
-1
+1
+1
+6
90°
80°
70°
60°
50°
40°
30°
20°
10°
0°
10°
20°
30°
40°
50°
60°
70°
80°
90°

Figure 8.56

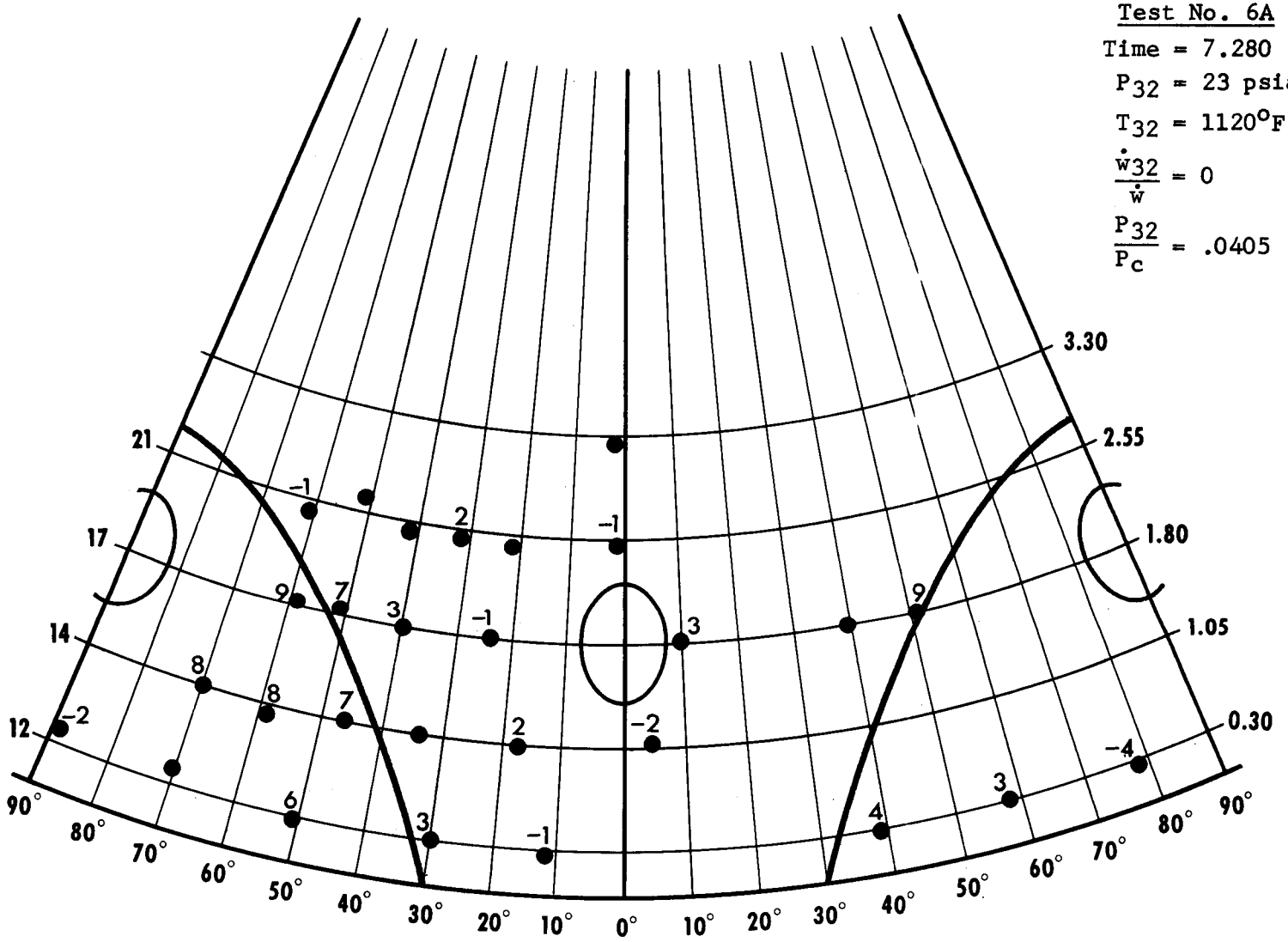
Test No. 6A
Time = 7.280 secs.
P_{32} = 23 psia
T_{32} = 1120°F
$\frac{\dot{w}_{32}}{\dot{w}}$ = 0
$\frac{P_{32}}{P_c}$ = .0405
3.30
2.55
1.80
1.05
0.30
21
17
14
12
90°
80°
70°
60°
50°
40°
30°
20°
10°
0°

Figure 8.57

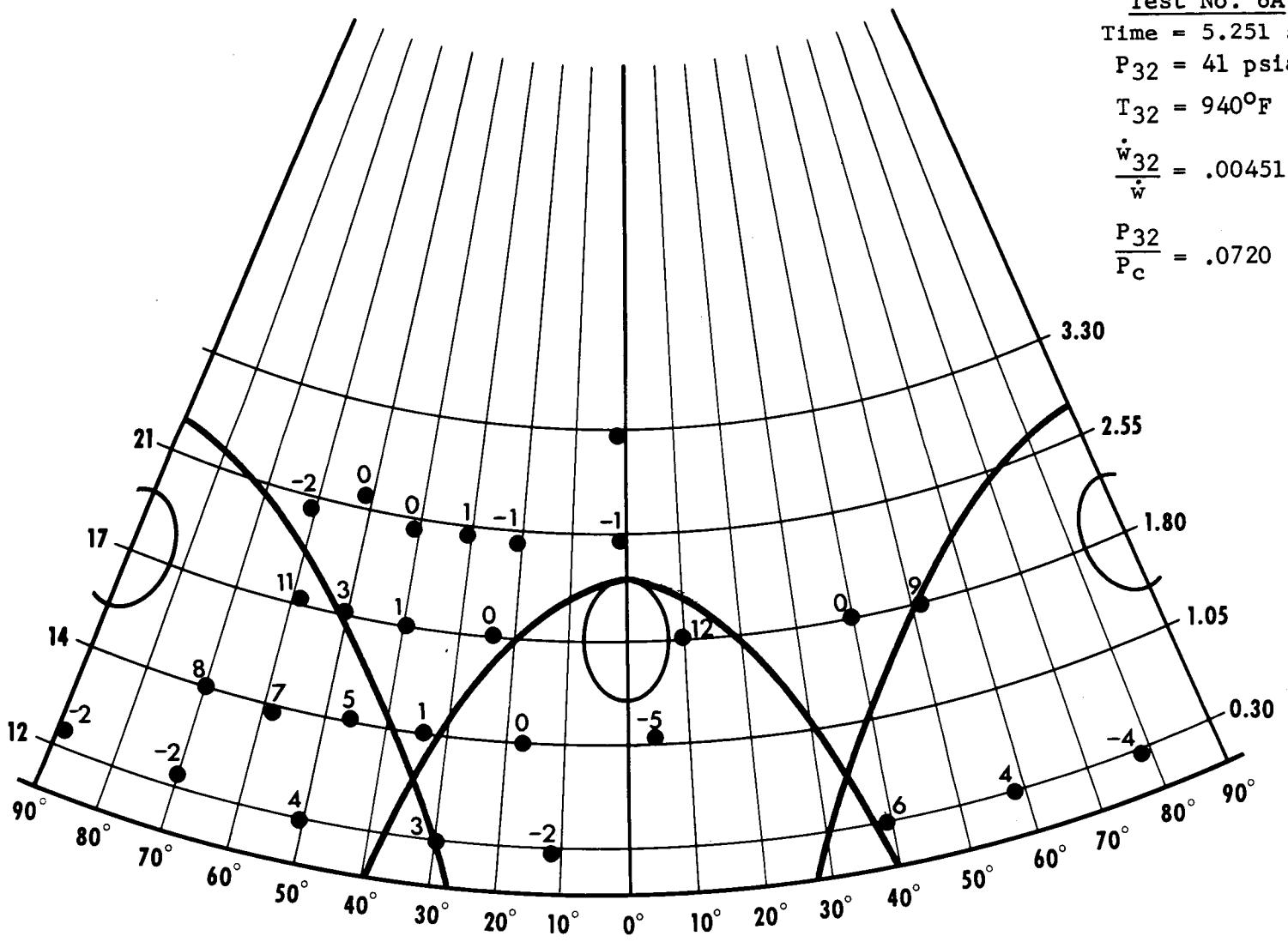
Test No. 6A
Time = 5.251 secs.
P32 = 41 psia
T32 = 940°F
ẇ32/ẇ = .00451
P32/Pc = .0720
3.30
2.55
1.80
1.05
0.30
21
17
14
12
90° 80° 70° 60° 50° 40° 30° 20° 10° 0° 10° 20° 30° 40° 50° 60° 70° 80° 90°

Figure 8.58

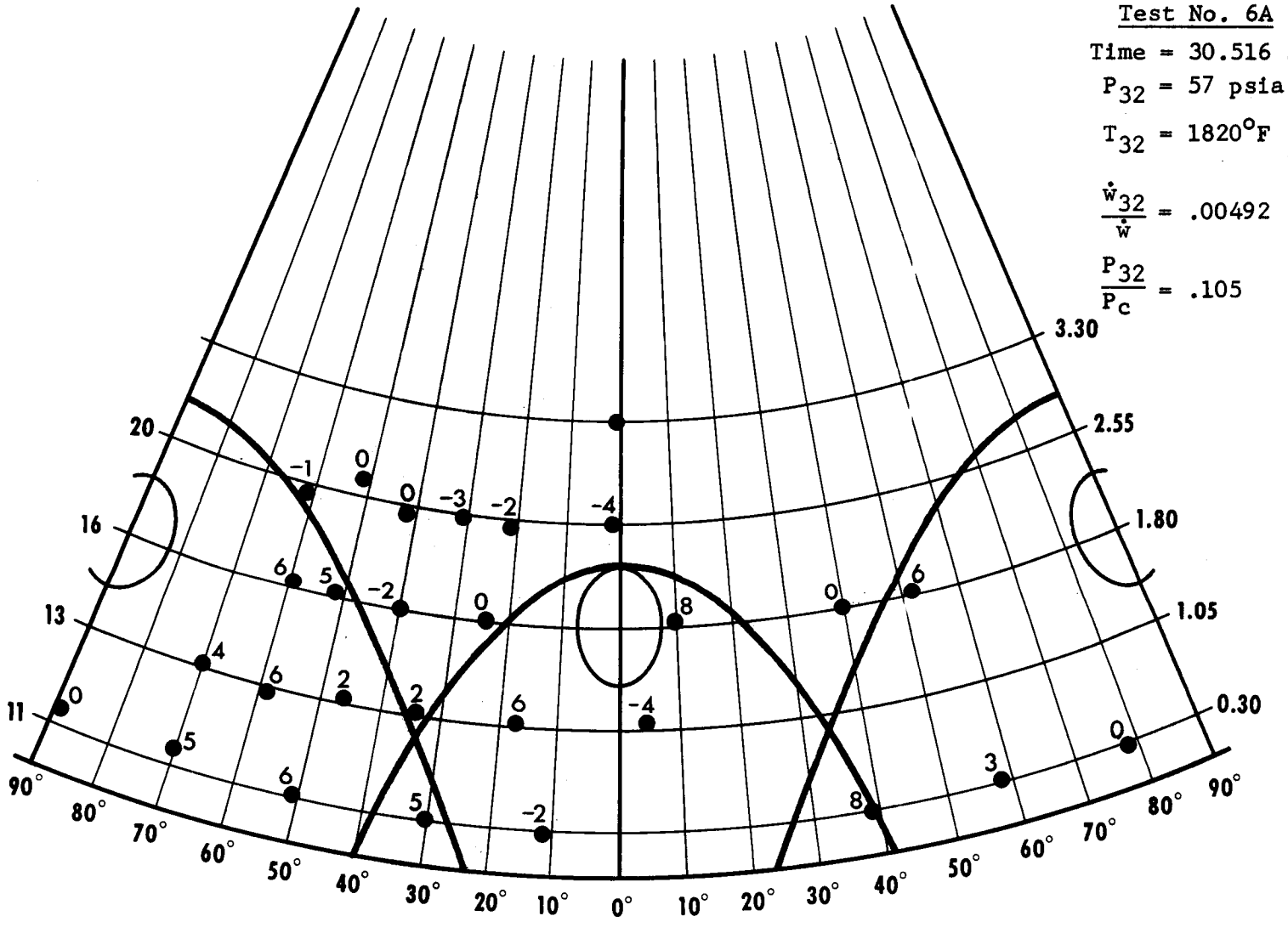
Test No. 6A
Time = 30.516 secs.
P_{32} = 57 psia
T_{32} = 1820°F
$\frac{\dot{w}_{32}}{\dot{w}}$ = .00492
$\frac{P_{32}}{P_c}$ = .105
3.30
2.55
1.80
1.05
0.30
20
16
13
11
90° 80° 70° 60° 50° 40° 30° 20° 10° 0° 10° 20° 30° 40° 50° 60° 70° 80° 90°

Figure 8.59

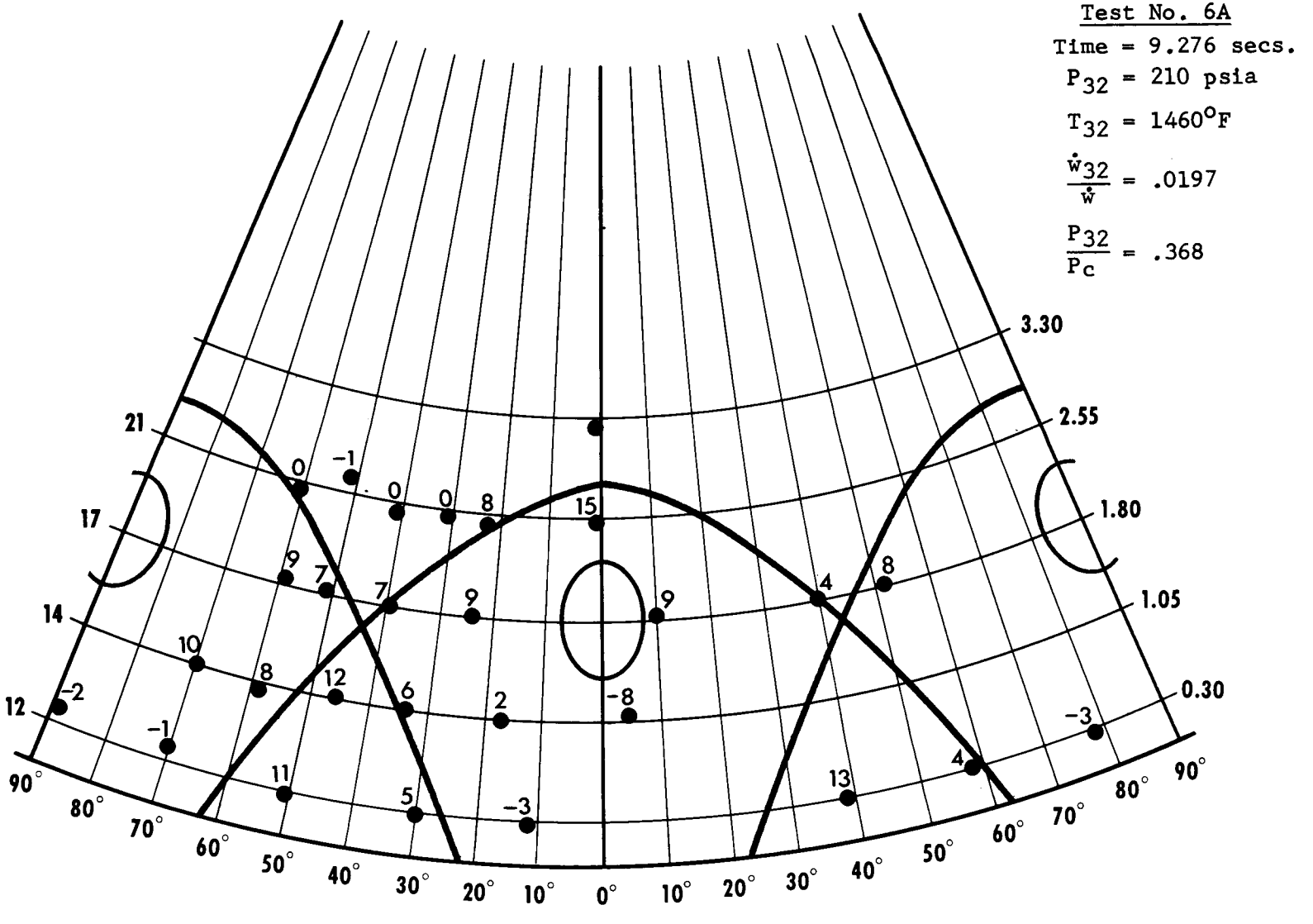
Test No. 6A
Time = 9.276 secs.
P_{32} = 210 psia
T_{32} = 1460°F
$\frac{\dot{w}_{32}}{\dot{w}}$ = .0197
$\frac{P_{32}}{P_c}$ = .368
3.30
2.55
1.80
1.05
0.30
21
17
14
12
90° 80° 70° 60° 50° 40° 30° 20° 10° 0° 10° 20° 30° 40° 50° 60° 70° 80° 90°

Figure 8.60

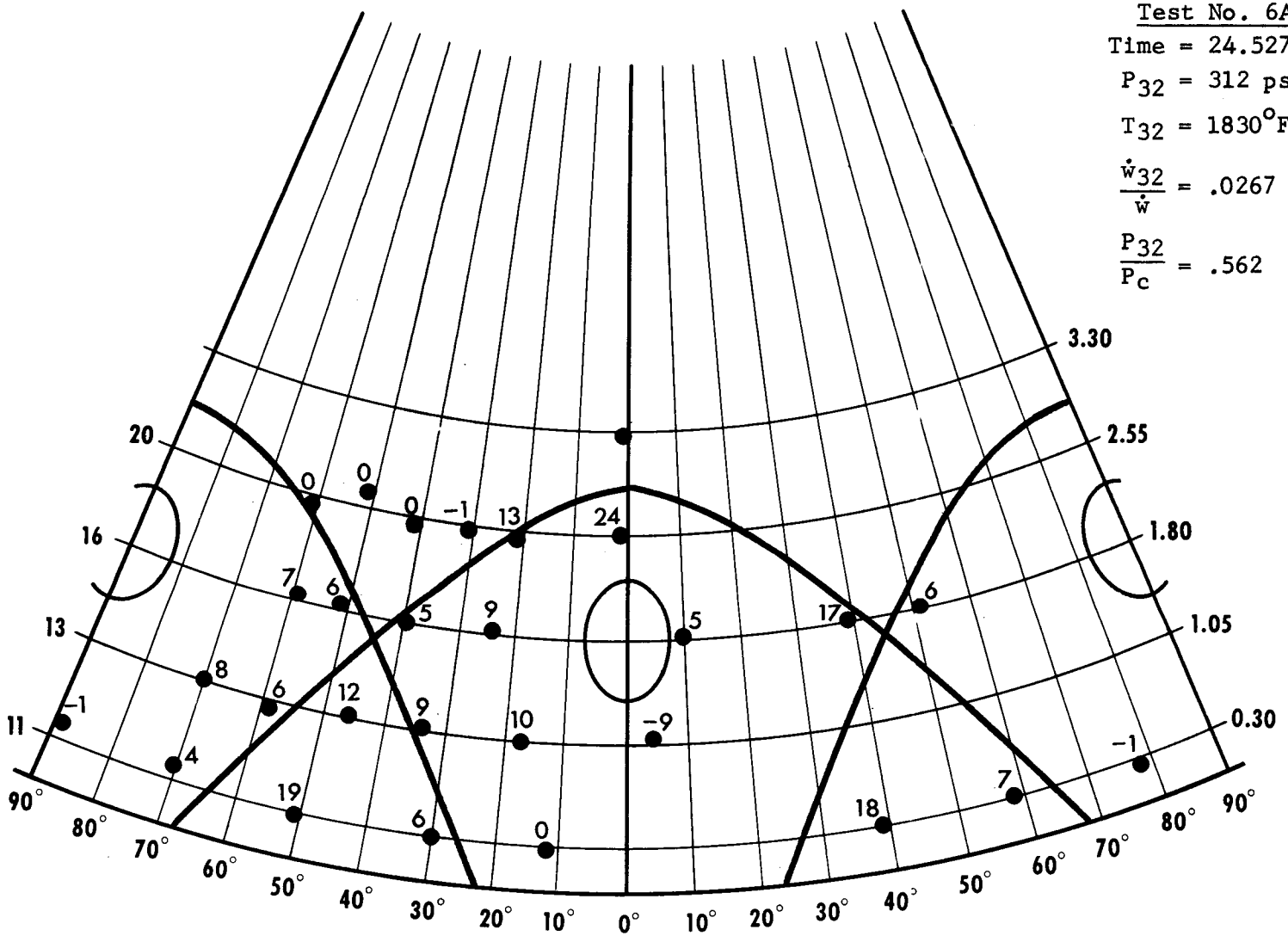
Test No. 6A
Time = 24.527 secs.
P32 = 312 psia
T32 = 1830°F
ẇ32/ẇ = .0267
P32/Pc = .562
3.30
2.55
1.80
1.05
0.30
20
16
13
11
90°
80°
70°
60°
50°
40°
30°
20°
10°
0°
0 0 0 -1 13 24
7 6 5 9 5 17 6
8 6 12 9 10 -9 -1
-1 4 19 6 0 18 7
-1

Figure 8.61

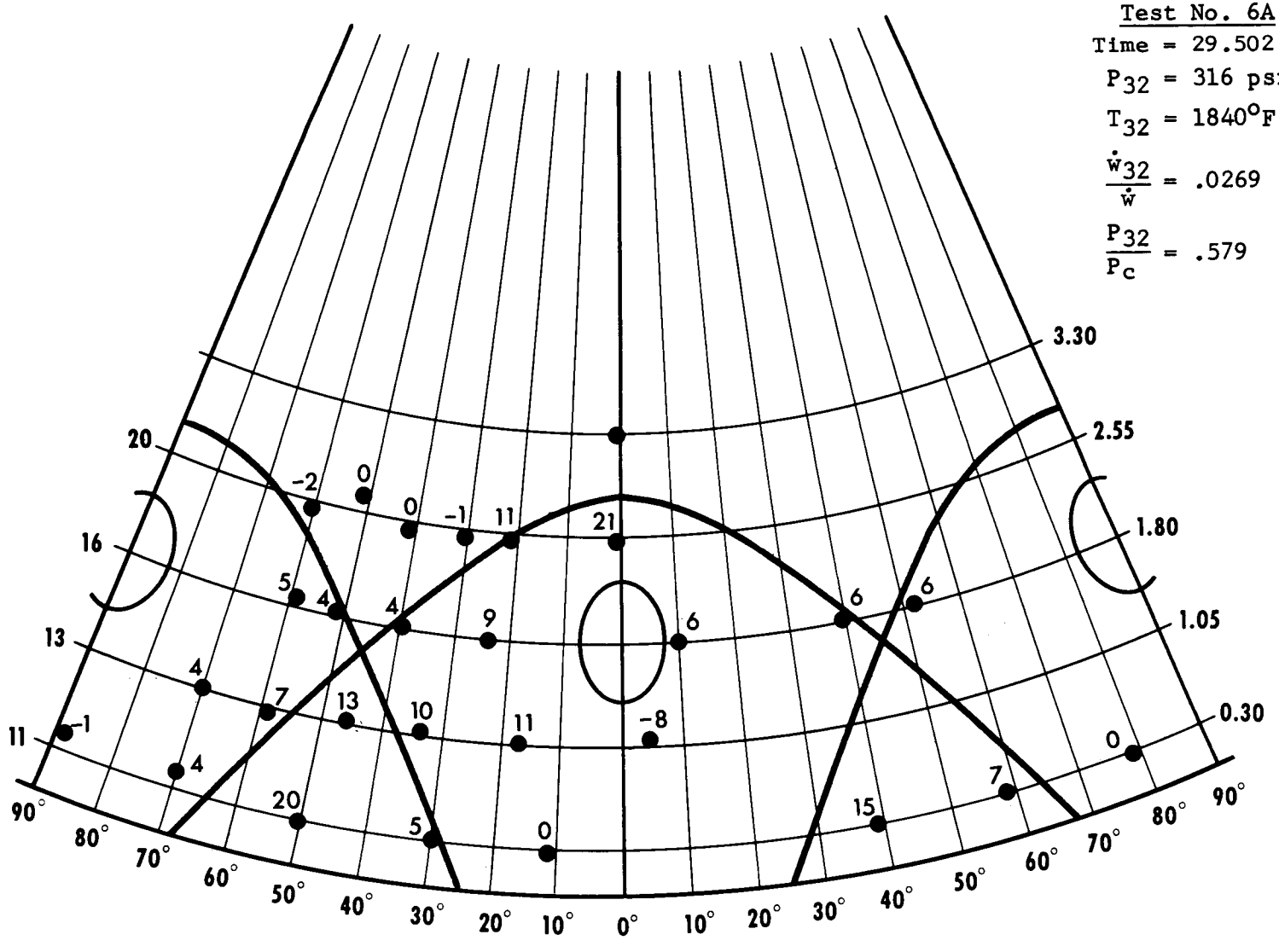
Test No. 6A
Time = 29.502 secs.
P_{32} = 316 psia
T_{32} = 1840°F
$\frac{\dot{w}_{32}}{\dot{w}}$ = .0269
$\frac{P_{32}}{P_c}$ = .579
3.30
2.55
1.80
1.05
0.30
20
16
13
11
90° 80° 70° 60° 50° 40° 30° 20° 10° 0° 10° 20° 30° 40° 50° 60° 70° 80° 90°

Figure 8.62

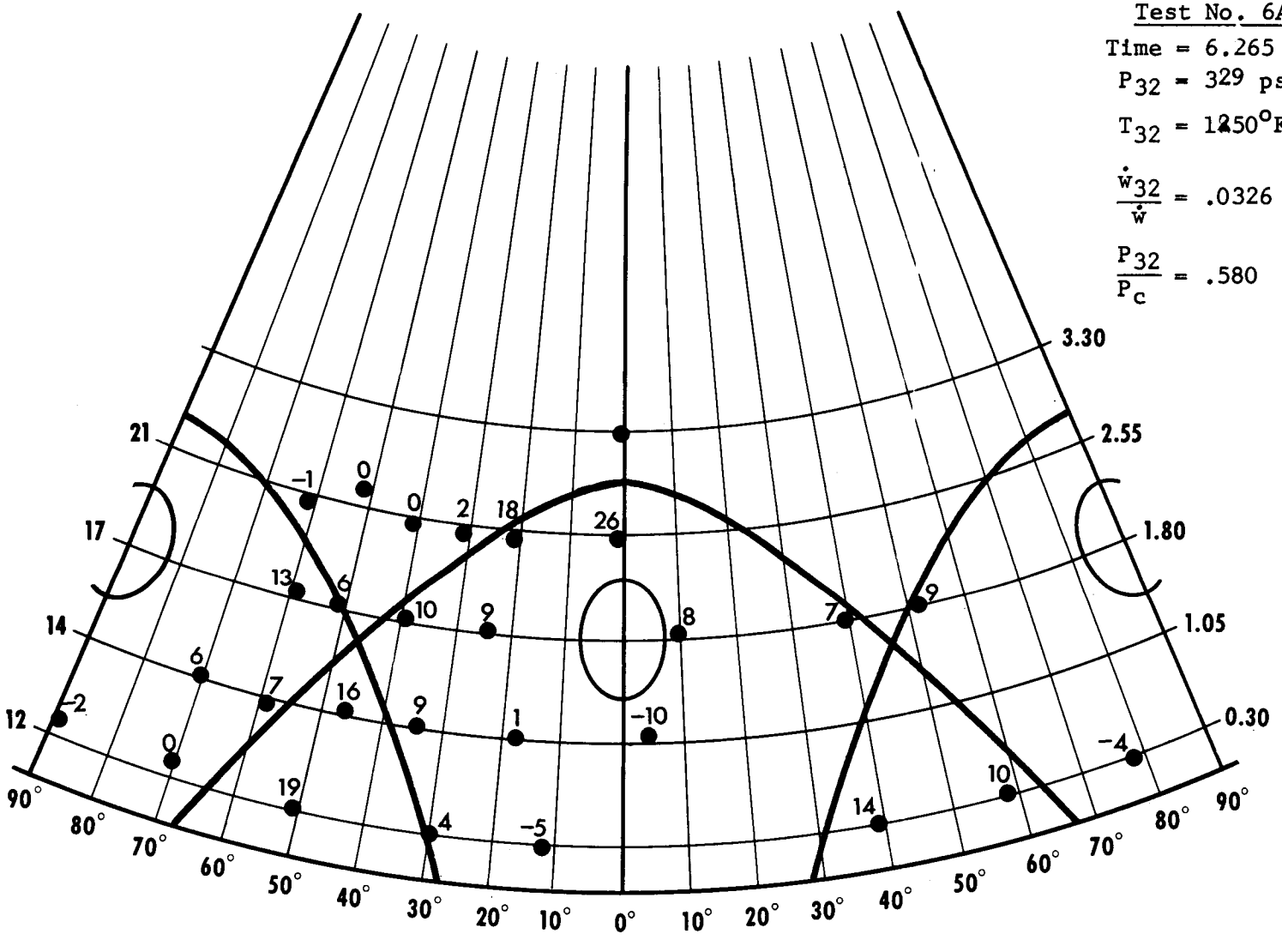
Test No. 6A
Time = 6.265 secs.
P32 = 329 psia
T32 = 1250°F
ẇ32/ẇ = .0326
P32/Pc = .580
3.30
2.55
1.80
1.05
0.30
21
17
14
12
90°
80°
70°
60°
50°
40°
30°
20°
10°
0°
10°
20°
30°
40°
50°
60°
70°
80°
90°
-1
0
0
2
18
26
13
6
10
9
8
7
9
6
7
16
9
1
-10
-2
0
19
4
-5
14
10
-4

Figure 8.63

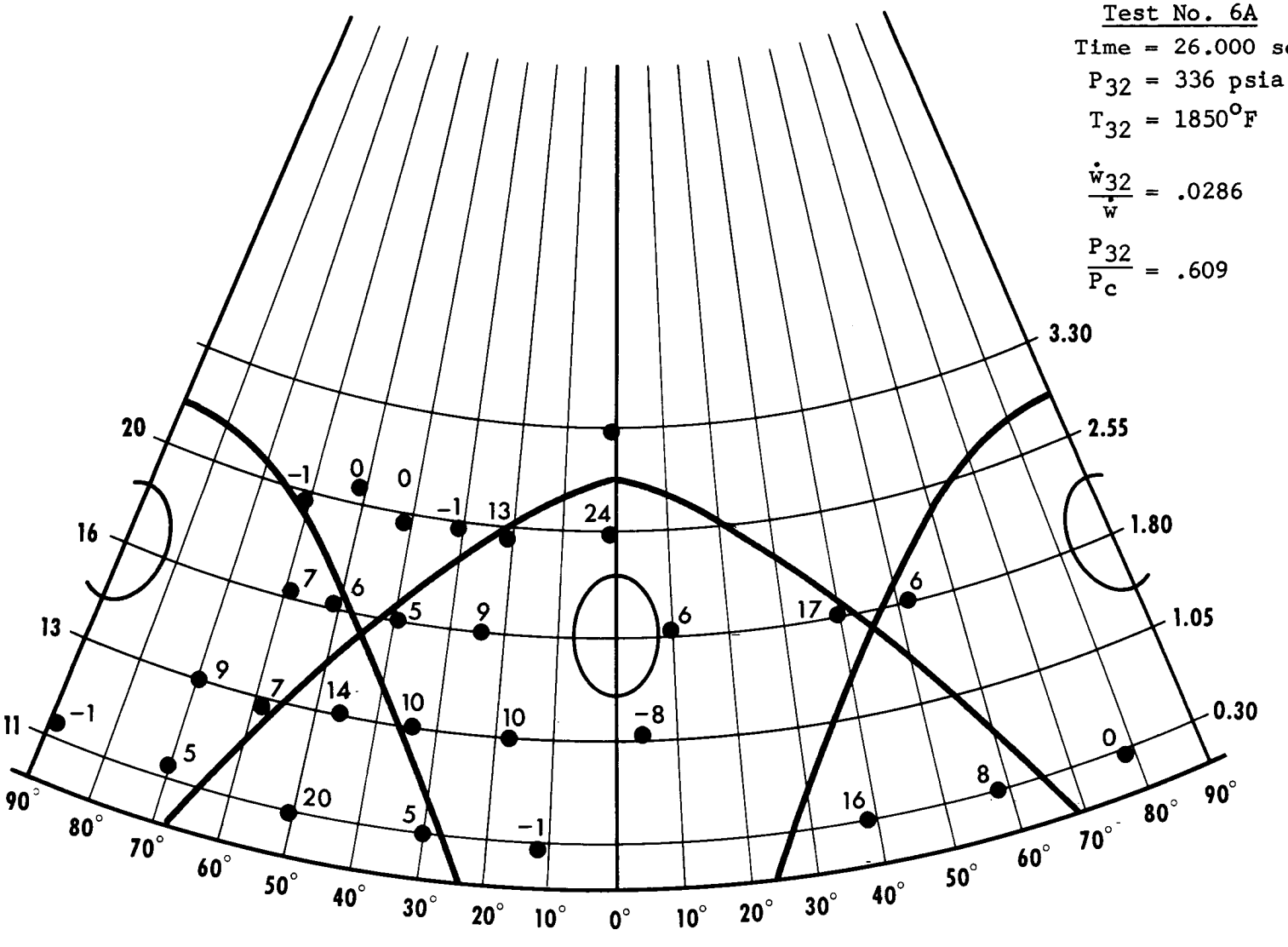
Test No. 6A
Time = 26.000 secs.
P32 = 336 psia
T32 = 1850°F
ẇ32/ẇ = .0286
P32/Pc = .609
3.30
2.55
1.80
1.05
0.30
20
16
13
11
90°
80°
70°
60°
50°
40°
30°
20°
10°
0°
10°
20°
30°
40°
50°
60°
70°
80°
90°
-1
0
0
-1
13
24
7
6
5
9
6
17
6
9
7
14
10
10
-8
-1
5
20
5
-1
16
8
0

Figure 8.64

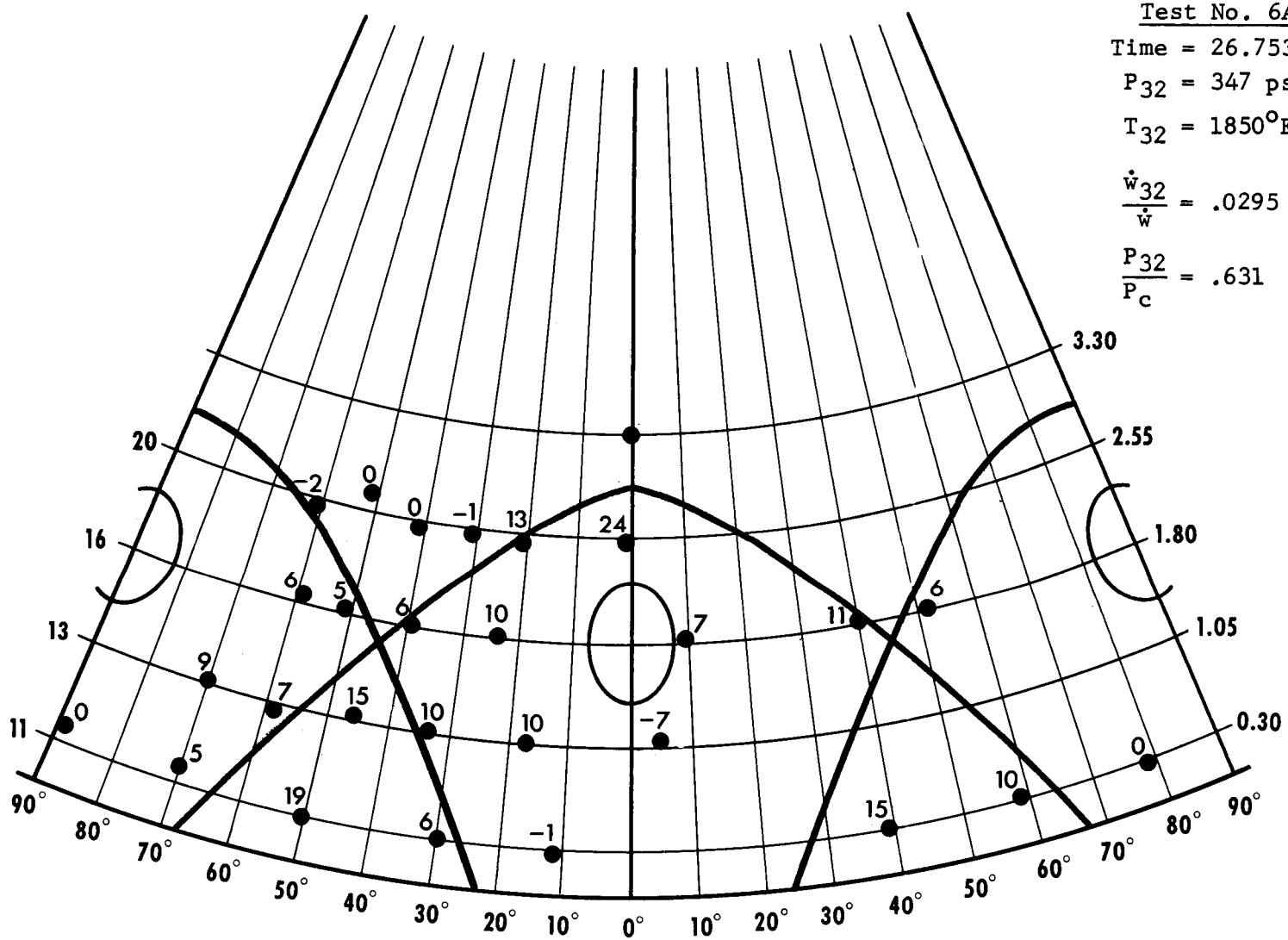
Test No. 6A
Time = 26.753 secs.
P_{32} = 347 psia
T_{32} = 1850°F
$\frac{\dot{w}_{32}}{\dot{w}}$ = .0295
$\frac{P_{32}}{P_c}$ = .631
3.30
2.55
1.80
1.05
0.30
20
16
13
11
90° 80° 70° 60° 50° 40° 30° 20° 10° 0° 10° 20° 30° 40° 50° 60° 70° 80° 90°

Figure 8.65

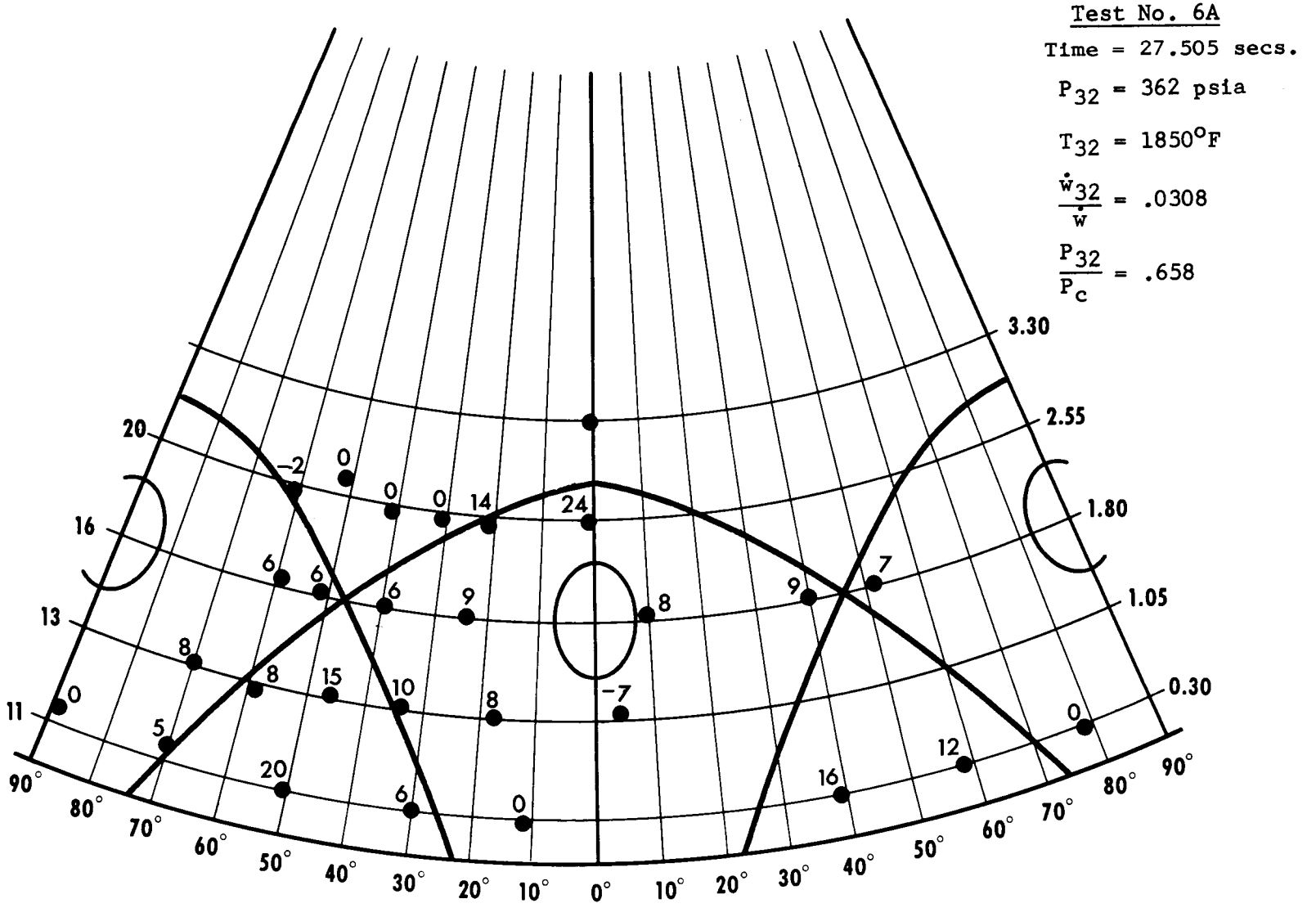
Test No. 6A
Time = 27.505 secs.
P_{32} = 362 psia
T_{32} = 1850°F
$\frac{\dot{w}_{32}}{\dot{w}}$ = .0308
$\frac{P_{32}}{P_c}$ = .658
3.30
2.55
1.80
1.05
0.30
20
16
13
11
90° 80° 70° 60° 50° 40° 30° 20° 10° 0° 10° 20° 30° 40° 50° 60° 70° 80° 90°
-2 0 0 0 14 24
6 6 6 9 8 9 7
8 8 15 10 8 -7
0 5 20 6 0 16 12 0

Figure 8.66

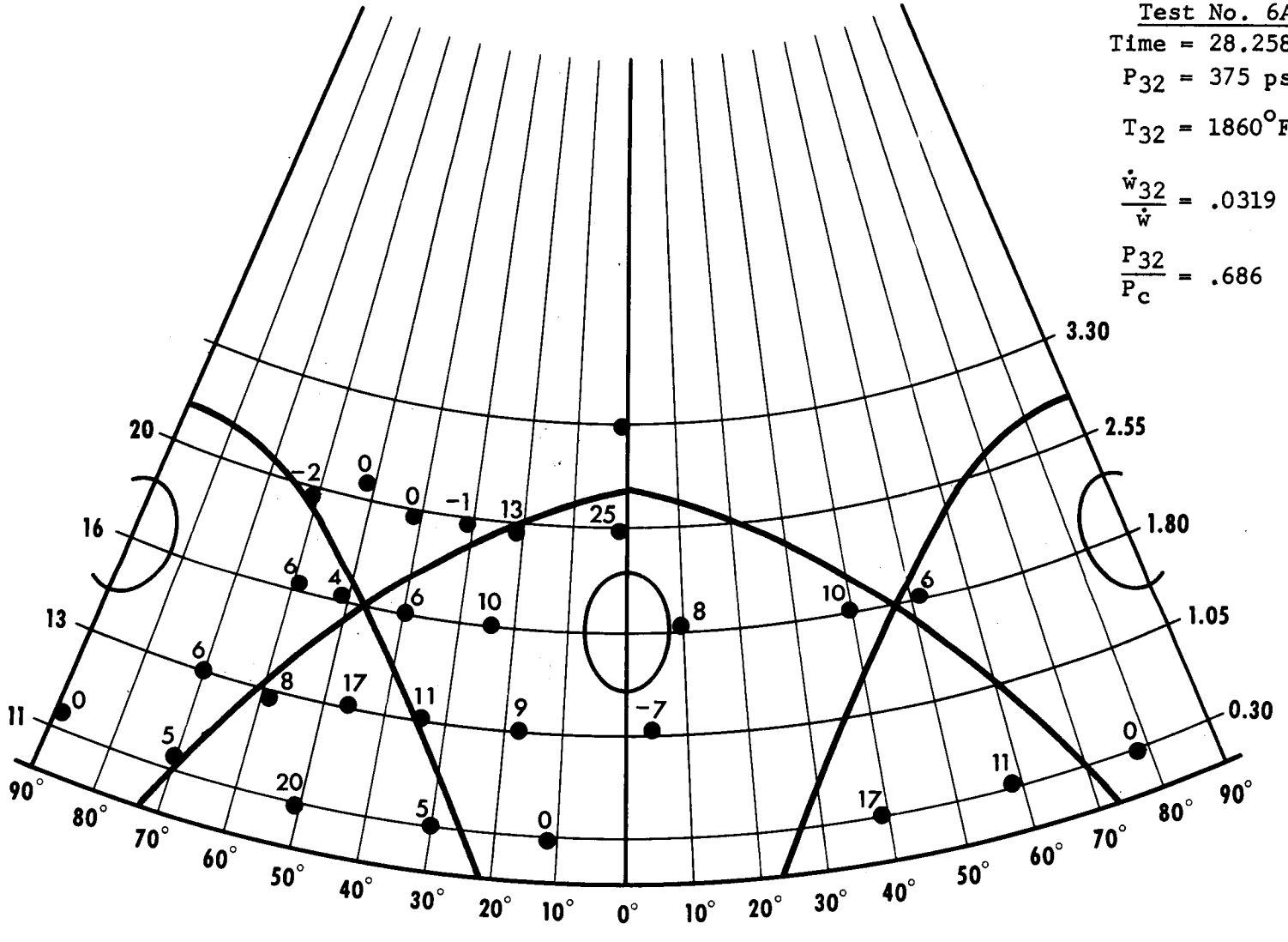
Test No. 6A
Time = 28.258 secs.
P_{32} = 375 psia
T_{32} = 1860°F
$\frac{\dot{w}_{32}}{\dot{w}}$ = .0319
$\frac{P_{32}}{P_c}$ = .686
3.30
2.55
1.80
1.05
0.30
20
16
13
11
90° 80° 70° 60° 50° 40° 30° 20° 10° 0° 10° 20° 30° 40° 50° 60° 70° 80° 90°

Figure 8.67

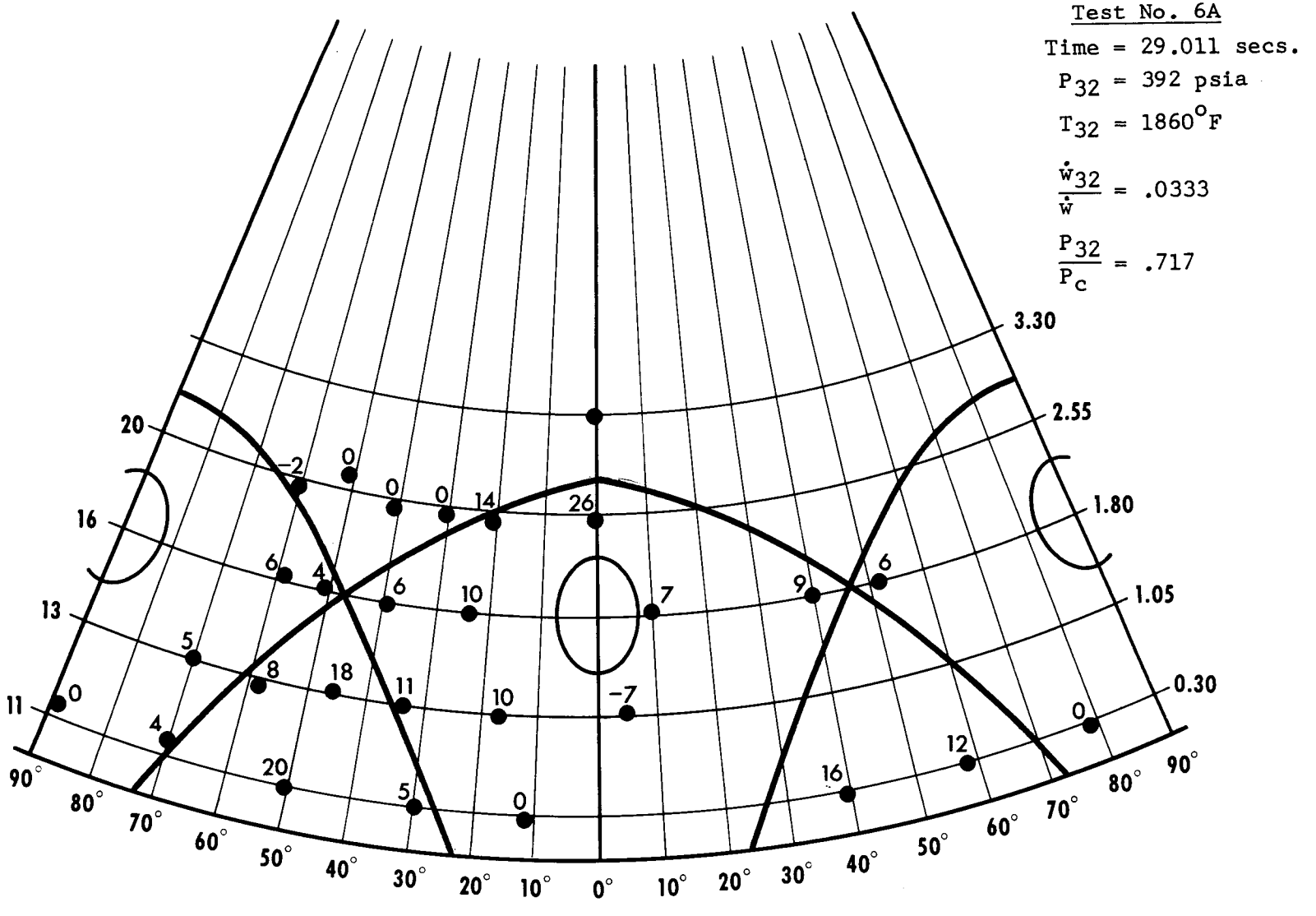
Test No. 6A
Time = 29.011 secs.
P32 = 392 psia
T32 = 1860°F
ẇ32/ẇ = .0333
P32/Pc = .717
3.30
2.55
1.80
1.05
0.30
20
16
13
11
90° 80° 70° 60° 50° 40° 30° 20° 10° 0° 10° 20° 30° 40° 50° 60° 70° 80° 90°
-2 0 0 0 14 26
6 4 6 10 7 9 6
5 8 18 11 10 -7
0 4 20 5 0 16 12 0

Figure 8.68

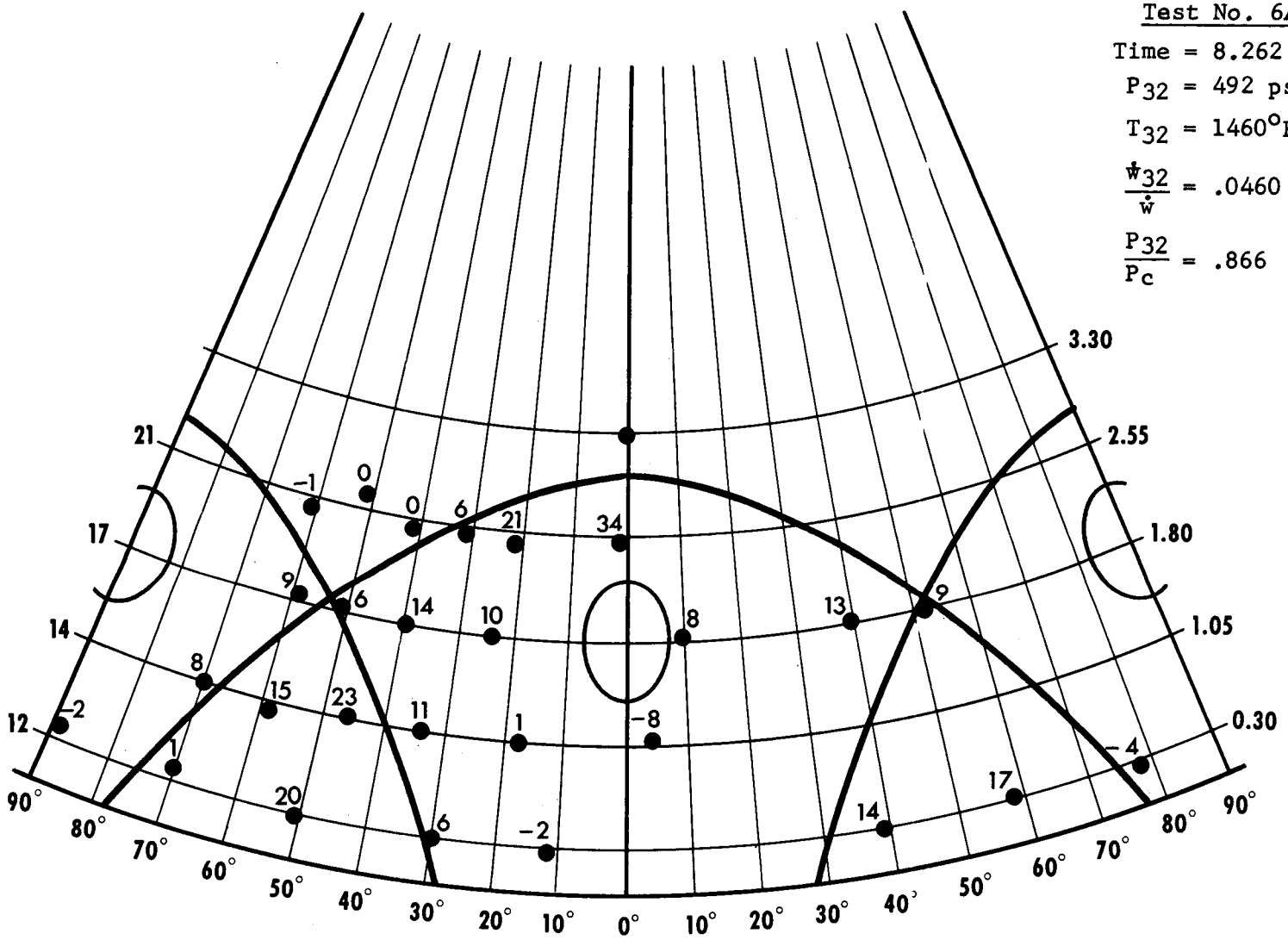
Test No. 6A
Time = 8.262 secs.
P32 = 492 psia
T32 = 1460°F
ẇ32/ẇ = .0460
P32/Pc = .866
3.30
2.55
1.80
1.05
0.30
21
17
14
12
90°
80°
70°
60°
50°
40°
30°
20°
10°
0°
10°
20°
30°
40°
50°
60°
70°
80°
90°
-1
0
0
6
21
34
9
6
14
10
8
13
9
8
15
23
11
1
-8
-4
-2
1
20
6
-2
14
17

Figure 8.69

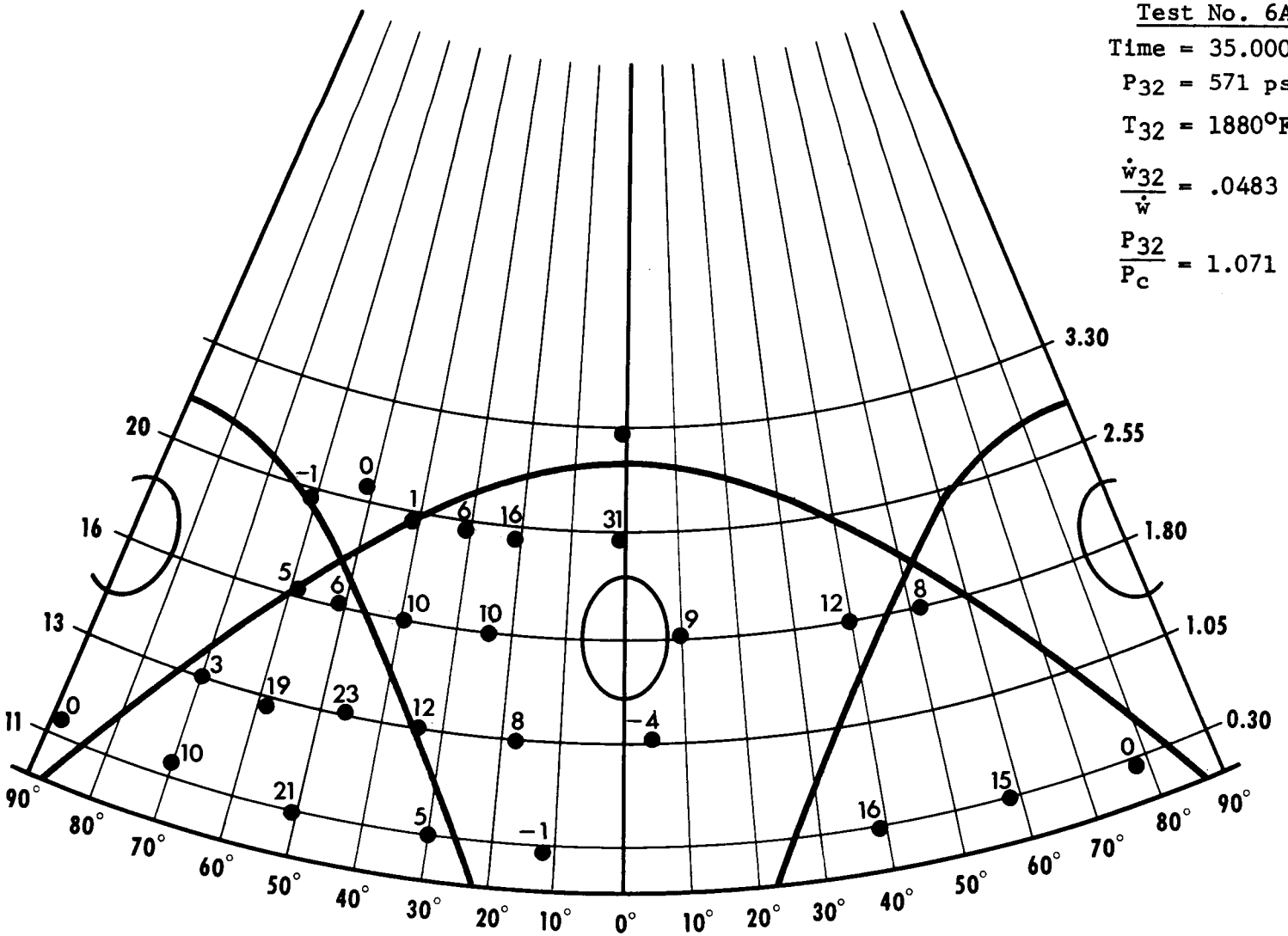
Test No. 6A
Time = 35.000 secs.
P32 = 571 psia
T32 = 1880°F
ẇ32/ẇ = .0483
P32/Pc = 1.071
3.30
2.55
1.80
1.05
0.30
20
16
13
11
90°
80°
70°
60°
50°
40°
30°
20°
10°
0°
10°
20°
30°
40°
50°
60°
70°
80°
90°

Figure 8.70

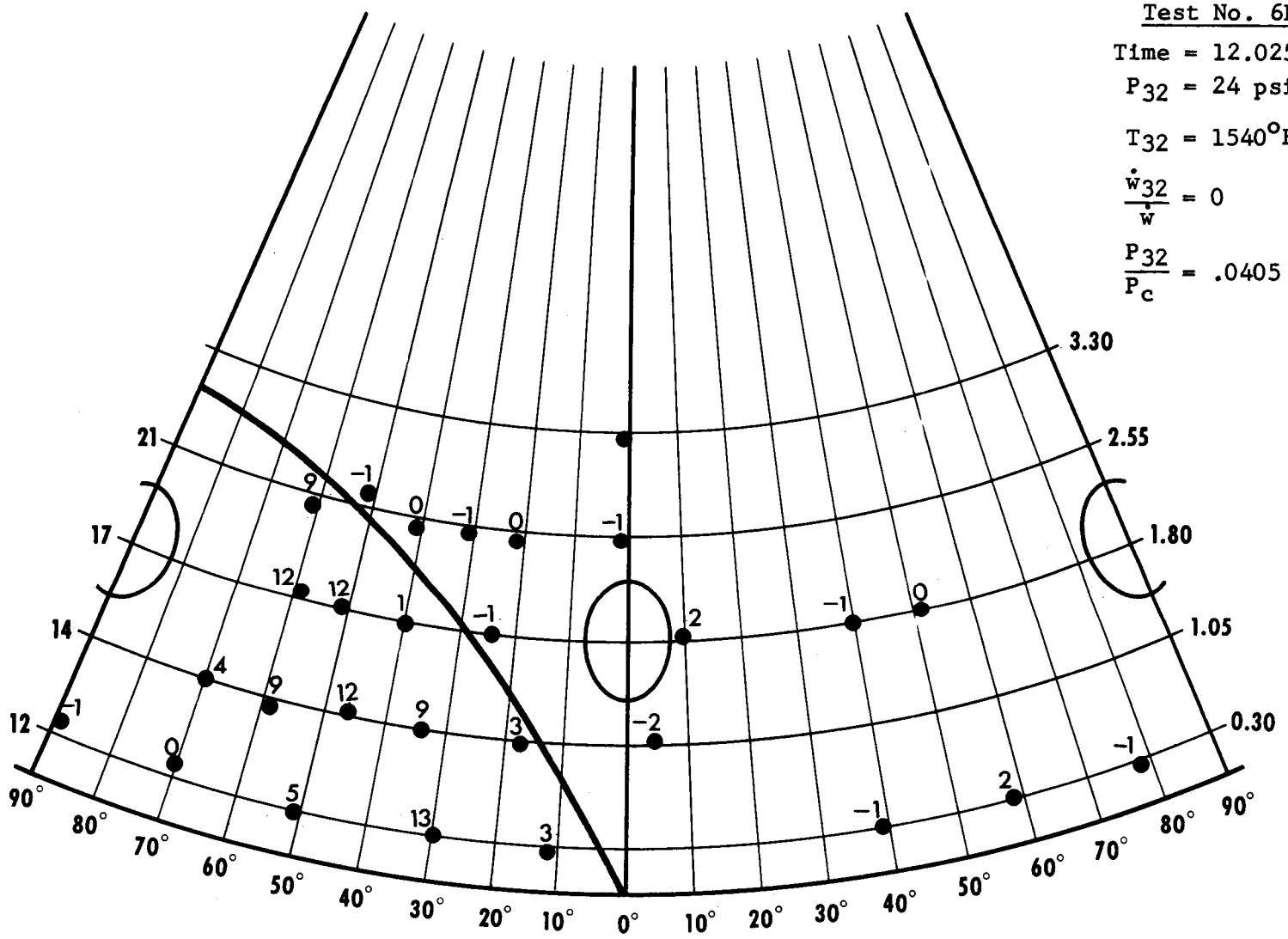
Test No. 6B
Time = 12.025 secs.
P_{32} = 24 psia
T_{32} = 1540°F
$\frac{\dot{w}_{32}}{\dot{w}}$ = 0
$\frac{P_{32}}{P_c}$ = .0405
3.30
2.55
1.80
1.05
0.30
21
17
14
12
90° 80° 70° 60° 50° 40° 30° 20° 10° 0° 10° 20° 30° 40° 50° 60° 70° 80° 90°

Figure 8.71

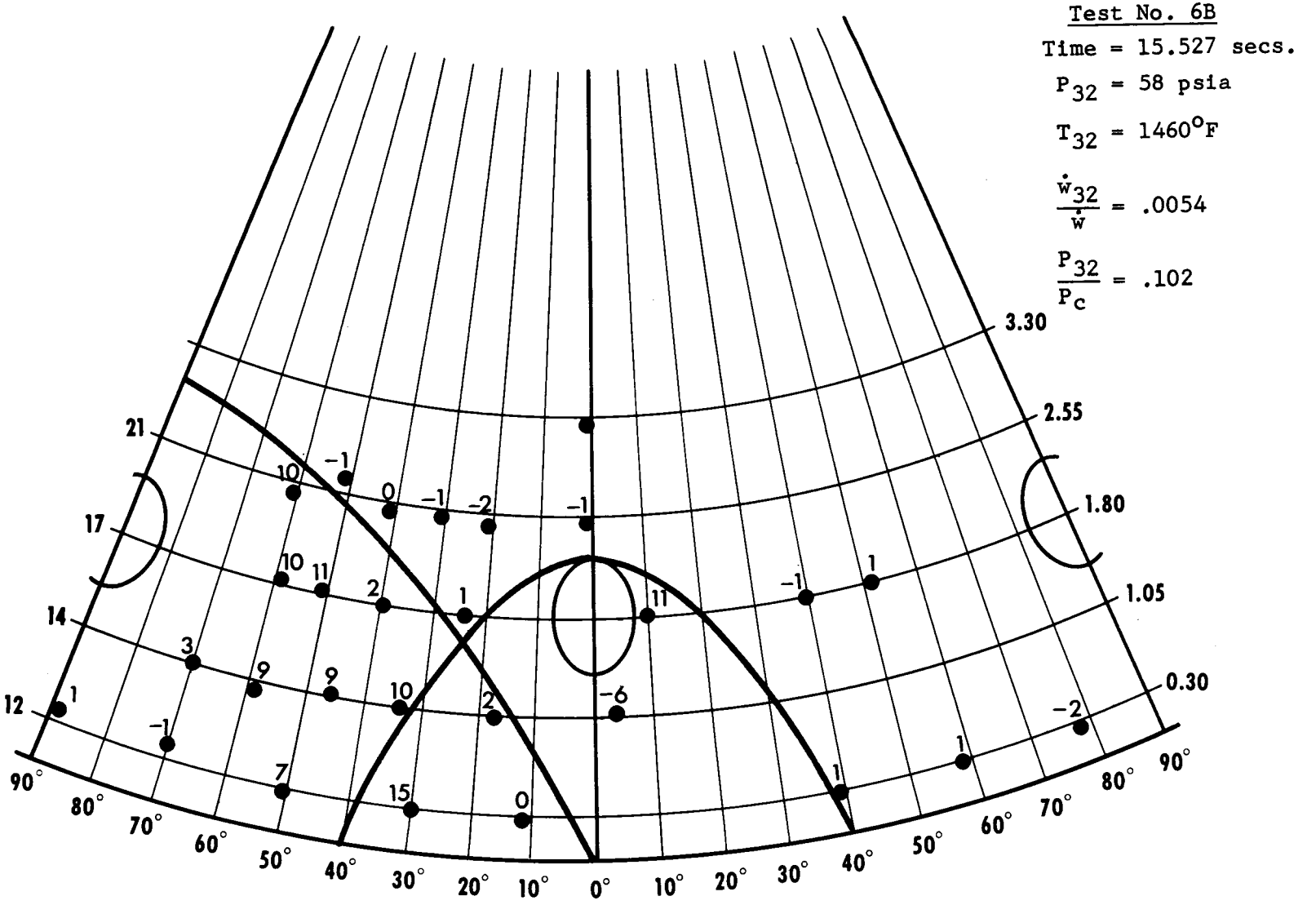
Test No. 6B
Time = 15.527 secs.
P_{32} = 58 psia
T_{32} = 1460°F
$\frac{\dot{w}_{32}}{\dot{w}}$ = .0054
$\frac{P_{32}}{P_c}$ = .102
3.30
2.55
1.80
1.05
0.30
21
17
14
12
90° 80° 70° 60° 50° 40° 30° 20° 10° 0° 10° 20° 30° 40° 50° 60° 70° 80° 90°

Figure 8.72

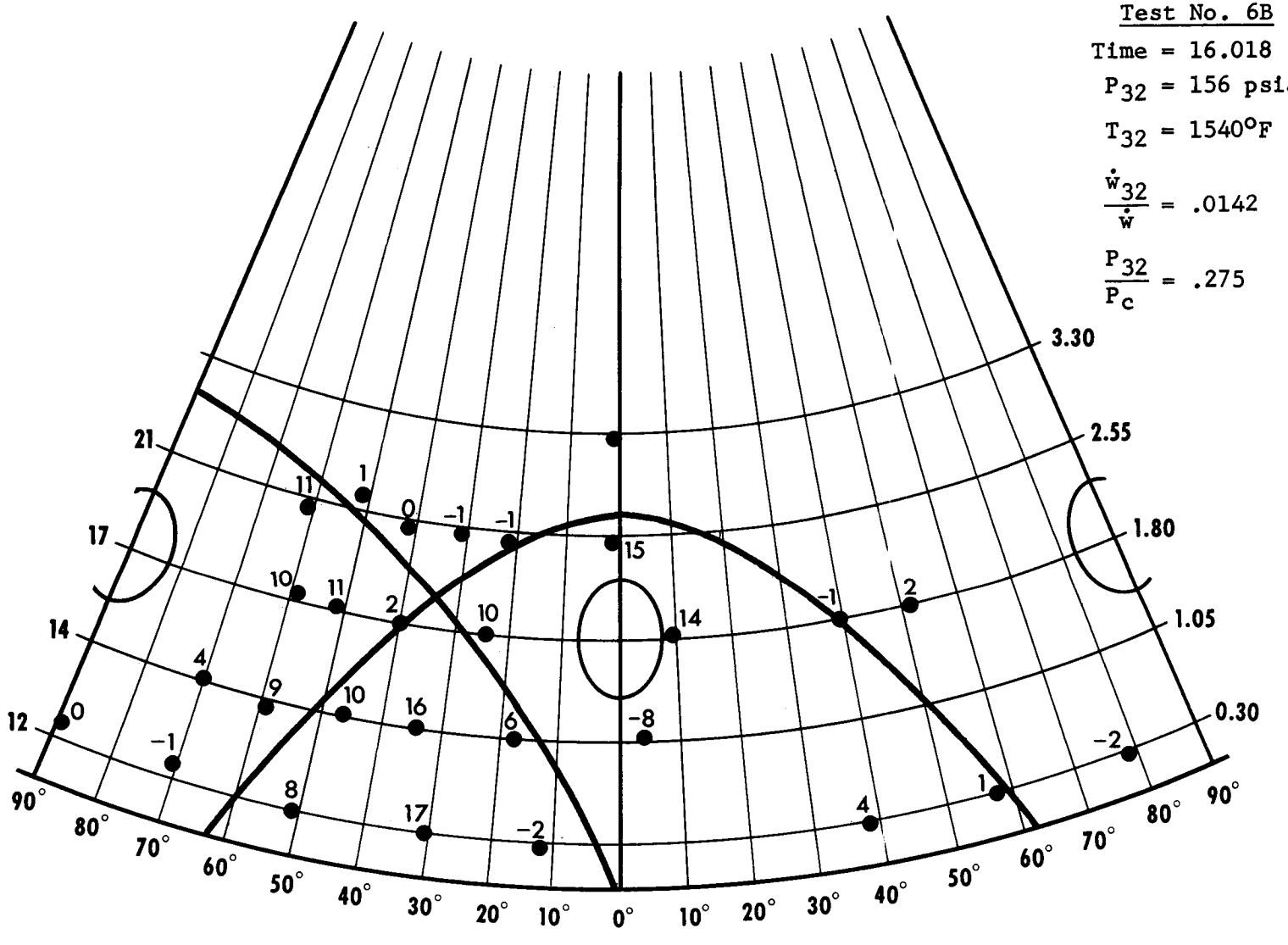
Test No. 6B
Time = 16.018
P_{32} = 156 psia
T_{32} = 1540°F
$\frac{\dot{w}_{32}}{\dot{w}}$ = .0142
$\frac{P_{32}}{P_c}$ = .275
3.30
2.55
1.80
1.05
0.30
21
17
14
12
90°
80°
70°
60°
50°
40°
30°
20°
10°
0°
10°
20°
30°
40°
50°
60°
70°
80°
90°

Figure 8.73

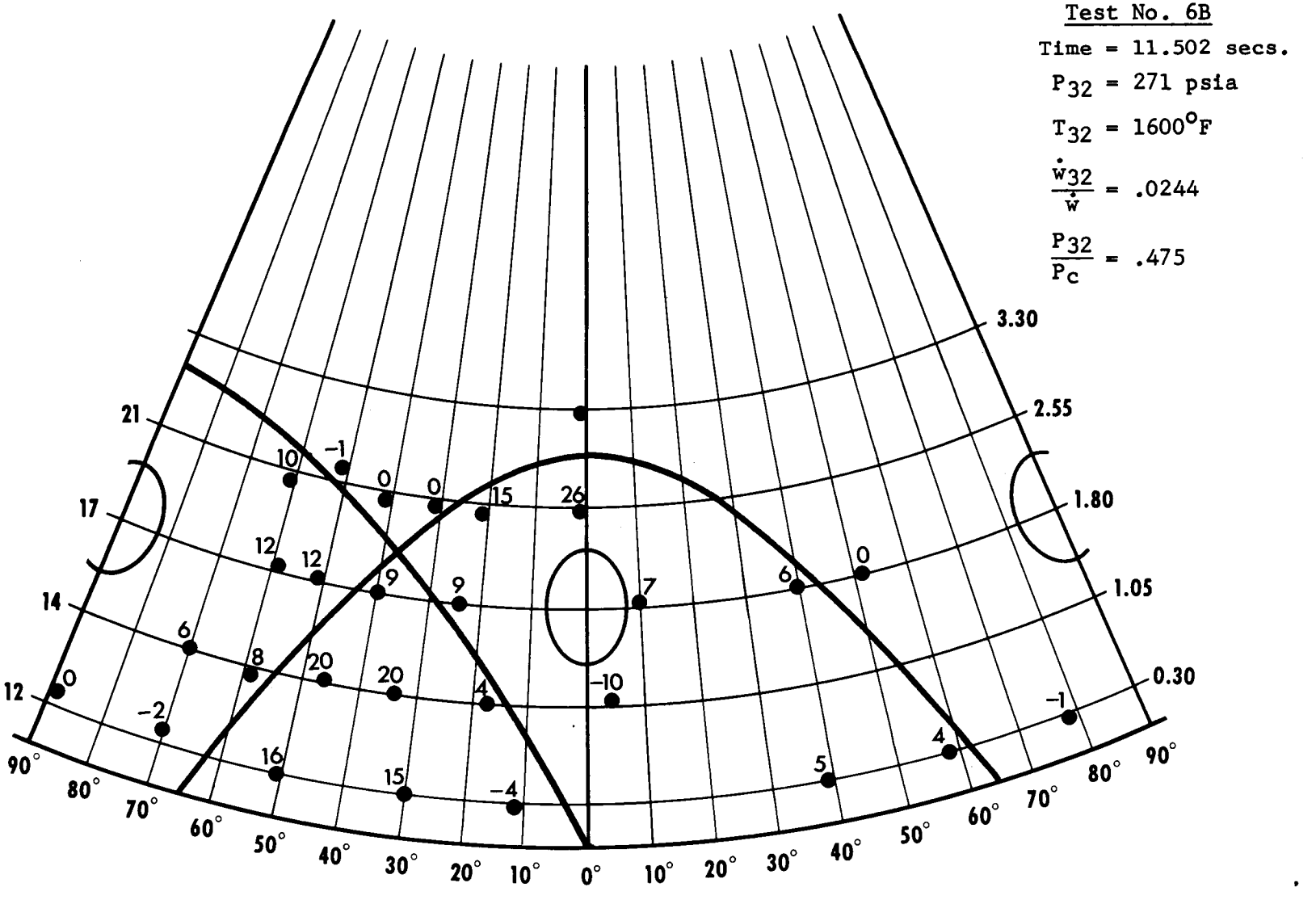
Test No. 6B
Time = 11.502 secs.
P32 = 271 psia
T32 = 1600°F
ẇ32/ẇ = .0244
P32/Pc = .475
3.30
2.55
1.80
1.05
0.30
21
17
14
12
90°
80°
70°
60°
50°
40°
30°
20°
10°
0°
10°
20°
30°
40°
50°
60°
70°
80°
90°
10
-1
0
0
15
26
12
12
9
9
7
6
0
6
8
20
20
4
-10
0
-2
-1
16
15
-4
5
4

Figure 8.74

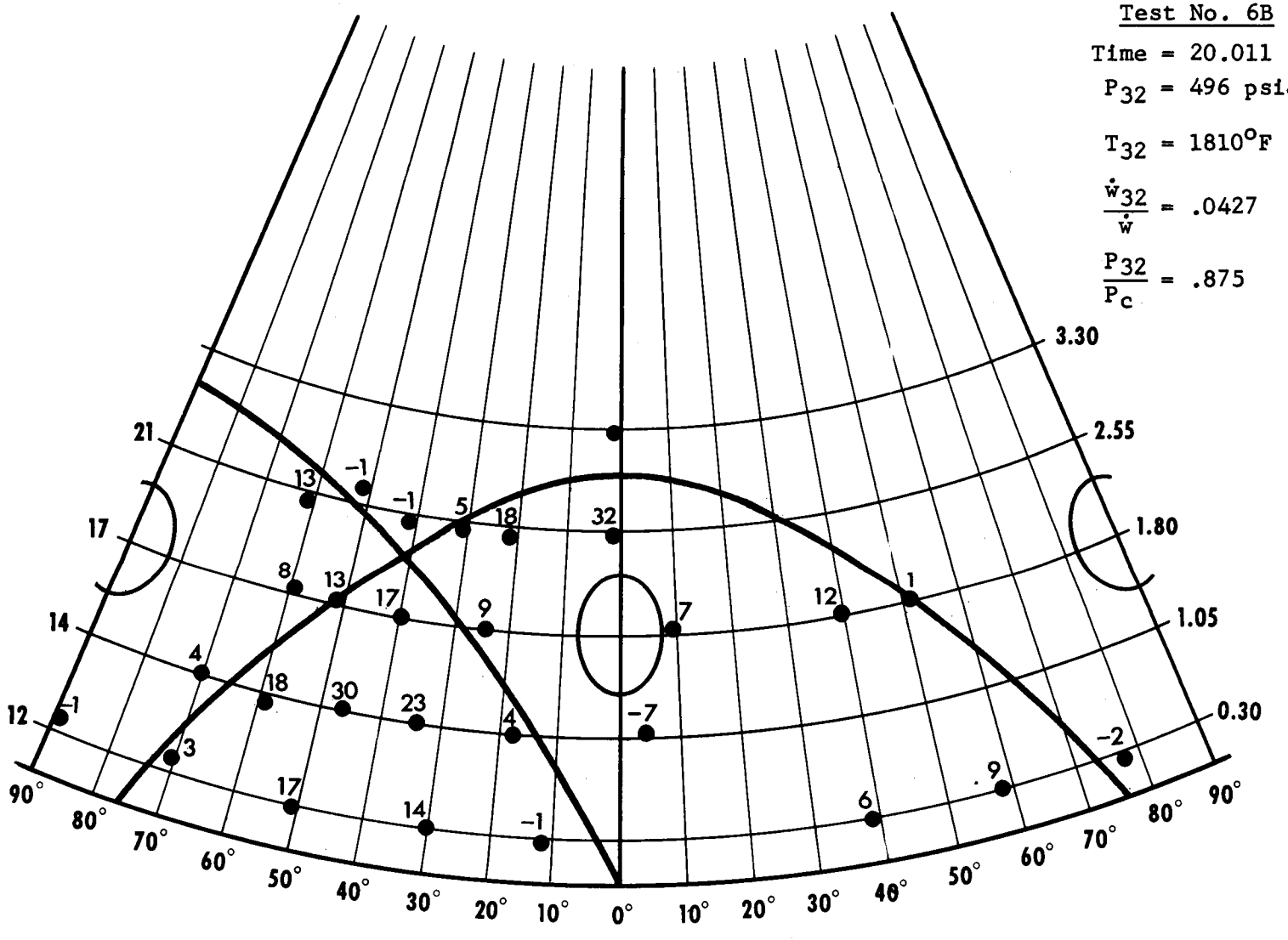
Test No. 6B
Time = 20.011 secs.
P_{32} = 496 psia
T_{32} = 1810°F
$\frac{\dot{w}_{32}}{\dot{w}}$ = .0427
$\frac{P_{32}}{P_c}$ = .875
3.30
2.55
1.80
1.05
0.30
21
17
14
12
90°
80°
70°
60°
50°
40°
30°
20°
10°
0°
10°
20°
30°
40°
50°
60°
70°
80°
90°
13
-1
-1
5
18
32
8
13
17
9
7
12
1
4
18
30
23
4
-7
-1
3
17
14
-1
6
9
-2

Figure 8.75

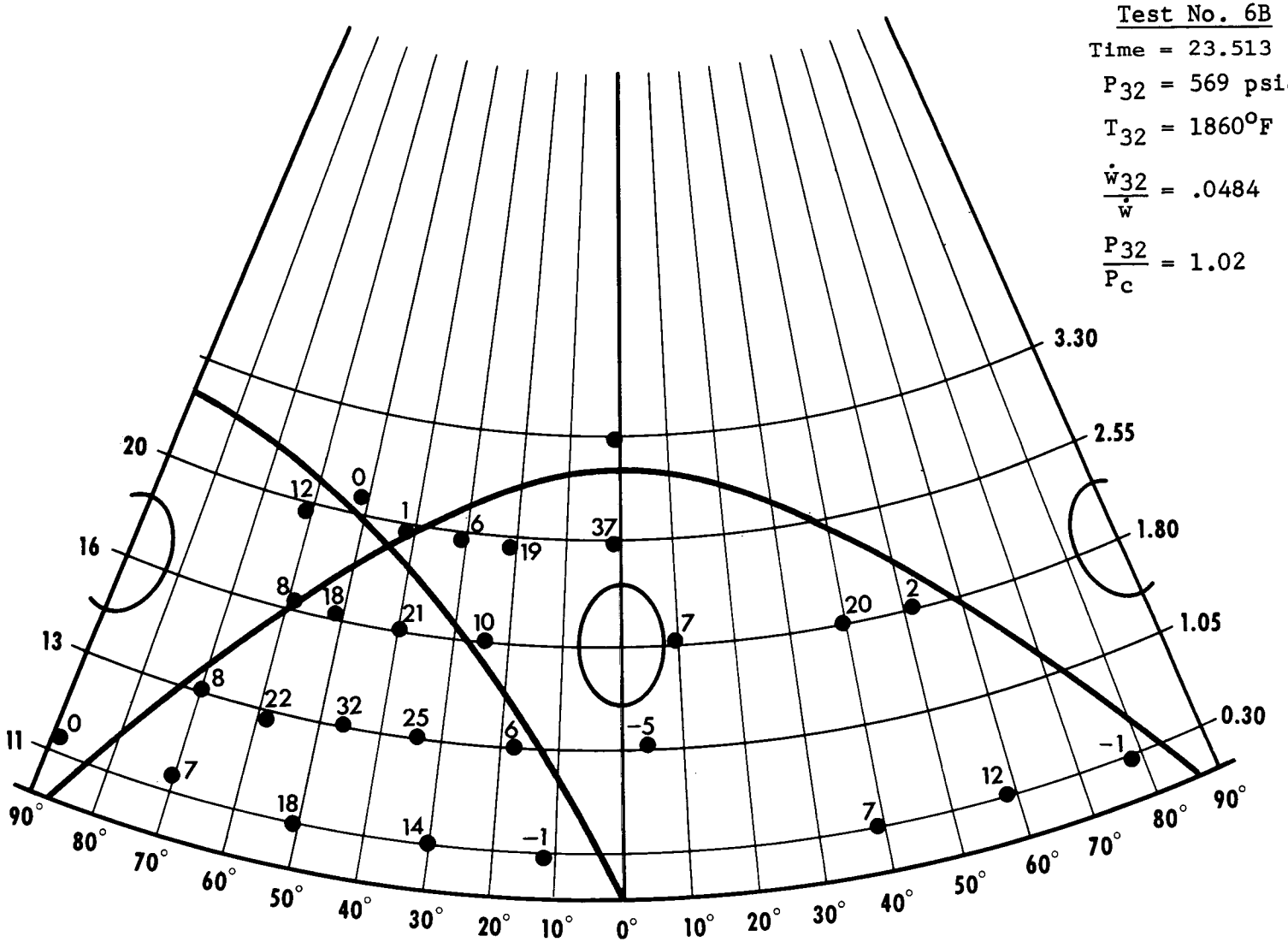
Test No. 6B
Time = 23.513 secs.
P_{32} = 569 psia
T_{32} = 1860°F
$\frac{\dot{W}32}{\dot{W}}$ = .0484
$\frac{P_{32}}{P_c}$ = 1.02
3.30
2.55
1.80
1.05
0.30
20
16
13
11
90°
80°
70°
60°
50°
40°
30°
20°
10°
0°
10°
20°
30°
40°
50°
60°
70°
80°
90°
12
0
1
6
19
37
8
18
21
10
7
20
2
8
22
32
25
6
−5
0
7
18
14
−1
7
12
−1

Figure 8.76

Figure 8.77 Composite of Static Pressure Versus Injector Pressure-Yaw Plane - Test 1

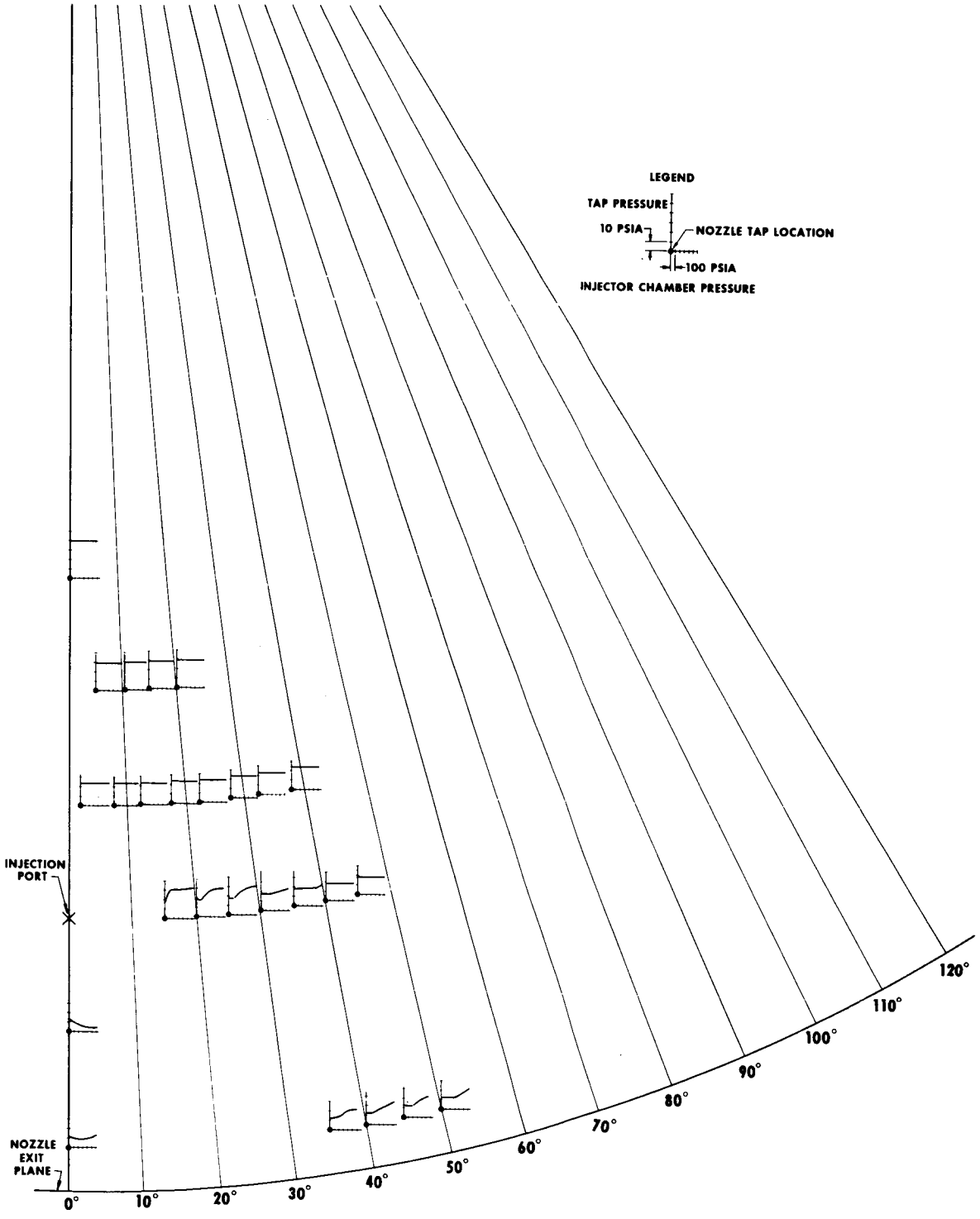

Figure 8.78 Composite of Static Pressure Versus Injector Pressure-Yaw Plane - Test 2

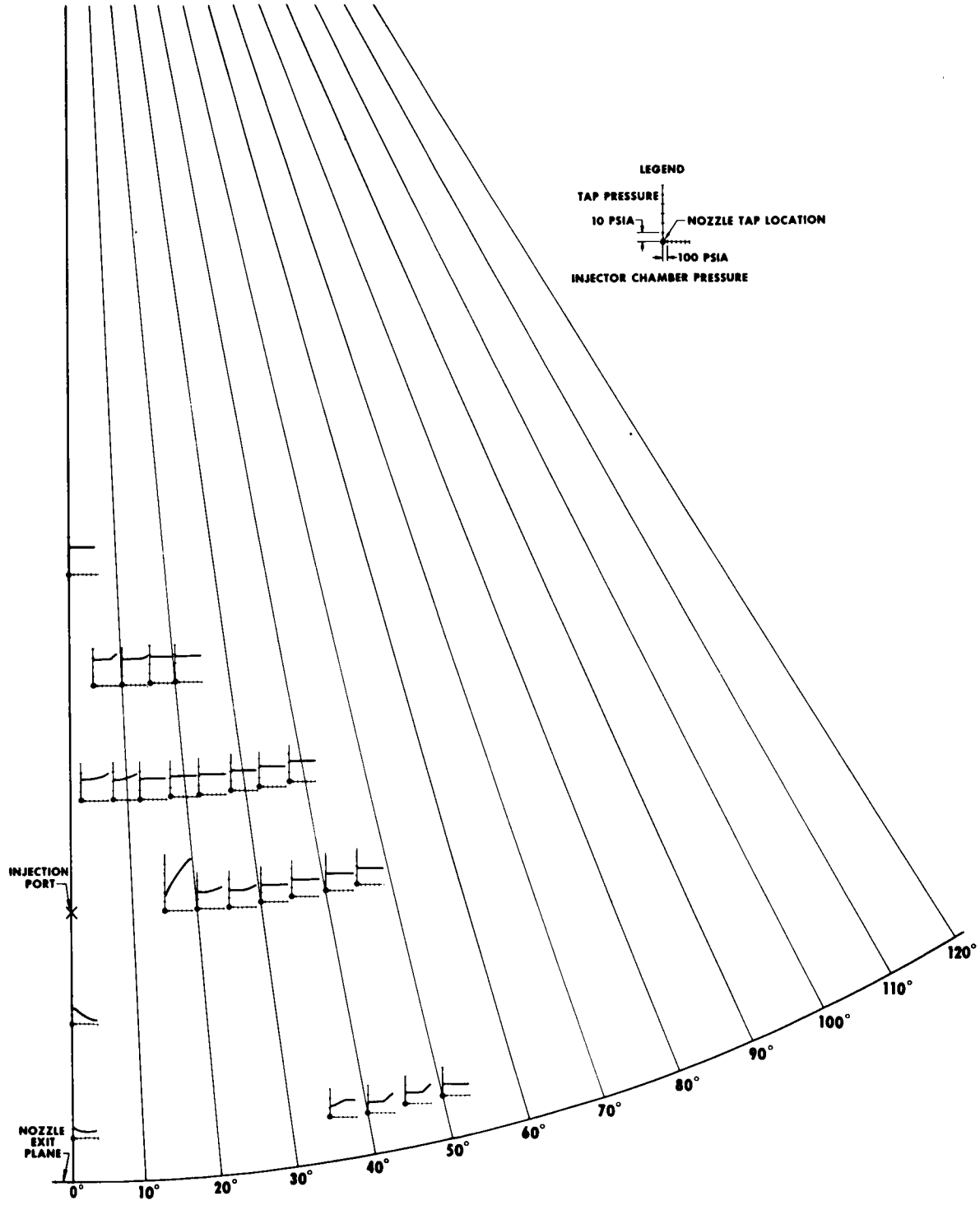

Figure 8.79 Composite of Static Pressure Versus Injector Pressure-Yaw Plane - Test 3

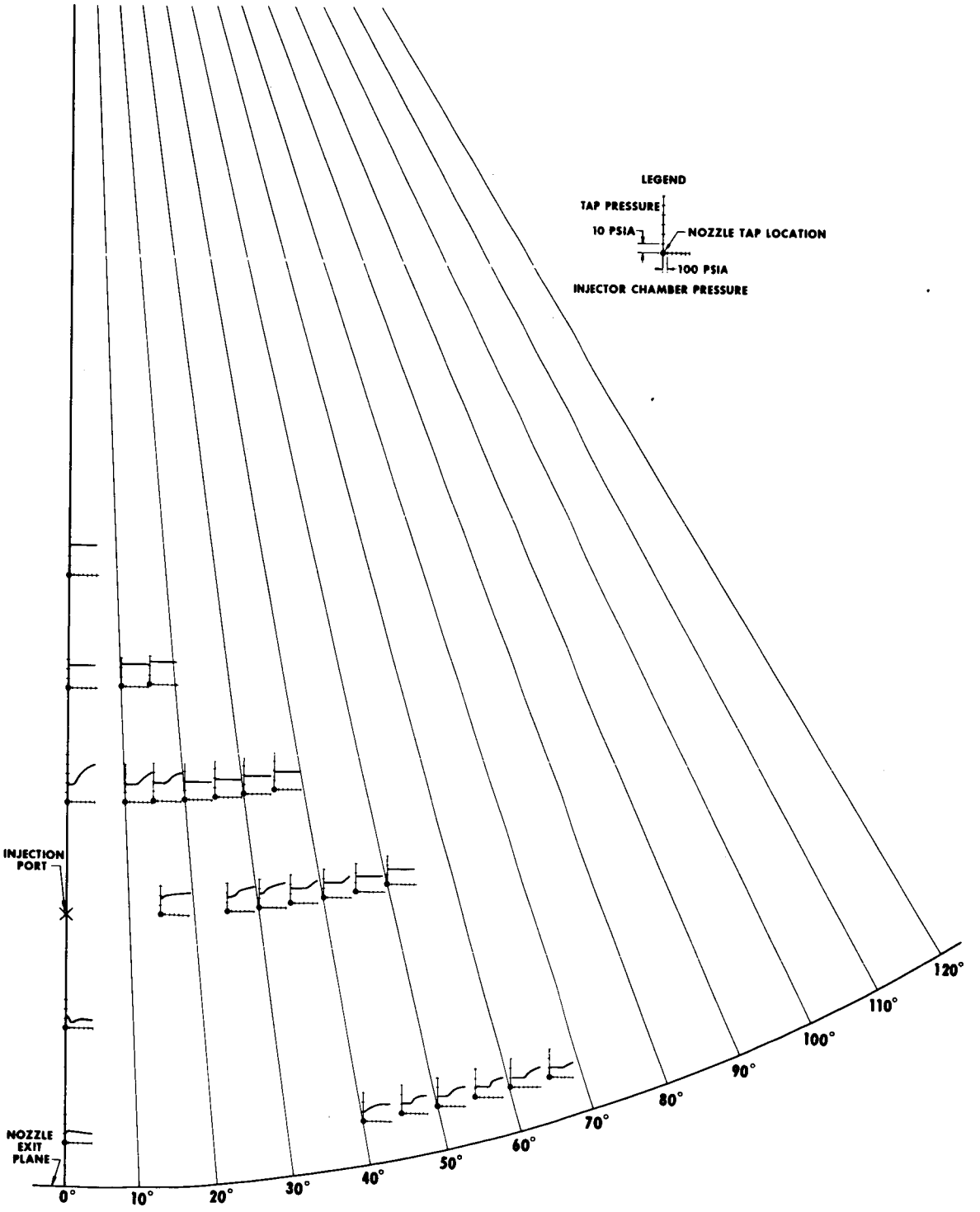

Figure 8.80 Composite of Static Pressure Versus Injector Pressure-Yaw Plane - Test 4

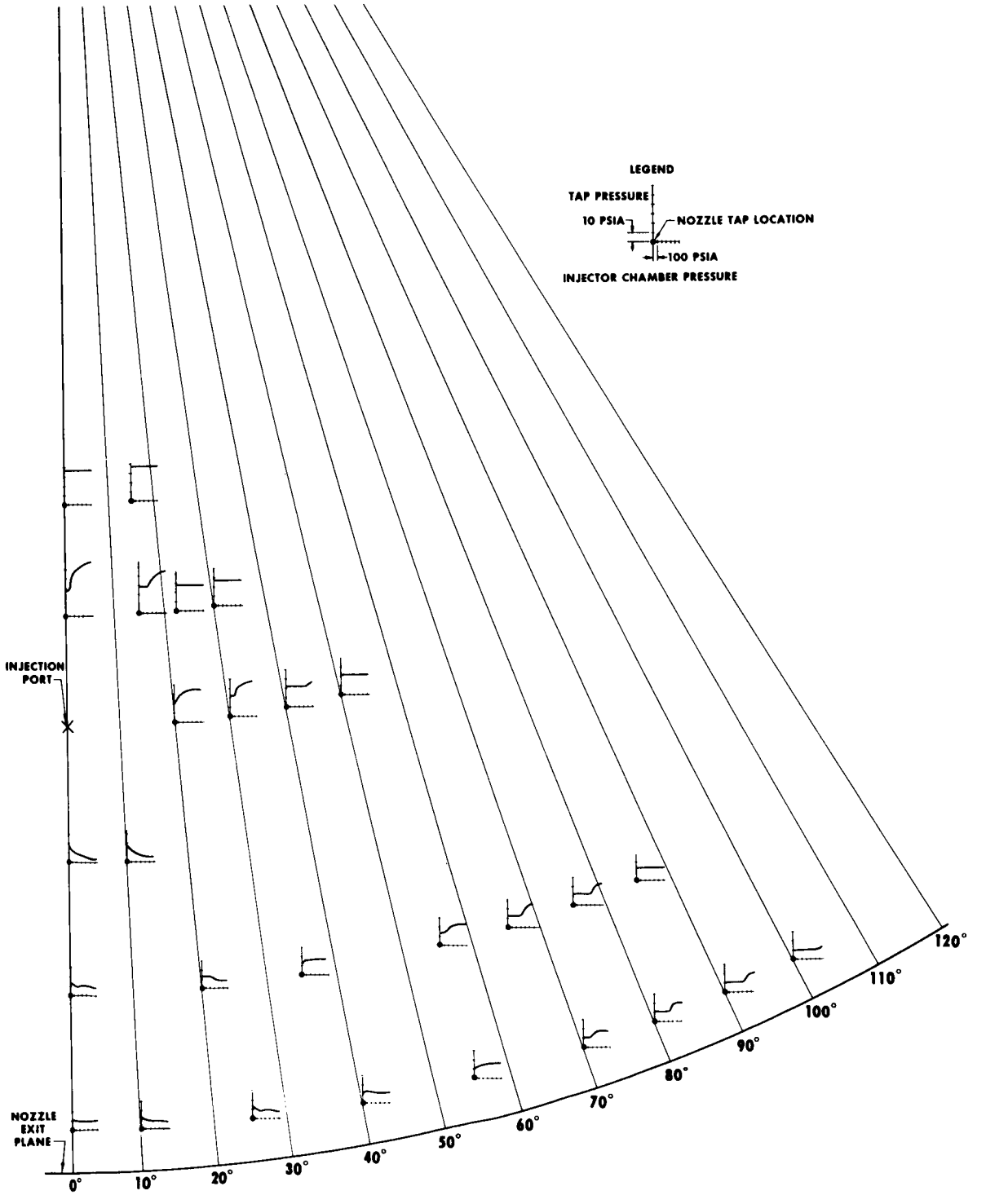

Figure 8.81 Composite of Static Pressure Versus Injector Pressure-Yaw Plane - Test 5

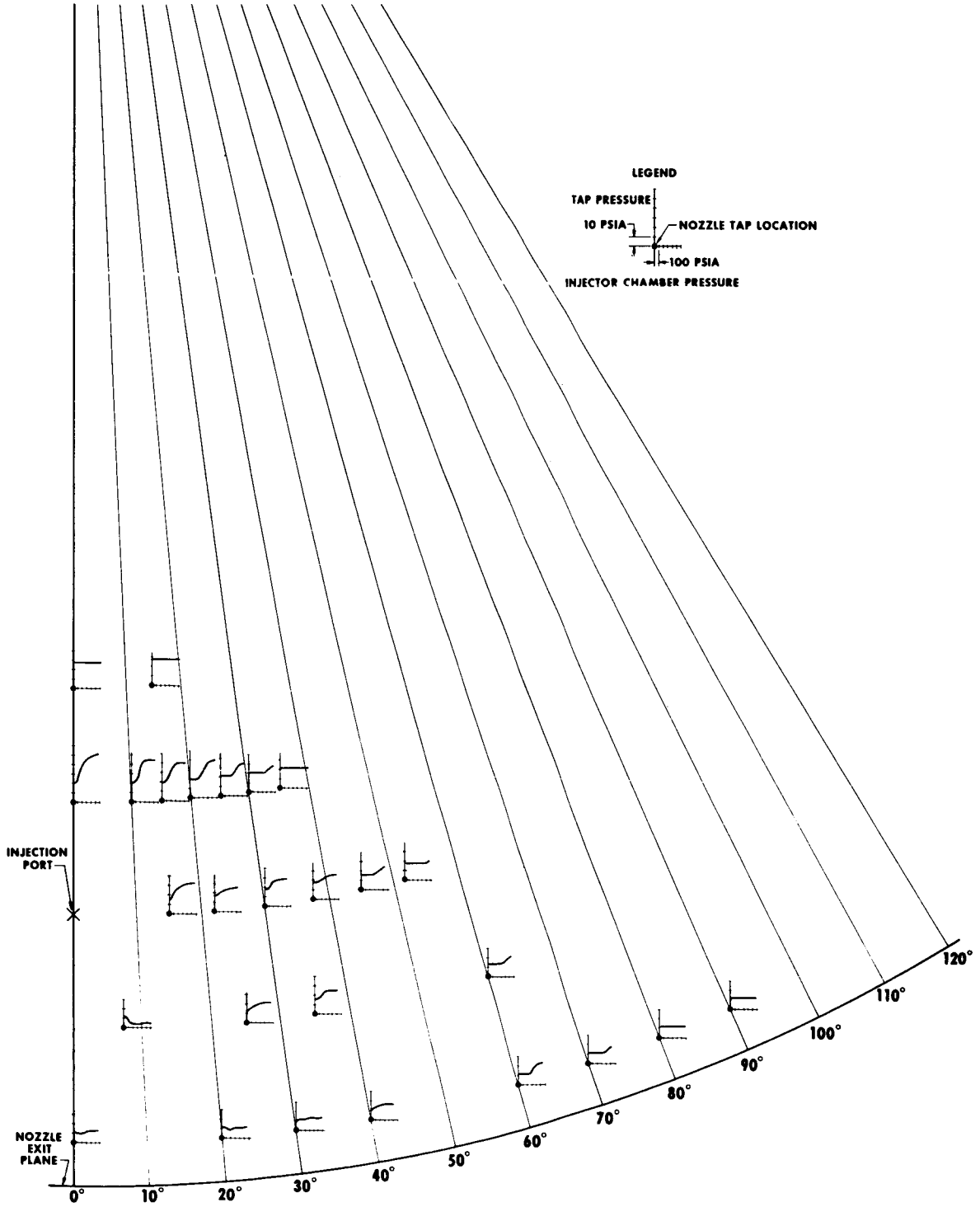

Figure 8.82 Composite of Static Pressure Versus Injector Pressure - Test 6 - Yaw Plane With Null Pitch Signal

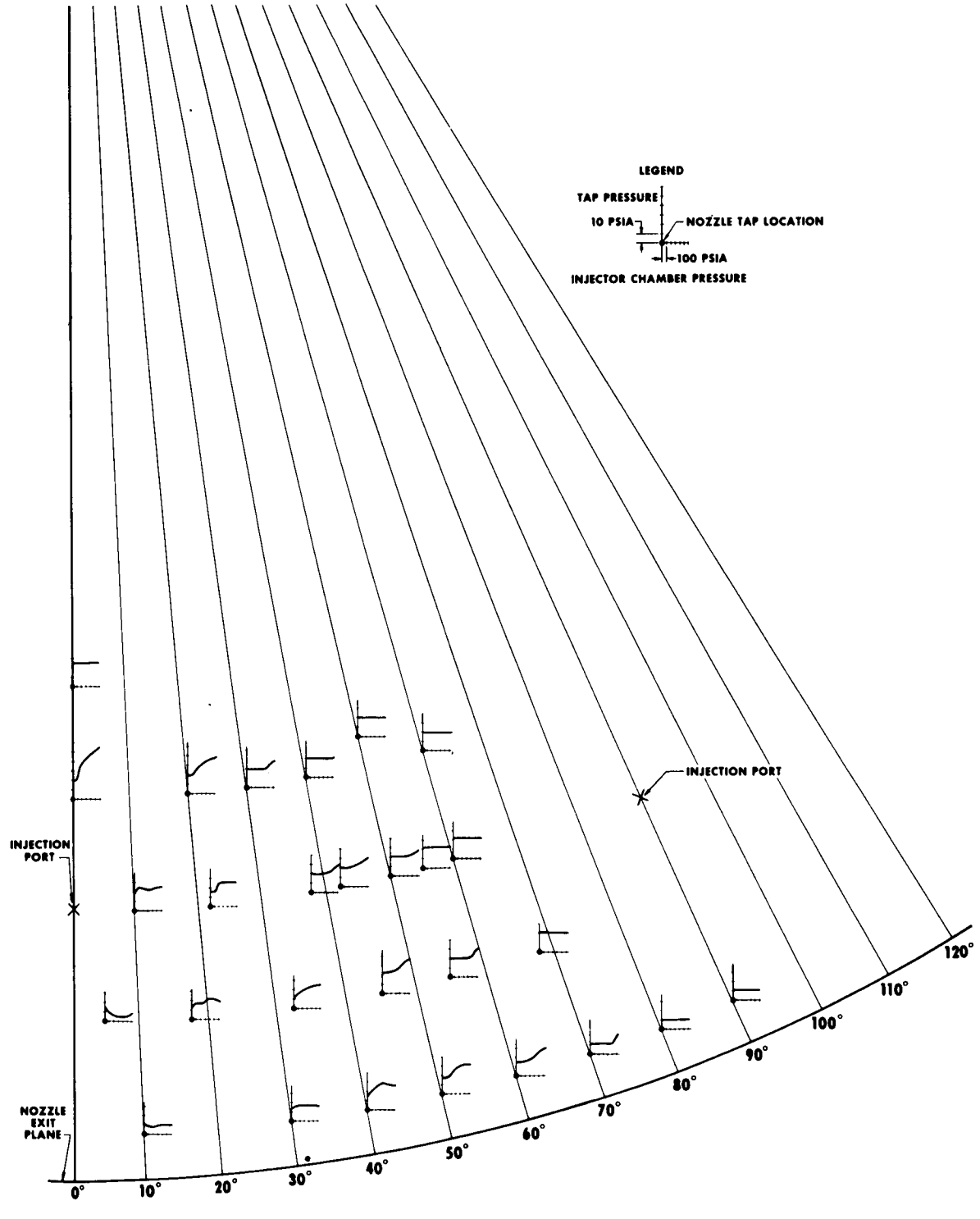

Figure 8.83 Composite of Static Pressure Versus Injector Pressure - Test 6 - Yaw Plane With Full Pitch Signal

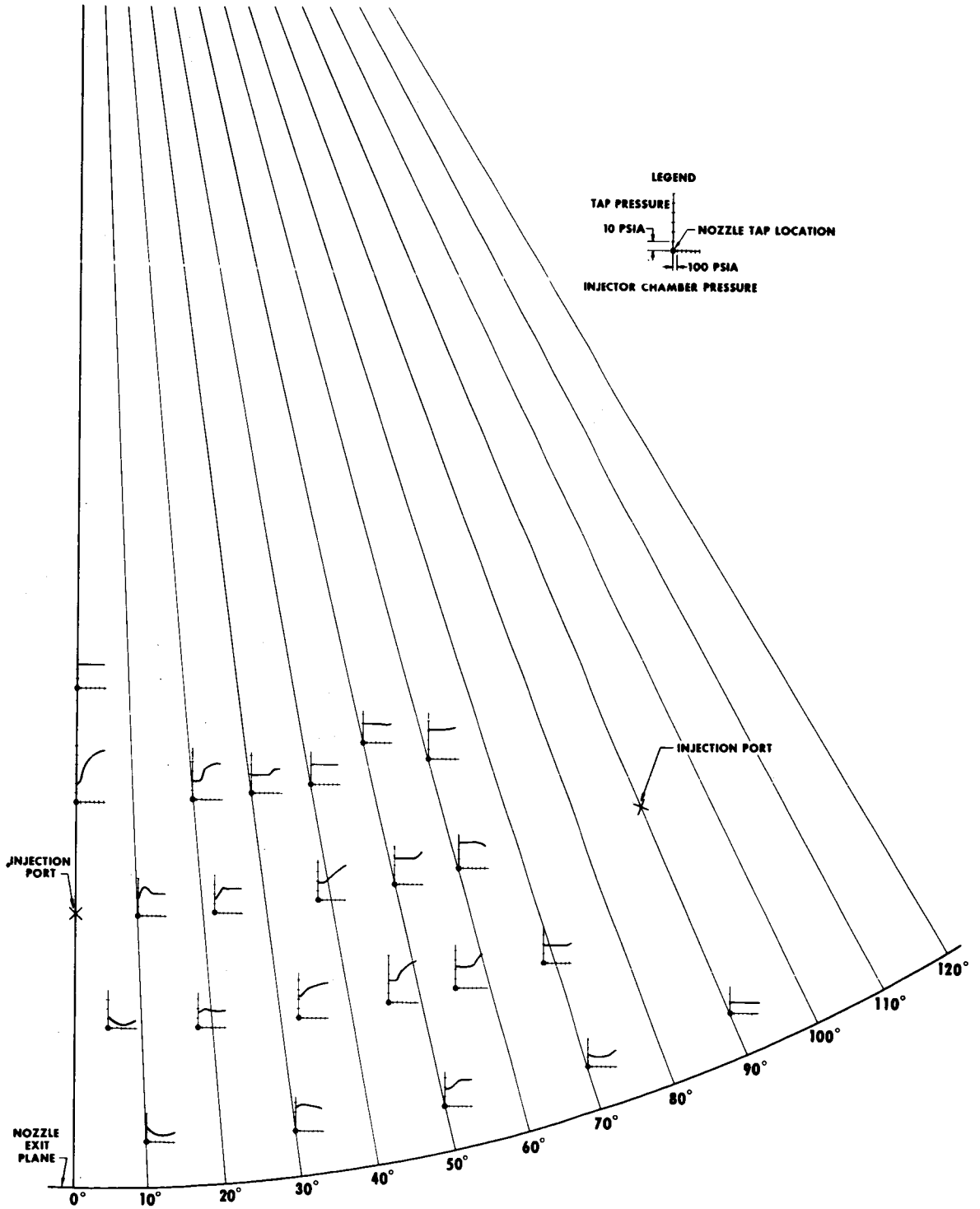

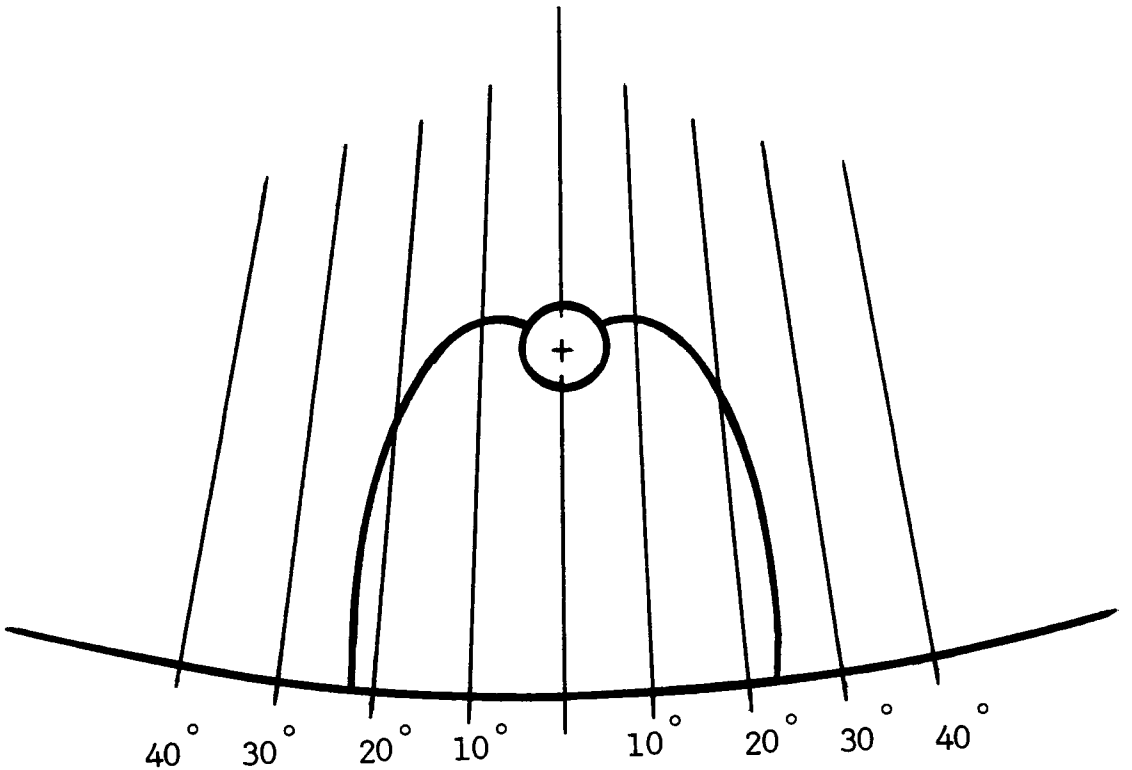

Figure 8.84 Erosion Pattern - Test 3

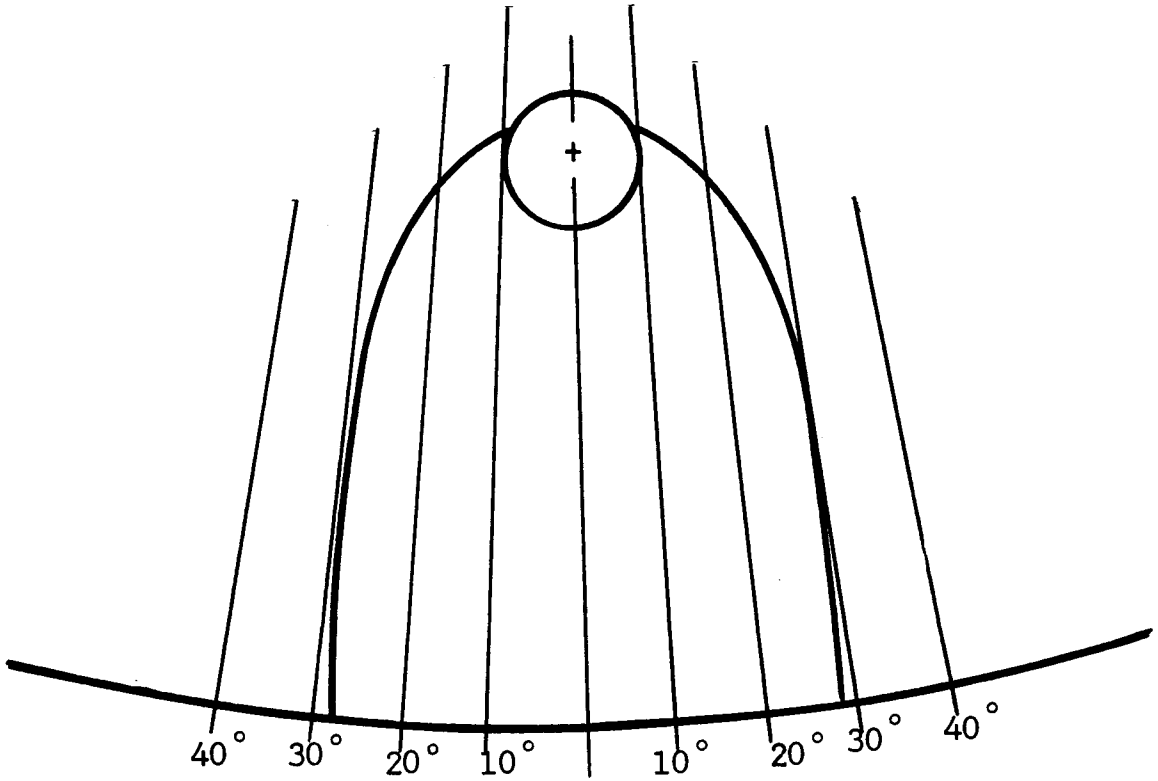

Figure 8.85 Erosion Pattern - Test 4

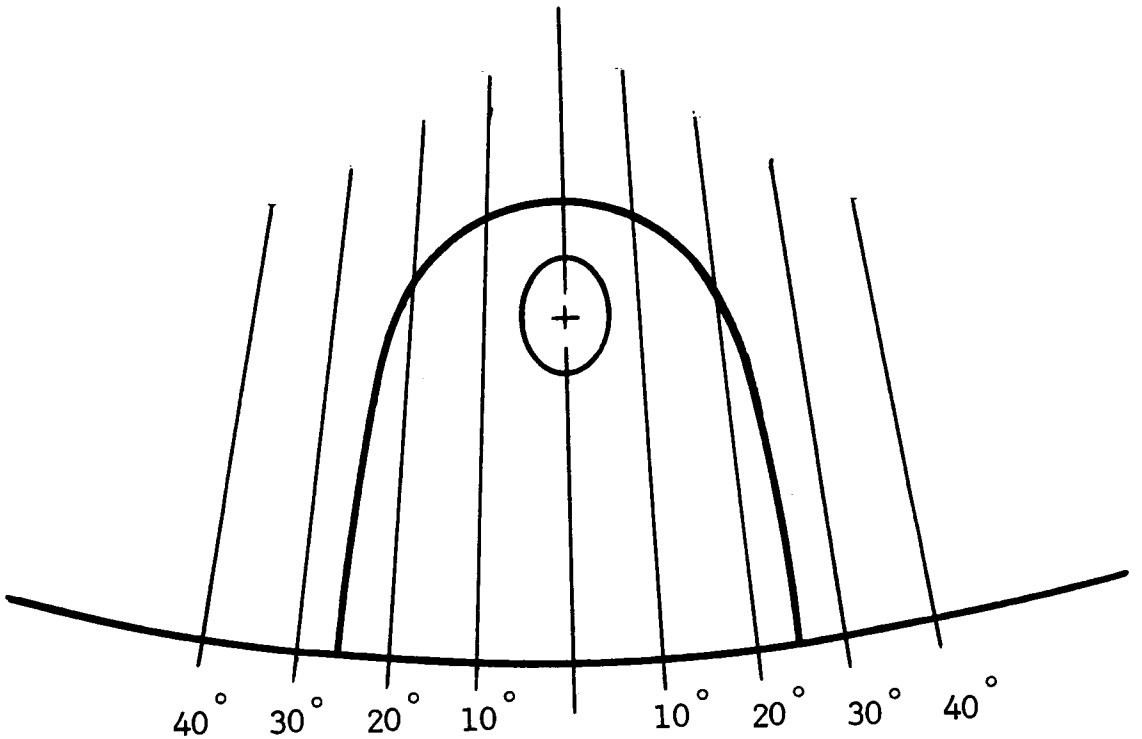

Figure 8.86 Erosion Pattern - Test 5

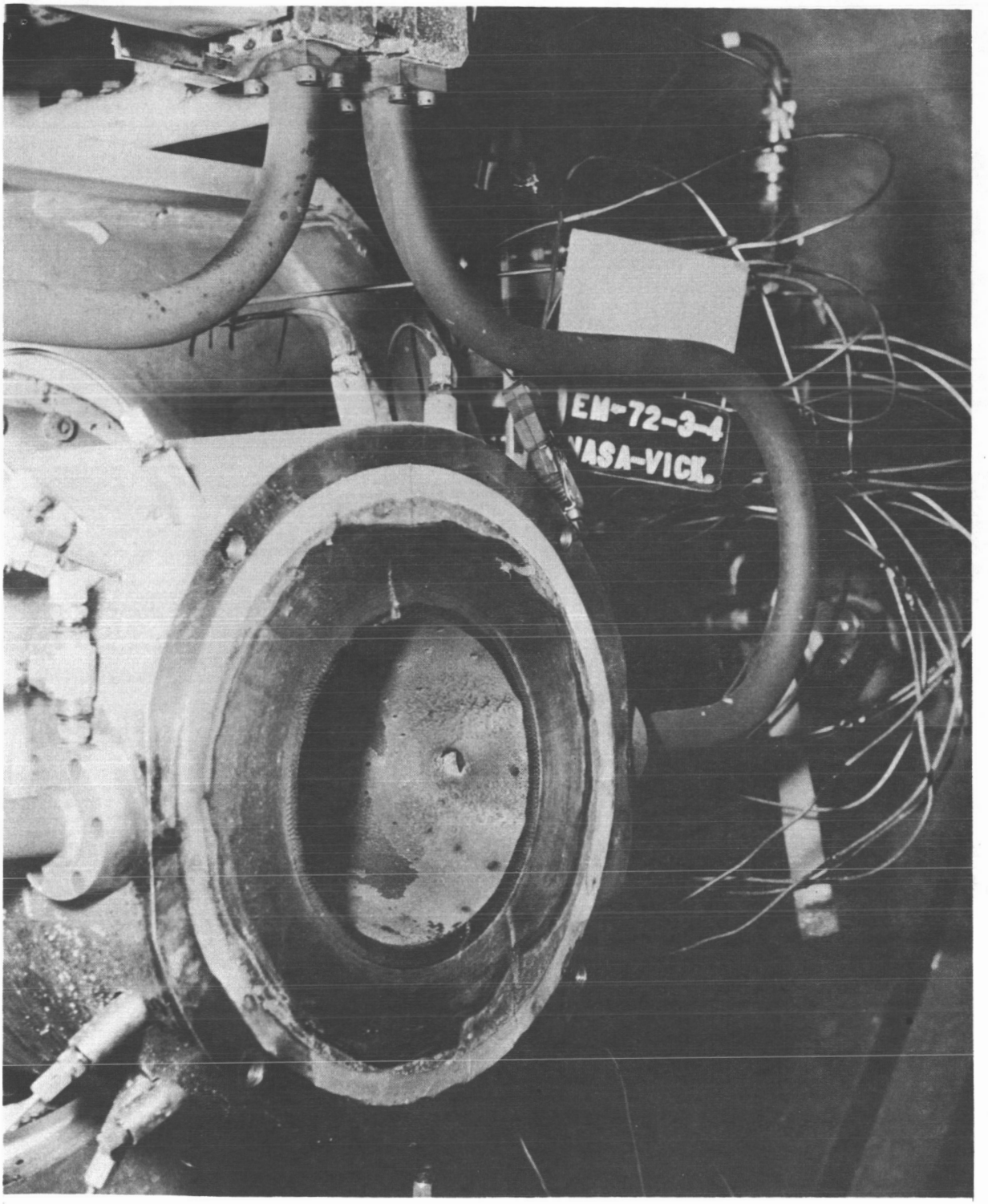

FIGURE - 8.87

Erosion Pattern in Nozzle Exit Cone - Test 5

SECTION 9

COMPARISONS BETWEEN TEST RESULTS AND THEORETICAL MODEL

The most direct means for evaluating the theoretical model is to compare predicted side force with the actual results. To further evaluate the model and to explain any difference from predicted side force, the shock patterns are examined with respect to shock shape and excess pressure distribution relative to the model prediction.

9.1 Actual and Theoretical Side Force

The side force theoretically expected from a secondary injection nozzle can be determined from the chamber pressure of that nozzle. The theoretical relationship between chamber pressure and side force per injector for each test is given in Figure 4.5. Net theoretical side force is the difference between the two forces expected from opposed nozzles in an axis of injection. Net theoretical side force values are listed in Tables 7.2 and 7.3 for selected points in Tests 1 through 6. Figure 9.1 shows the relationship between predicted and measured side force for Tests 1 through 6. The end point of each line on the figure indicates the maximum side force obtained in the test. The data

points on which these lines are based are shown in Figure 9.2 through 9.7.

Some inferences in regard to the mathematical model can be made from Figure 9.1. The results of the two sonic injection tests (1 and 3) are very close to the predicted results. For all four tests employing supersonic injection, theoretical values are higher than measured side force. In Test 2, the poor performance of the motor probably caused the slope of the theoretical versus measured side force line to be higher than it should be. Nevertheless, the mathematical model is clearly predicting side forces for supersonic injection that are higher than experimental results indicate. Since the forces predicted by the model are based on certain pressures acting on certain areas along the wall of the primary nozzle, comparison of the shock patterns given in Section 8 with the model presented in Section 4 should serve as a basis for modifying the mathematical model.

9.2 Actual and Theoretical Shock Location and Pressure Distribution

If the oblique shock caused by secondary injection assumes the conical shape on which the model is based, the geometry of the

shock-nozzle wall interface appears as shown in Figure 9.8. Theoretical values for X and θ are obtained through the calculation procedure given in Section 4. From the geometry of the intersection of two cones, the azimuth of the shock on the nozzle wall in the injection plane and at the exit plane can be calculated as:

$$\Phi_j = 2 \arcsin \left[\frac{X \cos \alpha}{D_j} \left(\tan \alpha + \tan [\theta - \alpha] \right) \right] \qquad (9.1)$$

$$\Phi_e = 2 \arcsin \left[\frac{L_j + X \cos\alpha}{D_e} \left(\tan \alpha + \tan [\theta - \alpha] \right) \right] \qquad (9.2)$$

Theoretical values for X, θ, Φ_j, Φ_e, and other design parameters for null flow conditions (equal flow through opposed injection nozzles) are listed in the upper part of Table 9.1. In the lower part of the table, values of X, Φ_j, and Φ_e determined for null flow conditions from the shock patterns of Section 8 are given. The experimental shock angle can be calculated from this data and the geometry as,

$$\theta_{exp} = \alpha + \arctan \left(\frac{D_e}{L_j} \sin \frac{\Phi_c}{2} - \tan\alpha - \frac{D_j}{L_j} \sin \frac{\Phi_j}{2} \right) \qquad (9.3)$$

where θ_{exp} is the only conical angle with axis along the wall

that can pass through the experimental Φ_j and Φ_e points obtained from the shock patterns. If a straightforward calculation for the shock apex of such a cone were made, the distance between injection point and the shock apex would be greater than the measured value of X because the top of the shock cone is rounded off by the pressure and momentum forces of the primary stream.

Some observations can now be made regarding the correlation of theoretical and experimental shock location and pressure distribution. In Test 2, the primary nozzle flow conditions were not at the design point and were unstable. Experimental shock pattern results were affected by this situation. From Table 9.1, it is evident that:

1. The shock is wider than expected in the injection plane and at the primary nozzle exit.
2. The shock angle itself is always larger than predicted.
3. The shock apex is not as far upstream as the model indicated because it is rounded off.
4. The actual pressures observed in the shock patterns

of Section 8 for the area upstream of the injection port are lower than those predicted for the separated and shock regions.

5. The model assumes zero side force contribution downstream of the injection port, but the shock patterns show that a sizeable percentage of the side force is generated by excess pressure in the downstream region.

Test			1	2	3	4	5 & 6
Injectant Mach Number	M_j		1.0	1.833	1.0	1.398	1.556
Injectant Pressure Ratio	P_j/P_{jc}		0.546	0.1705	0.546	0.328	0.261
Injectant Chamber Pressure	P_{jc}	(psia)	427	468	265	300	300
Average Pressure, Separated Region	$\overline{P_s}$	(psia)	126.4	79.1	97.7	98.4	78.4
Separation Pressure	P_s	(psia)	73.1	78.7	74.1	98.4	79.1
Average Pressure, Shock Region	$\overline{P_2}$	(psia)	67.4	72.6	68.4	91.0	72.8
Distance Along Wall to Shock Apex	X	(in)	1.116	1.404	1.375	1.321	1.702
Distance Along Axis to Exit	L_j	(in)	1.731	1.731	1.731	2.90	1.731
Accomodation Height	h	(in)	0.471	0.569	0.557	0.525	0.585
Theoretical Conical Shock Angle	θ	(deg)	34.7	35.0	34.9	36.6	35.4
Injection Plane Shock Azimuth (eq. 9.1)	Φ_j	(deg)	16	20	19.5	23	24
Exit Plane Shock Azimuth (eq. 9.2)	Φ_e	(deg)	34	37	37	38	41
			---	---	---	---	---
Measured Distance To Shock Apex	X	(in)	0.70	1.75	1.00	0.99	1.07
Measured Injection Plane Shock Azimuth	Φ_j	(deg)	36	28	32	36	43
Measured Exit Plane Shock Azimuth	Φ_e	(deg)	55	50	55	79	66
Conical Shock Angle (eq. 9.3)	θ_{exp}	(deg)	37	40	42	44	43

Table 9.1

Theoretical and Experimental Shock Parameters at Null Flow Conditions

	Type of Injection	Nozzle Location	Angle of Injection
1	Sonic	75%	⊥ Motor Axis
2	Supersonic	75%	⊥ Motor Axis
3	Sonic	75%	⊥ Motor Axis
4	Supersonic	60%	⊥ Motor Axis
5	Supersonic	75%	20° Upstream
6	Supersonic	75%	20° Upstream

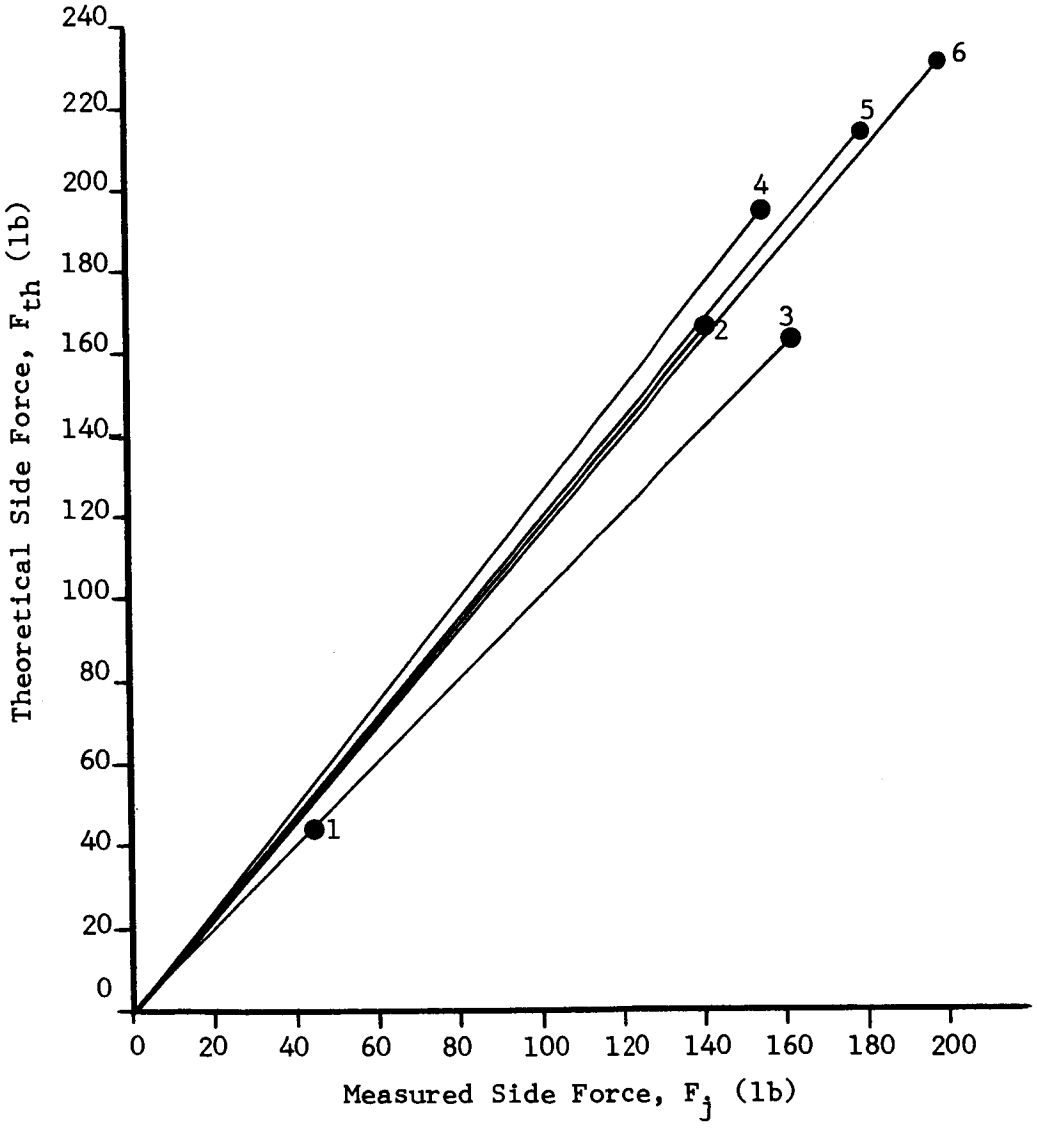

Figure 9.1 Theoretical Versus Measured Side Force - Tests 1 thru 6

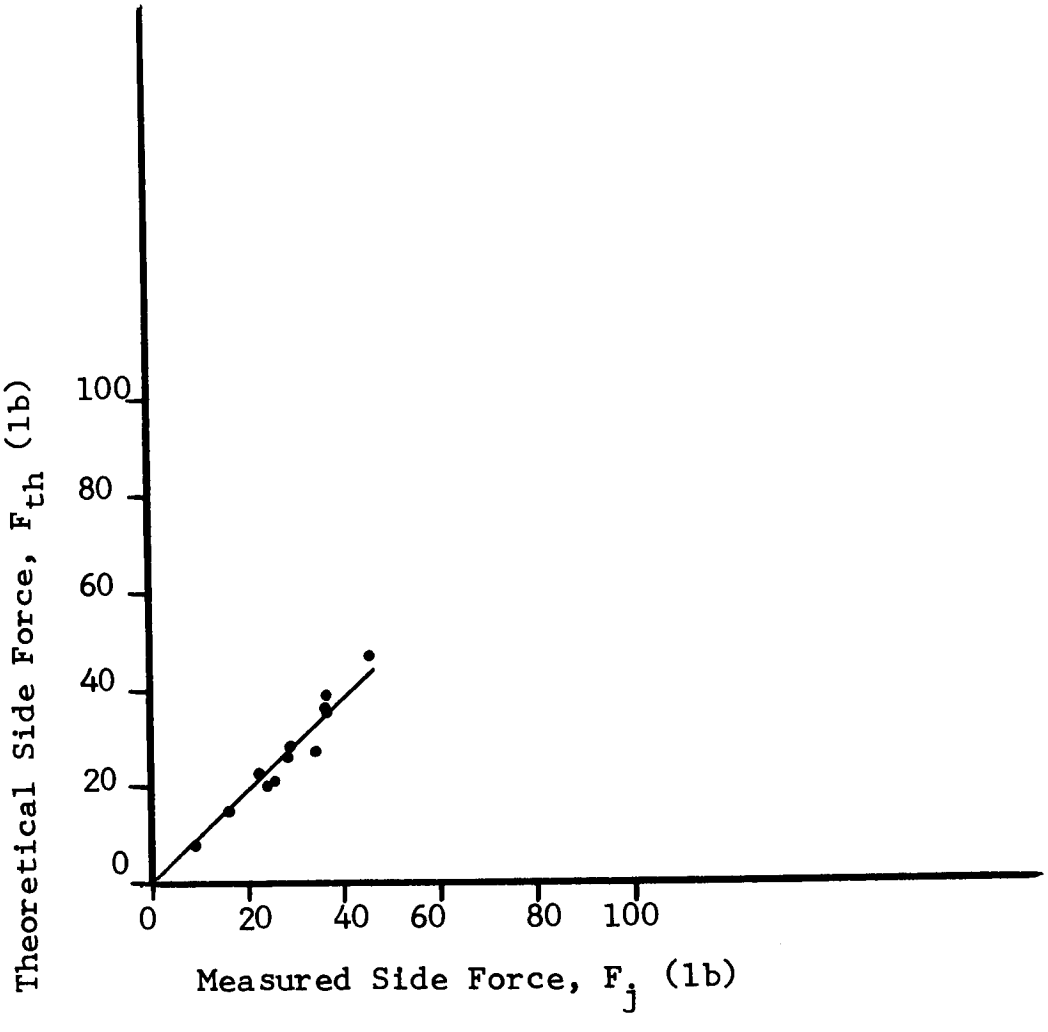

Figure 9.2 Theoretical Versus Measured Side Force - Test 1

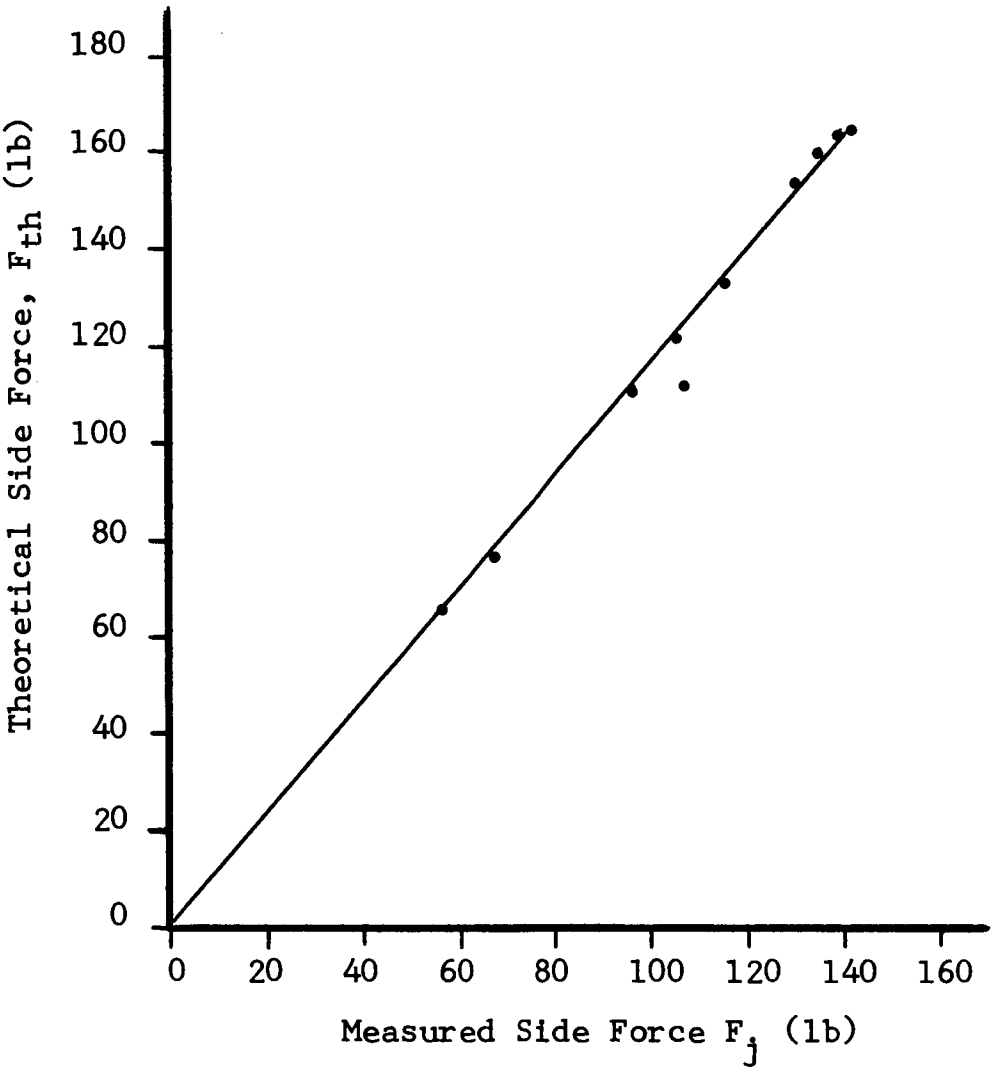

Figure 9.3 Theoretical Versus Measured Side Force - Test 2

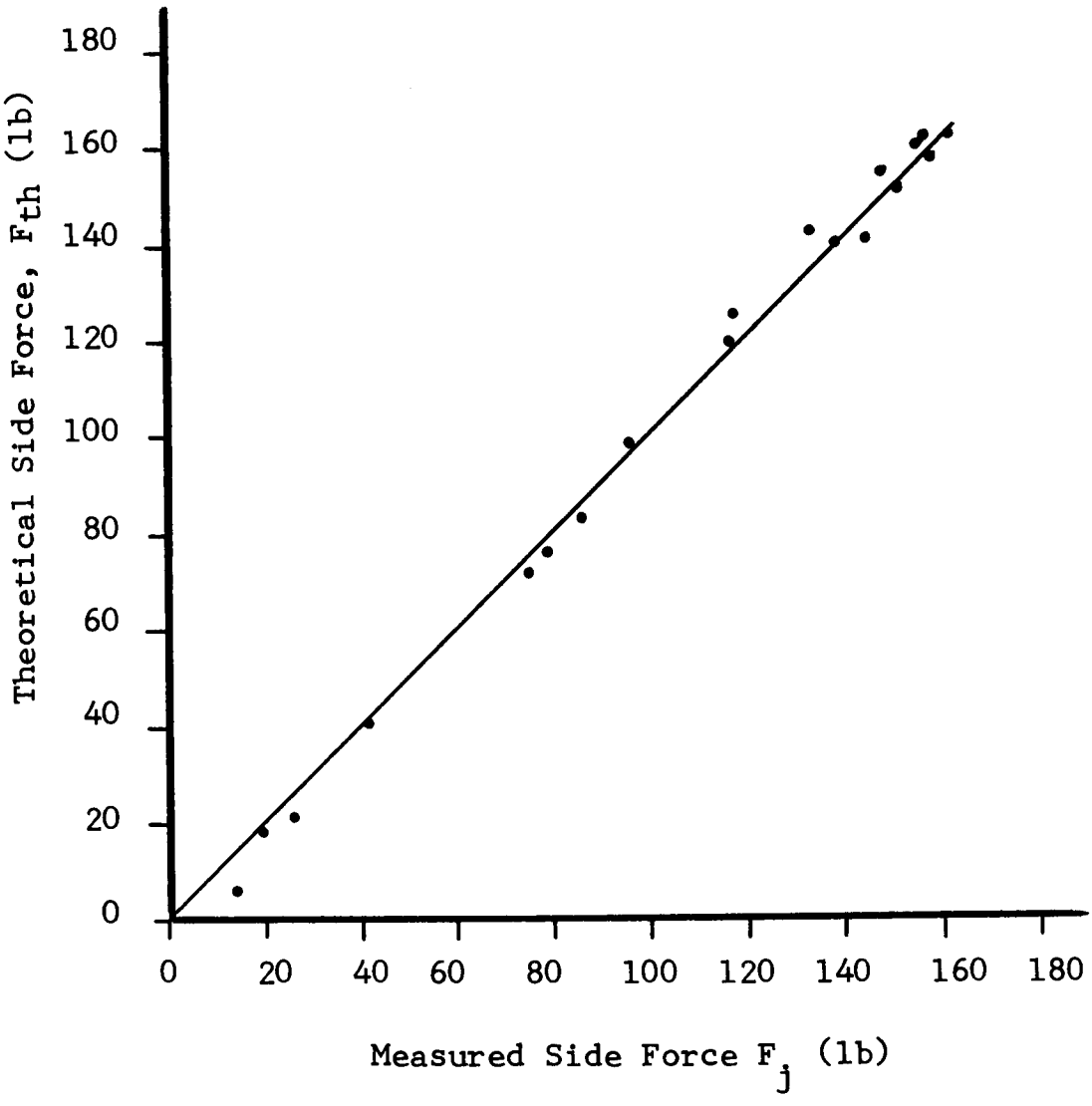

Figure 9.4 Theoretical Versus Measured Side Force - Test 3

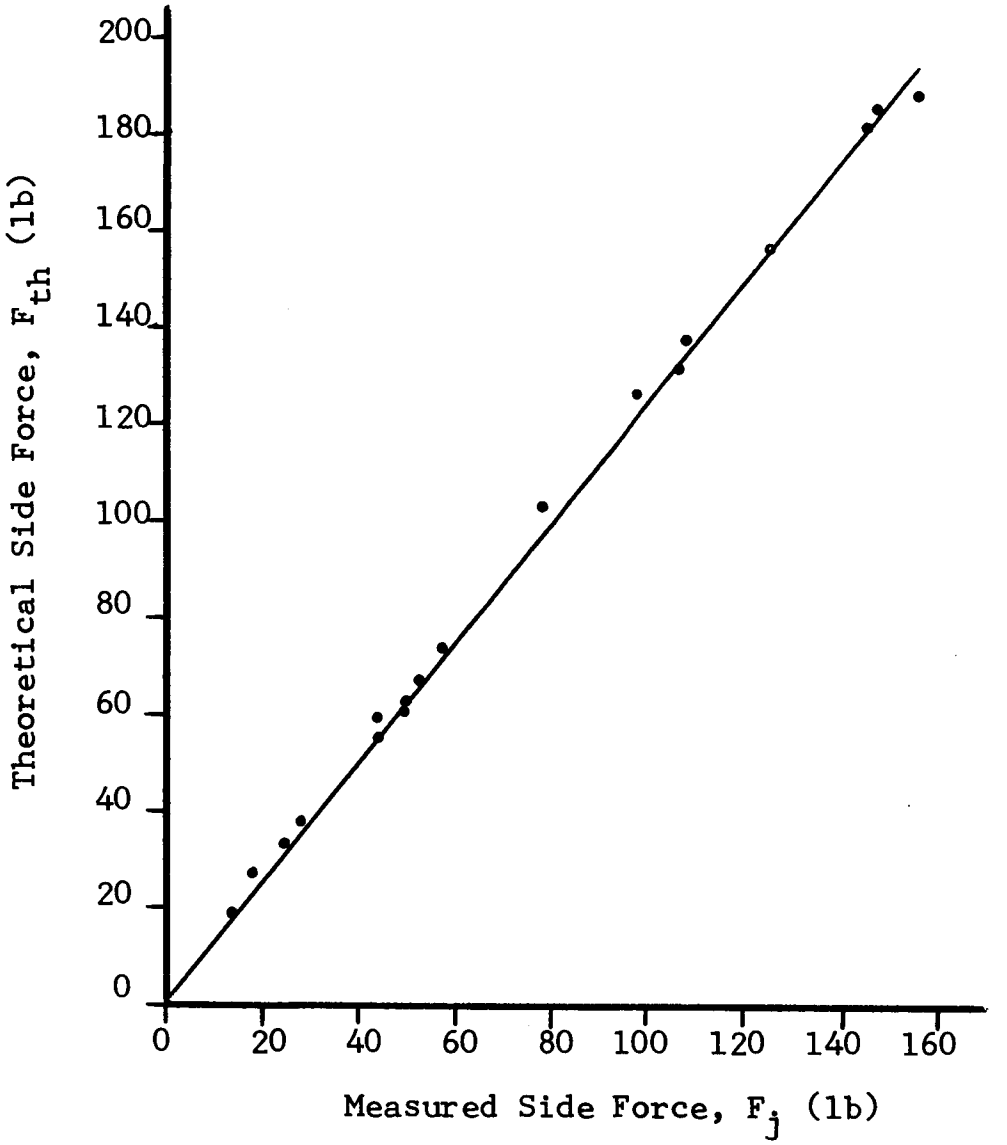

Figure 9.5 Theoretical Versus Measured Side Force - Test 4

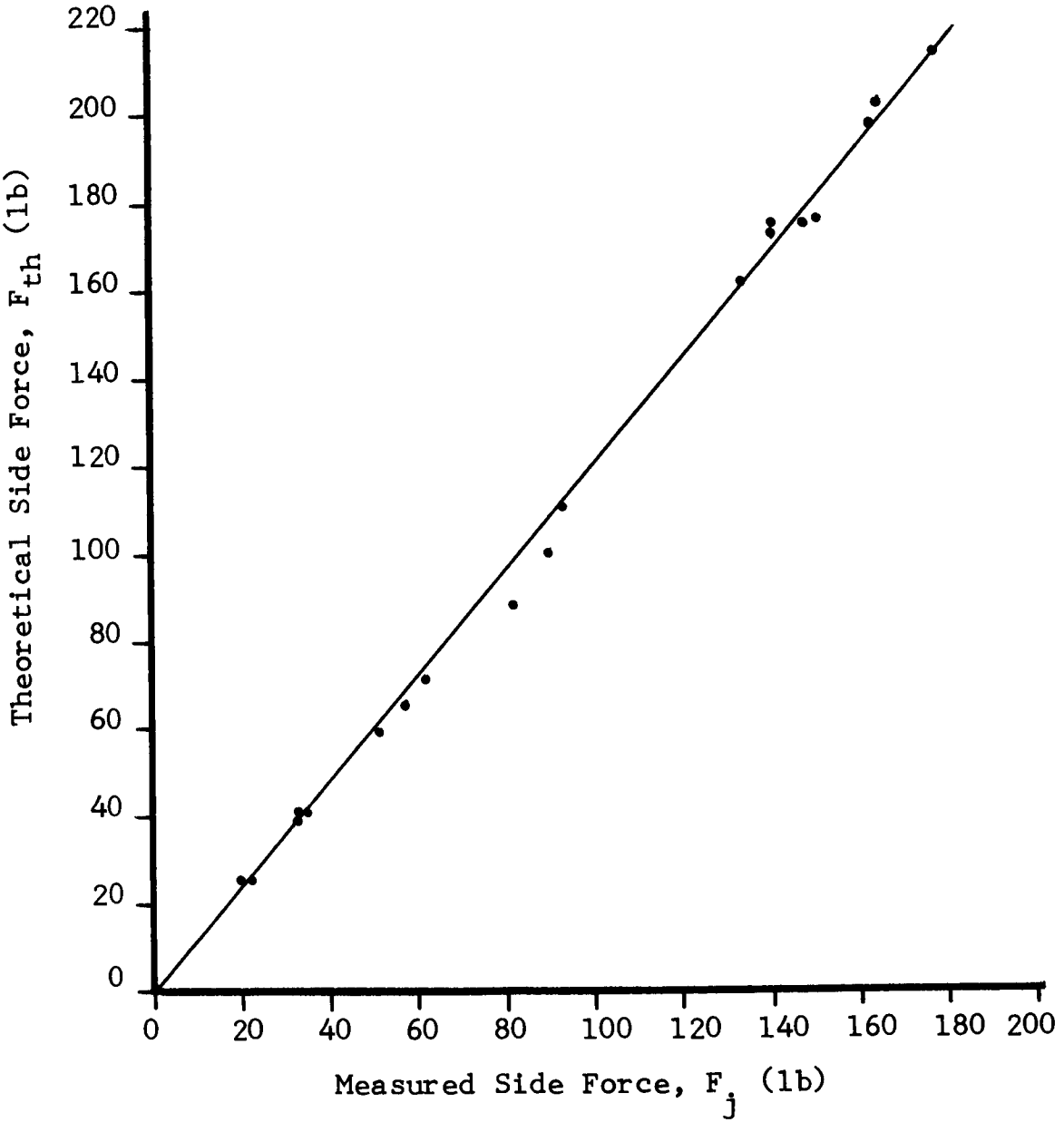

Figure 9.6 Theoretical Versus Measured Side Force - Test 5

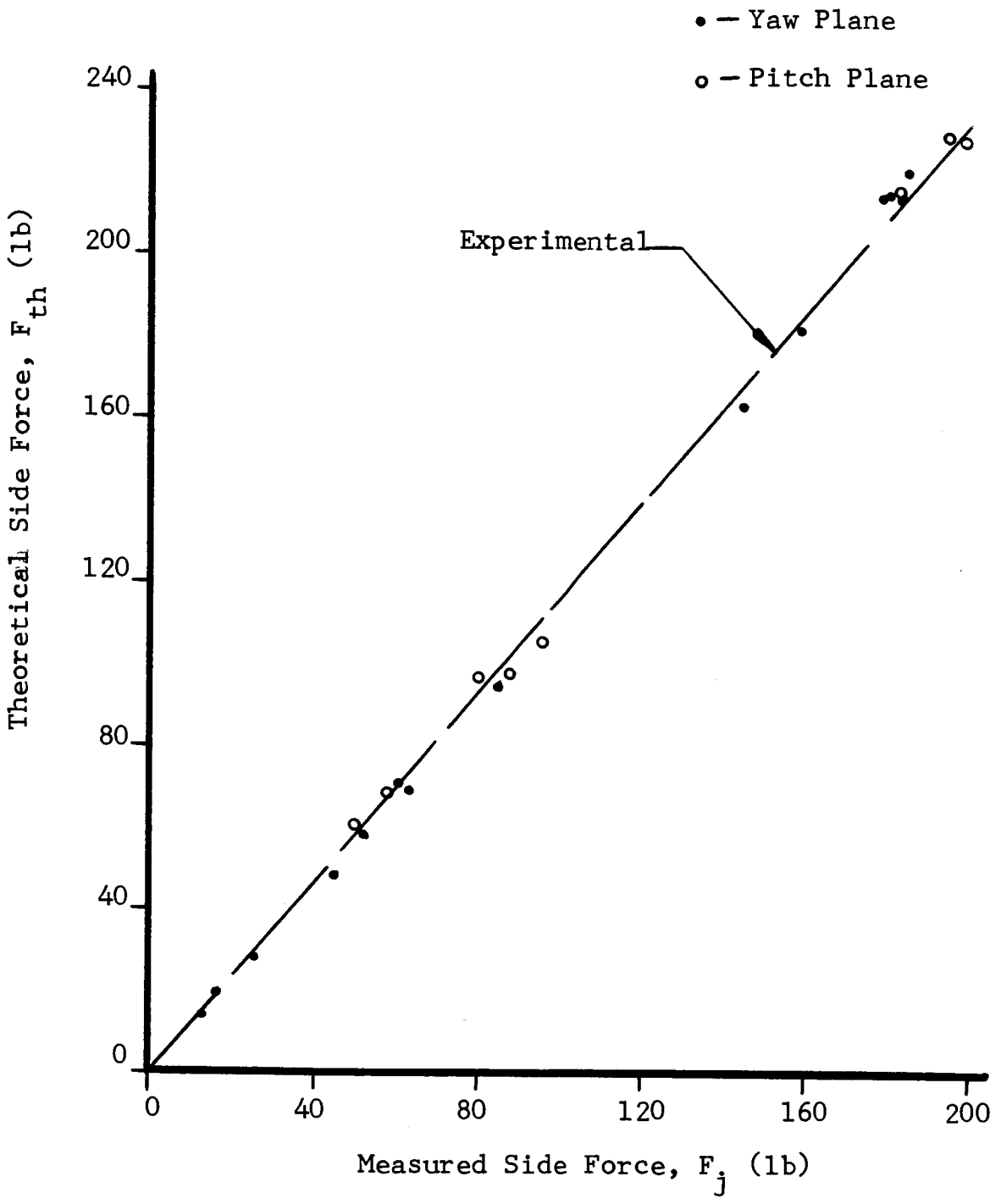

Figure 9.7 Theoretical Versus Measured Side Force - Test 6

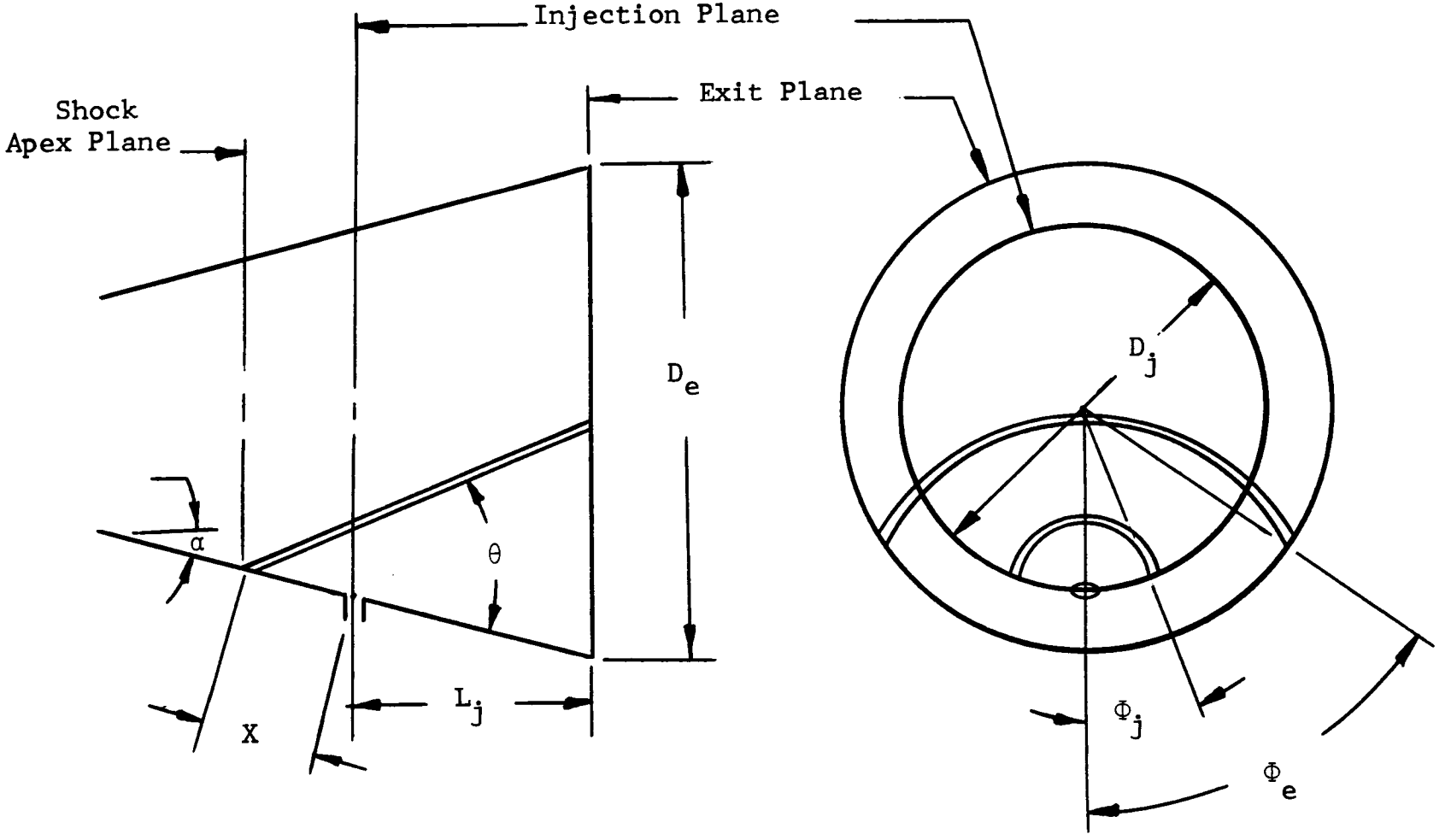

Figure 9.8 Geometry of Oblique Shock With Respect to Nozzle Wall

SECTION 10

REVIEW OF MATHEMATICAL MODEL

In Section 9, certain basic differences are noted between the experimental results and the mathematical model of Wu, Chapkis, and Mager[1] presented in Section 4. In this Section, the experimental information regarding the shock structure is summarized. Then, the relation of the experimental information to existing theoretical approaches is discussed. Finally, a design procedure for gaseous secondary injection is presented.

10.1 Shock Structure

Based on the shock patterns found in the tests and on Schlieren photographs of cold gas injection found throughout the literature, the upstream shock profile is probably as shown in Figure 10.1. The induced shock is greatly rounded just upstream of the injected flow. The presence of this induced shock triggers a small secondary shock. It is this bow shock that forms the shock outline on that part of the shock patterns upstream of the injection port. Between the main shock and the separated region upstream of the injection nozzle is a zone of spiral

flow. This spiral flow is the cause of the erosion channels shown in Figures 8.84 to 8.86. In tests with injection normal to the motor axis as shown in Figure 10.1, the channel runs into the injection port. With upstream injection, the shock structure is moved upstream, and the erosion channel is cut around the upstream side of the injection port as shown in Figure 8.86.

Between the injection port and motor exit plane, the distinct flow regimes exist within the shock structure. There is an inner core of secondary gas flow. Surrounding this core is a large mixing zone containing a spiral flow that is very strong along the inner core. Enclosing the system is the main shock. These three regimes are shown at the exit plane in Figure 10.2. The erosion caused by the spiral flow appears next to the inner core. The main shock forms a conical angle θ over the inner portion of the exit plane. Near the wall, however, the shock is larger than θ. The conical angle θ_{exp} measured from the shock patterns and recorded in Table 9.1 is always larger than calculated angle θ. This extension of the main shock may be

caused by a continuation of the bow shock effect of Figure 10.1 all around the main shock structure.

The above shock description is consistent with and, in part, based on the work of Charwat and Allegre[6].

10.2 Discussion of Theoretical Approaches

The first consideration in attempting to establish a mathematical model that is consistent with test results is to somehow modify the model presented in Section 4. Although it is possible to improve on some of the approximations, the assumption that side force contribution from wall pressures downstream of the injection point is zero cannot be modified within the mathematical model. At present, there appears to be no way of logically extending the theoretical approach to cover the complex flow patterns and pressure distributions downstream of the injection port.

The next course of action is to look at other mathematical models. A summary of most of these models may be found in Reference 5. Most analyses of the secondary injection phenomena deal with the shock structure and pressure distributions along the motor nozzle wall. These approaches, therefore, run into the same

problems encountered by the model of Wu, Chapkis, and Mager.

One different approach involves the use of blast wave theory. Blast wave theory was originally applied to secondary injection by Broadwell[7]. Equation 19 in Reference 7 is expressed in a form suitable for calculating specific impulse ratio. Applying the parameters for Tests 1 through 6 to that equation and comparing the results with the test data from Table 7.4 produces the following table.

Test	Specific impulse ratio, $\frac{I_j}{I}$, blast wave theory	Specific impulse ratio, $\frac{I_j}{I}$, test results
1	0.73	0.96
2	0.93	1.13
3	0.73	1.19
4	0.80	1.09
5	0.85	1.45
6	0.85	1.44

An extensive comparison of the models of References 1 and 7 and some discussion of other approaches may be found in a recent report by Guhse[8].

10.3 Design Procedure

In the absence of a scientifically derived model which correctly predicts shock structure and side force for injection of a secondary gas into a rocket motor nozzle, a procedure for designing a secondary injection system is now presented. This procedure evolved as the data from each test in the series was analyzed. Empirical data is added to the design procedure of Section 4.1 to produce a system design that should result in maximum side force. The equations apply specifically to a conical motor nozzle, but the equations may be modified to suit the actual contour of a given rocket nozzle.

The first step is to select an angle of injection. Upstream injection definitely produces greater side force. Not enough experimental information is available to choose an angle that produces a maximum side force. The 20^{o} angle used in Test 5 and 6 or possibly a 30^{o} upstream injection angle are advised. With too large an angle, the momentum force of the secondary jet is reduced, and some undesirable effects may appear in the shock structure.

The second step is to design the injector nozzles. Supersonic injection should be used. The throat area of the injection nozzle is designed to produce the maximum injector chamber pressure compatible with the remainder of the secondary system. The exit area is tentatively designed in the following manner. Assume any reasonable injection point. Design the exit areas according to the procedure given in Section 4.1. Since test results showed actual pressures to be somewhat lower than the theoretical, it may be desirable to set the injector exit pressure somewhat lower than theoretical separation pressure at step 5. Having $P_j = 0.9\ P_s$ is suggested. This allows for a greater area ratio, a higher exit Mach number, and, as a result, a higher side force.

Given the tentative injection point and injector design, the third step is to calculate the shock azimuth at the exit of the motor nozzle. Determine the values of θ and X from the mathematical model at full flow conditions. The effective shock angle along the nozzle wall (now defined a ψ) is always greater than θ. The test results showed the difference ($\psi - \theta$) to be as much as eight degrees (see Table 9.1). With this as a guide, some value for

ψ must be chosen. For injection at primary stream Mach numbers similar to those of the Tests 1 through 6, choice of $\psi = 40^{o}$ is reasonable. Next, define a distance Y as a chord in the plane of injection connecting the injection point to the actual shock azimuth, Φ_j, in that plane. From empirical data, calculate Y = 1.1 X. From the system geometry of a cone with conical angle ψ passing through a point determined by Y, the shock azimuth at the exit, Φ_e, is calculated as

$$\Phi_e = 2 \arcsin \left\{ \frac{L_j}{D_e} \left[\tan (\psi-\alpha) + \tan \alpha + \frac{Y}{L_j} \right] \right\} \qquad (10.1)$$

Some of the angles and distances of equation 6.1 are shown in Figure 9.8.

For maximum side force, Φ_e must be less than 90^{o}. When Φ_e is greater than 90^{o}, a large portion of the high-pressure distribution inside the shock is either wasted on a portion of the wall at right angles to the desired direction of side force or even creates a negative side force component. For best results, a design value of Φ_e equal to 75 or 80 degrees is desirable. This provides a small safety factor if the design value is lower than

that produced in the actual system. If, then, the calculated Φ_e of equation 10.1 is between 75 and 80 degrees, the design is completed. If not, a new injection point is assumed, and the process is repeated until Φ_e from equation 10.1 falls within the desired range.

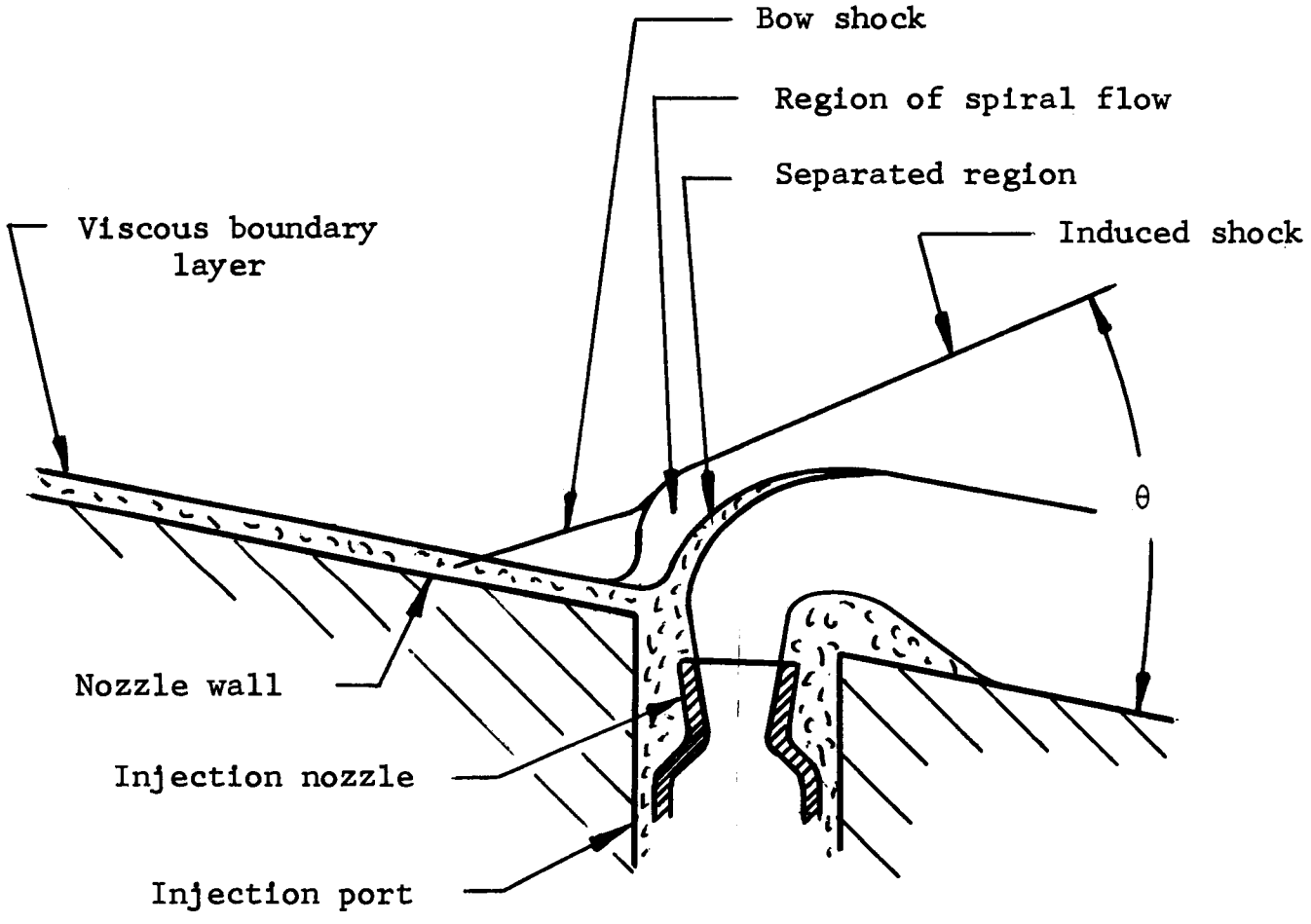

Figure 10.1 Upstream Shock Profile

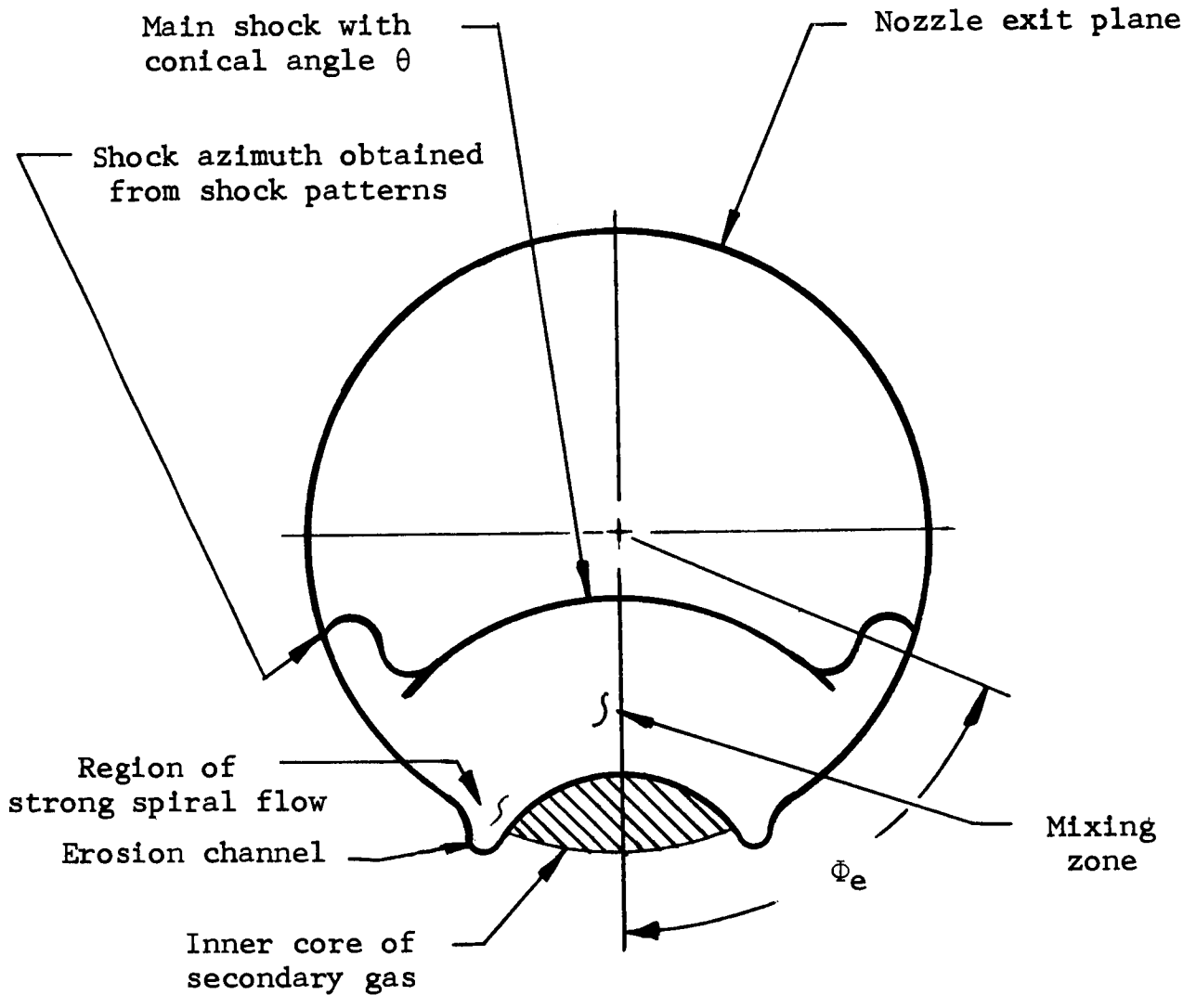

Figure 10.2 Shock Structure at Motor Nozzle Exit Plane

SECTION 11

SUMMARY OF EFFECTS OF PARAMETER VARIATIONS ON SIDE FORCE

Information regarding the effects on side force of variation of specific parameters come from three sources. First of all is the experimental data from this series of tests. Secondly, there is experimental information reported by others. The third source lies in the consensus of predictions by the various theoretical analyses. In this Section, conclusions regarding effects of parameter variations are made. These conclusions are drawn from all three sources. A simple means for approximating side force is proposed on the basis of the concluded effects of parameter variation.

11.1 Effect of Primary Stream Mach Number

Some difference of opinion can be found in the literature regarding the effect of primary stream Mach number. The reason for this probably lies in the placement of the shock structure downstream of the injection point. Since there is a positive contribution to side force from the downstream pressure distributions, it is necessary that the injection port be as far

upstream as possible. The limiting factor in upstream positioning of the injection port is the location of the shock on the nozzle wall near the exit plane. If the shock azimuth is 90^{o}, the high-pressure area just inside the shock is being wasted. If the azimuth is greater than 90^{o}, the high-pressure area produces a negative contribution to side force. When experimenters vary port locations inside a nozzle in order to check effects of different primary stream Mach numbers, the results can well be influenced by the downstream shock distribution. Given a primary nozzle configuration, a designer should use a procedure like the one given in Section 10.3 rather than choose injection location on the basis of primary stream Mach numbers.

11.2 Effect of Secondary Gas Temperature

During the first few seconds after ignition of the secondary system, the injector chamber temperatures steadily rise up to their design point of $1800^{o}F$. During that rise time, it is possible to see the effect of temperature on the side force produced by a given secondary mass flow. Calculations show that side force is directly proportional to the square root of the absolute total temperature of the secondary gas.

11.3 Effect of Injection Angle

Almost unanimously, the various mathematical models predict an increase in side force as the angle of injection is turned upstream from the normal to the motor axis. As the angle is increased, a maximum point is reached before the loss in secondary jet momentum force due to the injection angle becomes significant. When the angle is increased further, serious disturbances in the primary flow may occur and cause a decrease in axial thrust.

Results from Tests 5 and 6 show the improvement in side force, magnification factor, and specific impulse ratio for 20^{o} upstream injection. If some allowances are made for other parameter variations in Tests 2 and 4, it appears that 20^{o} upstream injection produces a fifteen percent increase in specific impulse ratio over that of supersonic injection normal to the motor axis. Experimental information from other sources usually shows side force increase for upstream injection, but these sources do not agree upon a specific relationship between injection angle and side force. This phase of the investigation of secondary injection phenomena probably has a greater need of more experimental data than any other.

11.4 Effect of Injection Mach Number and Pressure

Some general comments can be made in regard to injection Mach number. Total side force increases with an increase in secondary jet momentum, and the jet momentum is proportional to exit Mach number. Within the limitations imposed by pressure matching requirements, the Mach number should be as high as possible.

Theoretically, the most efficient injection system is one whose injector exit pressure matches the pressure in the upstream separation region of the induced shock. This theory is in agreement with results of this series of tests as well as tests of most other experimenters. In order to obtain the proper exit pressure along with a high Mach number, the chamber pressure of the injection nozzles should be as high as possible. With higher chamber pressure, the divergent section of the injection nozzle requires a larger expansion ratio in order to produce the required exit pressure. In turn, a larger expansion ratio produces a higher Mach number.

The relationship between chamber pressure, exit pressure, and

Mach number is illustrated in Figure 11.1. The curves are based on a parameter variation study using the calculation procedure given in Section 4. The intersection of the two curves at the left indicates the minimum chamber pressure at which P_j can be equal to or greater than P_s for the given system. As injector throat area is decreased, P_{jc} is increased. For supersonic injection, the expansion ratio of the injection nozzle is increased in order to match P_j and P_s as P_{jc} is increased. Over the range of P_{jc} studied, M_j increases from 1 to 1.83. For sonic injection, P_j increases according to the critical pressure ratio as the decreasing throat area increases P_{jc}. The curves show an increase in F_s for supersonic injection and a decrease for sonic injection. The test results are in qualitative agreement with these curves.

11.5 Side Force Calculations in Preliminary Design

In preliminary work, a TVC system designer is interested in obtaining an approximate value for the side force his system can produce. Magnification factor data from this series of tests indicates a magnification factor of two for pressure-matched

supersonic injection normal to the motor axis from a properly designed injection point. The momentum force of an injected supersonic jet is given by the equation

$$\left(\dot{m}_j v_j\right) = \dot{m}_j M_j \sqrt{\frac{g\gamma_j R_j T_{jc}}{1 + \frac{1}{2}(\gamma_j - 1)M_j^2}} \qquad (11.1)$$

In equation 11.1, M_j is usually the only unknown term. The value of M_j is determined after the proper design procedures are performed. As a first-order approximation, $M_j = 1.5$ may be applied for sea-level motor nozzle applications; and $M_j = 2.4$ may be used with an altitude nozzle. If an additional approximation that side force is inversely proportional to the cosine of the injection angle is used, then the preliminary design equation for side force from one nozzle is

$$F_s = \frac{2\,\dot{m}_j M_j}{\cos \varepsilon} \sqrt{\frac{g\gamma_j R_j T_{jc}}{1 + \frac{1}{2}(\gamma_j - 1)M_j^2}} \quad , \; 0 \leq \varepsilon \lesssim 30^{\circ} \qquad (11.2$$

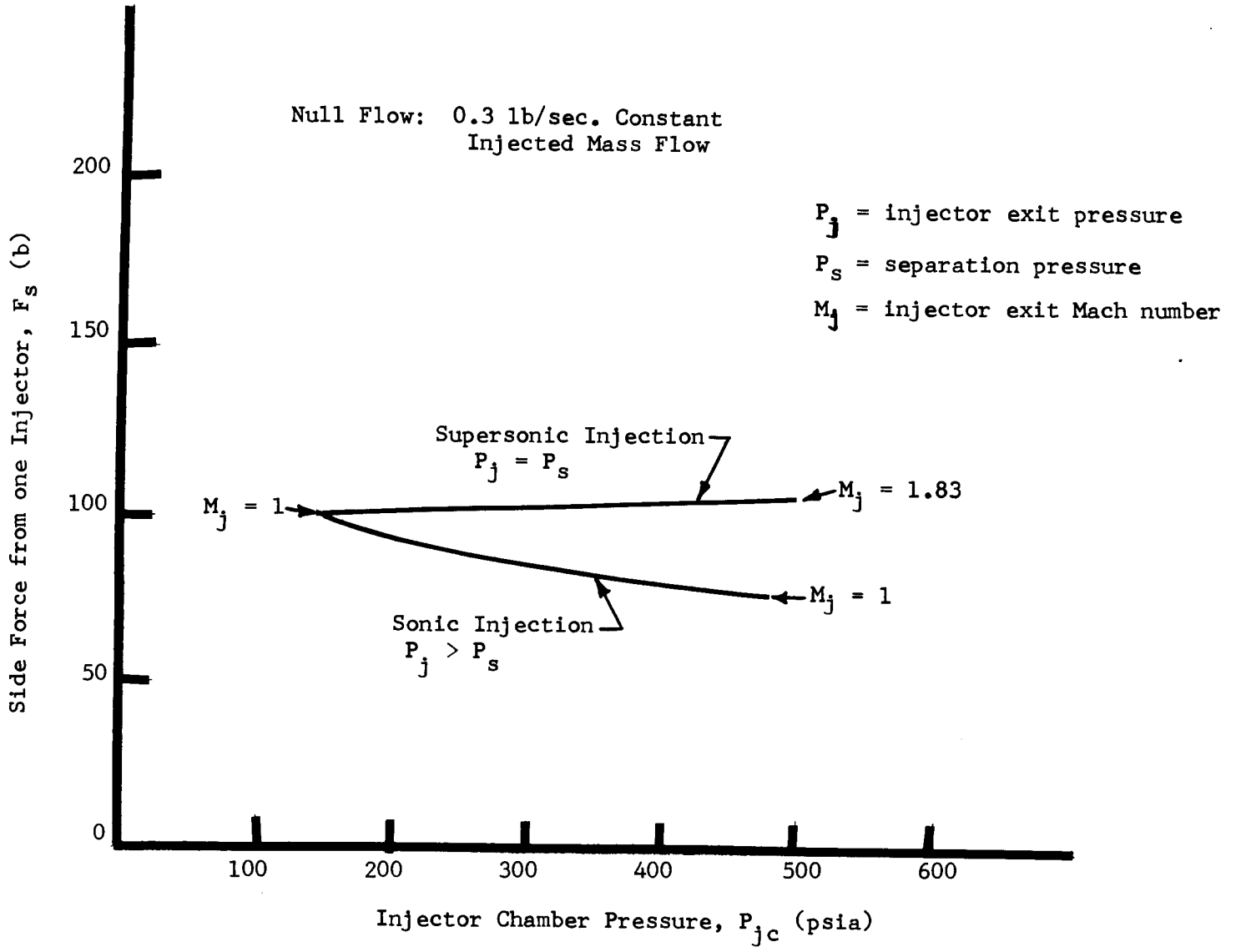

Figure 11.1 Theoretical Comparison of Supersonic and Sonic Injection

SECTION 12

DYNAMIC RESPONSE - THEORETICAL APPROACHES

The components involved in determining the dynamic response of secondary injection are shown in Figure 12.1. In each control plane, the flow of high temperature gas is divided by the control valve to the chambers of the two secondary injection nozzles. Secondary injection into the primary nozzle creates a side force, F_{app}, which is applied to the rocket motor mounted on a thrust stand. The load cells of the thrust stand in the control plane provide the resultant force, F_{meas}.

In this system, ΔP_{jc} and F_{meas} are measurable quantities. Data acquisition and reduction of these quantities for purposes of dynamic analysis is discussed in Paragraph 12.1. Equations for the thrust stand are given in Paragraph 12.2. Approaches toward determining F_{app} and the transfer function of the secondary injection mechanism are presented in Paragraph 12.3. Test data and the application of the analysis to it begins in Section 13.

12.1 Data Acquisition and Reduction

For dynamic analysis, it is necessary to work from high-speed digital plots or from the analog Visicorder traces. The magnitudes

and time relationships of the measured quantities must be determined from one or both of these sources.

There are some difficulties inherent in each of these two forms. Data for digital plots pass through a 50 cps filter which may cause some attenuation and time delay in signals with high frequency components. Each point in a digital plot is made at a certain time associated with the sampling sweep in which it was recorded. This time may differ from the time the data point was acquired. For instance, for a 300 sample per second acquisition and plot rate, the actual time and plotted time may differ as much as 3-1/3 milliseconds. One possible source of difficulty in the analogue trace is the actual positioning of the plotting device over the graph paper with respect to obtaining exact time and magnitude scaling.

On the Visicorder trace, magnitude and time scaling must be done indirectly since no grid appears on the trace itself. Magnitude scaling comes from the calibration steps preceding the run. Time scaling is based on the timing points running along the top and bottom of the trace.

The characteristics of the data itself may be seen on the Visicorder

reproduction included in the test data of Section 14. On a programmed sinusoid, the chamber pressures usually appear as a clean sine wave. There is no difficulty in obtaining the peak to peak amplitude on either Visicorder or plotted data. The programmed steps, however, are not sharp steps on the chamber pressure curves. The dynamics of the valve and manifolding are the limiting factors. Given this condition for step inputs, it is better to concentrate on frequency response data for determining the dynamics of secondary injection.

The characteristics of side force data present some difficulty. In order for a thrust stand to possess high response capabilities, it must have a relatively high spring rate and a low damping factor. When such a thrust stand is subjected to a force input along one axis, such as the thrust of the primary engine, the stand will vibrate at its damped natural frequency in the other planes. This low-amplitude oscillation is present for all modes of yaw or pitch excitation - steady state, sine wave, step, or ramp. The transfer function of the thrust stand in the yaw or pitch plane does not cover this cross-coupling effect. When the vibration level is small compared to the applied force, the vibrations can be eliminated graphically from the analog signal

available on the Visicorder trace. To recover the side force signal from digital plots, it is required that the plotting rate be at least seven times faster than the frequency of the vibration. Maximum vibration frequency encountered in the test was 30 cps; therefore, the minimum plot rate required is 210 samples per second. The results of sinusoid data reduction from 300 sps plots and from 20 inch per second Visicorder run compare favorably, but some difference still exists in the side force wave shapes from the two sources.

12.2 Thrust Stand

In Tests 3 through 6 of the series, a six-degree-of-freedom thrust stand was used. Sinusoidal inputs were applied to the yaw plane. The effective rocket motor and thrust stand geometry in that plane is shown in Figure 12.2. The nomenclature used in the following analysis is found in Table 12.1. The use of the subscripts 34 and 56 results from the numbers assigned to the load cells in the Data Acquisition System.

Equations from the lightly damped two-degree-of-freedom system shown in Figure 12.2 are:

$$m\ddot{z} + D\dot{z} + 2kz + k(\ell_2-\ell_1)\theta_1 = F_{app}$$

$$J\ddot{\theta}_1 + \mu\ddot{\theta}_1 + k(\ell_2^2 + \ell_1^2)\theta_1 + k(\ell_2-\ell_1)z = (\ell_2+\ell_3)F_{app}$$

When all initial conditions are zero, the equations with Laplace notation are:

$$[mS^2 + DS + 2k]z + k(\ell_2-\ell_1)\theta_1 = F_{app}$$

$$k(\ell_2-\ell_1)z + [JS^2 + \mu S + k(\ell_2^2 + \ell_1^2)]\theta_1 = (\ell_2+\ell_3)F_{app}$$

When F_{app} is sinusoidal, S may be replaced by $j\omega$, and the steady-state frequency response equations become:

$$[2k - m\omega^2 + j\omega D]z + k(\ell_2-\ell_1)\theta_1 = F_{app}$$

$$k(\ell_2-\ell_1)z + [k(\ell_2^2 + \ell_1^2) - j\omega^2 + j\omega\mu]\theta_1 = (\ell_2+\ell_3)F_{app}$$

The relationship between the load cell displacements and the z and θ_1 variables are given by:

$$x_{56} = z + \ell_2\theta_1$$

$$x_{34} = z - \ell_1\theta_1$$

After substitution, the problem may be solved for F_{56} or F_{34} as a function of F_{app}. Since F_{56} is the larger of the two load cell

readings, it is used in the resultant equation:

$$\frac{F_{56}}{F_{app}} = \frac{(\ell_1+\ell_2)(\ell_1+\ell_2+\ell_3) - \frac{\omega^2}{k}\left[m\,\ell_2(\ell_2+\ell_3)+J\right] + j\frac{\omega}{k}\left[\mu+D\ell_2(\ell_2+\ell_3)\right]}{(\ell_1+\ell_2)^2 - \frac{\omega^2}{k}\left[\frac{\mu D}{k} + 2J+m\,(\ell_1^2+\ell_2^2)\right] + \frac{\omega^4 mJ}{k^2} + j\frac{\omega}{k}\left[2\mu+D(\ell_1^2+\ell_2^2) - \frac{\omega^2}{k}(JD+\mu m)\right]} \tag{12.1}$$

All terms except μ and D on the right side of the equation are either known or can be calculated directly. Although the system is lightly damped, μ and D cannot be neglected. Approximate values for these two damping terms can be based on the system response to a programmed step input.

12.3 Determination of Secondary Injection Transfer Function

The secondary injection fluid mechanism is assumed to have a transfer function of the form $\frac{a}{S+b}$. Referring to Figure 12.1, for a sinusoidal input,

$$\frac{F_{app}}{\Delta P_{jc}} = \frac{a}{j\omega+b}$$

where the ratio $\frac{a}{b}$ is determined from the steady-state results. The thrust stand transfer function is given in terms of F_{56} in equation 12.1. For any input frequency, a magnitude and a phase angle can be calculated for $\frac{F_{56}}{F_{app}}$. From the test data, the

magnitude and phase angle of $\frac{F_{56}}{\Delta P_{jc}}$ can be measured. Then, for any ω,

$$\frac{F_{app}}{\Delta P_{jc}} = \frac{a}{j\omega+b} = \frac{\left|\frac{F_{56}}{\Delta P_{jc}}\right|}{\left|\frac{F_{56}}{F_{app}}\right|} \left(\angle \frac{F_{56}}{\Delta P_{jc}} - \angle \frac{F_{56}}{F_{app}} \right) \qquad 12.2$$

Equation 12.2 can be solved for both real and imaginary parts. Since $\frac{a}{b}$ is already known, solution for either real or imaginary terms will give the complete solution.

Theoretically, this approach is very simple and straight-forward. Two independent equations may be solved for the same unknown for each frequency tested. The results are easily obtained in practice, however, only when the first resonant frequency of the $\frac{F_{56}}{F_{app}}$ transfer function occurs for values of ω greater than b. The test results given in the next section of this report show that the test stand reaches its first resonance point for ω less than b.

Table 12.1 Nomenclature

a	Numerator of Secondary Injection Transfer Function	$\frac{(in^2 rad)}{sec.}$
b	Corner Frequency for Secondary Injection	(rad/sec)
D	Translational Damping Term	(lb.sec/ft)
F_{app}	Force Applied to System by Secondary Injection	(lb)
F_{meas}	Sum of Load Cell Readings: $F_{meas}=F_{34}+F_{56}$	(lb)
F_{34}	Force on Forward Load Cell: $F_{34}=k\ x_{34}$	(lb)
F_{56}	Force on Aft Load Cell: $F_{56}= k\ x_{56}$	(lb)
J	System Moment of Inertia about Center of Gravity	(slug ft^2)
k	Spring Constant of Load Cells	(lb/ft)
ℓ_1	Distance Between Forward Load Cell and Center of Gravity	(ft)
ℓ_2	Distance Between Center of Gravity and Aft Load Cell	(ft)
m	System Mass	(slugs)
ΔP_{jc}	Difference in Injector Chamber Pressures	(psi)
x_{34}	Deflection of Forward Load Cell	(ft)
x_{56}	Deflection of Aft Load Cell	(ft)
z	Lateral Translation of System Center of Gravity	(ft)
θ_1	System Rotation about Center of Gravity	(rad)
μ	Rotational Damping Term	(ft.lb.sec)

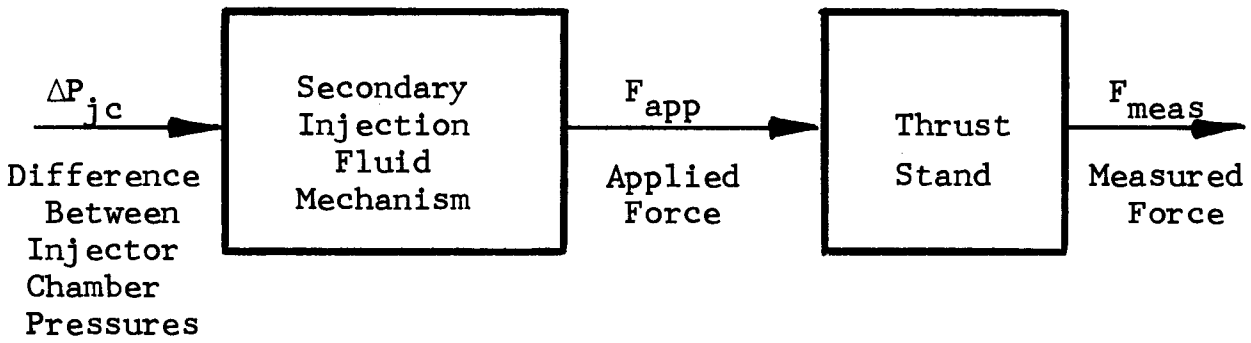

Figure 12.1 Block Diagram of SITVC Components

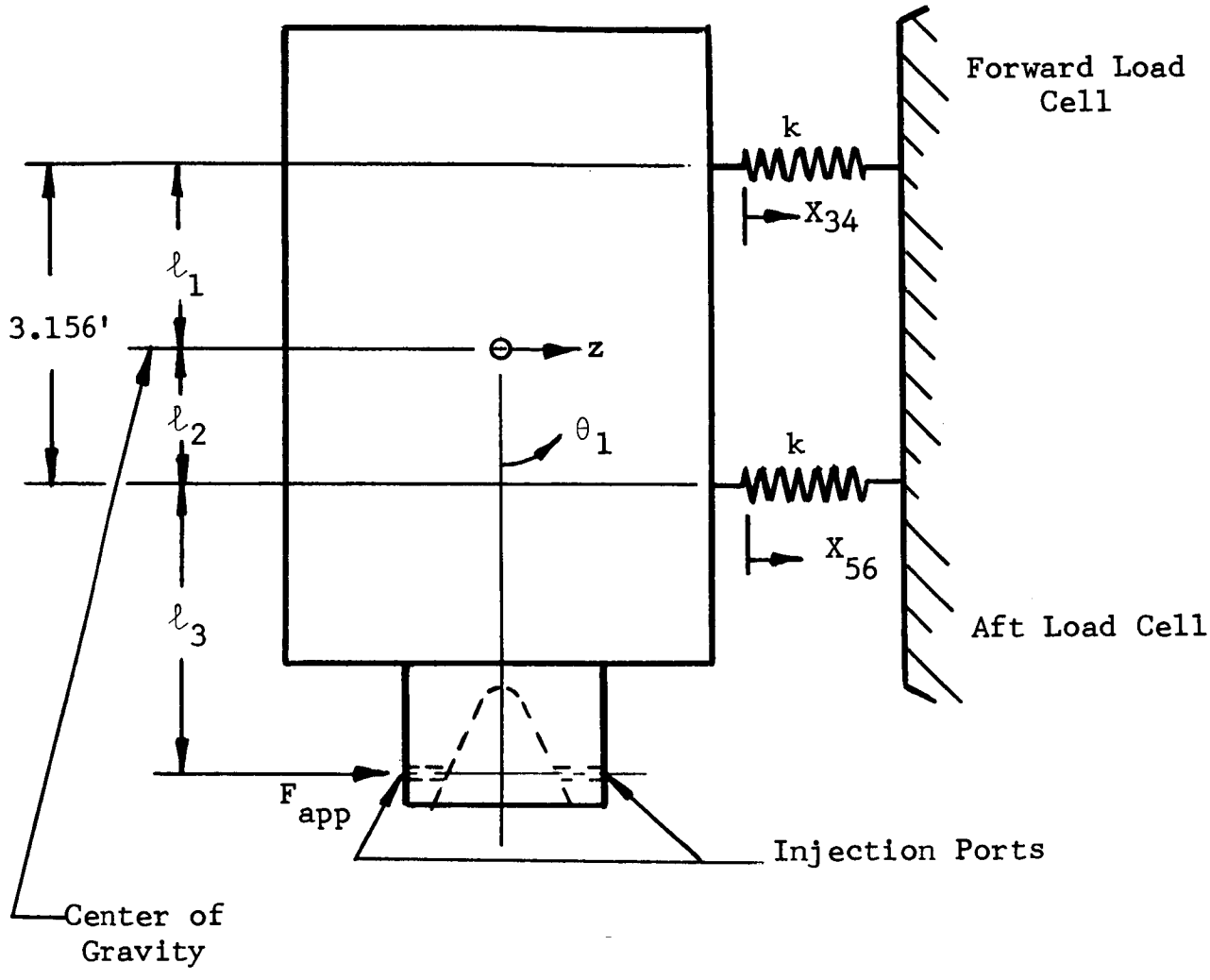

Figure 12.2 Rocket Motor and Thrust Stand Geometry - Yaw Plane

SECTION 13

FREQUENCY RESPONSE - TEST DATA

In order to obtain the transfer function of the secondary injection fluid mechanism, the analysis given in Section 12 is now applied to frequency response data from Tests 4, 5, and 6. Representative curves of system response characteristics are also given.

13.1 Transfer Function Calculations

Applicable system parameters appear in Table 13.1. The $\frac{a}{b}$ ratio is calculated from the steady-state data for the respective tests. Examination of Visicorder traces for the tests indicated that system damping for each test is about one-tenth of critical damping. Some of these Visicorder traces are reproduced in Section 14. Applying the 0.1 damping ratio to both translational and rotational vibration of the system, average values of D and μ are found to be

$D = 1900$ lb sec/ft

$\mu = 4500$ ft lb sec

The above parameters are next substituted into equation 12.1.

For Test 4,

$$\frac{F_{56}}{F_{app}} = \frac{12.80 - \frac{160.9\omega^2}{10^6} + j\,\frac{8180\omega}{10^6}}{9.96 - \frac{377\omega^2}{10^6} + \frac{3.05\omega^4}{10^9} + j\left(0.01860\omega - \frac{0.311\omega^3}{10^6}\right)} \qquad (13.1)$$

For Test 5,

$$\frac{F_{56}}{F_{app}} = \frac{13.11 - \frac{177.8\omega^2}{10^6} + j\,\frac{8660\omega}{10^6}}{9.96 - \frac{387\omega^2}{10^6} + \frac{3.29\omega^4}{10^9} + j\left(0.01843\omega - \frac{0.322\omega^3}{10^6}\right)} \qquad (13.2$$

For Test 6,

$$\frac{F_{56}}{F_{app}} = \frac{13.11 - \frac{190.0\omega^2}{10^6} + j\,\frac{8320\omega}{10^6}}{9.96 - \frac{436\omega^2}{10^6} + \frac{4.10\omega^4}{10^9} + j\left(0.01862\omega - \frac{0.360\omega^3}{10^6}\right)} \qquad (13.3$$

Calculated magnitude and phase angle of $\frac{F_{56}}{F_{app}}$ at the frequencies applied in Tests 4, 5, and 6 are given in Tables 13.2, 13.3, and 13.4. Also in these three tables are the values of magnitude and phase angle of $\frac{F_{56}}{\Delta P_{jc}}$ as determined from the test data. The accuracy of the $\frac{F_{56}}{\Delta P_{jc}}$ phase angle measurements is limited by the factors mentioned in Section 12.1. Magnitude and phase angle of $\frac{F_{app}}{\Delta P_{jc}}$ are then calculated by application of Equation 12.2. With the assumptions made, it is impossible to have a positive angle for $\frac{F_{app}}{\Delta P_{jc}}$; however the low positive and negative angles calculated at low frequencies are encouraging since they indicate that the applied force of secondary injection at those frequencies is approximately in phase with the injector chamber pressures.

Values of a and b given in Tables 13.2, 13.3, and 13.4 are calculated directly from the equation $\frac{F_{app}}{\Delta P_{jc}} = \frac{a}{j\omega+b}$ for each condition in which the $\frac{F_{app}}{\Delta P_{jc}}$ angle is negative. Results for frequencies less than 10 cps are doubtful because of the small phase angles involved. In Test 6, the system is very near its first resonance point with a 20 cps input. Therefore, this data point cannot be used. The three points remaining are 10 and 15 cps

of Test 4 and 10 cps of Test 5. All these points show a value of b near 210 radians per second. Ratios of a to b at these points are reasonably close to the actual ratios (given in Table 13.1) determined by static test data.

On this basis, the corner frequency of the secondary injection fluid mechanism is calculated as 35 cps, where the corner frequency is defined as $\frac{b}{2\pi}$. This means that the response of secondary injection is expected to be down 3 decibels at 35 cps, with a corresponding phase angle of -45^{o}.

13.2 System Response Characteristics

Figures 13.1, 13.2, and 13.3 give representative curves for the frequency response of the system components. Figure 13.1 shows the response of valve position as indicated by the feedback transducer, of differential injection nozzle chamber pressure, and of measured side force compared to the programmed input signal during Test 4. The same ratios are plotted for Test 6 in Figure 13.2. Data from other tests tend to produce similar characteristics.

To illustrate the effect of the test stand on programmed frequencies above 15 cps, the ratio of measured side force to difference in injector chamber pressures is plotted for Tests 4, 5, and 6 in Figure 13.3.

13.3 Effect of Test Stand Dynamics

It is obvious from the results obtained from the frequency response tests that the limiting factor in obtaining good repeatable data is the performance of the test stand. To achieve fast response a low damping factor is required, however a low damping factor produces a higher level of oscillation with a resulting large noise to signal ratio, and a larger decay time for step induced oscillations. The use of an electrical filtering network to smooth out the force level traces has basically the same effect as increasing the stand damping, in that it introduces a delay into the system which is very difficult to analyze.

Test Number	4	5	6
J (slug ft^2)	84	86	95
k (lb/ft)	1.043×10^6	1.043×10^6	1.043×10^6
ℓ_1 (ft)	2.08	2.03	2.09
ℓ_2 (ft)	1.08	1.13	1.07
ℓ_3 (ft)	0.894	0.990	0.990
m (slug)	39.5	41.5	47
$\frac{a}{b}$ (in^2)	.265	.34	.33

Table 13.1 System Parameters

Frequency (cps)		3	5	10	15
$\frac{F_{56}}{F_{app}}$ (eq. 13.1)	magnitude	1.295	1.318	1.419	1.615
	phase angle	-1.3^{o}	-2.2^{o}	-4.9^{o}	-8.3^{o}
$\frac{F_{56}}{\Delta P_{jc}}$ (test data)	magnitude (in^2)	0.36	0.42	0.42	0.61
	phase angle	-4^{o}	-9^{o}	$-21\frac{1}{2}^{o}$	$-32\frac{1}{2}^{o}$
$\frac{F_{app}}{\Delta P_{jc}}$ (eq. 12.2)	magnitude (in^2)	0.278	0.319	0.296	0.378
	phase angle	-2.7^{o}	-6.8^{o}	-16.6^{o}	-24.2^{o}
a $\left(\frac{in^2\ rad}{sec}\right)$		111	84.5	65	86
b $\left(\frac{rad}{sec}\right)$		400	265	210	210

Table 13.2 Test 4 Frequency Response Calculations

Frequency (cps)		3	5	10
$\frac{F_{56}}{F_{app}}$ (eq. 13.2)	magnitude	1.329	1.351	1.454
	phase angle	-1.3^{o}	-2.1^{o}	-4.7^{o}
$\frac{F_{56}}{\Delta P_{jc}}$ (test data)	magnitude (in^2)	0.46	0.46	0.48
	phase angle	0^{o}	$-3\frac{1}{2}^{o}$	$-21\frac{1}{2}^{o}$
$\frac{F_{app}}{\Delta P_{jc}}$ (eq. 12.2)	magnitude (in^2)	0.346	0.340	0.330
	phase angle	1.3^{o}	-1.4^{o}	-16.8^{o}
a $\left(\frac{in^2\ rad}{sec}\right)$		---	435	72
b $\left(\frac{rad}{sec}\right)$		---	1280	220

Table 13.3 Test 5 Frequency Response Calculations

Frequency (cps)		3	8	20
$\frac{F_{56}}{F_{app}}$ (eq. 13.3)	magnitude	1.330	1.415	2.31
	phase angle	-1.3^{o}	-3.8^{o}	-15.7^{o}
$\frac{F_{56}}{\Delta P_{jc}}$ (test data)	magnitude (in^2)	0.44	0.48	6.0
	phase angle	-1^{o}	-3^{o}	-80^{o}
$\frac{F_{app}}{\Delta P_{jc}}$ (eq. 12.2)	magnitude (in^2)	0.331	0.339	2.60
	phase angle	0.3^{o}	0.8	-64.3^{o}
a $\left(\frac{in^2\ rad}{sec}\right)$		---	---	362
b $\left(\frac{rad}{sec}\right)$		---	---	605

Table 13.4 Test 6 Frequency Response Calculations

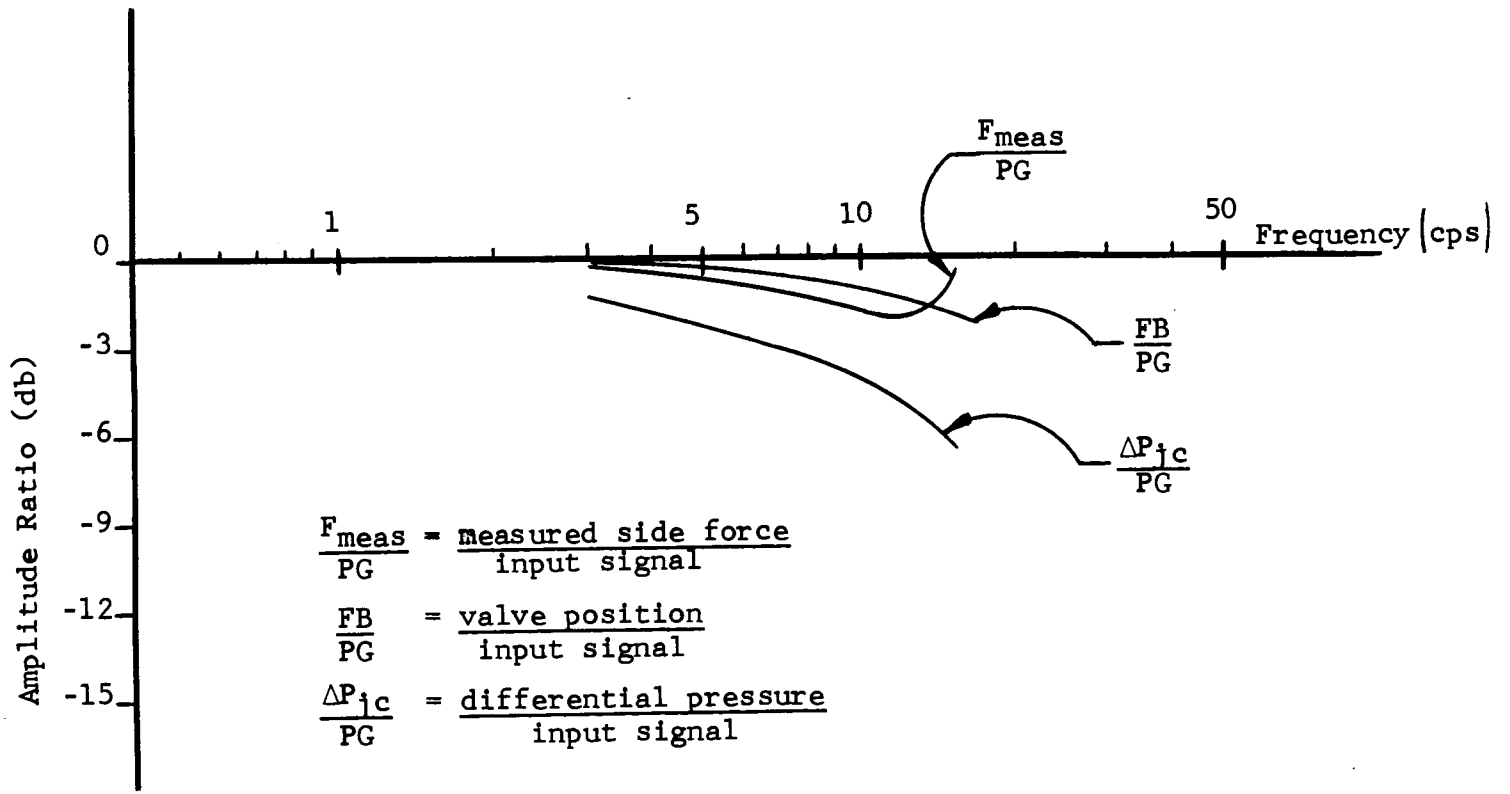

Figure 13.1 System Response Characteristics - Test 4

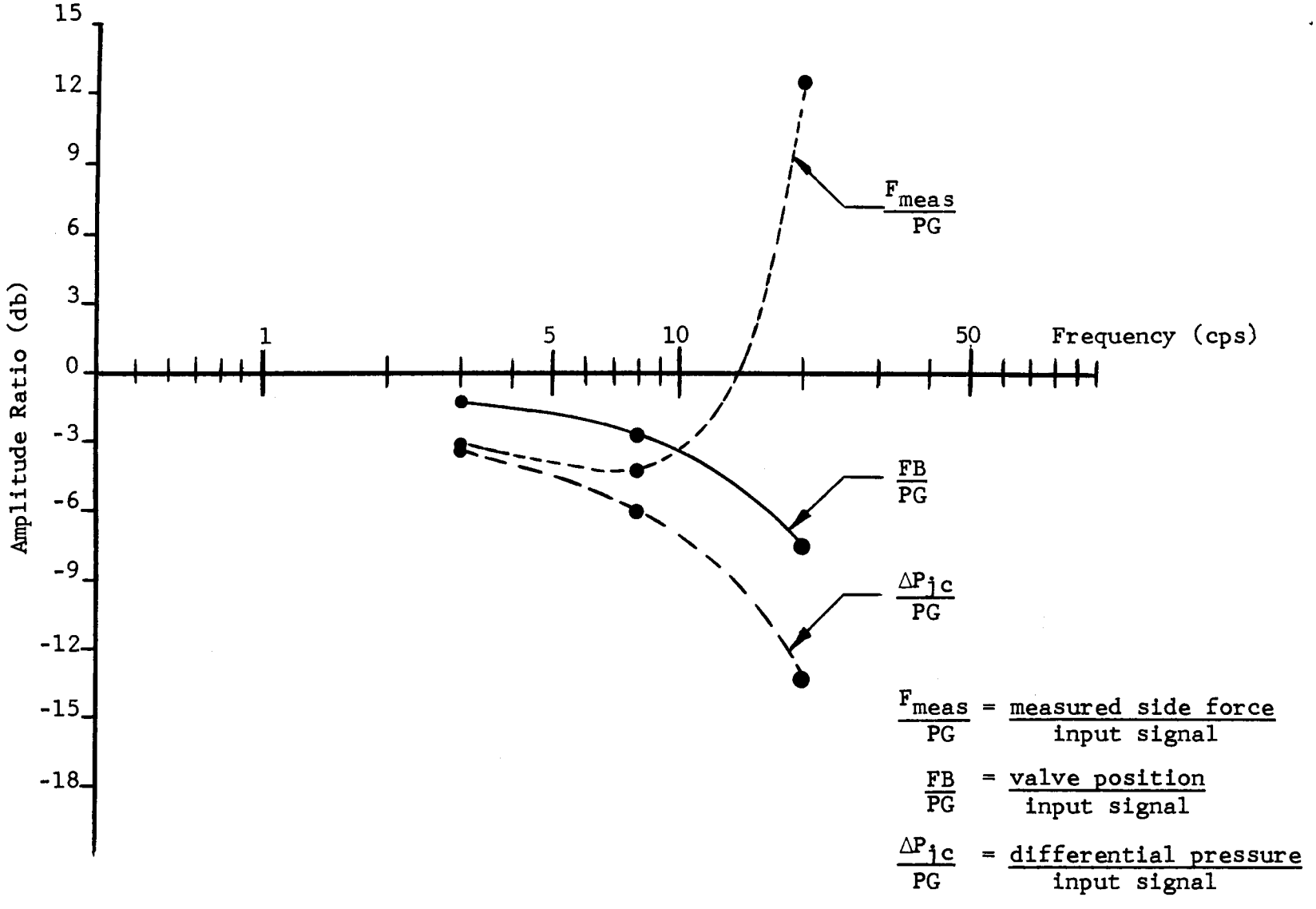

Figure 13.2 System Response Characteristics - Test 6

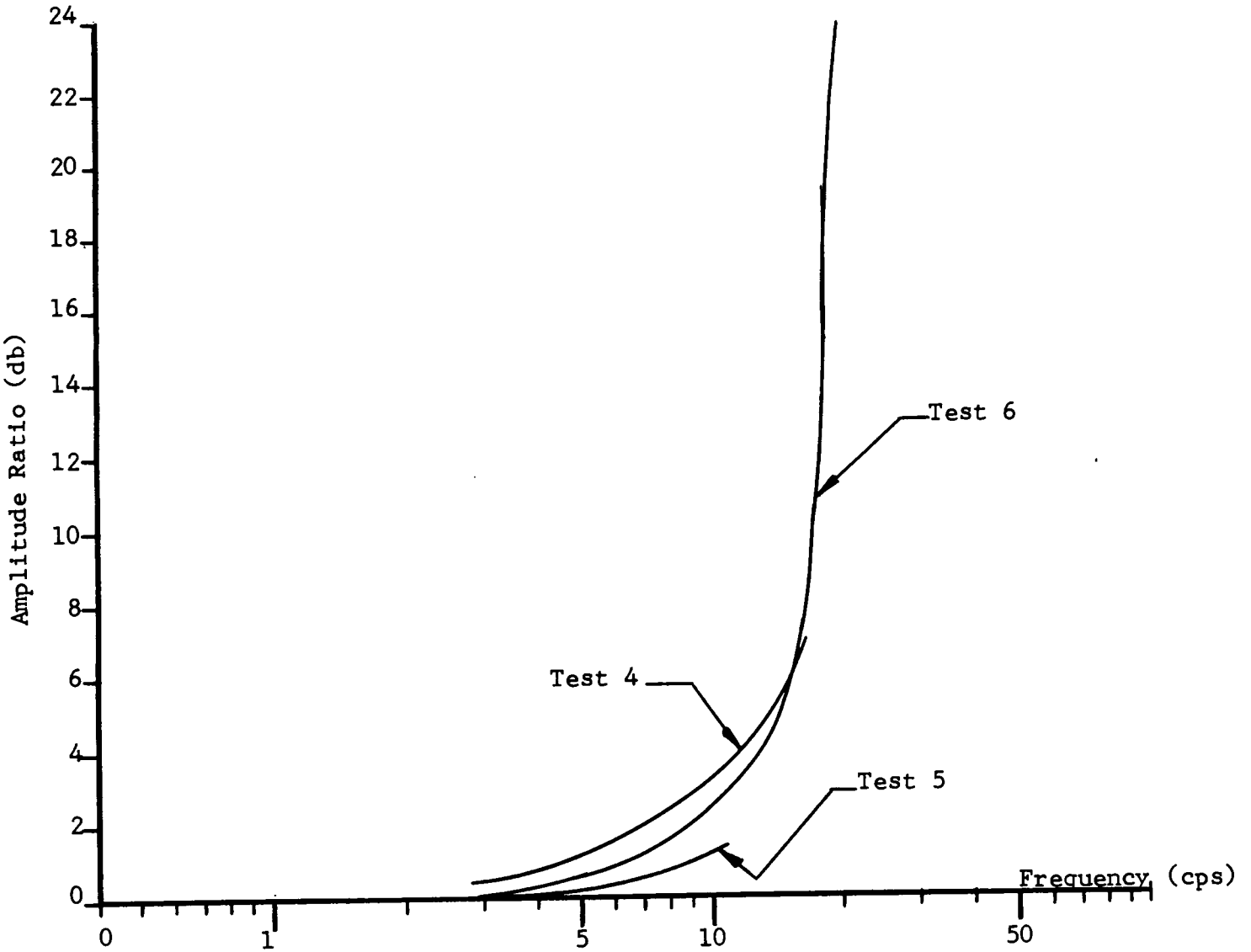

Figure 13.3 Frequency Response of $\frac{F_{meas}}{\Delta P_{jc}}$ $\frac{\text{measured side force}}{\text{differential pressure}}$

SECTION 14

SYSTEM CONTROL QUALITIES

The object of this section of the report is to delineate the control qualities of the secondary injection TVC system.

In general terms certain characteristics are required to make a good control system. These can be summarized under the following headings.

i Repeatibility

ii Minimum threshold effect

iii No discontinuities throughout the full operating cycle

iv Linearity of output to input

v Minimum hysteresis

The experimental results of this program have shown that the TVC system performed excellently in these specific areas.

Figures 14.1 and 14.2 are photographic reproductions of a Visicorder trace of Test 4 run at 1 inch per second. They show the overall relationship between the valve input program,

the valve position, the left and right injection nozzle pressures and the resultant side forces. The more salient features are detailed in the following paragraphs.

14.1 Repeatibility

Figure 14.3 is a digital plot of the period from 11 to 17 seconds of Test 5. This was plotted at a rate of 300 discrete points per second. It shows the net side force generated by four equal input steps. The oscillations superimposed on the steps are due to the ringing of the test stand, and make the determination of the exact force level very difficult. It does however illustrate the typical repeatibility characteristics of the system.

14.2 Minimum Threshold Effect

The threshold of a control system is defined as the smallest input signal to which the output responds.

The response of the system to small input steps is shown on a digital plot in Figure 14.4 for Test 4. These were the smallest input signals used during the experimental program, and represent a level of 3.5% of the maximum available signal.

The upper trace is the pressure differential between the injector nozzles, and the lower is the resultant net side force. Again the oscillations and force level scale factor make a very acurate measurement impossible, but the response of the output (i.e., side force) is apparent.

It is not possible to state a minimum threshold level, except that it is below 3.5% of maximum.

14.3 Smoothness of Output

Figure 14.5 presents the system response to an input ramp and step plotted from the digital data of Test 4.

The upper trace is the pressure differential between the two injector nozzles and the lower is the resultant side force. The differential pressure is plotted as an absolute value and therefore does not become negative. The input signal however was a ramp from a negative pressure differential through null to a positive differential.

The side force trace shows the movement from a negative to positive level with no discontinuity about the zero or null position.

14.4 Output Linearity

The linearity of the output signal with respect to the input can be seen for the ramp input on Figure 14.5. An averaging line has been drawn through the high frequency oscillations to emphasize this point.

14.5 Hysteresis

Hysteresis in a secondary injection TVC system can be defined as the difference in the value at any specific side force level when approached from an increasing or a decreasing injection differential pressure. It is fundamentally a measure of the various frictions existing in the system. The term friction being used here to describe fluid friction as well as mechanical friction.

The friction level is very dependent on the amount of oscillations present, since high frequency vibration or dither can significantly reduce the amount of friction. Because of this, no attempt has been made to quantitatively evaluate the hysteresis, since from Figures 14.3, 14.4 and 14.5 it is obvious that the test installation was subjected to high frequency oscillations throughout the test firings.

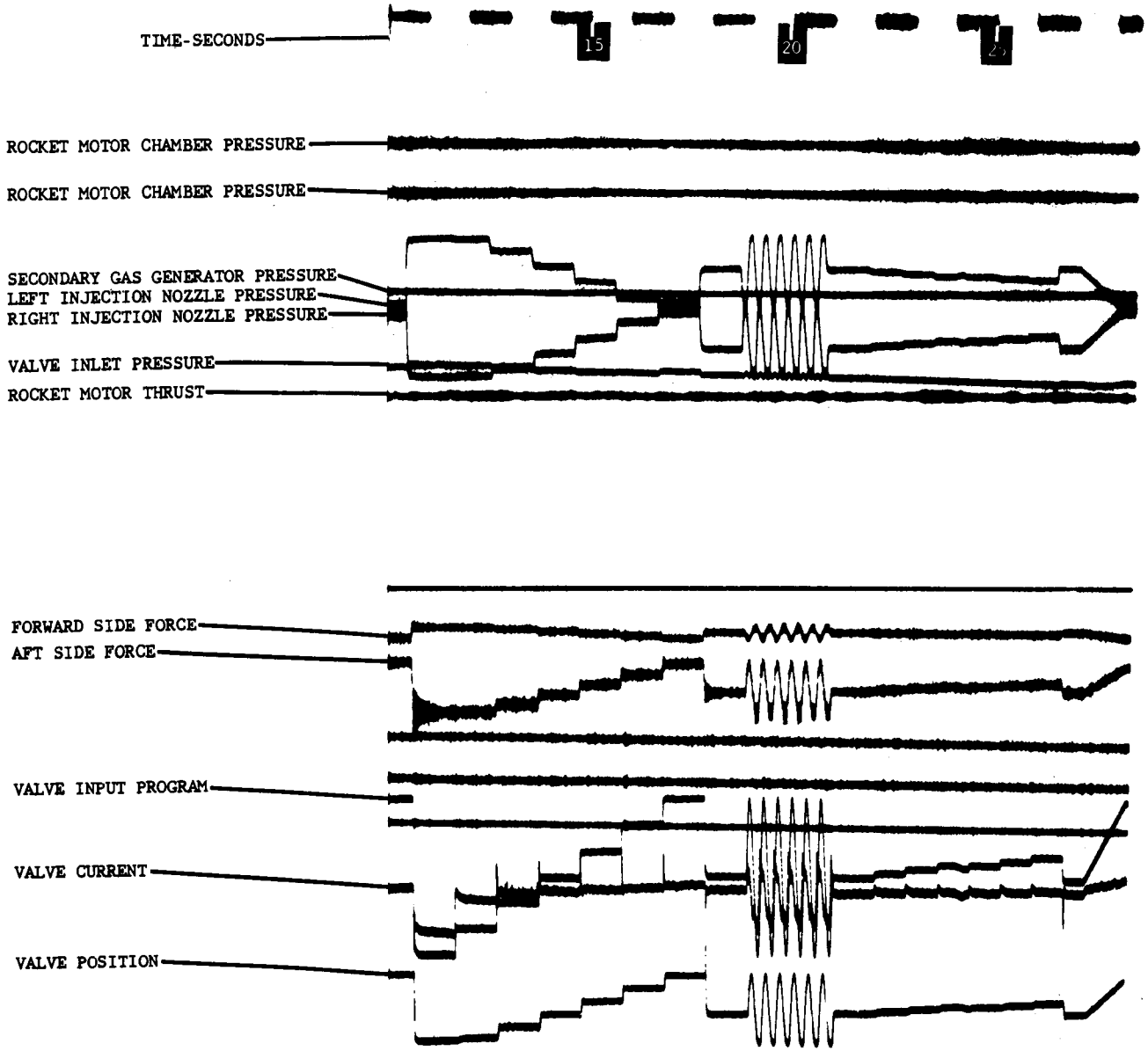

Figure 14.1 Visicorder Trace - Test No. 4

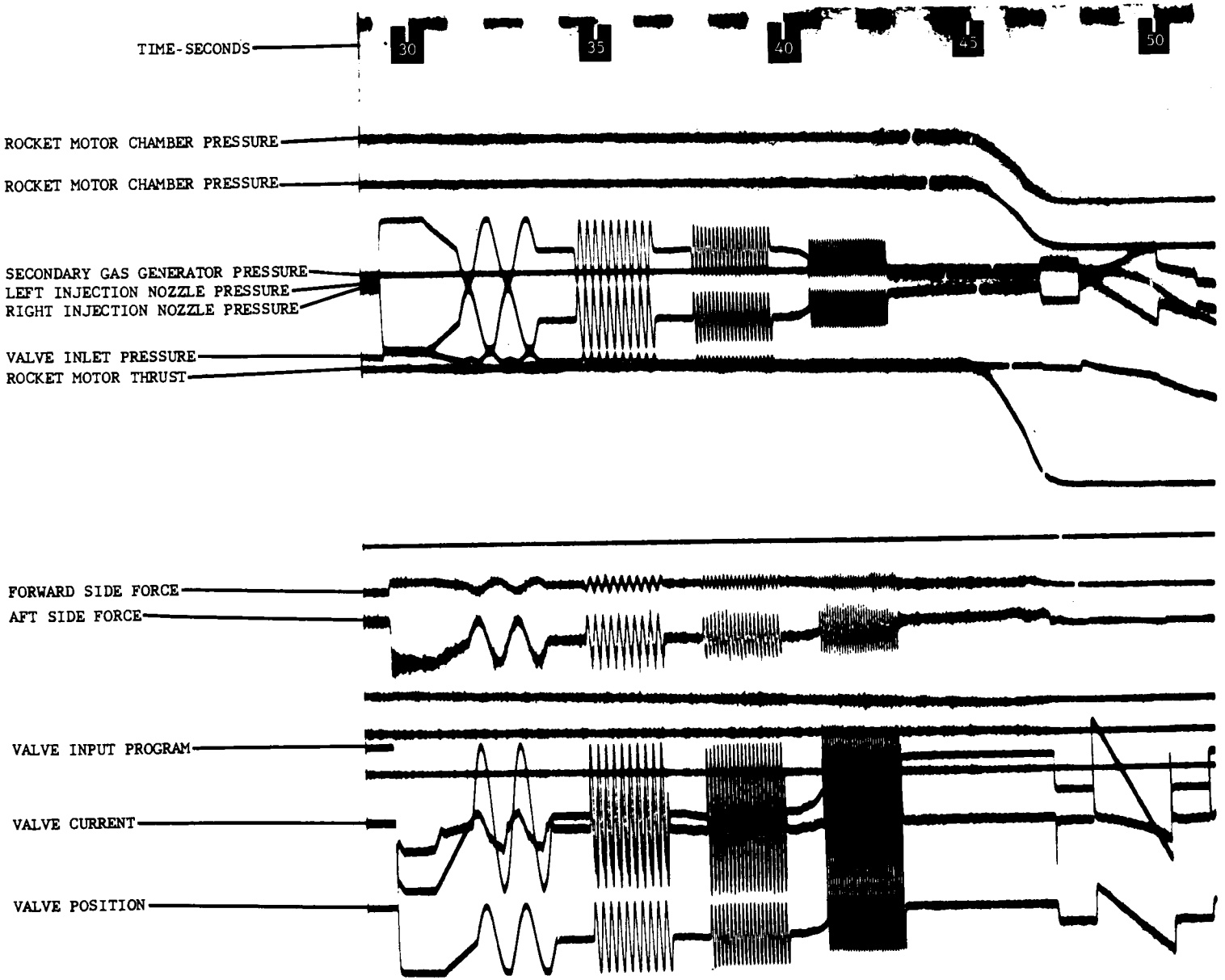

Figure 14.2 Visicorder Trace - Test No. 4

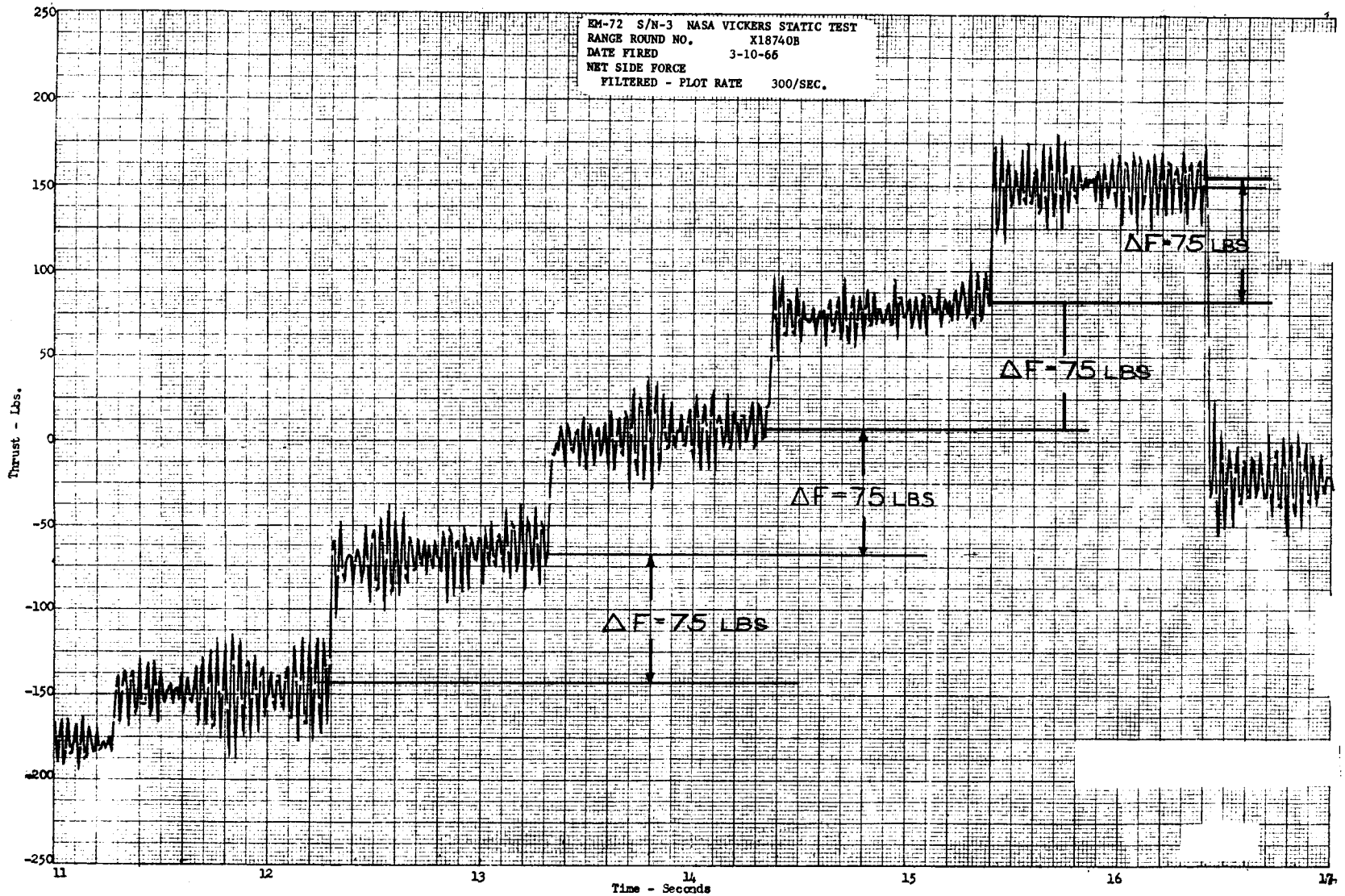

Figure 14.3 Digital Plot Test 5. 11 to 17 Seconds.

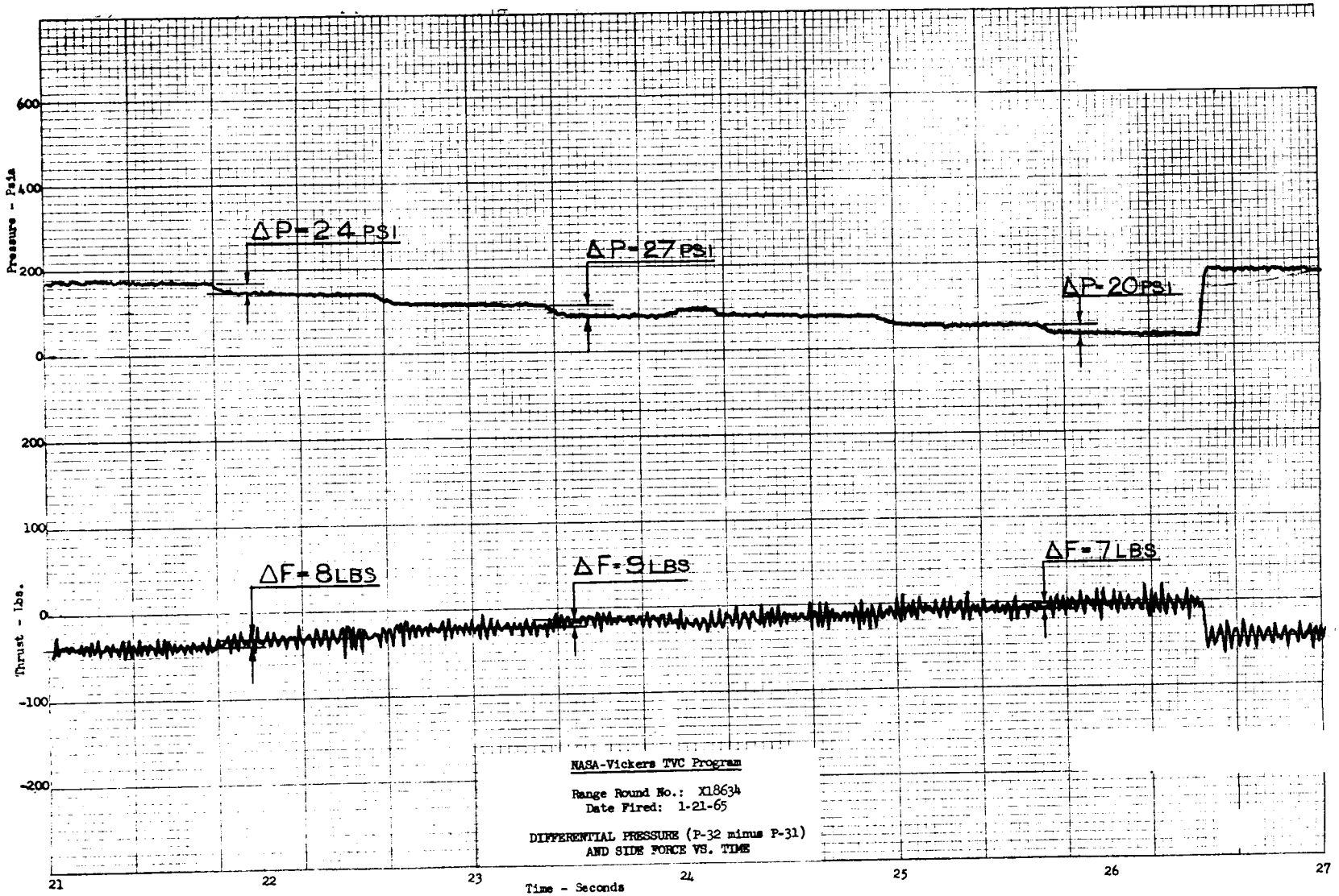

Figure 14.4 Response of System to Small Input Levels Test 4.

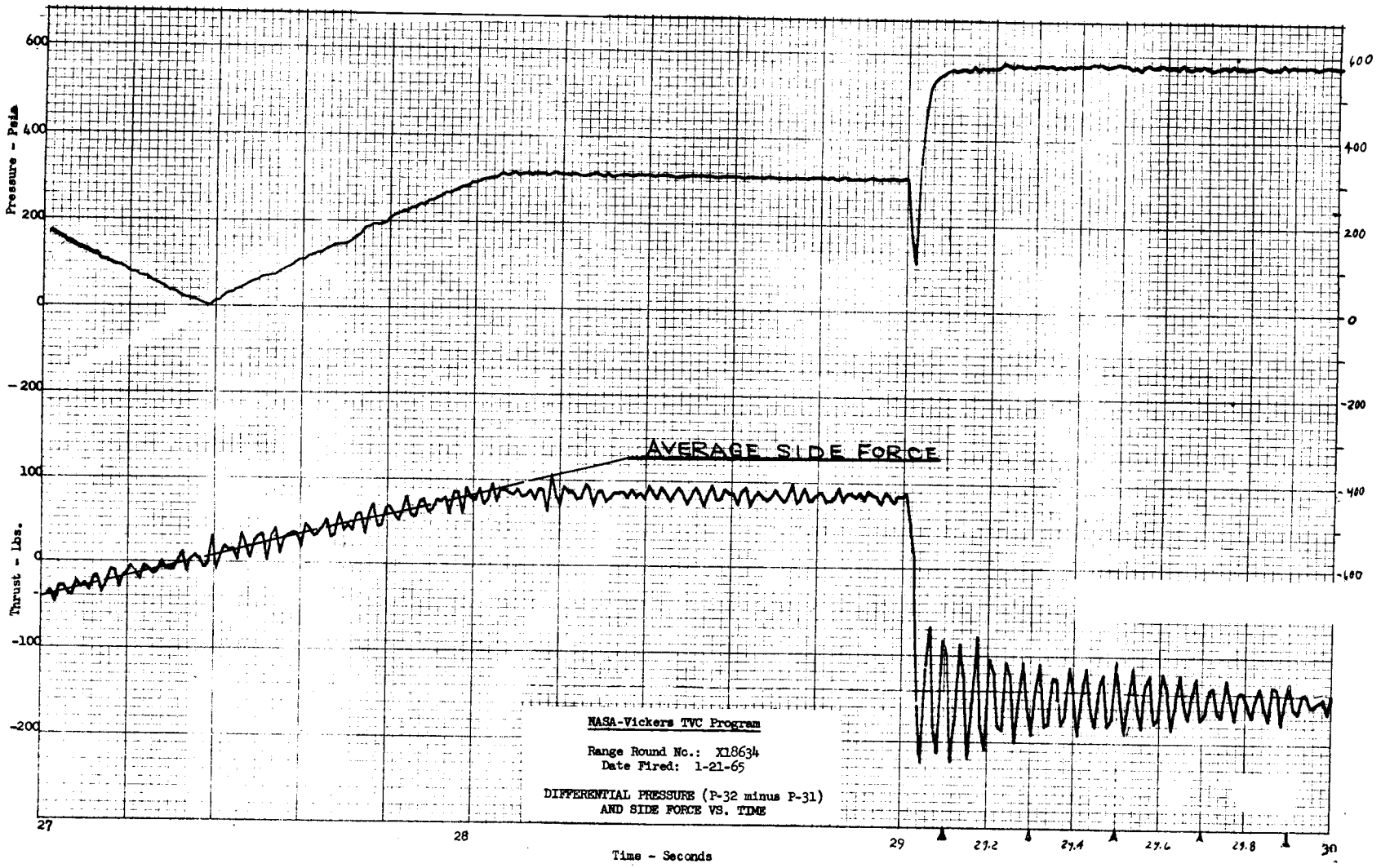

Figure 14.5 Response of System to Ramp Input Test 4.

SECTION 15

CONCLUSIONS AND RECOMMENDATIONS

15.1 Conclusions

The results of this study program have proven the performance capabilities of a continuous flowing proportional secondary injection TVC system using 2000°F gas as the injectant fluid.

The side force levels and specific impulse ratios achieved lie well within the regime of hot gas injection as shown in Figure 7.8.

The dynamic characteristics of the system are predictable, and the control qualities are excellent. This study shows that a system of this type can be directly applied to an operational vehicle. An axial thrust augmentation of 1 to 2% of the motor thrust was achieved. The continuous flowing feature of this system produced no adverse effects on the internal aerodynamics of the rocket motor.

No mathematical model has been found that correctly predicts all aspects of the gaseous secondary injection phenomena. However, the information gained from the experimental data

has verified certain trends predicted by the theoretical analyses and has shown the physical causes for some of the errors found in the models. Combining the theoretical approaches with experimental evidence now makes possible a reasonable procedure for designing a secondary injection thrust vector control system.

15.2 Current Related Work

The work performed on this contract is currently being extended under contract NAS 1-4102. An identical secondary injection system and rocket motor are being used with a 37.5:1 area ratio nozzle to investigate the system performance under simulated altitude conditions. The effect of injection nozzle location and injection angle, and operation with two axes injection will be examined.

In conjunction with this effort a flight-weight proportional two stage pressure feedback valve to operate with the 2000°F gas is also being developed to replace the breadboard model for one system test.

This valve has been designed with a view to uprating its temperature capability in the future to 5500°F.

As part of contract NAS 1-4102, a materials and stress analysis is being performed to provide a valve potential of 5500°F with aluminized propellant.

15.3 Recommendations

1. With the conclusion of contract NAS 1-4102 the necessary components and performance requirements will exist to design, develop and test a flight-weight system.

   It is recommended that a flight test program be carried out, using the flight-weight pressure feedback valve, to operationally test a 2000°F solid propellant proportional secondary injection system.

2. It is also recommended that a development and test program be initiated to extend the capability of the two stage pressure feedback valve for use with a 5500°F aluminized propellant.

3. It is recommended that further experimental work be done along the lines of this contract especially in the area of optimizing the injection angle of the secondary gas.

4. More work needs to be carried out on the analytical model of gaseous secondary injection as it is applied to a rocket nozzle. The inaccuracies in existing models lie in the area of three dimensional flow including the effects downstream of the injection port.

5. A complete study of the dynamics of the secondary injection phenomenum was limited by the response of the test stand.

   It is recommended that further work be performed in this area to extend the knowledge of the frequency bandwidth of the phenomenum.

APPENDIX

SAMPLE OF DATA PROCESSING AND INSTRUMENTATION REQUIREMENTS

Pickup Assignments

A. High Speed (300 sps)

1. Secondary Nozzle Chamber Pressure (4)
2. Gas Generator Pressure (2)
3. Valve Inlet Pressure (2)
4. Motor Chamber Pressure (1)
5. Forward Thrust (2)
6. Side Thrust (yaw) (4)
7. Vertical Thrust (pitch) (6)
8. Thrust Vector Control Program (2)
9. Feedback Signal (2)
10. Torque Motor Current (2)

B. Low Speed (30 sps) and/or red core (400 sps)

1. Pressure Taps 3 through 30 (28)

C. Thermocouple

1. Secondary Nozzle Chamber Temperature (4)
2. Valve Inlet Temperature (2)

Output

A. Time Plots (0-60 seconds at 10 sps plot rate)

1. Pressure Taps (28)
2. Average Forward Thrust (1)
3. Average Total Side Thrust (yaw) (1)
4. Average Total Vertical Thrust (pitch) (1)
5. Secondary Nozzle Chamber Pressure (4)
6. Secondary Nozzle Chamber Temperature (4)
7. Gas Generator Pressure (2)
8. Valve Inlet Pressure (2)
9. Valve Inlet Temperature (2)
10. Motor Chamber Pressure (1)
11. Thrust Vector Control Program (2)
12. Feedback Signal (2)
13. Torque Motor Current (2)

B. Paired Time Plots (0-60 seconds at 10 sps plot rate)

1. Program and Corresponding Smoothed Side Force (2)
2. Yaw Program and Chamber Pressure of 90° Injector (1)
3. Pitch Program and Chamber Pressure of 180° Injector (1)
4. Smoothed Yaw and Chamber Pressure of 90° Injector (1)

5. Smoothed Pitch and Chamber Pressure of 180° Injector (1)

C. Analytical Shock Display

1. Included Angle = 90°
2. Number of Taps = 28
3. Number of Lines = 5
4. Line Spacing to be Consistent with Actual Pattern
5. Number of Printed Displays to be Assigned

D. Digital Printouts on same page at 100 sps for Entire Test

1. Time
2. Yaw Program
3. Chamber Pressure of 270° Injector (P31)
4. Chamber Pressure of 90° Injector (P32)
5. Differential Pressure (P32-P31)
6. Yaw (F3F4 avg. + F5F6 avg.)
7. Pitch (F7F8 avg. + F9F10 avg. + F11F12 avg.)
8. Chamber Pressure of 0° Injector
9. Chamber Pressure of 180° Injector
10. Pitch Program (if column space available)

E. Digital Printouts at 10 sps

1. Pressures P1 to P30, P33, P34, P38, and P39

2. Forces, F1 to F12

3. Feedback Signals FB1 and FB2

4. Valve Currents VC1 and VC2

F. Digital Printouts at 2 sps for Temperatures TC1 to TC6

G. Two-Channel X-Y Plotters (2)

1. Chamber Pressures of 90° and 270° Injectors Versus Time

2. Chamber Pressures of 0° and 180° Injectors Versus Time

H. Expanded Time Plots on 11 x 17 Graph at 300 sps Plot Rate

1. Axial Thrust (0 to 3 seconds)

2. Chamber Pressure P31 (36.7 to 37.0, 38.7 to 39.0, and 40.7 to 41.0 seconds)

3. Chamber Pressures P32 (36.7 to 37.0, 38.7 to 39.0, and 40.7 to 41.0 seconds)

4. Yaw (36.7 to 37.0, 38.7 to 39.0, and 40.7 to 41.0 seconds)

Instrumentation Calibration Procedure

Prior to the static firing an instrumentation channel check (not including a drift check) will be conducted. Another calibration will be available if it is required by the computer program (Minneapolis-Honeywell Static Channel Performance Evaluation Abstract #01-013).

The regular calibration listing and the listing from Performance Evaluation Program will be made available to the Range immediately for review and evaluation prior to the pre-firing system check.

Following the static test the DAS transcribed tape and the Redcore firing tape will be delivered to Computing for reduction. Another instrumentation channel check will be conducted utilizing the pre-firing and post-firing calibration. Both a linearity and drift check will be run.

The regular calibration listing and the listing from the evaluation program will be reviewed and evaluated by the Range, cognizant Instrumentation Engineer, and Test Engineer prior to the release of any data.

Before either listings or graphs are prepared, a percent channel difference will be calculated between P1 and P2, and the A and B side of all the thrust gages. The results will be listed in the data package. If the channel difference is below one percent for the two channels, the average will be used for all graphs. The printouts will contain the individual channels and the average of the two channels.

LIST OF REFERENCES

(1) Wu, J. M., Chapkis, R. L., and Mager, A., "Approximate Analysis of Thrust Vector Control by Fluid Injection," ARS Journal, December, 1961, pages 1677-1685.

(2) Mager, A., "On the Model of the Free, Shock-Separated, Turbulent Boundary Layer," Journal Aeronautical Science, February, 1956, Volume 23, pages 181-184.

(3) Ames Research Staff, "Equations, Tables, and Charts for Compressible Flow," NACA TR-1135, 1953.

(4) Hammitt, A. G., and Murthy, K.R.A., "Approximate Solutions for Supersonic Flow Over Wedges and Cones," AFOSR TN 59-304, Rep. 449 Princeton University, April 1959.

(5) Kallis, J. M., and Adelberg, M., "Recent Advances in the Fluid Dynamics of Gas Injection for Thrust-Vector and Trajectory Control (u)," CPIA Publication 18A, AD 346945 Bulletin of the Interagency Solid Propulsion Meeting, July 1963, pages 341-389, CONFIDENTIAL.

(6) Charwat, A. F., and Allegre, J., "Interaction of a Supersonic Stream and a Transverse Supersonic Jet," AIAA Journal, November 1964, Volume 2, No. 11, pages 1965-1972.

(7) Broadwell, J. E., "Analysis of the Fluid Mechanics of Secondary Injection for Thrust Vector Control," AIAA Journal, May 1963, Volume 1, No. 5, pages 1067-1075.

(8) Guhse, R. D., "An Experimental Investigation of Thrust Vector Control by Secondary Injection," NASA Contractor Report, NASA CR-297, September 1965.

"The aeronautical and space activities of the United States shall be conducted so as to contribute . . . to the expansion of human knowledge of phenomena in the atmosphere and space. The Administration shall provide for the widest practicable and appropriate dissemination of information concerning its activities and the results thereof."

—NATIONAL AERONAUTICS AND SPACE ACT OF 1958

NASA SCIENTIFIC AND TECHNICAL PUBLICATIONS

TECHNICAL REPORTS: Scientific and technical information considered important, complete, and a lasting contribution to existing knowledge.

TECHNICAL NOTES: Information less broad in scope but nevertheless of importance as a contribution to existing knowledge.

TECHNICAL MEMORANDUMS: Information receiving limited distribution because of preliminary data, security classification, or other reasons.

CONTRACTOR REPORTS: Technical information generated in connection with a NASA contract or grant and released under NASA auspices.

TECHNICAL TRANSLATIONS: Information published in a foreign language considered to merit NASA distribution in English.

TECHNICAL REPRINTS: Information derived from NASA activities and initially published in the form of journal articles.

SPECIAL PUBLICATIONS: Information derived from or of value to NASA activities but not necessarily reporting the results of individual NASA-programmed scientific efforts. Publications include conference proceedings, monographs, data compilations, handbooks, sourcebooks, and special bibliographies.

Details on the availability of these publications may be obtained from:

SCIENTIFIC AND TECHNICAL INFORMATION DIVISION

NATIONAL AERONAUTICS AND SPACE ADMINISTRATION

Washington, D.C. 20546